

**How Tibiofemoral Alignment Effects the Medial-Lateral Compartment Loading in the
Knee Joint During Tai Chi Gait, a Musculoskeletal Modeling Approach**

by

Colin James Holtkamp

A thesis submitted to the Graduate Faculty of
Auburn University
in partial fulfillment of the
requirements for the Degree of
Master of Science

Auburn, Alabama
August 8, 2020

Key Words: Musculoskeletal Modeling, Knee Model, Tai Chi, Compartmental Loading, Joint
Contact Forces, OpenSim

Copyright 2020 by Colin James Holtkamp

Approved by

David G. Beale, Chair, Professor, Mechanical Engineering
Wei Liu, Associate Professor, Biomedical Affairs and Research
Robert L. Jackson, Professor, Mechanical Engineering

Abstract

Osteoarthritis of the knee joint is one of the most common disabling diseases in the United States particularly among elderly people. Even though no disease altering cure currently exists that rectifies the degenerative nature of OA, some studies have shown that moderate, intermittent mechanical loading of the articular cartilage can stimulate cell synthesis and maintain homeostasis by means of rehabilitative exercise. One exercise that has drawn the attention of researchers and clinicians is Tai Chi, a Chinese ancient martial art recently turned therapeutic exercise. Tai Chi has been shown to increase joint stability, balance, and help manage pain in patients with OA. Therefore, the aim of this study is twofold: The first aim, is to understand how Tai Chi gait effects mediolateral compartmental loading of the knee joint relative to Normal Walking. The second aim is to understand how tibiofemoral malalignment effects mediolateral compartmental loading of the knee for Tai Chi gait relative to Normal Walking. Results for both research questions were resolved through a musculoskeletal modeling approach. One 28-year-old male subject, weighing 77.11 kilograms, and a height of 1.75 meters was used to conduct this study. One Yang style Tai Chi gait and one Normal Walking gait at self-selected walking speed was measured with 3D gait analysis. The gait data was then used to generate a musculoskeletal model in OpenSim that resolves the medial and lateral knee joint contact loads of a model with subject specific tibiofemoral alignment. A standard joint reaction analysis with muscle forces generated by static optimization was used to compare the mediolateral compartmental contact loads in the right knee during stance phase of Tai Chi and Normal Walking gait. Subsequent joint reaction analyses were conducted to analyze the effects of tibiofemoral malalignment, varus and valgus malalignment ($\pm 8^\circ$ offset from normal tibiofemoral alignment), on compartmental loading for both Tai Chi and Normal Walking. This study found that the mean total, mean medial, and mean lateral joint contact loads where all

significantly higher for Tai Chi (333.77% BW, 152.23%BW, and 181.54%BW respectively) than for Normal Walking (211.29% BW, 120.23%BW, and 91.06%BW, respectively), p value <0.005 . However, in terms of load distribution, the medial compartment accepted a significantly smaller percentage of the mean total load for Tai Chi, 27.35%TL, than for Normal Walking, 54.35%TL. Medial compartmental unloading of knee was also observed in late stance phase of Tai Chi gait. Therefore, it can be concluded that Tai Chi gait reduces the load distribution on the medial compartment and increases the load distribution on the lateral compartment. This observation is consistent with the hypothesis that a reduced external knee adduction moment will reduce medial compartment loading in the knee joint for Tai Chi. Finally, when analyzing the medial and lateral joint contact loads for a varus and valgus tibiofemoral malalignment, the medial compartment showed a higher sensitivity to change in load per degree malalignment than the lateral compartment for Tai Chi. For Normal Walking, the reciprocal was observed. These findings elucidate an altered mechanical loading pattern for Tai Chi gait relative to Normal Walking. This change in mechanical loading could help stimulate cell synthesis within the articular cartilage of the knee and help maintain homeostasis, ultimately improving total joint health. Therefore, there is strong evidence to support the hypothesis that Tai Chi is a good rehab exercise for patients with osteoarthritis of the knee.

Acknowledgments

First, I would like to thank my lovely wife who has stood by me throughout this long process. She has always encouraged me and helped me stay focused on the task at hand. Secondly, I would like to thank my parents who have always stood by me in every season of life and have graciously provided opportunities for me to pursue my dreams, including this one, an opportunity to pursue a master's degree. Third, I would like to thank Dr. Beale and Dr. Liu for giving me the opportunity to research the area of biomechanics. Their guidance and advice have helped shape this work.

Last and most importantly, I would like to thank the Lord Jesus Christ and the Holy Spirit whom he has placed in the heart of all believers. I can honestly say that without him and his active counsel, I would have quit a long time ago. However, thanks be to him, I did not quit because, "He who began a good work in me will bring it to completion" (Philippians 1:6). I thank the Holy Spirit for being my counselor and teacher, for "He has come to teach me all things and bring to remembrance everything that he has taught me" (John 14:26). I especially want to thank him for graciously supplying the spirit of wisdom and revelation. Only by him have I been given the ability to comprehend highly technical work such as this. After completing this work, I am convinced that, "All the treasures of wisdom and knowledge are found in him, Christ" (Colossians 2:3). Thank you, Lord, for your faithfulness, grace, and mercy throughout this challenging process. To him be the glory forever and ever.

Table of Contents

Abstract.....	ii
Acknowledgments.....	iv
Table of Contents.....	v
List of Tables	viii
List of Figures.....	x
List of Abbreviations	xvi
Chapter 1: Background and Literature Review	1
1.1. Introduction.....	1
1.2. Knee Osteoarthritis	3
1.3. Anatomy of the Knee.....	4
1.4. Anatomy of Articular Cartilage	6
1.5. Mechanical Loading Effects on Cartilage and OA	10
1.6. Tibiofemoral Alignment Effects Compartmental Mechanical Loading of The Knee	13
1.7. Non-Invasive Treatments for Osteoarthritis	17
1.8. Intro to Tai Chi.....	20
1.9. Musculoskeletal Modeling.....	22
1.9.1. Intro to Musculoskeletal Modeling.....	22
1.9.2. Human Subject Testing and Data Collection with Motion Capture	23
1.10. Musculoskeletal Modeling in OpenSim.....	26
1.10.1. The Model.....	28
1.10.2. Scaling.....	32
1.10.3. Inverse Kinematics.....	34
1.10.4. Residual Reduction Analysis	35
1.10.5. Static Optimization	38
1.10.6. Computed Muscle Control.....	39
1.10.7. Muscle Driven Forward Dynamics.....	42
1.10.8. Joint Reaction Analysis.....	43
1.11. Computational Modeling.....	45
1.11.1. Low Fidelity Knee Models	48
1.12. Conclusion and Motivation for this Research.....	51
Chapter 2: Methods and Procedures	53
2.1. Introduction.....	53
2.2. Human Subject Data	53
2.3. Preparing Data for OpenSim Import.....	54

2.4. The Musculoskeletal Model.....	55
2.5. The Modeling Process and Standard Workflow	60
2.5.1. Preliminary Model Adjustments	61
2.5.2. Scaling.....	66
2.5.3. Inverse Kinematics.....	69
2.5.4. Residual Reduction Analysis	70
2.5.5. Computed Muscle Control.....	73
2.5.6. Static Optimization	74
2.5.7. Joint Reaction Analysis.....	74
2.5.8. Forward Dynamics.....	76
2.6. Gait Characteristics.....	76
2.7. Data Analyses	79
2.8. Statistical Analyses	81
Chapter 3: Results	83
3.1. Introduction.....	83
3.2. Joint Contact Forces of Tai Chi and Normal Walking for the Nominal Model	83
3.2.1. Nominal Normal Walking.....	83
3.2.2. Nominal Tai Chi	86
3.2.3. Varus Normal Walking.....	88
3.2.4. Varus Tai Chi.....	91
3.2.5. Valgus Normal Walking	93
3.2.6. Valgus Tai Chi	96
3.3. Comparing Results.....	98
3.3.1. Nominal Normal Walking Vs. Nominal Tai Chi.....	98
3.3.2. Normal Walking Altered Tibiofemoral Alignment	99
3.3.3. Tai Chi Altered Tibiofemoral Alignment	102
3.3.4. Normal Walking Altered TFA Vs. Tai Chi Altered TFA.....	105
Chapter 4: Discussion of the Results	108
4.1. Nominal Normal Walking Vs. Nominal Tai Chi.....	108
4.1.1. Influence of Muscle Forces on Joint Contact Loading.....	108
4.1.2. Influence of Medial and Lateral Muscle Forces on Compartmental Load Distribution	112
4.1.3. Influence of EKAM on Compartmental Load Distribution.....	115
4.2. Normal Walking Altered TFA Vs. Tai Chi Altered Tai Chi	127
4.3. Discussion Summary	128
Chapter 5: Validation.....	129
5.1. Intro to Model Validation Process	129
5.2. Current Validation Process	131
5.2.1. Calibration Process	132
5.2.2. Internal validation.....	136

5.2.3. Independent Validation.....	137
5.3. Validation Results and Discussion.....	141
5.3.1. Calibration Results.....	141
5.3.2. Calibration Discussion.....	144
5.3.3. Internal Validation Results.....	146
5.3.4. Internal Validation Discussion.....	149
5.3.5. Independent Validation Results.....	150
5.3.6. Independent Validation Discussion.....	155
5.4. Validation Conclusion.....	158
5.5. Validation Future Recommendations.....	159
Chapter 6: Conclusion.....	161
6.1. Limitations.....	161
6.2. Future Recommendations.....	162
6.3. Conclusion.....	163
References.....	166
Appendix.....	176
Appendix A: Matlab Codes.....	176
A.1. Joint Center Calculation.....	176
A.2. RRA Parameter Extraction and Reduction Code.....	180
A.3. Internal validation Code.....	189
A.4. EKAM Calculation Code.....	192
Appendix B: RRA Data.....	195
Appendix C: Left Leg Joint Reaction Plots and Statistics.....	199
Appendix D: Left Leg Altered TFA Plots and Statistics.....	209
Appendix E: Left Leg Muscle Forces and Contact Load Contributions.....	214
Appendix F: Calibration Results.....	218
Appendix G: Internal Validation Error Plots.....	222

List of Tables

Table 1: Threshold values for reducing residual forces and moments (Hicks et al.).....	38
Table 2: Scale factors calculated by the scale tool in OpenSim used to scale the model. Each scale factor corresponds to a specific bone segment (right and left) of the model.....	67
Table 3: Scaling marker weight factors used to scale the nominal model.....	67
Table 4: Scaling errors of the nominal model (TFA=177.16 deg.) used in this study	69
Table 5: Kinematic coordinate weights used for Normal Walking and Tai Chi trials	69
Table 6: Threshold for residual forces, torques and coordinate errors about the pelvis for reducing residuals during residual reduction analysis.....	70
Table 7: Final residual “hand of god” forces, moments, and coordinate errors about the pelvis in the ground reference frame for the nominal model for Normal Walking trail. Green values are sufficient, yellow values are “Tolerable”, and red values are “Insufficient”.....	71
Table 8: Final residual “hand of god” forces, moments, and coordinate errors about the pelvis in the ground reference frame for the nominal model for Tai Chi trail. Green values are sufficient, yellow values are “Tolerable”, and red values are “Insufficient”	71
Table 9: Statistical results calculated for the Normal Walking, right and left knee, stance phase, nominal tibiofemoral alignment, TFA=177.16 degrees.	86
Table 10: Statistical results calculated for the Tai Chi, right and left knee, stance phase, nominal tibiofemoral alignment, TFA=177.16 degrees.	88
Table 11: Statistical results calculated for the Normal Walking, right and left knee, stance phase, varus tibiofemoral alignment, TFA=172 degrees.	91
Table 12: Statistical results calculated for the Tai Chi, right and left knee, stance phase, varus tibiofemoral alignment, TFA=172 degrees.	93
Table 13: Statistical results calculated for the Normal Walking, right and left knee, stance phase, valgus tibiofemoral alignment, TFA=188 degrees.	96
Table 14: Statistical results calculated for the Normal Walking, right and left knee, stance phase, valgus tibiofemoral alignment, TFA=188 degrees.	98
Table 15: Statistical comparisons of normalized joint contact forces for the right knee nominal alignment of Tai Chi and Normal Walking.....	99
Table 16: Statistical comparisons of normalized joint contact forces for the right knee altered tibiofemoral alignment of Normal Walking.	102
Table 17: Statistical comparisons of normalized joint contact forces for right knee altered tibiofemoral alignment of Tai Chi.	105
Table 18: Percent difference of normalized joint contact force data comparisons of right knee varus and valgus tibiofemoral alignment for Tai Chi and Normal Walking.	106
Table 19: Normalized percent difference per degree of malalignment of normalized joint contact force data comparisons of right knee varus and valgus tibiofemoral alignment for Tai Chi and Normal Walking.....	107
Table 20: Mean sum medial side muscle force and lateral side muscle forces that contribute the medio-lateral compartmental joint contact loads in the right knee.	115
Table 21: Statistical data for the EKAM calculated about the left and right knees of stance phase for Normal Walking and Tai Chi gait.....	118
Table 22: Statistical results of paired t-tests for the difference of means for kinematic coordinates calculated by inverse dynamics and forward dynamics. All values are for the right leg stance phase of the Normal Walking trial.	143
Table 23: The mean the percent differences in kinematic coordinate values at all time steps for inverse kinematics and forward dynamics throughout right leg stance phase of gait for the Normal Walking trial.	144
Table 24: Defines each moment calculation, Figure 91, about the right knee used for internally validating the muscle forces calculations for Tai Chi gai.	148
Table 25: Internal validation results of moments calculated about the right and left knee joints for stance phase of Normal walking and Tai Chi gait, where the errors are the difference in inverse dynamic flexion/extension moment and the muscle force flexion/extension moment about the left and right knees.....	149
Table 26: Statistical values for muscle activations from independent validation, EMG activations, OpenSim reference activations, and the activations from the Normal Walking trial in this study.....	154

Table 27: Influential muscle force confidence levels based on calibration and independent validation results for normal walking of the nominal TFA model.....157

Table 28: RRA iterative residual “hand of god” forces and moments on the pelvis for Nominal Normal Walking TFA=177.16. All parameters shown were minimized until they could not be minimized any further. Green= sufficient value, yellow=tolerable value, and red=insufficient value. Threshold values can be found in Table 6.....195

Table 29: RRA iterative residual “hand of god” forces and moments on the pelvis for Varus Normal Walking TFA=172. All parameters shown were minimized until they could not be minimized any further. Green= sufficient value, yellow=tolerable value, and red=insufficient value. Threshold values can be found in Table 6.....196

Table 30: RRA iterative residual “hand of god” forces and moments on the pelvis for Valgus Normal Walking TFA=188. All parameters shown were minimized until they could not be minimized any further. Green= sufficient value, yellow=tolerable value, and red=insufficient value. Threshold values can be found in Table 6.....196

Table 31: RRA iterative residual “hand of god” forces and moments on the pelvis for Nominal Tai Chi TFA=177.16. All parameters shown were minimized until they could not be minimized any further. Green= sufficient value, yellow=tolerable value, and red=insufficient value. Threshold values can be found in Table 6.197

Table 32: RRA iterative residual “hand of god” forces and moments on the pelvis for Varus Tai Chi TFA=177.16. All parameters shown were minimized until they could not be minimized any further. Green= sufficient value, yellow=tolerable value, and red=insufficient value. Threshold values can be found in Table 6.197

Table 33: RRA iterative residual “hand of god” forces and moments on the pelvis for Valgus Tai Chi TFA=177.16. All parameters shown were minimized until they could not be minimized any further. Green= sufficient value, yellow=tolerable value, and red=insufficient value. Threshold values can be found in Table 6.198

Table 34: Statistical comparisons of normalized joint contact forces for the left knee nominal alignment of Tai Chi and Normal Walking.....208

Table 35: Statistical comparisons of normalized joint contact forces for the left knee altered tibiofemoral alignment of Normal Walking.....212

Table 36: Statistical comparisons of normalized joint contact forces for the left knee altered tibiofemoral alignment of Tai Chi.212

Table 37: Percent difference of normalized joint contact force data comparisons of left knee varus and valgus tibiofemoral alignment for Tai Chi and Normal Walking.212

Table 38: Normalized percent difference per degree of malalignment of normalized joint contact force data comparisons of left knee varus and valgus tibiofemoral alignment for Tai Chi and Normal Walking.....213

Table 39: Mean sum medial side muscle force and lateral side muscle forces that contribute the medio-lateral compartmental joint contact loads in the left knee.217

Table 40: Statistical results of paired t-tests for the difference of means for kinematic coordinates calculated by inverse dynamics and forward dynamics. All values are for the left leg stance phase of the Normal Walking trial.....218

Table 41: The mean the percent differences in kinematic coordinate values at all time steps for inverse kinematics and forward dynamics throughout left leg stance phase of gait for the Normal Walking trial.219

List of Figures

Figure 1: Bone segments (femur, tibia and patella) comprising the right knee joint. Image courtesy of (Dan).	5
Figure 2: Anatomy of soft tissues namely ligaments and articular cartilage in the knee joint. Photo courtesy of (Seedhom, “Transmission of the Load in the Knee Joint with Special Reference to the Role of the Menisci. Part I. Anatomy, Analysis and Apparatus”)	6
Figure 3: Various Zones of the Articular Cartilage. (A) Shows the sparse placement of Chondrocytes within the cartilage ECM. (B) Shows the collagen fiber orientation in the various zones within the cartilage ECM. Image courtesy of (Sophia Fox et al.)	7
Figure 4: Displacement and stress curves vs. time plot shows the time dependent viscoelastic behavior of articular cartilage in compression. Image courtesy of (Cohen et al.).....	9
Figure 5: Radiographic imaging of healthy right knee (A) and an Osteoarthritic knee (B). Medial joint space narrowing, and the formation of osteophytes can be seen in (B). Image modified from (Altman et al.).	12
Figure 6: Outlines the effects that cyclic mechanical loading has in promoting healthy cartilage homeostasis as well as the degenerative effects mechanical loading has on cartilage when permanent deformation in mechanical loading occurs from injury change. Picture courtesy of (Andriacchi et al.).....	13
Figure 7: Mechanical axis of the femur (A), anatomical axis of the femur (B), mechanical axis of the tibia (C), and anatomical axis of the tibia (D) for the left leg defined in the literature. This photo was modified from (Krackow).	14
Figure 8: Normal alignment of tibiofemoral mechanical axis (A), tibiofemoral alignment (TFA) angle and mechanical tibiofemoral angle (MTFA) formed by tibial and femoral mechanical axes (B), valgus and varus angle formed by the anatomical axes of the femur and tibia (C) and (D) respectively, mechanical axis of lower extremity (MALE) formed by a varus knee alignment (E) and valgus knee alignment (F) respectively. All images are of the left leg. This photo was modified from (Krackow).....	15
Figure 9: Knee Adduction Moment generated about the knee joint center of a static normal aligned knee (A), a static varus aligned knee (B), and a dynamic varus aligned knee (C) (Johnson, F. ; Leitzl, S; Waugh). The resultant external knee adduction moment (EKAM) results in larger medial knee joint contact load (D) (Andriacchi et al.). Image modified from (Johnson, F. ; Leitzl, S; Waugh) and (Andriacchi et al.).....	16
Figure 10: Representation of how a single motion capture camera does not directly calculate the position of each marker rather multiple cameras are used in conjunction with a weighted least squares (WLS) approximation to calculate the position of each marker.....	24
Figure 11: Flow chart of the data collection process which serves as the primary inputs for the musculoskeletal model and subsequent simulations.....	26
Figure 12: Anatomical directions and the global coordinate system as defined by OpenSim	28
Figure 13: OpenSim Rigid Body Definitions: Proximal segments are parent bodies, green, while distal segments are child bodies, blue, respectively when considering a joint of two bone segments. P_0 , B_0 , and G_0 are the origins of parent body, child body, and ground anatomical reference frames respectively. P and B are any point in the parent and child body respectively. Photo adapted from (Seth, Sherman, et al.).....	29
Figure 14: Hill-type muscle Model which helps characterize the force generation of a muscle. The was modified to produce the Thelen2003Muscle model used in OpenSim MS Modeling framework. Image courtesy of (Thelen).....	31
Figure 15: Experimental and virtual marker locations used for scaling OpenSim MSMs. Image courtesy of OpenSim documentation (Delp, Anderson, et al.) (Seth, Hicks, et al.).....	32
Figure 16: RRA Feedback Control Loop Block Diagram. Image courtesy of (Anderson et al.).....	37
Figure 17: CMC Feedback Control Loop Block Diagram. Image courtesy of (Thelen and Anderson).....	40
Figure 18: (a) Three link mechanism of the right leg, (b) Rendering of the virtual muscles which cause relative motion at the knee and ankle joints in OSM, (c) Simplified muscle lines if action and GRF on the right leg, (d) FBD of tibia used in joint reaction analysis.	43
Figure 19: 3 DOF Planar Knee model were the tibia rotates and translates in the sagittal plane as a function of knee flexion angle. Photos (A) and (B) courtesy of (Delp, Loan, et al.) and (Seth, Sherman, et al.) respectively.....	49
Figure 20: Instrumented Knee Implant responsible for measuring knee joint contact loads <i>in-vivo</i> for patients with total knee arthroplasty. Photos (A) and (B) adapted from (Graichen et al.) and (Halder et al.) respectively.	50
Figure 21: Flow chart of how to transform 3D gait data to be imported into OpenSim.....	55
Figure 22: Knee joint decomposition if the Medio-Lateral Knee (MLK) model used for this research study. Image courtesy of (Lerner et al.).....	56

Figure 23: Decomposed tibial segment of the mediolateral knee (MLK) model. (A) shows the right lower extremity with bone segments and muscle forces acting on the tibia. (B) Shows rigid body segments of the right femur, tibia, and foot. (C) Shows the isolated muscle forces and joint reaction loads. (D) Is a 3-D Free body diagram of the tibial segment for which a moment a force balance can be conducted such that the reaction loads at the medial and lateral condyles can be solved through a joint reaction analysis in OpenSim.58

Figure 24: Flow chart of all the OpenSim Analyses to generate compartmental tibiofemoral joint contact loads. This chart also includes simulations such as ID, CMC, and FD, which were used for validation.61

Figure 25: Markers used to calculate the right hip, knee, and ankle joint centers which from the tibiofemoral Alignment (TFA) angle. The TFA angle is the internal angle formed by the intersection of the tibial and femoral mechanical axes. Figure shows anterior (A) and posterior view (B).62

Figure 26: “Bell and Brand Pelvis” defined in V3D_Composite coordinate system in Visual-3D (C-Motion, Germantown, MD, USA). Figure modified from Visual-3D Wiki Documentation.64

Figure 27: Three different models used for this study with varying tibiofemoral alignment, nominal TFA=177.16 degrees (A), varus TFA=172 degrees (B), and valgus TFA=188 degrees (C).65

Figure 28: Nominal model with 37 virtual markers (pink) appended to the model (right). Static trial of 37 retroreflective markers (blue) measured by motion capture during data collection (left)66

Figure 29: Inputs and outputs for the Scale Tool in OpenSim. Imported files are blue while user defined inputs are black.....68

Figure 30: Rendering of the fully scaled nominal tibiofemoral alignment model used for this study.68

Figure 31: Inputs and outputs for the Inverse Kinematics Tool in OpenSim. Imported files are blue while user defined inputs are black70

Figure 32: Inputs and outputs for the Residual Reduction Analysis (RRA) Tool in OpenSim. Imported files are blue while user defined inputs are black.....72

Figure 33: Inputs and outputs for residual forces, moments, and coordinate errors data extraction using Matlab. This code extracts data from two files (blue) generated by each RRA iteration72

Figure 34: Inputs and outputs for the Computed Muscle Control (CMC) Tool in OpenSim. Imported files are blue while user defined inputs are black.....73

Figure 35: Inputs and outputs for the Static Optimization (STO) Tool in OpenSim. Imported files are in blue while user defined inputs are in black74

Figure 36: Inputs and outputs for the Joint reaction Analysis (JRA) Tool in OpenSim. Imported files are in blue while user defined inputs are in black75

Figure 37: Inputs and outputs for the Forward Dynamics (FD) Tool in OpenSim. Imported files are in blue while user defined inputs are in black76

Figure 38: Break down of the classic M-Shape of the vertical ground reaction force for right leg stance phase of Normal Walking. This GRF data comes from the Normal Walking trial used for this study.77

Figure 39: Subphases of the Tai Chi Gait Cycle used for this study: Double support I (A), Single support (B), Double support II (C), Swing (D). Photo courtesy of (Liu et al.).....78

Figure 40: Break down of the of the vertical ground reaction force for right leg stance phase of Tai Chi. This GRF data comes from the Tai Chi trial used for this study.78

Figure 41: Normalized joint contact loads of the total, medial, and lateral left and right knee compartments during stance phase of Normal Walking gait with nominal alignment, TFA=177.16 degrees.84

Figure 42: Right Medial and lateral normalized joint contact loads summed to show the total contact loads as a percentage of body weight during stance phase of Normal Walking gait with nominal alignment, TFA=177.16 degrees.85

Figure 43: Right Medial and lateral normalized joint contact load distribution as a percentage of the total contact load during stance phase of Normal Walking gait with nominal alignment, TFA=177.16 degrees.85

Figure 44: Normalized joint contact loads of the total, medial, and lateral right and left knee compartments during stance phase of Tai Chi gait with nominal alignment, TFA=177.16 degrees.86

Figure 45: Medial and lateral normalized joint contact loads summed to show the total contact loads as a percentage of body weight during stance phase of Tai Chi gait with nominal alignment, TFA=177.16 degrees.87

Figure 46: Medial and lateral normalized joint contact load distribution as a percentage of the total contact load during stance phase of Tai Chi gait with nominal alignment, TFA=177.16 degrees.88

Figure 47: Normalized joint contact loads of the total, medial, and lateral right knee compartments during stance phase of Normal Walking gait with varus alignment, TFA=172 degrees.89

Figure 48: Medial and lateral normalized joint contact loads summed to show the total contact loads as a percentage of body weight during stance phase of Normal Walking gait with varus alignment, TFA=172 degrees.90

Figure 49: Medial and lateral normalized joint contact load distribution as a percentage of the total contact load during stance phase of Normal Walking gait with varus alignment, TFA=172 degrees.	90
Figure 50: Normalized joint contact loads of the total, medial, and lateral right knee compartments during stance phase of Tai Chi gait with varus alignment, TFA=172 degrees.	91
Figure 51: Medial and lateral normalized joint contact loads summed to show the total contact loads as a percentage of body weight during stance phase of Tai Chi gait with varus alignment, TFA=172 degrees.	92
Figure 52: Medial and lateral normalized joint contact load distribution as a percentage of the total contact load during stance phase of Tai Chi gait with varus alignment, TFA=172 degrees.	93
Figure 53: Normalized joint contact loads of the total, medial, and lateral right knee compartments during stance phase of Normal Walking gait with valgus alignment, TFA=188 degrees.....	94
Figure 54: Medial and lateral normalized joint contact loads summed to show the total contact loads as a percentage of body weight during stance phase of Normal Walking gait with valgus alignment, TFA=188 degrees.....	95
Figure 55: Medial and lateral normalized joint contact load distribution as a percentage of the total contact load during stance phase of Normal Walking gait with valgus alignment, TFA=188 degrees.	95
Figure 56: Normalized joint contact loads of the total, medial, and lateral right knee compartments during stance phase of Tai Chi gait with valgus alignment, TFA=188 degrees.	96
Figure 57: Medial and lateral normalized joint contact loads summed to show the total contact loads as a percentage of body weight during stance phase of Tai Chi gait with valgus alignment, TFA=188 degrees.....	97
Figure 58: Medial and lateral normalized joint contact load distribution as a percentage of the total contact load during stance phase of Tai Chi gait with Valgus alignment, TFA=188 degrees.	98
Figure 59: Normalized, right knee, stance phase, total joint contact loads of Normal Walking gait for nominal (TFA=177.16 deg.), varus (TFA=172 deg.), and valgus (TFA=188 deg.) tibiofemoral alignments.....	101
Figure 60: Normalized, right knee, stance phase, medial compartment joint contact loads of Normal Walking gait for nominal (TFA=177.16 deg.), varus (TFA=172 deg.), and valgus (TFA=188 deg.) tibiofemoral alignments	101
Figure 61: Normalized, right knee, stance phase, lateral compartment joint contact loads of Normal Walking gait for nominal (TFA=177.16 deg.), varus (TFA=172 deg.), and valgus (TFA=188 deg.) tibiofemoral alignments	102
Figure 62: Normalized, right knee, stance phase, total joint contact loads of Tai Chi gait for nominal (TFA=177.16 deg.), varus (TFA=172 deg.), and valgus (TFA=188 deg.) tibiofemoral alignments.....	104
Figure 63: Normalized, right knee, stance phase, medial compartment joint contact loads of Tai Chi gait for nominal (TFA=177.16 deg.), varus (TFA=172 deg.), and valgus (TFA=188 deg.) tibiofemoral alignments.....	104
Figure 64: Normalized, right knee, stance phase, lateral compartment joint contact loads of Tai Chi gait for nominal (TFA=177.16 deg.), varus (TFA=172 deg.), and valgus (TFA=188 deg.) tibiofemoral alignments.....	105
Figure 65: Normalized muscle forces that traverse the right knee during stance phase for Normal Walking, nominal tibiofemoral alignment (TFA=177.16deg.)	109
Figure 66: Normalized muscle forces that traverse the right knee during stance phase for Tai Chi, nominal tibiofemoral alignment (TFA=177.16deg.)	109
Figure 67: Normalized joint contact forces compared to the sum of the three most influential muscle forces (Sum Isolated Muscle Forces), rectus femoris, lateral gastrocnemius, medial gastrocnemius and the total muscle forces that traverse the right knee, stance phase, Normal Walking, nominal tibiofemoral alignment (TFA=177.16)	110
Figure 68: Normalized joint contact forces compared to the sum of the three most influential muscle forces (Sum Isolated Muscle Forces), medial and lateral gastrocnemius, vastus medialis, vastus lateralis, vastus intermedius, rectus femoris, muscle forces that traverse the right knee, stance phase, Tai Chi, nominal tibiofemoral alignment (TFA=177.16).....	111
Figure 69: Diagram of the anatomical locations of most influential muscles that contribute to the joint contact load of the right knee. (A) Shows the location of the medial and lateral gastrocnemius muscles in the calf. (B) Shows the rectus femoris and the vastus intermedius muscles in the quadricep. (C) Shows the vastus medialis and the vastus lateralis in the quadricep.	113
Figure 70: Summed normalized muscle forces for the medial and the lateral sides compared to the medial and lateral joint contact forces of the right knee during stance phase of Tai Chi gait.....	114
Figure 71: Summed normalized muscle forces for the medial and the lateral sides compared to the medial and lateral joint contact forces of the right knee during stance phase of Normal Walking gait.....	114
Figure 72: External Knee adduction moment (EKAM) arm as a function of stance phase (A) and the EKAM as a function of stance phase (B). Measurements were taken from the same data set but calculated in another study (Jagodinsky et al.) and (Liu et al.) respectively.	116
Figure 73: External knee adduction moment normalized by body mass of the left and right knees for stance phase of Tai Chi and Normal Walking.....	118

Figure 74: External knee adduction moment for altered tibiofemoral alignment, nominal TFA=177.16, varus TFA=172, and valgus TFA=188, about the left and right knees for stance phase of Normal Walking gait.	119
Figure 75: External knee adduction moment for altered tibiofemoral alignment, nominal TFA=177.16, varus TFA=172, and valgus TFA=188, about the left and right knees for stance phase of Tai Chi gait.	119
Figure 76: Simulated EKAM for right leg stance phase of Tai Chi overlaid against the Nominal Tai Chi joint contact loads.	120
Figure 77: Simulated EKAM for left leg stance phase of Tai Chi overlaid against the Nominal Tai Chi joint contact loads.	121
Figure 78: Simulated EKAM for right leg stance phase of Normal Walking overlaid against the Nominal Normal Walking joint contact loads.	123
Figure 79: Simulated EKAM for left leg stance phase of Normal Walking overlaid against the Nominal Normal Walking joint contact loads.	124
Figure 80: Workflow of the validation process used for this study to validate the kinematic and muscle force results for Tai Chi and Normal Walking.	132
Figure 81: The following OpenSim simulations compose the calibration analysis workflow. Results from each simulation serve as inputs for the next.	133
Figure 82: Unstable forward dynamic simulation that results in abnormal model motion during gait.	135
Figure 83: Raw EMG signal for medial gastrocnemius of the left leg, stance phase of the independent test subject from the grand challenge study.	138
Figure 84: Left rectus femoris EMG signal rectified and normalized for percent maximum voluntary contraction for stance phase of the independent test subject from the grand challenge study.	138
Figure 85: Left medial gastrocnemius EMG signal rectified and normalized for percent maximum voluntary contraction for stance phase of the independent test subject from the grand challenge study.	139
Figure 86: Left lateral gastrocnemius EMG signal rectified and normalized for percent maximum voluntary contraction for stance phase of the independent test subject from the grand challenge study.	139
Figure 87: Calibration results for the Normal Walking trial of the nominal model. A comparison of the inverse kinematic and forward dynamic X translational coordinate of the pelvis for right leg, stance phase.	141
Figure 88: Calibration results for the Normal Walking trial of the nominal model. A comparison of the inverse kinematic and forward dynamic Y & Z translational coordinates of the pelvis for right leg, stance phase.	142
Figure 89: Calibration results for the Normal Walking trial of the nominal model. A comparison of the inverse kinematic and forward dynamic rotations of the hip, knee, and ankle coordinates for right leg, stance phase.	142
Figure 90: Anteroposterior, X-component, ground reaction force measured at the right calcaneus by the force plate for stance phase of Tai Chi gait.	146
Figure 91: Normalized moment comparisons used for internal validation of the right and left knee stance phase for Normal Walking gait.	147
Figure 92: Normalized moment comparisons used for internal validation of the right and left knee stance phase for Tai Chi gait.	147
Figure 93: Rectus femoris muscle activation comparisons of EMG, Normal Walking, and the OpenSim reference models. The EMG data is the normalized muscle activation of the left rectus femoris from an independent subject. Right and left muscle activations are shown for the Normal Walking and OpenSim reference models. All activations are a function stance phase.	151
Figure 94: Medial gastrocnemius muscle activation comparisons of EMG, Normal Walking, the OpenSim reference models. The EMG data is the normalized muscle activation of the left medial gastrocnemius from an independent subject. Right and left muscle activations are shown for the Normal Walking and OpenSim reference models. All activations are a function stance phase.	152
Figure 95: Lateral gastrocnemius muscle activation comparisons of EMG, Normal Walking, the OpenSim reference models. The EMG data is the normalized muscle activation of the left lateral gastrocnemius from an independent subject. Right and left muscle activations are shown for the Normal Walking and OpenSim reference models. All activations are a function stance phase.	152
Figure 96: Normalized joint contact loads for the right knee, stance phase, nominal tibiofemoral alignment compared against the respective vertical component ground reaction force.	161
Figure 97: Normalized joint contact loads of the total, medial, and lateral left knee compartments during stance phase of Normal Walking gait with nominal alignment, TFA=177.16 degrees.	199
Figure 98: Left medial and lateral normalized joint contact loads summed to show the total contact loads as a percentage of body weight during stance phase of Normal Walking gait with nominal alignment, TFA=177.16 degrees.	199

Figure 99: Left medial and lateral normalized joint contact load distribution as a percentage of the total contact load during stance phase of Normal Walking gait with nominal alignment, TFA=177.16 degrees.	200
Figure 100: Normalized joint contact loads of the total, medial, and lateral left knee compartments during stance phase of Tai Chi gait with nominal alignment, TFA=177.16 degrees.	200
Figure 101: Left medial and lateral normalized joint contact loads summed to show the total contact loads as a percentage of body weight during stance phase of Tai Chi gait with nominal alignment, TFA=177.16 degrees.	201
Figure 102: Left medial and lateral normalized joint contact load distribution as a percentage of the total contact load during stance phase of Tai Chi gait with nominal alignment, TFA=177.16 degrees.	201
Figure 103: Normalized joint contact loads of the total, medial, and lateral left knee compartments during stance phase of Normal Walking gait with varus alignment, TFA=172 degrees.	202
Figure 104: Left medial and lateral normalized joint contact loads summed to show the total contact loads as a percentage of body weight during stance phase of Normal Walking gait with varus alignment, TFA=172 degrees.	202
Figure 105: Left medial and lateral normalized joint contact load distribution as a percentage of the total contact load during stance phase of Normal Walking gait with varus alignment, TFA=172 degrees.	203
Figure 106: Normalized joint contact loads of the total, medial, and lateral left knee compartments during stance phase of Tai Chi gait with varus alignment, TFA=172 degrees.	203
Figure 107: Left medial and lateral normalized joint contact loads summed to show the total contact loads as a percentage of body weight during stance phase of Tai Chi gait with varus alignment, TFA=172 degrees.	204
Figure 108: Left medial and lateral normalized joint contact load distribution as a percentage of the total contact load during stance phase of Tai Chi gait with varus alignment, TFA=172 degrees.	204
Figure 109: Normalized joint contact loads of the total, medial, and lateral left knee compartments during stance phase of Tai Chi gait with valgus alignment, TFA=188 degrees.	205
Figure 110: Left medial and lateral normalized joint contact loads summed to show the total contact loads as a percentage of body weight during stance phase of Normal Walking gait with valgus alignment, TFA=188 degrees.	205
Figure 111: Left medial and lateral normalized joint contact load distribution as a percentage of the total contact load during stance phase of Normal Walking gait with valgus alignment, TFA=188 degrees.	206
Figure 112: Normalized joint contact loads of the total, medial, and lateral left knee compartments during stance phase of Tai Chi gait with valgus alignment, TFA=188 degrees.	206
Figure 113: Left medial and lateral normalized joint contact loads summed to show the total contact loads as a percentage of body weight during stance phase of Tai Chi gait with valgus alignment, TFA=188 degrees.	207
Figure 114: Left medial and lateral normalized joint contact load distribution as a percentage of the total contact load during stance phase of Tai Chi gait with valgus alignment, TFA=188 degrees.	207
Figure 115: Normalized, left knee, stance phase, total joint contact loads of Normal Walking gait for nominal (TFA=177.16 deg.), varus (TFA=172 deg.), and valgus (TFA=188 deg.) tibiofemoral alignments.	209
Figure 116: Normalized, left knee, stance phase, total joint contact loads of Tai Chi gait for nominal (TFA=177.16 deg.), varus (TFA=172 deg.), and valgus (TFA=188 deg.) tibiofemoral alignments.	209
Figure 117: Normalized, left knee, stance phase, medial joint contact loads of Normal Walking gait for nominal (TFA=177.16 deg.), varus (TFA=172 deg.), and valgus (TFA=188 deg.) tibiofemoral alignments.	210
Figure 118: Normalized, left knee, stance phase, medial joint contact loads of Tai Chi gait for nominal (TFA=177.16 deg.), varus (TFA=172 deg.), and valgus (TFA=188 deg.) tibiofemoral alignments.	210
Figure 119: Normalized, left knee, stance phase, lateral joint contact loads of Normal Walking gait for nominal (TFA=177.16 deg.), varus (TFA=172 deg.), and valgus (TFA=188 deg.) tibiofemoral alignments.	211
Figure 120: Normalized, left knee, stance phase, lateral joint contact loads of Tai Chi gait for nominal (TFA=177.16 deg.), varus (TFA=172 deg.), and valgus (TFA=188 deg.) tibiofemoral alignments.	211
Figure 121: Normalized muscle forces that traverse the left knee during stance phase for Normal Walking, nominal tibiofemoral alignment (TFA=177.16deg.)	214
Figure 122; Normalized muscle forces that traverse the left knee during stance phase for Tai Chi, nominal tibiofemoral alignment (TFA=177.16deg.)	214
Figure 123: Normalized joint contact forces compared to the sum of the three most influential muscle forces (Sum Isolated Muscle Forces), rectus femoris, lateral gastrocnemius, medial gastrocnemius and the total muscle forces that traverse the left knee, stance phase, Normal Walking, nominal tibiofemoral alignment (TFA=177.16).	215
Figure 124: Normalized joint contact forces compared to the sum of the three most influential muscle forces (Sum Isolated Muscle Forces), medial and lateral gastrocnemius, vastus medialis, vastus lateralis, vastus intermedius, rectus	

femoris, muscle forces that traverse the left knee, stance phase, Tai Chi, nominal tibiofemoral alignment (TFA=177.16).....	215
Figure 125: Summed normalized muscle forces for the medial and the lateral sides compared to the medial and lateral joint contact forces of the left knee during stance phase of Tai Chi gait.....	216
Figure 126: Summed normalized muscle forces for the medial and the lateral sides compared to the medial and lateral joint contact forces of the left knee during stance phase of Tai Chi gait.....	216
Figure 127: Calibration results for the Normal Walking trial of the nominal model. A comparison of the inverse kinematic and forward dynamic rotations of the hip, knee, and ankle coordinates for left leg, stance phase.....	218
Figure 128: Calibration results for the Tai Chi trial of the nominal model. A comparison of the inverse kinematic and forward dynamic X translational coordinate of the pelvis for right leg, stance phase.....	219
Figure 129: Calibration results for the Tai Chi trial of the nominal model. A comparison of the inverse kinematic and forward dynamic Y & Z translational coordinates of the pelvis for right leg, stance phase	220
Figure 130: Calibration results for the Tai Chi trial of the nominal model. A comparison of the inverse kinematic and forward dynamic rotations of the hip, knee, and ankle coordinates for right leg, stance phase.....	220
Figure 131: Calibration results for the Tai Chi trial of the nominal model. A comparison of the inverse kinematic and forward dynamic rotations of the hip, knee, and ankle coordinates for left leg, stance phase.....	221
Figure 132: Moment Error, i.e. the error between the moments about the knee generated mu the muscle forces and the inverse dynamics moment, calculated by Equation 47 about the right knee joints for stance phase Normal Walking.....	222
Figure 133: Moment Error, i.e. the error between the moments about the knee generated mu the muscle forces and the inverse dynamics moment, calculated by Equation 47 about the left knee joints for stance phase Normal Walking.....	222
Figure 134: Moment Error, i.e. the error between the moments about the knee generated mu the muscle forces and the inverse dynamics moment, calculated by Equation 47 about the right knee joints for stance phase Tai Chi.	223
Figure 135: Moment Error, i.e. the error between the moments about the knee generated mu the muscle forces and the inverse dynamics moment, calculated by Equation 47 about the left knee joints for stance phase Tai Chi.	223

List of Abbreviations

AJC	Ankle Joint Center
ACL	Anterior Cruciate Ligament
ASIS	Anterior Superior iliac Spine
BW	Body Weight
COM	Center of Mass
COP	Center of Pressure
CMC	Computed Muscle Control
DOF	Degrees of Freedom
EMG	Electromyography
EKAM	External Knee Adduction Moment
EMC	Extracellular Matrix
FMA	Femoral Mechanical Axis
FE	Finite Element
FD	Forward Dynamics
FIE	Forward Inverse Error
FBD	Free Body Diagram
GC	Generalized Coordinates
GUI	Graphical User Interface
GDP	Gross Domestic Product
GRF	Ground Reaction Force
HJC	Hip Joint Center

ID	Inverse Dynamics
IK	Inverse Kinematics
JRA	Joint Reaction Analysis
KAM	Knee adduction Moment
KJC	Knee Joint Center
KOA	Knee Osteoarthritis
LCL	Lateral Collateral Ligament
LG	Lateral Gastrocnemius
MLA	Majority Load Accepted
MVC	Maximum Voluntary Contraction
MALE	Mechanical Axis of the Lower Extremity
MTFA	Mechanical Tibiofemoral Angle
MCL	Medial Collateral Ligament
MG	Medial Gastrocnemius
MLK	Medio-Lateral Knee (Model)
MC	Motion Capture
MS	Musculoskeletal
MSM	Musculoskeletal Model
OSM	OpenSim
OA	Osteoarthritis
%BW	Percent Body Weight
%MVC	Percent Maximum Voluntary Contraction
PCL	Posterior Cruciate Ligament

PSIS	Posterior Superior Iliac Spine
RF	Rectus Femoris
RRA	Residual Reduction Analysis
RLA	Right Lateral Ankle
RLK	Right Lateral Knee
RMA	Right Medial Ankle
RMK	Right Medial Knee
ST	Stance Time
STO	Static Optimization
TC	Tai Chi
TMA	Tibial Mechanical Axis
TFA	Tibiofemoral Alignment
TKA	Total Knee Arthroplasty
WLS	Weighted Least Squares

Chapter 1: Background and Literature Review

1.1. Introduction

The knee joint is fundamental in everyday activities such as walking, running, and moving around. The knee is one of the largest and most complex diarthrotic joints in the human body and is integral to weight bearing and locomotion. Thus, maintaining adept knee joint health is critical in maintaining a healthy and pain free quality of life (Yildiz et al.). The most common antagonistic threat to good knee health is osteoarthritis (OA) (Dieppe and Lohmander). Osteoarthritis of the knee is a degenerative disease that involves the degradation of articular cartilage in the knee joint (Dieppe and Lohmander). Articular cartilage is avascular, and as result, healing is slow and seemingly null (Griffin and Guilak). The degenerative process of OA is nearly irreversible and will continually progress until properly treated, generally by total knee arthroplasty (TKA) for end-stage knee OA (Rönn et al.). TKA is an invasive surgery with many potential risks that can be traumatic and is preferred to be avoided if possible (Rönn et al.). Thus, non-surgical treatments and non-invasive rehab methods are advantageous to patients diagnosed with knee osteoarthritis (KOA), particularly among elderly people where healing from traumatic surgery can be physically and mentally taxing. While complete restoration of total knee health is not likely once OA has begun, rehab exercises have shown evidence of stimulating healthy cartilage maintenance, thus slowing OA progression and improving diagnosed patients' quality of life (Kan et al.). One non-invasive exercise technique of interest that could prove to be advantageous is Tai Chi, an ancient Chinese martial art, now turned exercise among a growing population (Barnes et al.). Previous investigations have found that Tai Chi is an effective technique to reduce pain and improve physical function, along with other health related benefits (Wang, Schmid, Hibberd, Kalish,

Roubenoff, Roness, and McAlindon). Minimal investigations into the efficacy of these outcomes have been conducted; thus, further investigations are needed.

Historically, it is believed that mechanical loading, i.e. the forces and moments about the knee joint that are resolved at the femoral condyle points of contact, is a large contributing factor in OA progression (Griffin and Guilak). Conversely, recent studies have shown that mild intermittent mechanical loading from exercise can stimulate cell synthesis and help maintain cartilage homeostasis (M. Christopher). Subsequently, tibiofemoral alignment plays a large role in mediolateral compartmental loading of the knee, and thus medial knee OA progression (Sharma et al.) (Miyazaki et al.). In order to fully understand the efficacy of mechanical loading for various exercises on OA mitigation, it is important to know the force distributions acting on the medial and femoral condyles of the femur. *In-vivo* measurements of the medial and lateral joint contact forces on the knee have been recorded in patients with instrumented tibial knee implants (Fregly et al.) (Halder et al.) (Kim et al.). However, *in-vivo* measurements of knee joint contact forces are invasive and not ideal for experimentation purposes (Hume). Additionally, patients with instrumented knee implants are sparse and data is not readily available for unique exercises such as Tai Chi (Fregly et al.).

Musculoskeletal modeling (MSM) software such as OpenSim (OSM), has aided in trying to characterize knee joint contact mechanics (Hast et al.). Validated musculoskeletal (MS) models have been created in OSM to resolve the compartmental loading (i.e. tibiofemoral contact forces on the medial and lateral femoral condyles) of the knee joint during normal gait (Lerner et al.) (Saxby et al.) (Gerus et al.). Understanding the effects of compartmental loading during gait can

help elucidate other alternative exercises that aid in stimulating joint health. While compartmental loading of the knee using MSM has been analyzed for normal gait, very little research has been conducted to analyze compartmental loading for Tai Chi gait. Therefore, the aim of this study is to answer two fundamental questions: How does Tai Chi effect the mediolateral compartmental loading of the knee compared to that of Normal Walking? And subsequently, how does tibiofemoral malalignment effect the compartmental loading of the knee during Tai Chi gait? Understanding knee joint compartmental loading will aid in understanding the pathogenesis of OA and the effectiveness of current non-invasive exercise treatments for patients with KOA (Adouni and Shirazi-Adl)

1.2. Knee Osteoarthritis

The pathogenesis of OA has long been studied and is well understood. Osteoarthritis is a degenerative disease that involves the degradation of articular cartilage within synovial joints (Dieppe and Lohmander). The degradation process is said to be contributed to biochemical and biomechanical factors (Van C. Mow et al.). Affecting roughly 10% of males and 18% females over the age of 60, osteoarthritis is the most common joint disease in the United States and worldwide (Plotnikoff et al.) (Murray and Lopez) (Yuqing Zhang, D.Sc and Joanne M. Jordan, MD). OA is more common among women within the total population. However, in age groups younger than 45 years old, OA is more prevalent in males (Yuqing Zhang, D.Sc and Joanne M. Jordan, MD). OA is more common in the United States and Europe than any other regions of the world and is increasing. Such increases are a result of an aging population and the increase in obesity prevalence (Yuqing Zhang, D.Sc and Joanne M. Jordan, MD). In western societies the socioeconomic impact is staggering. Not only has this disease caused a financial burden equivalent

to 1% to 2.5% of western countries gross domestic product (GDP), but patients' total quality of life has been negatively impacted as well (March and Bachmeier). The high financial burden comes from the direct costs of surgeries and lengthy hospital stays, while indirect costs result from loss of financial productivity due to the disabling nature of the disease (Hiligsmann et al.). OA is one of the leading cause of disability in the United States among older individuals (Lawrence), and no cure currently exists that offers disease modifying effects (M. Christopher). Therefore, it is important to stimulate research in order to find a cure given the overwhelming socioeconomic impact of osteoarthritis.

1.3. Anatomy of the Knee

The knee joint is composed of 3 bone segments: the femur, tibia, and the patella **Figure 1**. The distal epiphysis of the femur is comprised of two spherical protrusions, one medial and one lateral in the frontal plane. These protrusions are called femoral condyles. The femoral condyles are primarily responsible for accepting the contact load induced from the tibia onto the femur during ambulation and muscle co-contraction. The hyaline articular cartilage lines the subchondral bone of the femoral condyles creating a smooth nearly friction free surface which the tibial plateau can articulate (Whitman), **Figure 2**. The proximal tibia is referred to the tibial plateau. On the surface of the tibial plateau is the tibial articular cartilage and the meniscus. The meniscus is a soft elastic tissue composed of fibroelastic cartilage (Fithian et al.). The primary function of the meniscus is to absorb and distribute loads between the tibial and femoral cartilage surfaces during mechanical loading (Kurosawa et al.).

The relative motion of the tibia with respect to the femur is constrained by muscles and ligaments across the knee joint. The main ligaments that constrain the knee are the anterior cruciate ligament (ACL), posterior cruciate ligament (PCL), medial collateral ligament (MCL) and lateral collateral ligament (LCL) (Abulhasan and Grey). The transverse ligament holds the medial and lateral menisci firmly to the tibial plateau. The cupping of the meniscus around the femoral condyles also serves to facilitate rotation of the tibia relative to the femur (Seedhom, “Transmission of the Load in the Knee Joint with Special Reference to the Role of the Menisci. Part I. Anatomy, Analysis and Apparatus”). The patellar tendon attaches the patella to the tibial tubercle creating a moment arm which allowing the quadriceps to generate knee extension moment about the knee joint in the sagittal plane (Cox and Hubbard), **Figure 2**.

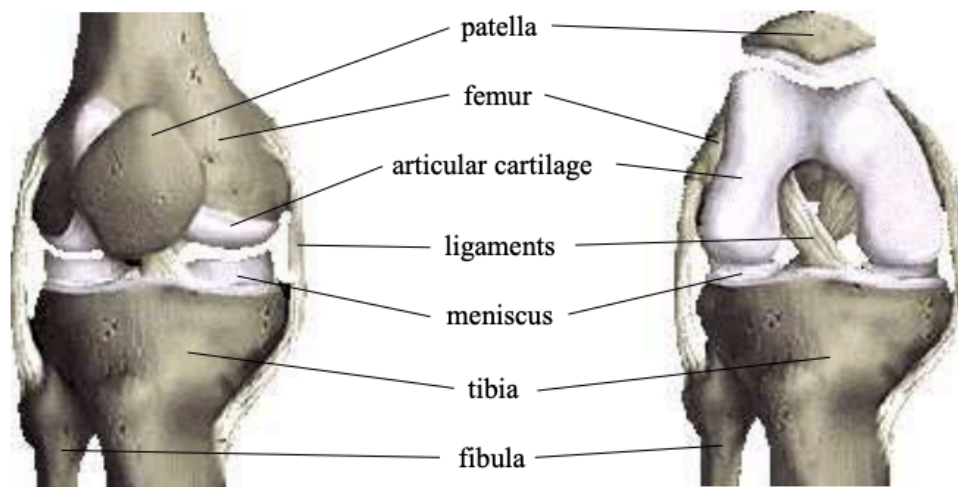


Figure 1: Bone segments (femur, tibia and patella) comprising the right knee joint. Image courtesy of (Dan).

The subchondral bone of the distal femur and tibial plateau (proximal tibia) are lined by hyaline articular cartilage seen in **Figure 1**, (Van C. Mow et al.).

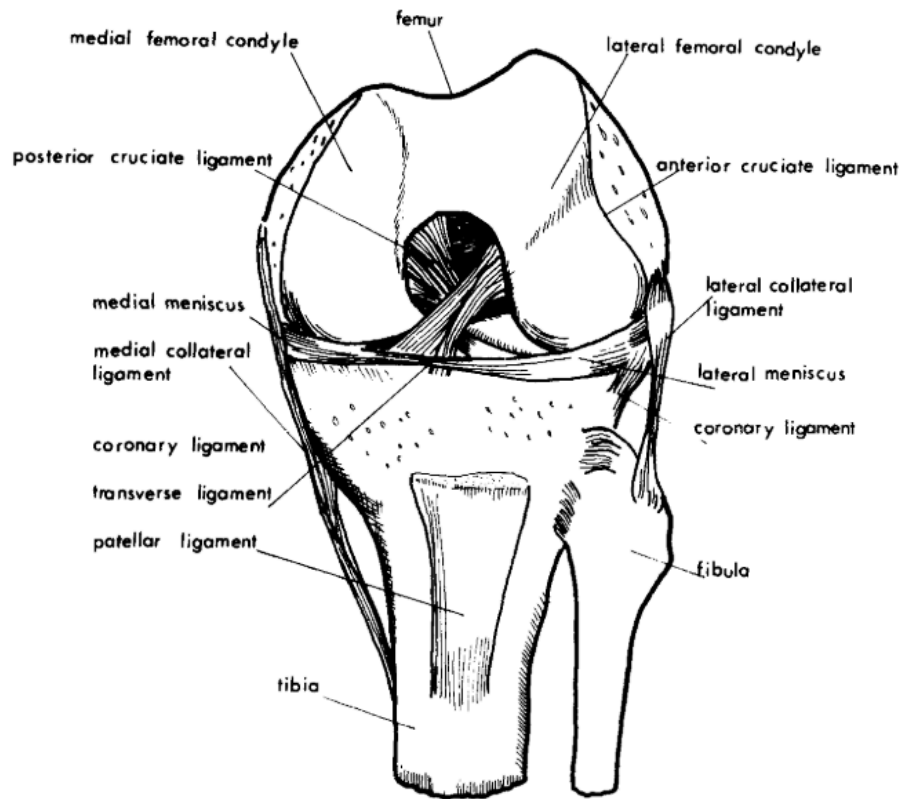


Figure 2: Anatomy of soft tissues namely ligaments and articular cartilage in the knee joint. Photo courtesy of (Seedhom, “Transmission of the Load in the Knee Joint with Special Reference to the Role of the Menisci. Part I. Anatomy, Analysis and Apparatus”)

1.4. Anatomy of Articular Cartilage

Articular cartilage tissue is roughly 2 to 4 mm thick and covers the subchondral bone of the femoral condyles and tibial plateau in the knee joint (Sophia Fox et al.). Unlike other tissues, cartilage is avascular and is primarily composed of type II collagen fibers, proteoglycans, chondrocytes and water (Cohen et al.). Other non-collagenous proteins, glycoproteins and water dissolved(Harrington et al.) electrolytes are present in lesser amounts (Cohen et al.). The cartilage tissue is arranged into an extracellular matrix (ECM) with a sparse distribution of highly specialized cells called Chondrocytes (Fujisawa et al.), **Figure 3A**. The main function of a chondrocyte is to deposit cartilage matrix which is responsible for cartilage cell turnover

(Musumeci). The avascular nature of cartilage has antagonist and protagonist functions. There are no blood vessels or nerves within the ECM; therefore, the articular cartilage provides a pain free, smooth surface through which bones can articulate (Houard et al.). Conversely, the lack of blood vessels in the ECM restrict cell synthesis. Thus, Articular cartilage has a slow healing process relative to other ossified bone (Griffin and Guilak). Cell synthesis is strictly left to chondrocytes within the ECM (Sophia Fox et al.). The half-life of collagen fibers within the ECM is said to range from a couple of decades to 400 years (Sophia Fox et al.). Another study has predicted the half-life of collagen fibers to be about 117 years (Verzijl et al.). Furthermore, the ECM matrix turnover can be longer than a human lifetime. This is long considering ossified bone remodels once every 10 years (Manolagas). Therefore, given the slow growth and turnover nature of hyaline cartilage, it is extremely important to maintain good cartilage health in order to prevent injury.

The ECM within articular cartilage is composed of collagen fibers that vary in orientation depending on the layer (Sophia Fox et al.). Thus, cartilage can be subcategorized into three primary zones based on collagen fiber orientation as seen in **Figure 3B**.

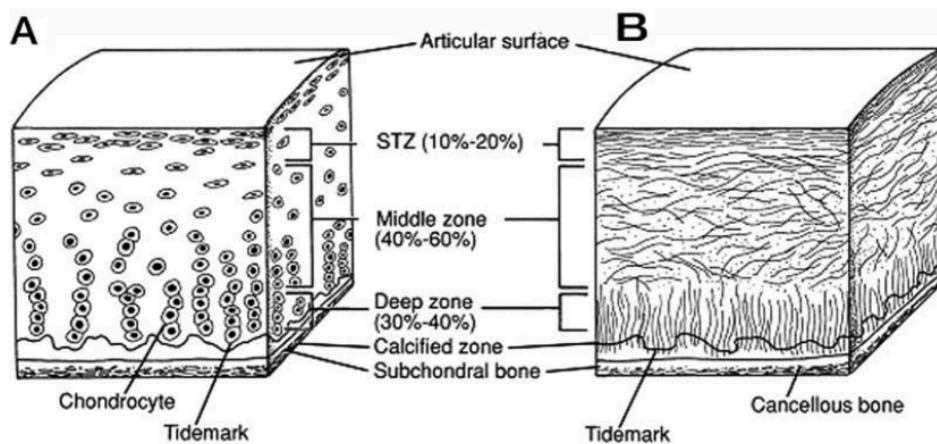


Figure 3: Various Zones of the Articular Cartilage. (A) Shows the sparse placement of Chondrocytes within the cartilage ECM. (B) Shows the collagen fiber orientation in the various zones within the cartilage ECM. Image courtesy of (Sophia Fox et al.)

The three zones that compose the articular cartilage are the superficial, middle, and deep zones. The superficial zone is composed of compact transverse fibers, tangent to the articulation surface, which provide a resistance to abrasion and shear stress at the surface and just below the surface during joint loading and contact. The middle zone's collagen fiber orientation is more random and sparse which provide a good transition zone between the superficial and deep zones. The middle zone experiences both normal stress and shear stress; therefore, the fibers are orientated adequately. The fiber orientation of the deep zone is normal to the articulation surface. This orientation resists high normal stresses and ultimately protects the calcified bone layer and the subchondral bone beneath the deep zone from high local stress environments (Whitman).

The multiphasic nature of articular cartilage makes the material properties unique and difficult to quantify (Lu and Mow). There are three primary phases of articular cartilage that characterize its material behavior. First, the solid phase is characterized by the material properties of the collagen fibers and their orientation as they are suspended within the ECM (V. C. Mow et al.). The second phase is a fluid phase which stems from the high moisture content of articular cartilage. The ECM is composed of about 80% water by weight (Linn and Sokoloff). Lastly, the ion phase contributes to the mechanical properties through the avenue of the electromagnetic repulsion of Na^+ , Ca^{++} , and Cl^- electrolytes that are dissolved within the ECM (Lai et al.). All three phases contribute to the unique mechanical behavior of articular cartilage. Within the cartilage matrix the ECM the collagen fibers are suspended in interstitial gelatin like fluid mainly composed of water. Synovial fluid within the joint is responsible for transferring the nutrients to the cartilage and other cells within the ECM (Sophia Fox et al.). Fluid flow is manifested within the ECM when the cartilage experiences a local stress produced by contact from mechanical loading. The fluid flows from high

pressure environments to the low-pressure environments until equilibrium pressure is reached (Sophia Fox et al.). The significance of this phenomena is twofold. First, the fluid flow across collagen fibers generates local turbulence in the fluid which helps transport nutrients within the ECM, ultimately promoting cell synthesis (Sophia Fox et al.). Secondly, the material behavior of the cartilage matrix is viscoelastic (Kwan et al.). Therefore, the young modulus is time dependent and cannot be characterized by one value. The viscoelastic behavior of the cartilage is characterized by creep and stress relaxation (Cohen et al.). The time dependent stress and strain curves of articular cartilage loaded in compression can be seen in **Figure 4**.

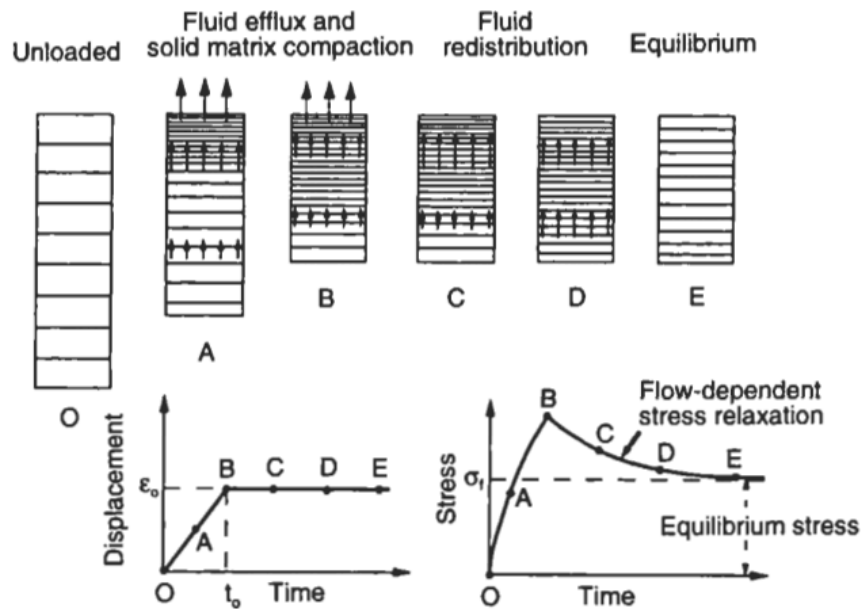


Figure 4: Displacement and stress curves vs. time plot shows the time dependent viscoelastic behavior of articular cartilage in compression. Image courtesy of (Cohen et al.)

When the cartilage is loaded, the stress will increase during compression from weight acceptance during stance phase and max out at an instantaneous peak. As time continues, fluid flows from high pressure to low pressure until an equilibrium pressure is reached. Simultaneously, the collagen fibers are stretched until an equilibrium stress is reached within the cartilage matrix. This time dependent process of approaching pressure and stress equilibrium is called the stress-

relaxation phase (Kwan et al.). The unique material behavior of cartilage makes the Young's Modulus difficult to quantify, because it is highly nonlinear and cannot be characterized by a single value. Direct experimental measurements have been conducted through cadaveric studies to resolve the material properties of cartilage (Thambyah et al.). However, many limitations exist at this step. Previous studies have shown that a single Young's Modulus that characterizes the compression phase can be used for computational purposes (Lu and Mow). Therefore, Isotropic material properties can be used as an approximation for the true material behavior of articular cartilage.

1.5. Mechanical Loading Effects on Cartilage and OA

Mechanical loading plays a role in maintaining overall cartilage health. However, overuse or extreme loading can have a negative effect on cartilage health. Both cartilage health and cartilage breakdown (i.e. osteoarthritis) are heavily influenced by mechanical loading (Andriacchi and Mündermann). Intermittent hydrostatic stress is believed to be good at promoting cartilage health (Ikenoue et al.). The cyclic loading of the cartilage produces fluid flow within the ECM which ultimately promotes cartilage homeostasis and healthy cartilage maintenance (M. Christopher). Conversely, octahedral shear stress promotes increased chondrocyte metabolism and ultimately leads to cartilage ossification (Lane Smith et al.). Fiber reinforced materials tend to yield and fail due to high shear stress (Lance and Robinson). Unfortunately, shear is unavoidable within the ECM due to the nature of the contact loading. However, cartilage growth starts from young age and even proceeds ossified bone formation (Whitman). Through the mechanotransductive growth behavior, cartilage matrix grows and conditions itself such that the cartilage can handle areas of high shear from repetitive and uniform mechanical loading patterns (Seedhom, "Conditioning of

Cartilage during Normal Activities Is an Important Factor in the Development of Osteoarthritis”). The mechanotransductive growth process takes a long time to develop. Additionally, the remodeling process of the ECM takes a long time given the half-life of collagen fibers is believed to be about 117 years which yields a slow turnover rate of hyaline cartilage (Verzijl et al.) (Li and Xu). Therefore, when a mechanical loading pattern is permanently changed due to injury, increased laxity, neuromuscular changes, aging, increased obesity, or a permanently altered gait cycle, the local fiber orientation is not built to handle the new local stress environment. As a result the cartilage is more likely to yield (Andriacchi et al.). Permanently altered knee kinematics results in abnormal remodeling of tissue and is believed to be the most pragmatic cause of Osteoarthritis in the knee (Loeser et al.). Due to the slow nature of cartilage cell synthesis, repetitive altered mechanical loading overwhelms the chondrocyte’s ability to remodel a cartilage matrix sturdy enough to handle the new local stress environment. Thus, the rate of cartilage degeneration exceeds that of cartilage formation. The result is a net loss of cartilage (Gudmann et al.) (Tchetina et al.). As the cartilage begins to yield, ossification of the hyaline cartilage is stimulated, at which point the cartilage matrix begins to turnover into calcified bone. Cartilage thinning and calcified bone spurs, i.e. osteophytes. can be seen in the radio graphic images in **Figure 5**.

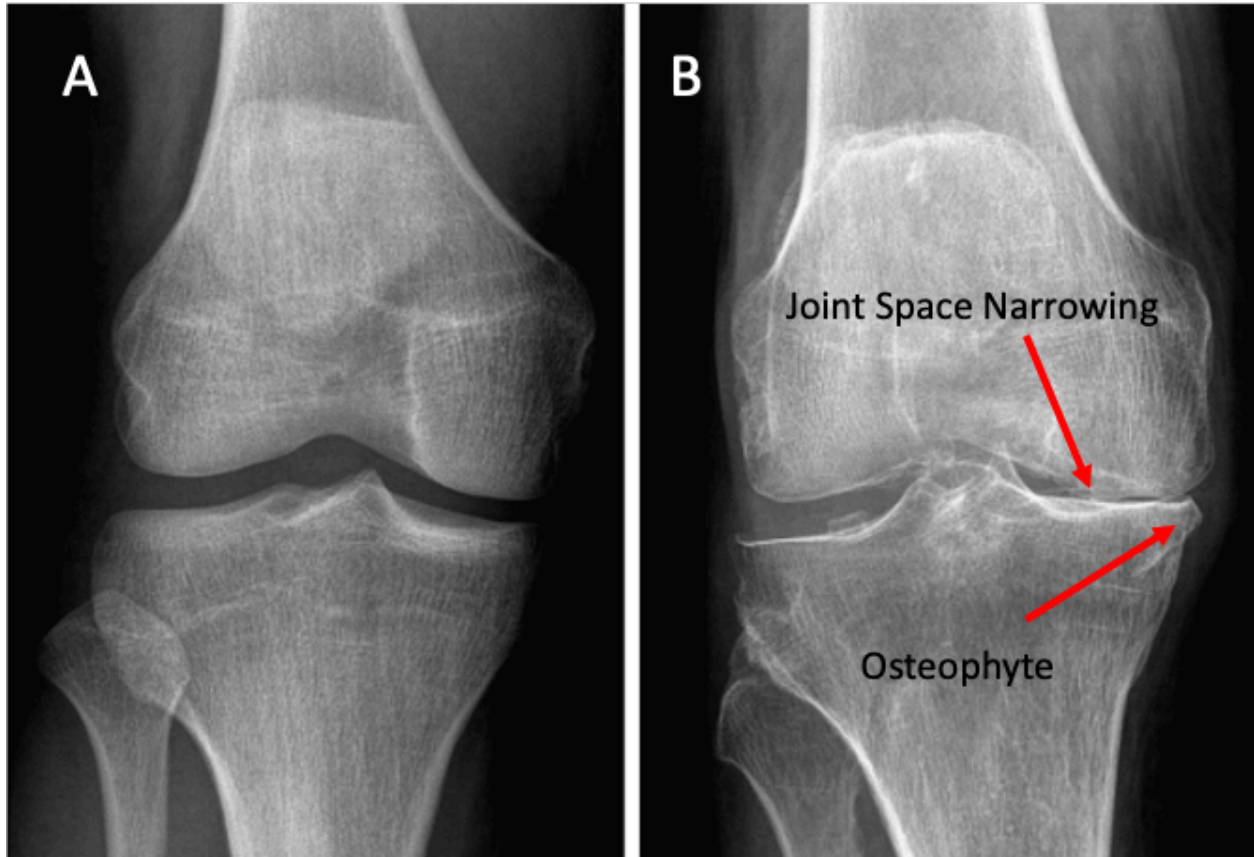


Figure 5: Radiographic imaging of healthy right knee (A) and an Osteoarthritic knee (B). Medial joint space narrowing, and the formation of osteophytes can be seen in (B). Image modified from (Altman et al.).

Thus, the pathogenesis of osteoarthritis has begun. The degradation process of articular cartilage is degenerative and often painful and debilitating. **Figure 6** gives a visual explanation of how the normal cartilage homeostasis is maintained through normal mechanical loading and how the degenerative OA process begins due to altered gait or injury.

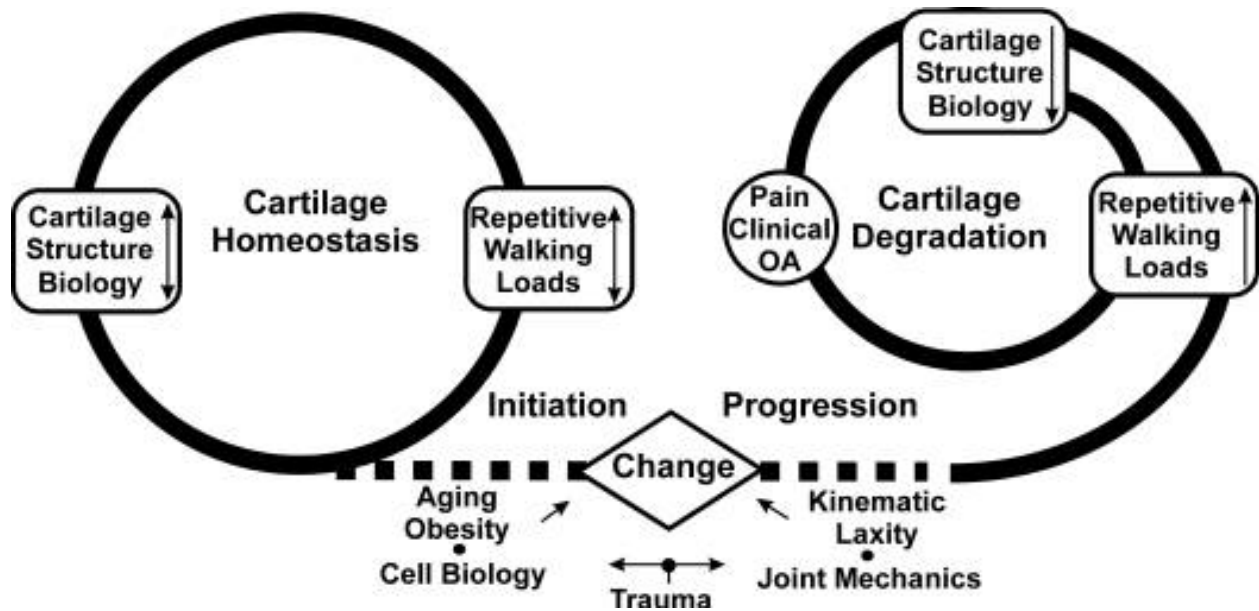


Figure 6: Outlines the effects that cyclic mechanical loading has in promoting healthy cartilage homeostasis as well as the degenerative effects mechanical loading has on cartilage when permanent deformation in mechanical loading occurs from injury change. Picture courtesy of (Andriacchi et al.).

1.6. Tibiofemoral Alignment Effects Compartmental Mechanical Loading of The Knee

Tibiofemoral alignment (TFA) of the knee plays a large role in the mechanical loading of medial and lateral compartments of the knee joint (Sharma et al.). The mechanical axis of the femur is defined as the line joined by the apex of the femoral condyles and the center of the femoral head (Krackow), **Figure 7A**. The anatomical axis of the femur is defined by the line that traverses the shaft of the femur, **Figure 7B**. The mechanical and anatomical axes of the tibia are both defined as the line that connects the apex of the proximal tibia and the apex of the distal tibia, **Figure 7C** and **Figure 7D** respectively.

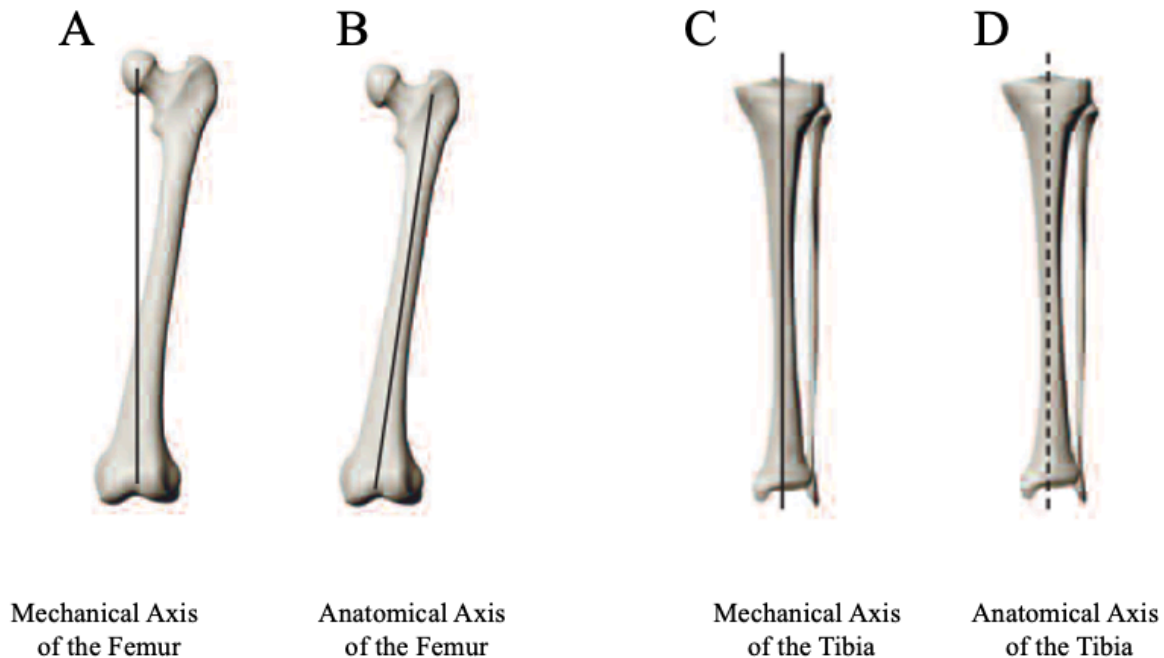


Figure 7: Mechanical axis of the femur (A), anatomical axis of the femur (B), mechanical axis of the tibia (C), and anatomical axis of the tibia (D) for the left leg defined in the literature. This photo was modified from (Krackow).

The mechanical axes of the femur and tibia intersect at the apex of the knee joint forming the mechanical tibiofemoral angle (MTFA) or the mechanical axis of deviation, **Figure 8B**. The MTFA allows the clinicians to assess the degree of malalignment of the tibia with respect to the femur (Krackow). The angular complement of the MTFA is referred to as the tibiofemoral alignment angle, (TFA) angle (Maini et al.). When the TFA angle is 180 degrees, tibiofemoral alignment is recognized as normal alignment (Krackow), **Figure 8A**. The line that connects the center of the femoral head to the apex of the distal tibia is referred to as the mechanical axis of the lower extremity (MALE), **Figure 8E** and **Figure 8F**. The varus-valgus angle is often defined as the angle formed by the intersection of the femoral and tibial anatomical axes (Yang et al.), **Figure 8D**. Therefore, a normal alignment typically results in about 5-7 degree valgus angle (Johnson, F. ; Leitl, S; Waugh). When the knee joint center is positioned lateral of the MALE, a varus angle is

formed, **Figure 8E**. Conversely, when the knee joint center is positioned medial of the MALE, a valgus angle is formed, **Figure 8F**.

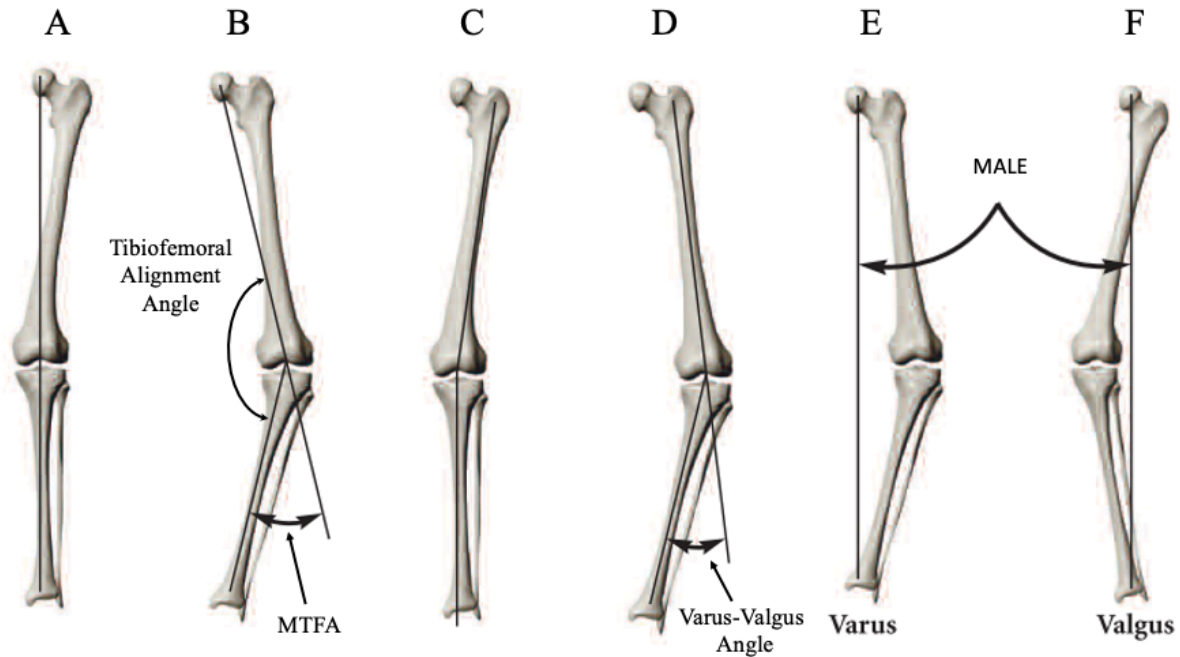


Figure 8: Normal alignment of tibiofemoral mechanical axis (A), tibiofemoral alignment (TFA) angle and mechanical tibiofemoral angle (MTFA) formed by tibial and femoral mechanical axes (B), valgus and varus angle formed by the anatomical axes of the femur and tibia (C) and (D) respectively, mechanical axis of lower extremity (MALE) formed by a varus knee alignment (E) and valgus knee alignment (F) respectively. All images are of the left leg. This photo was modified from (Krackow).

Tibiofemoral alignment plays a major role in joint contact force distribution. Studies have shown that patients with medial compartment knee OA tend to have a more distinguished varus knee alignment, **Figure 8D**, thus a higher external knee adduction moment (EKAM) about the knee joint (Nie et al.). The external knee adduction moment is the frontal plane moment about the knee joint that is calculated by the product of the ground reaction force (GRF) vector acting at the foot and its perpendicular distance to the knee joint center defined by **Equation 1** and shown in **Figure 9** (Fregly).

$$\vec{M}_{EKAM} = \vec{r}_{\perp} \vec{F}_{GRF} \quad (1)$$

Where \vec{M}_{EKAM} is the external knee adduction moment about the knee joint, \vec{r}_{\perp} is the perpendicular distance from the GRF vector to the knee joint center which acts as a moment arm, and \vec{F}_{GRF} is the ground reaction force vector measured between the ground and the foot of the subject. The EKAM is a clinically useful measure to investigate initiation and progression of OA (Andriacchi). As seen in **Figure 9A-C**, the EKAM is dependent on tibiofemoral alignment (Johnson, F. ; Leitl, S; Waugh). A larger varus aligned TFA angle is more likely to have a larger EKAM because of the increase in moment arm about the knee joint center (Nie et al.), **Figure 9B**. Subsequently, the joint contact force distribution on the medial and lateral condyles of the knee are dependent on the magnitude of the EKAM, **Figure 9D**.

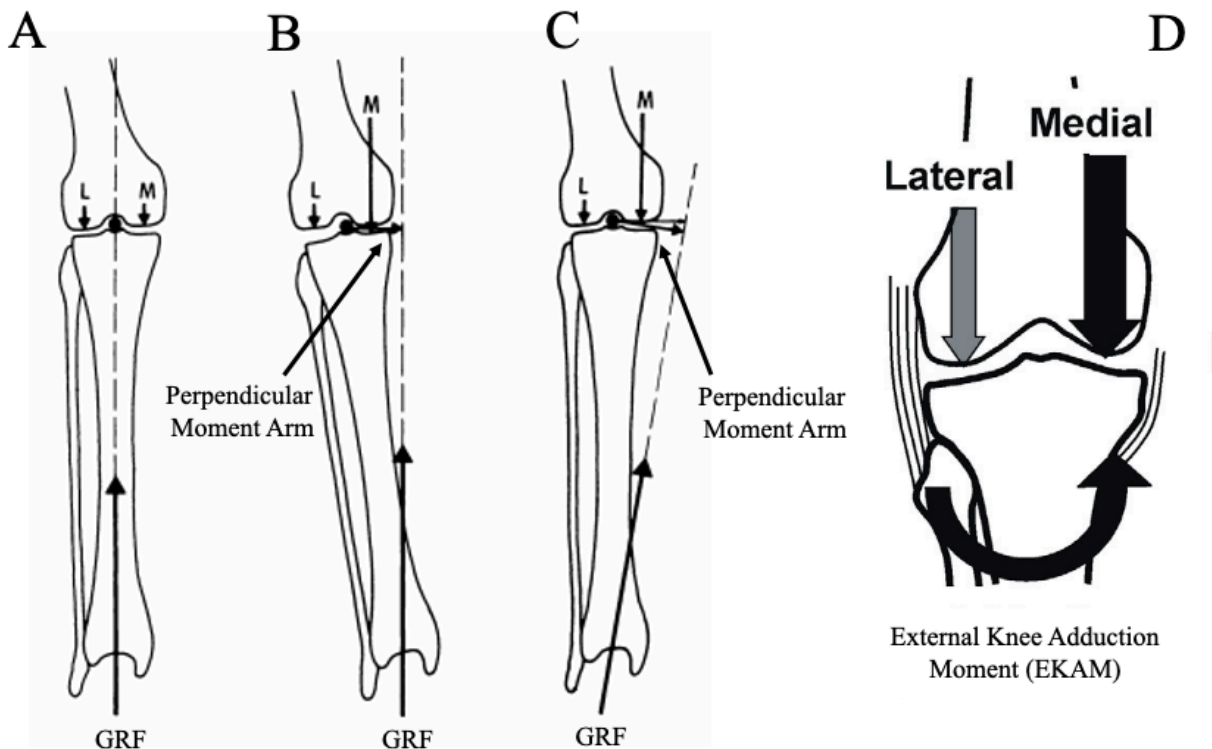


Figure 9: Knee Adduction Moment generated about the knee joint center of a static normal aligned knee (A), a static varus aligned knee (B), and a dynamic varus aligned knee (C) (Johnson, F. ; Leitl, S; Waugh). The resultant external knee adduction moment (EKAM)

results in larger medial knee joint contact load (D) (Andriacchi et al.). Image modified from (Johnson, F. ; Leidl, S; Waugh) and (Andriacchi et al.).

Thus, patients with higher EKAMs will experience more medially loaded knee joints resulting in higher contact forces on the medial femoral condyle (Miyazaki et al.). Under normal varus-valgus alignment, the medial compartment tends to absorb about 70-75 percent of the total knee contact load (Hsu et al.). Given that the medial knee compartment experiences higher contact loads, more wear is often seen in the medial compartment of the knee. Thus, medial knee OA is common among individuals (Magalhães and Kirkwood). As the medial compartment of the knee begins to wear and degenerate, early stages of medial compartment knee OA begin to set in. Medial compartment joint thinning is also present which leads to an exacerbated varus angle of the knee and results in higher medial loading. Higher medial loading results in more medial cartilage degeneration and even greater varus angles of the knee. This degenerative cycle will continue over time until properly treated, generally by total knee arthroplasty. Therefore, exercises that reduce the EKAM thus reducing the medial compartment load in the knee joint could prove to be beneficial in preventing and managing pain and progression in early onsets of OA.

1.7. Non-Invasive Treatments for Osteoarthritis

Osteoarthritis is a degenerative irreversible disease that involves the degradation of articular cartilage matrix resulting in cartilage thinning and premature ossification of bone. Severe cases of OA are typically identified on radiographic imaging by joint thinning and the presence of bony spurs called osteophytes (Dieppe and Lohmander). No disease altering treatments currently exist for patients with OA. The degenerative effects of end-stage OA will continue until properly treated, typically through total knee arthroplasty (Rönn et al.). While TKA surgery is often successful, the

durability of prosthetic components is low, lasting only about 15-20 years. Therefore, TKA should only be conducted in patients over the age of 60 and avoided if possible (Rönn et al.). There are also many other risks associate with TKA such as loosening of components, patellofemoral problems, infections and knee stiffness (Rönn et al.). Additionally, studies have shown that TKA surgery can often leave patients with persistent postoperative residual pain (Lundblad et al.). Therefore, non-invasive treatments are advantageous to patients with KOA. While no disease altering treatments that reverse the degradation process of cartilage currently exist, recent studies have suggested evidence that dynamic moderate exercise in patients with KOA could potentially have symptom-modifying effects and has the potential to exert OA disease modifying effects (M. Christopher). While it is unlikely that moderate dynamic loading through exercise alone will be successful in reversing the progression of OA, moderate exercise could prove to be more effective as a preventative maintenance technique to preserve cartilage homeostasis, promote cellular synthesis, and preserve overall joint health (M. Christopher). Some studies have shown that moderate exercise and aerobic exercise can reduce pain, increase joint function and reduce OA progression (Peungsuwan et al.)(Péloquin et al.)(Ebnezar et al.)(Geneen et al.)(Lauche et al.)(Roddy et al.)(Bennell et al.).

One study analyzed the effectiveness of Thai exercise accompanied with a traditional massage to manage pain, improve walking ability, and total quality of life among older individuals with knee osteoarthritis (Peungsuwan et al.). Thai exercise is a popular exercise in Thailand among elderly people which utilizes a series of slow flow-like motions of the lower extremities accompanied by the use of a wand. The wand is used for balance and increased muscle enhancement of the upper extremities. The messaging was used intermittently between exercise routines. After having

patients perform the exercises regularly for 1 year, the results concluded that Thai exercise and massage show significant improvements in the patients ability to walk normally, improved pain management, improved function, and an improved total quality of life (Peungsuwan et al.).

Another study analyzed the effectiveness of physical activity on patients over the age of 50 with knee osteoarthritis by incorporating aerobic exercises, strength training, and stretching exercises for an extended period of time (Péloquin et al.). After training for three months, the experimental group showed significant improvements in arthritic pain, ability to walk and bend down, aerobic capacity, hamstring and lower back flexibility, quadricep and hamstring strength, and the perception of changes related to osteoarthritis of the knee, compared to the control group. However, there were no significant changes in joint tenderness, isokinetic strength of the quadriceps, and overall health perception. This study concluded that the program was effective in helping patients improve their ability to cope with KOA by maintaining their independence, ultimately improving their total quality of life (Péloquin et al.).

Another, study analyzed the effects of hatha yoga therapy on functional disability, pain, and flexibility in patients with knee osteoarthritis as a potential remedy for knee OA (Ebnezar et al.). Two hundred and fifty patients with symptomatic knee OA were randomly assigned to receive hatha yoga therapy or an alternative therapeutic treatment which involves transcutaneous electrical stimulation and ultrasound treatment. After 3 months of training and treatment, the hatha yoga therapy group showed significant improvements in walking pain, range of knee flexion, joint tenderness, and swelling compared to the alternative therapy treatment. This study concluded hatha yoga is more effective than other therapies previously used in society. These findings suggest that

hatha yoga can be an effective measure to treat patients with symptomatic knee osteoarthritis, by improving problematic symptoms associated with osteoarthritis (Ebnezar et al.).

Non-surgical alternatives such as physical exercise have shown promise in their ability to treat patients with knee OA. However, more needs to be done to confirm their efficacy. Other exercises have shown promise as well. One exercise of interest that is still in the early stages of biomechanical research is Tai Chi Chuan which has shown promise for treating patients with knee OA (Wang, Schmid, Hibberd, Kalish, Roubenoff, Roncs, Okparavero, et al.).

1.8. Intro to Tai Chi

The primary focus of this research is to understand and characterize the compartmental loading distribution of the knee joint through musculoskeletal modeling of Tai Chi (TC) gait. Understanding the compartmental loading of TC gait could elucidate the potential efficacy of mechanical based therapies that aid in cartilage maintenance and potential stimulation of anti-inflammatory signals involved in cartilage homeostasis (M. Christopher). Originating in 17th century China, Tai Chi was initially developed as form of martial art. However, in recent years it has been utilized as an aerobic exercise (Barnes et al.). TC involves a series of slow-moving postures and forms characterized by an upright, balanced low center of gravity due to high flexion at the knee relative to normal athletic posture (Fransen et al.). The forms are combined into a series of forward and backward cascading flowlike movements that emphasize a soft yet strong body posture and a calm, concentrated mind (Wayne and Kaptchuk). Widely popular among elderly people, TC has proven to have both psychological and physiological health benefits, such as increased lower limb strength, enhanced balanced and postural stability, improved flexibility,

reduced depression, and higher quality of life (Wang, Schmid, Iversen, Harvey, Fielding, Driban, Price, et al.). Many studies have been done to elucidate the hypothesis that TC could be a possible therapeutic and physiological remedy for patients with KOA. Though there has been controversy of the patient reported outcomes, previous studies generally agree that TC is an effective exercise to manage short term (12-week trials) reduction in pain and increased total quality of life (Wang, Schmid, Hibberd, Kalish, Roubenoff, Rones, and McAlindon)(Lauche et al.)(Wang, Schmid, Iversen, Harvey, Fielding, Driban, Price, et al.)(Lee et al.)(Yan et al.). Other studies have concluded that TC is an effective rehab exercise for improvements in physical function and joint stiffness (Wang, Schmid, Hibberd, Kalish, Roubenoff, Rones, and McAlindon)(Lauche et al.)(Yan et al.). Though there is still disagreement over whether or not TC is directly synergistic in improving OA symptoms, there is growing evidence to support the beneficial aspects of TC for patients with OA. One study concluded the TC has benefits in management of KOA and should be available in rehabilitative programs as an alternative remedy for patients with OA (Yan et al.). Due to the slow movement nature of the exercise, TC has shown itself to be superior to other rehab exercises for elderly people because its slow fluid-like, back and forth movements with the flexed knee reportedly promote mobility and balance as well as gradual increase in muscle strength without exasperating any of the symptoms that other rehab exercise negatively impact (Yan et al.). While TC has shown signs of symptom improvements of KOA, the direct efficacy if TC's benefit on patients with OA is still unclear (Lee et al.). Musculoskeletal modeling could aid in understanding how knee joint mechanics behaves during normal Tai Chi exercises, which could lead to benefactors of mechanical loading on preserving cartilage health.

It is still unclear how compartmental loading is distributed throughout stance phase of TC gait. Understanding how contact forces behave on the medial and femoral condyles could help elucidate the pathogenesis of Tai Chi as an effective rehab exercise for patients with Knee OA. From previous investigations it is clear that compartmental loading of the knee is directly correlated the knee adduction moment (Nie et al.). One study concluded that there was a significant reduction in peak external knee adduction moment (EKAM), about 25-47%, throughout the stance phase of Tai Chi gait compared to that of Normal Walking gait, suggesting that the medial compartment contact force would be significantly reduced if it were measured *in-vivo* (Liu et al.). To our knowledge, no *in-vivo* joint contact measurements have been recorded for TC gait. Thus, musculoskeletal modeling simulations would be beneficial to help elucidate the medio-lateral joint contact forces in the knee.

1.9. Musculoskeletal Modeling

1.9.1. Intro to Musculoskeletal Modeling

Computer aided musculoskeletal modeling has been around since the late 1960's (Paul). With rapid improvements in computers and motion capture (MC) technology, the accuracy and reliability of MSM has increased as well (Mündermann et al.). Musculoskeletal modeling has proven itself to have many pragmatic applications. Musculoskeletal modeling enables doctors and researchers to accurately measure and simulate human body motion, better plan for surgeries, understand pathogenesis of musculoskeletal disorders such as cerebral palsy, plan for corrective surgeries, and better understand metabolic muscle consumption (Blemker et al.). As it pertains to this research, many attempts have been made to characterize the contact behavior of the knee using multibody dynamics software in conjunction with finite element (FE) solvers to resolve pressure

distributions of the tibiofemoral and patellofemoral contact locations during ambulation. Understanding joint contact mechanical loading i.e. centers of pressure (COP) and force and moment magnitudes will aid in understanding the pathogenesis of OA and the effectiveness of current non-invasive exercise treatments for patients with KOA (Adouni and Shirazi-Adl).

1.9.2. Human Subject Testing and Data Collection with Motion Capture

The musculoskeletal modeling process begins by measuring the motion of a human test subject with motion capture technology. The primary components of the motion capture system are the test subject, communicative markers, ground reaction force plates, and motion capture cameras. Human motion or gait for example can be measured by recording the time history locations of each communicative marker in 3-D space. The communicative markers are placed on bony landmarks on the human body to reduce human muscle artifact (Maiwald et al.). A minimum of three non-collinear markers must be placed on each segment of the body in order accurately capture the pose of a rigid body in 3-D space (Colyer et al.). The markers communicate with the cameras on a passive or active platform. Passive markers operate when the motion capture (MC) cameras send out infrared retroreflective signal. That signal is reflected off the markers and back to the cameras (Richards). The active markers operate by flashing a unique signal typically through infrared light emission which can be seen by the motion capture cameras (Maletsky et al.). The markers are then calibrated and synchronized with the ground reaction force plates and other markers such that the time history locations and Ground reaction forces can be simultaneously measured. One drawback of the active markers is that they require an onboard power source which adds weight and can potentially restrict the natural motion of the test subject (Maletsky et al.).

A minimum of two motion capture cameras are required to capture the 3-D motion of a subject (Colyer et al.). However, marker occlusion and small capture volumes promote the need to have many more cameras. The greater number of cameras typically correlates to reduced error, (Lluna et al.), and less gap filling from marker occlusions. The cameras do not measure the exact position of the markers but rather use a least squares algorithm in communication with other cameras to approximate the locations of each marker by minimize the normal distance between each approximate ray from each camera, as seen in **Figure 10** (Apuzzo).

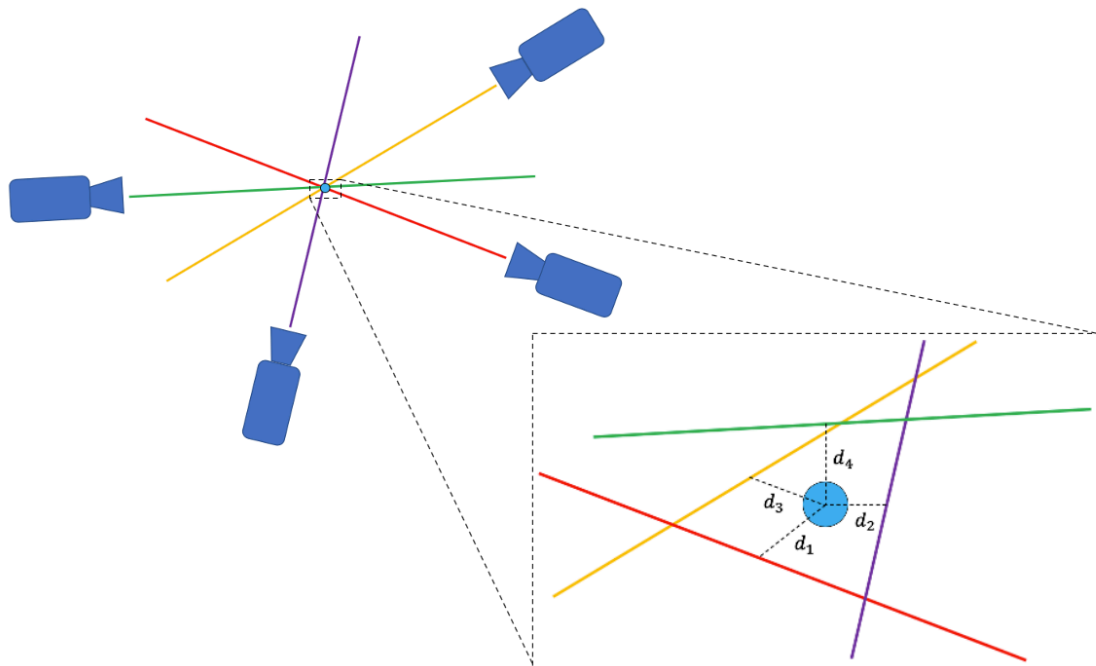


Figure 10: Representation of how a single motion capture camera does not directly calculate the position of each marker rather multiple cameras are used in conjunction with a weighted least squares (WLS) approximation to calculate the position of each marker.

Markers are placed on strategic bony landmarks such as the medial and lateral sides of the knee and ankle joints to allow researchers to identify joint centers. Thus anatomical reference frames can be appended to each bone segment (Donati et al.)(Cappozzo et al.). The marker trajectories are synchronized with the faceplate plate data. Marker trajectories alone will only suffice for

kinematic analysis of human motion. Ground reaction forces at the foot are needed in conjunction with marker trajectories are needed to generate kinetic analyses of human motion. Force plates in the floor of the gait lab record six important metrics, force and moments about the X, Y, and Z directions of the global reference frame. Centers of pressure from the foot in contact with the ground can be generated by combining the forces and moment recorded by the force plates. Accurate force plate measurements are necessary to generate accurate kinetic measurement of gait, which is an important factor in calculating joint contact forces at the knee (Scorza et al.).

The data collected by the cameras and force plates can be collected by number of different motion capture software platforms such as Vicon (VICON technology, Los Angeles, CA, USA), Motion Analysis (Motion Analysis Corp., Rohnert Park, CA, USA), and Optitrack (NaturalPoint, Inc., Corvallis, OR, USA) to name a few. Gait data is collected with one of these platforms and then post processed using another data processing software such as Visual 3D (C-Motion, Germantown, MD, USA). Extensive postprocessing procedures must be done before an accurate musculoskeletal model can be constructed. The marker positions are typically measured at a particular capture frequency, and can vary depending on the application (van der Kruk and Reijne). The data is generally clouded with noise from floor vibrations and soft tissue artifact; therefore, a filter is applied. One of the most commonly applied filters marker data is a lowpass Butterworth filter (Schreven et al.). The data is then processed and gap filled by fitting spline curves to the data where there are marker occlusions (Woltring). Once the marker data is completely postprocessed the data can be imported into a multibody dynamics musculoskeletal modeling software. A flow chart of the data collection process can be seen in **Figure 11**.

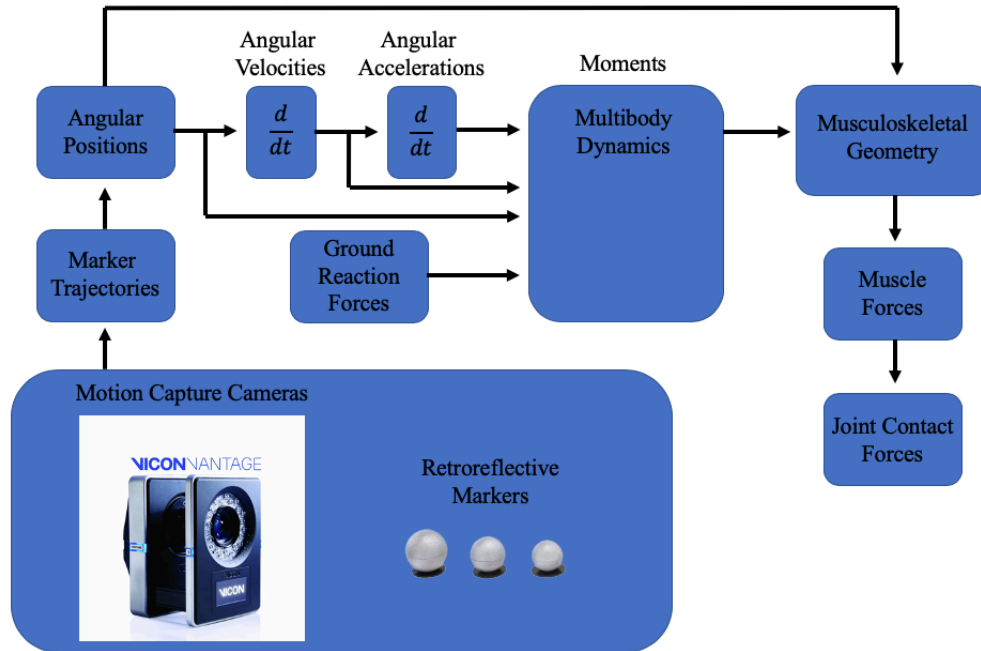


Figure 11: Flow chart of the data collection process which serves as the primary inputs for the musculoskeletal model and subsequent simulations

1.10. Musculoskeletal Modeling in OpenSim

OpenSim is a popular freely available software platform that was developed by biomechanical researchers at Stanford University, Stanford California (Delp, Anderson, et al.). Prior to the development of OSM, biomechanical researchers had difficulty reproducing results from previous experiments, thus hindering their ability to build upon previous research. This issue was primarily attributed to custom multibody dynamic codes which varied across the field (Hume). To minimize this gap, OSM has served to advance the field of biomechanics by creating a standard, freely available, musculoskeletal modeling platform where researchers and clinicians can access and build upon previous research, as well as conduct their own experiments. OpenSim is opensource and can be applied to suit any researchers needs. Additionally, the developers of OSM have created the SimTK repository where a growing community of researchers can access helpful resources, share their projects, and build upon other research (Delp, Anderson, et al.). OSM allows its users

to create and analyze multibody dynamic, musculoskeletal models of human movement such as walking, running, or even cycling (Seth, Sherman, et al.). Tools and plugins allow modelers to analyze their models on a more intuitive and pragmatic level. Some of those analyses include: Scaling, where models can be scaled to match the anthropometry of a test subject measured through motion capture, inverse kinematics, which allows joint angle positions, velocities, and accelerations to be generated from marker trajectories, Inverse dynamics, which allows joint forces and moments to be calculated from marker trajectories and ground reaction forces, computed muscle control and static optimization, to generate the muscle forces and excitations necessary to track measured kinematic data, joint reaction analysis, to calculate reaction loads between bone segments in the model, muscle driven forward dynamic analysis allow the MSM to track dynamic movements based on computed neuromuscular control, and many others as well. All of these analyses can be computed from the OpenSim Graphical User Interface (GUI) and are computationally light simulations. This makes the process of creating a muscle driven MSM from subject specific experimental data fast and easy for researchers and doctors looking to make reasonable cause and effect decisions based on pathological gait (Thelen and Anderson).

In order to model joint contact at the knee, a number of analyses must be first conducted which serve as inputs for a joint reaction analysis. Those steps include Scaling, Inverse Kinematics (IK), Residual Reduction Analysis (RRA), Computed Muscle Control (CMC) or Static Optimization (STO), and finally a Joint Reaction Analysis (JRA). The fundamentals of how these analyses are computed is described in detail below.

1.10.1. The Model

Musculoskeletal modeling and analysis begin by creating or selecting an existing MS model. Upon download OSM provides a number of existing MS models to get started. The SimTK repository has other more advanced modes that can be download for more intensive purposes. Simply put an MS model is an organized set of equations that define of rigid links, joints, and actuators (Hicks et al.). A set of rigid links, i.e. bones, are connected by joints which are constrained by a set of prescribed degrees of freedom (DOF) designed to mimic the actual motion of each joint in the human body. Muscles act as linear actuators that generate motions within the multibody system relative to the prescribed DOF. To eliminate confusion, it is important to note how OSM defines its global coordinate reference frame with respect to anatomical directions, **Figure 12**.

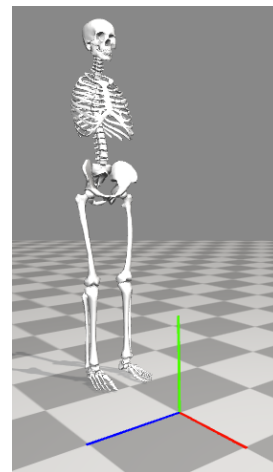
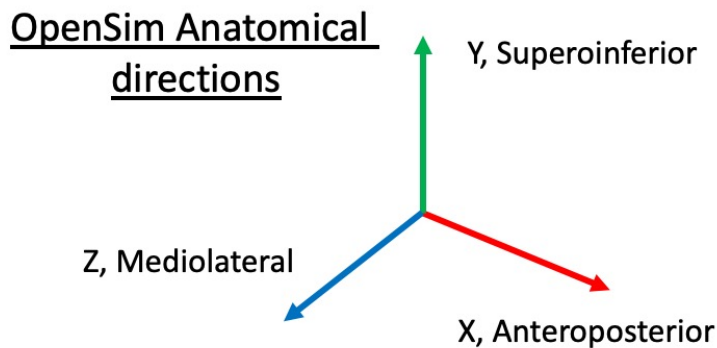


Figure 12: Anatomical directions and the global coordinate system as defined by OpenSim

The MS model consists of a set of local anatomical reference frames appended to each bone. The entire the system resides in a global reference frame. As seen in **Figure 13**, OSM defines each proximal bone, green, segment as the parent body while the distal segment, blue, is the child body.

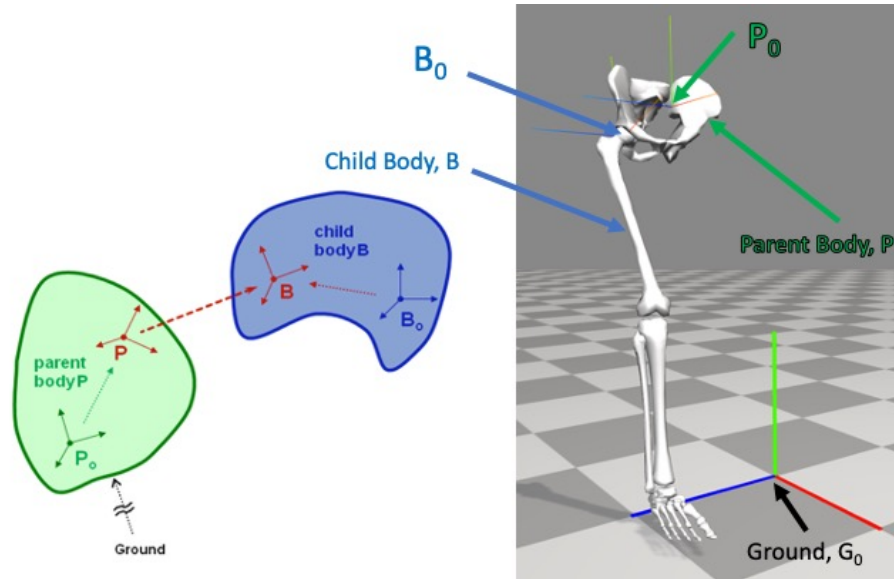


Figure 13: OpenSim Rigid Body Definitions: Proximal segments are parent bodies, green, while distal segments are child bodies, blue, respectively when considering a joint of two bone segments. P_0 , B_0 , and G_0 are the origins of parent body, child body, and ground anatomical reference frames respectively. P and B are any point in the parent and child body respectively. Photo adapted from (Seth, Sherman, et al.).

Joints are modeled such that they mimic the natural motion of joints in the human body. The hip joint for example is defined by three degrees freedom, rotation about the X, Y, and Z axis in the pelvic anatomical reference frame. The knee joint on the other hand is more complex. While the most obvious degree of freedom, is rotation in the sagittal plane, joint laxity and ligament elasticity allow the tibia to translate and rotate in all three directions relative to the femur. Thus, the knee joint is more accurately a 6 DOF joint. Because internal/external rotation, abd/adduction, and all translations of the tibia relative to the femur are difficult to measure with motion capture, most MS models define the knee joint as 3 DOF joint, rotation about the z axis and translation in the x and y directions within the sagittal plane. The axis of rotation of the knee joint translates in the sagittal plane as a function of knee flexion angle, thus simulating the articulating nature of the femoral head on the tibial plateau, similar to that of a cam and follower (Arnold et al.)(Blemker et al.). While this simplification is convenient for computational purposes, it does not give an accurate

representation of the true knee joint kinematics, which is generally needed for knee contact modeling (Hume).

The model also contains muscles which serve as linear actuators that generate motion in accordance with the prescribed DOF at each joint. Muscles are complex organizations of soft tissues that generate a contractive tensile force exclusively (Thelen). Muscle force and activation generated by muscle contraction is multivariate and is a function of physiological cross-sectional area, sarcomertric length, pennation angle, contractile velocity, and the material properties of the muscle fibers and tendons, governed by **Equation 2** (Millard et al.).

$$\vec{F}_{Muscle} = f(A_m, l_{sarcomere}, V_{contraction}, E_{eff}, \alpha) \quad (2)$$

Where A_m is the physiological cross-sectional area of the muscle, $l_{sarcomere}$ is the sarcometric length, $V_{contraction}$ is the contractile velocity, E_{eff} is the effective elastic modulus of the muscle fibers and tendons, and α is the pennation angle of the muscle. Given the multivariate nature of muscle force generation, modeling an accurate muscle is not straight forward. However, Dr. Derryl G. Thelen from The University of Wisconsin-Madison, Madison, WI was able to produce a muscle model that is an accurate representation of real-world muscle force generation. His model is called the Thelen2003Muscle, which is a modification of the hill-type muscle model and is implemented in OpenSim MSM framework (Thelen). A visual schematic of the hill-type muscle model can be seen in **Figure 14**. Another muscle model that is used in OpenSim MS models is the Millard2012EquilibriumMuscle, developed by Dr. Matthew Millard, at Stanford University, Stanford, CA (Millard et al.).

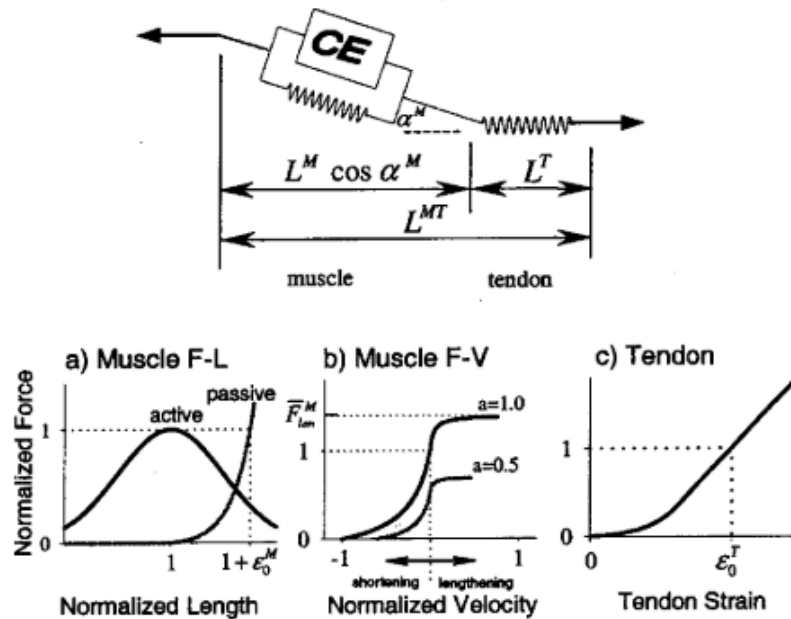


Figure 14: Hill-type muscle Model which helps characterize the force generation of a muscle. The was modified to produce the Thelen2003Muscle model used in OpenSim MS Modeling framework. Image curtesy of (Thelen).

Other MSMs parameters such as bone geometry, as well as tendon and ligament attachment points were primarily determined from cadaveric dissections (Arnold et al.). Given the unique subject specificity of the human body, the anthropometric accuracy of the MSM is limited. Therefore, the accuracy of each model has inherent limitations. This is known and accepted across the biomechanical field. However, given that OSM is so widely used in the field of biomechanics, OSM provides a standard benchmark for which researchers can compare MS models. Thus, reducing one area of variability within research projects (Delp, Anderson, et al.). Upon download, OSM provides a number of complex and simplified MS models. These models can be easily modified to any level of complexity to suit researchers needs.

1.10.2. Scaling

Once an appropriate MS model has been selected, the MS model must first be scaled before any meaningful analyses can be performed. It is important to match the anthropometric properties of the MSM to the experimentally measured test subject in order to reduce computational error (Lathrop et al.). Scaling is achieved by first comparing the anthropometric difference between the measured markers from the test subject and the virtual markers in the MS model. XYZ marker positions of a static pose are measured with motion capture, typically 2 to 3 seconds of data. The X,Y, and Z positions are then averaged for all markers at each time step to form a single set of experimental marker locations. The MS model has a set of virtual model markers that are positioned at strategic locations in local anatomical reference frames such that the position of the virtual markers closely resemble the locations of the measured markers, as seen in **Figure 15**.

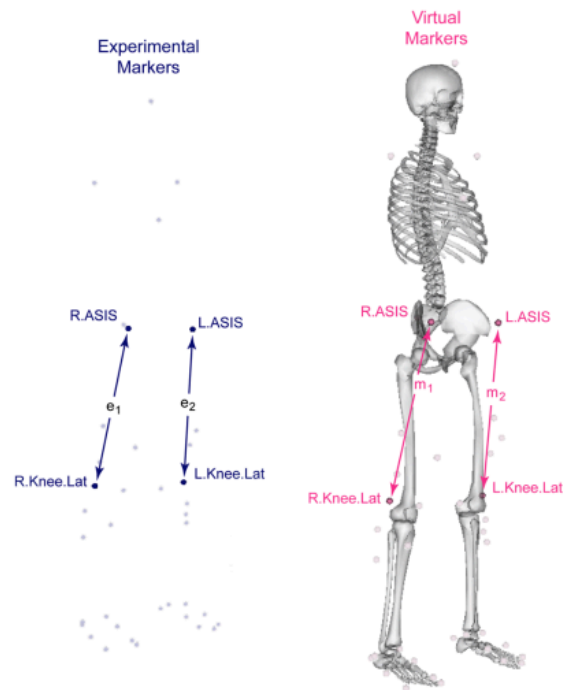


Figure 15: Experimental and virtual marker locations used for scaling OpenSim MSMs. Image courtesy of OpenSim documentation (Delp, Anderson, et al.) (Seth, Hicks, et al.).

Coordinate differences between two markers appended to a single segment are determined from marker pairs, for both the virtual and experimental markers. The virtual and experimental pairs are denoted, \mathbf{m}_i and \mathbf{e}_i respectively. Scale factors, \mathbf{s}_i , are then computed from **Equation 3**.

$$\mathbf{s}_i = \frac{\mathbf{e}_i}{\mathbf{m}_i} \quad (3)$$

Where \mathbf{s}_i is the segment specific scale factor, \mathbf{e}_i is the experimental marker pair, and \mathbf{m}_i is the virtual marker pair. Multiple marker pairs can be used to generate one scale factor for a particular segment. In which case the average is taken and defined by **Equation 4**.

$$\mathbf{S}_i = \frac{\sum_{i=1}^n \mathbf{s}_i}{n} \quad (4)$$

Where \mathbf{S}_i is the primary segment specific scale factor, \mathbf{s}_i are the secondary segment specific scale factors, and n is the number of marker pairs used to calculate the scale factor. The model geometry is then scaled according to each segment specific scale factor. Manual scale factors can be used as well. Other MS model properties such as joint frame locations, mass center locations, force application points, muscle attachment points, and mass and inertial properties are scaled proportionally using the scale factors. Muscles are configuration dependent, therefore muscle properties such as optimal fiber length and tendon slack length are scaled proportionally as well. Once the MS model has been scaled to match the experimental data, the virtual markers are relocated to match the locations of the experimental markers as close as possible. The degree to which the virtual markers relocate typically quantifies anthropometric error in the model due to scaling. This can be improved by repositioning the virtual marker locations such that they correspond to each relative marker location on the test subject.

1.10.3. Inverse Kinematics

Once the modeled has been scaled, an inverse kinematic analysis can be performed. The inverse kinematics tool transforms the individual marker trajectories into time dependent joint angular positions, velocities, and accelerations using Euler angles and numerical differentiation. Each model joint is now considered a generalized coordinate (GC), where the GC angle is denoted as q_i . For example, knee flexion angle is considered a generalized coordinate, where \dot{q}_i and \ddot{q}_i are the joint angular velocities and accelerations for each generalized coordinate. The inverse kinematic tool goes through each timestep of the experimental marker data and formulates a model pose such that the virtual markers and generalized coordinates best match the experimental markers and generalized coordinates. A best match model pose for each time step is determined by minimizing the marker and GC error of a weighted least squares (WLS) function given by **Equation 5**.

$$WLS = \sum_{i=1}^{markers} w_i (\bar{x}_i^{exp} - \bar{x}_i^{model})^2 + \sum_{j=1}^{joint\ angles} \omega_j (q_i^{exp} - q_i^{model})^2 \quad (5)$$

Where w_i is the marker error weighting term, ω_j is the coordinate error weighting term, \bar{x}_i^{exp} is the experimental marker position, \bar{x}_i^{model} is the virtual marker position, q_i^{exp} is the experimental GC, q_i^{model} is the virtual GC. Marker errors are defined by the positional difference between virtual and experimental marker locations. Similarly, coordinate errors are the difference in GC's between virtual and experimental coordinate values. The experimental GC's are typically computed during post processing step after data collection using Visual-3D software, (C-Motion, Germantown, MD, USA). A weighting term is assigned to each marker and GC error. The weighting term defines the degree of strength for which a respective marker or GC error should be minimized. Although challenging and time consuming, the error from IK can be improved by trial

and error adjustments of the weighting terms in the IK input files in OpenSim. Errors with larger weighting terms are more costly in the WLS function, and thus the IK solver will attempt to minimize that error to a greater magnitude (Delp, Anderson, et al.)(Seth, Hicks, et al.). After running the IK tool, a kinematic file containing GC positions, velocities, and accelerations (\mathbf{q}_i , $\dot{\mathbf{q}}_i$, and $\ddot{\mathbf{q}}_i$) at each time step, is generated that closely resembles the human body movement measured in the lab. Upon loading the kinematics file, movement of the MS model can now be viewed in the OpenSim GUI.

1.10.4. Residual Reduction Analysis

Residual reduction analysis (RRA) is a form of forward dynamic simulation used to reduce computational errors i.e. residuals in the musculoskeletal model. When dynamic MS models are formed from experimentally measured inputs, errors are often present. As a result, the model becomes dynamically inconsistent (Kuo). More precisely, the accelerations calculated from IK are not dynamically consistent with the ground reaction forces measured by the force plates, thus violating Newton's second law of motion defined by **Equations 6**.

$$\sum \vec{F} = m\vec{a} \quad (6)$$

The source of these errors typically comes from modeling assumptions i.e. the model has no upper extremities, scaling errors, noise, and other errors from the motion capture process (Kuo). In order to compensate for the dynamic inconsistency in the MS model, residual actuators are appended to the center of mass (COM) of the model, at the pelvis joint. The pelvis joint is defined as a 6 DOF joint with respect to the ground, 3 translations and 3 rotations about in all three anatomical directions. Therefore, the residual actuators are composed of three forces (F_x , F_y , F_z) and three moments (M_x , M_y ,

M_z) at the pelvis joint. The new, dynamically consistent form of newtons second law becomes

Equation 7,

$$\vec{F} + \vec{F}_{residual} = \sum_{i=1}^{segments} m_i \vec{a}_i \quad (7)$$

where, \vec{F} are the forces computed by inverse dynamics, m_i is the mass of each segment, \vec{a}_i is the center of mass acceleration of each segment, and $\vec{F}_{residual}$ are the residual forces computed from the residual actuators.

Although the presence of residual forces and moments are inevitable to achieve dynamic consistency, mathematical measures can be taken to reduce their influence in the MS model, thus the need for the residual reduction analysis. RRA is driven by a control solver that alters the generalized coordinate values in IK by tracking the MS models pose at small time steps ($T = .001s$). Actuator forces and torques $f_{act,i}$ at each joint needed to move the model forward from its previous pose $q_{rra,i}(t)$ to the next pose $\ddot{q}_{ik,i}(t + T)$ at the next time step $t_{j+1} = t_j + T$ is solved by minimizing an objective function J , given by **Equation 8** (Anderson et al.).

$$J(\vec{f}_{act}) = \sum_{i=1}^n w_i \left(\frac{f_{act,i}}{f_{act,i}^{opt}} \right)^2 + \sum_{i=1}^n \omega_i \left(\ddot{q}_{des,i}(t + T) - \ddot{q}_{rra,i}(t) \right)^2 \quad (8)$$

Where $f_{act,i}$ is the actuator force of the i^{th} coordinate, $f_{act,i}^{opt}$ is the optimal actuator force of the i^{th} coordinate, w_i is the weighting term of optimal force usage of the i^{th} coordinate, ω_i is the weighting term of the tracking error for the i^{th} coordinate acceleration, $\ddot{q}_{rra,i}(t)$ is the adjusted acceleration of the i^{th} coordinate, n is the number of GCs, and $\ddot{q}_{des,i}(t + T)$ is the desired acceleration of the i^{th} coordinate which is calculated by proportional derivative control theory defined by **Equation 9**.

$$\ddot{\mathbf{q}}_{des,i}(\mathbf{t} + T) = \ddot{\mathbf{q}}_{ik,i}(\mathbf{t} + T) + \mathbf{k}_v \left(\dot{\mathbf{q}}_{ik,i}(\mathbf{t}) - \dot{\mathbf{q}}_{rra,i}(\mathbf{t}) \right) + \mathbf{k}_p \left(\mathbf{q}_{ik,i}(\mathbf{t}) - \mathbf{q}_{rra,i}(\mathbf{t}) \right) \quad (9)$$

Where, $\ddot{\mathbf{q}}_{ik,i}(\mathbf{t} + T)$ is the acceleration if the i^{th} coordinate calculated at the subsequent time step computed by IK, \mathbf{k}_v and \mathbf{k}_p are the derivate and proportional gain terms respectively, $\dot{\mathbf{q}}_{ik,i}(\mathbf{t})$ and $\mathbf{q}_{ik,i}(\mathbf{t})$ are the velocity and positions of the i^{th} generalized coordinate calculated by IK, and $\dot{\mathbf{q}}_{rra,i}(\mathbf{t})$ and $\mathbf{q}_{rra,i}(\mathbf{t})$ are the velocity and position terms of the new set of generalized coordinates computed by RRA. A block diagram of the feedback control loop for RRA can be seen in **Figure 16**.

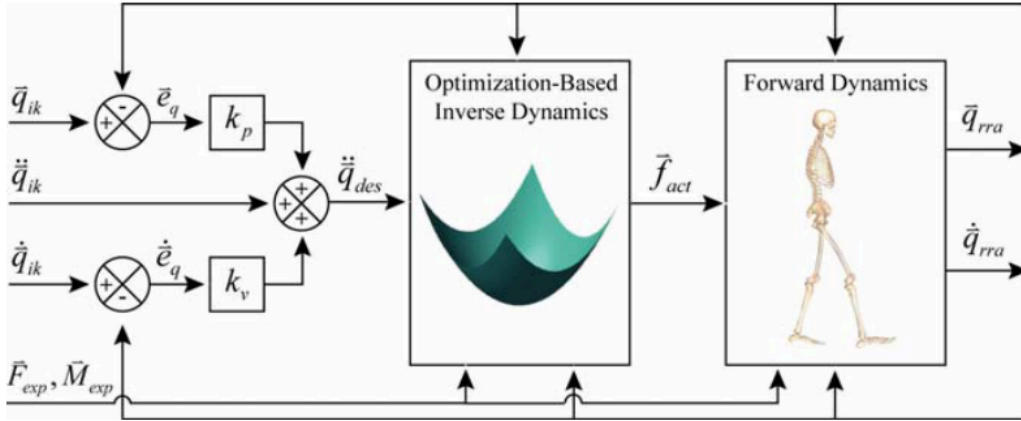


Figure 16: RRA Feedback Control Loop Block Diagram. Image courtesy of (Anderson et al.).

The new generalized coordinates generated by RRA allow the residuals to be reduced. The center of mass location is automatically adjusted to reduce the residuals, and new mass recommendations are given by the RRA tool for each bone to further reduce the residuals. The new mass values of the bones can be manually adjusted into the MS model for the GUI. The new set of GCs coupled with the new center of mass location and the adjusted mass recommendations can be iteratively solved to converge to a set of kinematics, center of mass, and mass properties that reduce the effects of residuals as much as possible. Convergence criterion can be seen in **Table 1** that best quantify

the level of residual sufficiency necessary to yield the best results. Ideally, all residual and coordinate error values of the model would be in the sufficient range.

Table 1: Threshold values for reducing residual forces and moments (Hicks et al.)

Threshold	Sufficient	Tolerable	Innsufficient
Max Residual Force	0-10 N	10-25 N	> 25 N
RMS Residual Force	0-5 N	5-10 N	> 10 N
Max Residual Moment	0-50 Nm	50-75 Nm	> 75 N
RMS Residual moment	0-30 Nm	30-50 Nm	> 50 N
Max Coordinate Error (Translation)	0-2 cm	2-5 cm	> 5 cm
RMS Coordinate Error (Translation)	0-2 cm	2-4 cm	> 4 cm
Max Coordinate Error (Rotation)	0-2 deg	2-5 deg	> 5 deg
RMS Coordinate Error (Rotation)	0-2 deg	2-5 deg	> 5 deg

1.10.5. Static Optimization

The static optimization tool is used to estimate the muscle force activations that are necessary to move the model from one-time step to the next. Using the Generalized coordinates calculated in IK or RRA, the static optimization tool computes the muscle forces at each step by solving a static force balance about each GC within the MS model by knowing the net joint torques at each coordinate computed with an inverse dynamic's algorithm (Pasdar et al.). Because the model muscle force cannot be computed analytically due to muscle redundancy, i.e. the model is statically indeterminant (Raikova), the muscle activations are computed by minimizing the sum squares of muscle activations defined by the objective function, J_{STO} , given by **Equation 10** (Pasdar et al.)(Anderson and Pandy).

$$J_{STO} = \sum_{i=0}^{n_{muscles}} (a_{i,j})^2 \quad (10)$$

Where,

$$a_{i,j} = \frac{F_{i,j}}{f(F_i^o, l_i, v_i)} \quad (11)$$

Where $\mathbf{a}_{i,j}$ is the muscle activation level of the i^{th} muscle in the model at the j^{th} time step, $\mathbf{F}_{i,j}$ is the i^{th} muscle force generated and the j^{th} time step. $f(\mathbf{F}_i^\circ, \mathbf{l}_i, \mathbf{v}_i)$ is the maximum force of the i^{th} muscle as a function of its force-length-velocity relationship, and n_{muscles} is the number of muscles in the model. The muscle forces are then resolved by a force balance at each generalized coordinate defined by **Equation 12**

$$\sum_{i=0}^{n_{\text{muscles}}} \mathbf{F}_i * \mathbf{r}_{i,j} = \boldsymbol{\tau}_j \quad (12)$$

Where,

$$\mathbf{F}_i = \mathbf{a}_{i,j} * f(\mathbf{F}_i^\circ, \mathbf{l}_i, \mathbf{v}_i) \quad (13)$$

Where \mathbf{a}_i is the activation level of the i^{th} muscle in the model, \mathbf{F}_i is the i^{th} muscle force, \mathbf{F}_i° is the maximum isometric force of the i^{th} muscle, \mathbf{l}_i is the sarcometric length, \mathbf{v}_i is the muscle velocity, $f(\mathbf{F}_i^\circ, \mathbf{l}_i, \mathbf{v}_i)$ is the muscle force-length-velocity relationship of each muscle, $\mathbf{r}_{i,j}$ is the moment arm made by each muscle, i , about each coordinate, j , and $\boldsymbol{\tau}_j$ is the torque calculated by inverse dynamics at each generalized coordinate. The static optimization tool is a beneficial tool that can accurately generate the muscle activations and forces needed to achieve a desired movement.

1.10.6. Computed Muscle Control

The computed muscle control tool utilizes a combination of forward dynamics, static optimization and proportion derivative control law to generate a feasible set of muscle excitations necessary to move a MSM such that it matches a desired set of generalized coordinate accelerations typically calculated by IK or RRA, **Figure 17**.

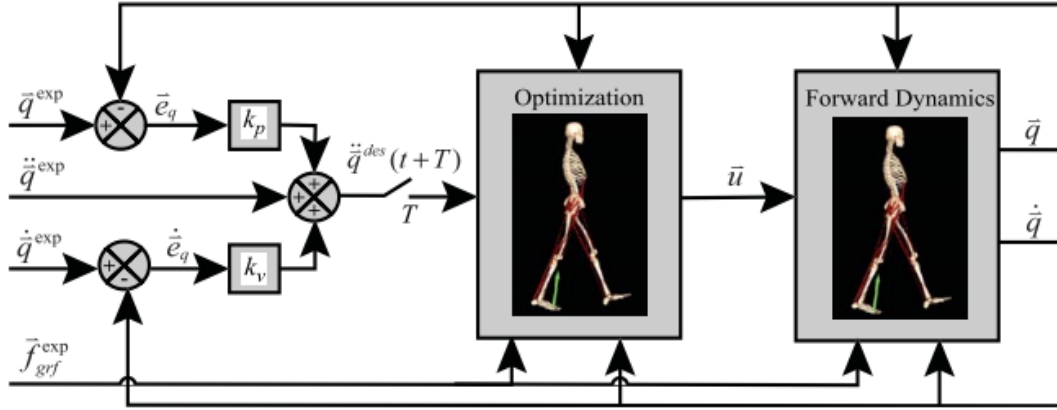


Figure 17: CMC Feedback Control Loop Block Diagram. Image courtesy of (Thelen and Anderson).

The muscle excitations are then used to produce a set of muscle forces used to produce movement in the MS model. CMC is computed by two fundamental steps. First, a set of desired accelerations must be computed using proportional derivative control that tracks the input generalize coordinates calculated by IK or RRA. The desired accelerations are defined by **Equation 14** with the generalized coordinated calculated by RRA as the coordinates to track.

$$\ddot{\mathbf{q}}_{des,i}(t+T) = \ddot{\mathbf{q}}_{RRA,i}(t+T) + \mathbf{k}_v \left(\dot{\mathbf{q}}_{RRA,i}(t) - \dot{\mathbf{q}}_i(t) \right) + \mathbf{k}_p \left(\mathbf{q}_{RRA,i}(t) - \mathbf{q}_i(t) \right) \quad (14)$$

Where $\ddot{\mathbf{q}}_{des,i}(t+T)$ is the desired GC accelerations at the subsequent time step, $\ddot{\mathbf{q}}_{RRA,i}(t+T)$ is the input GC acceleration generated by RRA at the subsequent time step, $\dot{\mathbf{q}}_{RRA,i}(t)$ and $\mathbf{q}_{RRA,i}(t)$ are the velocity and position of the input GCs calculated by RRA, $\dot{\mathbf{q}}_i(t)$ and $\mathbf{q}_i(t)$ are the model velocity and position GCs, \mathbf{k}_v and \mathbf{k}_p are the derivative and proportional feedback gain terms respectively, and T is the time step, typically $T = 0.01s$ (Thelen et al.).

Secondly, the actuator controls \mathbf{a}_j , i.e. muscle excitations are computed by minimizing an objective function, J_{CMC} , defined by **Equation 15**.

$$J_{CMC} = \sum_{j=1}^{muscles} w_j a_j^2 + \sum_{i=1}^{coordinates} \omega_i \left(\ddot{q}_{des,i}(t+T) - \ddot{q}_i(t) \right)^2 \quad (15)$$

Where a_j is the j^{th} muscle activation, $\ddot{q}_i(t)$ is the actual model generalized coordinate acceleration, w_j and ω_i are the weighting parameters for the muscle activations and the generalize coordinate tracking errors respectively (Thelen et al.). The objective function minimizes and distributes the muscle excitations across all muscles through static optimization. At each time step the model is held at a static pose with known external forces and accelerations, and thus a static optimization problem is computed so solve for the muscle excitations and the subsequent muscle forces needed to achieve the desire coordinate accelerations. Muscle excitations cannot be solved directly through analytical methods because muscle redundancies across joints exist. Therefore the model is statically indeterminant (Raikova). The objective function allows the muscle excitations to be computed through optimization despite muscle redundancy.

Typically, CMC will fail when the muscle forces needed to produce the desired accelerations cannot be achieved. This happens when the muscle excitation limit is exceeded resulting in muscle forces that are not strong enough to achieve the desired acceleration. In the event that this happens, reserve actuators can be appended to the model at each generalized coordinate to compensate for the lack of muscle force generation. The model will sparingly access reserve forces and torques from the reserve actuators to achieve the desired acceleration. Reduction of reserve actuator consumption can be regulated by how closely the model tracks the desired accelerations. This this is done by adjusting the coordinate tracking error weighting terms, ω_i . When the coordinate errors are more loosely tracked, reserve actuator consumption is reduced; therefore, a tradeoff exists which is a limitation of CMC. The forces in the model can be improved by iteratively tuning the

weighting parameters to give the most realistic excitation behavior. It is helpful to compare the excitation curves to experimentally calculate excitations through electromyography in order to validate the MS model muscle forces. Once the muscle forces are calculated, the MSM can be driven by the muscle forces alone, thus rendering a muscle driven model.

1.10.7. Muscle Driven Forward Dynamics

Once the muscle activations, forces, and residual forces have been computed by Computed muscle control, those outputs can be used as inputs to drive a muscle driven model forward in time using forward integration. Because there is no coordinate tracking from a PD controller, the model is open loop and therefore can become unstable if there are errors in the muscle forces or errors in the external loads being applied to the model. This is one way of internally validating the set of muscle forces generated by computed muscle control (Hicks et al.). If the kinematic errors between the generalized coordinate are small for IK results compared to forward dynamic results, then it is safe to assume that the muscle force set is sufficient to produce the desired motion being analyzed. However, this does not mean that the muscle activations are comparable to what is taking place *in-vivo*. Muscle activations should be validated against subject specific electromyogram (EMG) activation plots (Hicks et al.). However, if EMG data is not available to compare muscle activations from CMC, then a forward dynamic analysis can be a useful tool to determine if the set of muscle activations being produced by the computed muscle control algorithm is sufficient to drive the model forward in time.

1.10.8. Joint Reaction Analysis

A Joint Reaction Analysis is used to calculate the reaction forces and moments between rigid bodies at each joint in the MS Model. In order to solve for the joint reaction loads, model geometry, joint kinematics, external loads, and muscle forces must first be known and applied to the rigid body of interest. Model geometry can be obtained for anthropometric scale factors generated by the scale tool. COM accelerations of each body are calculated from joint kinematics by the inverse kinematics tool. External loads such as gravity and ground reaction forces measured by force plates and applied to the body in contact with the ground, typically to the calcaneus bone in the foot as seen in **Figure 18c**, are applied to the rigid body. Additionally, muscle forces calculated by CMC or STO are applied to the rigid body. A 3-D free body diagram (FBD) of the tibia, can be seen in **Figure 18d**.

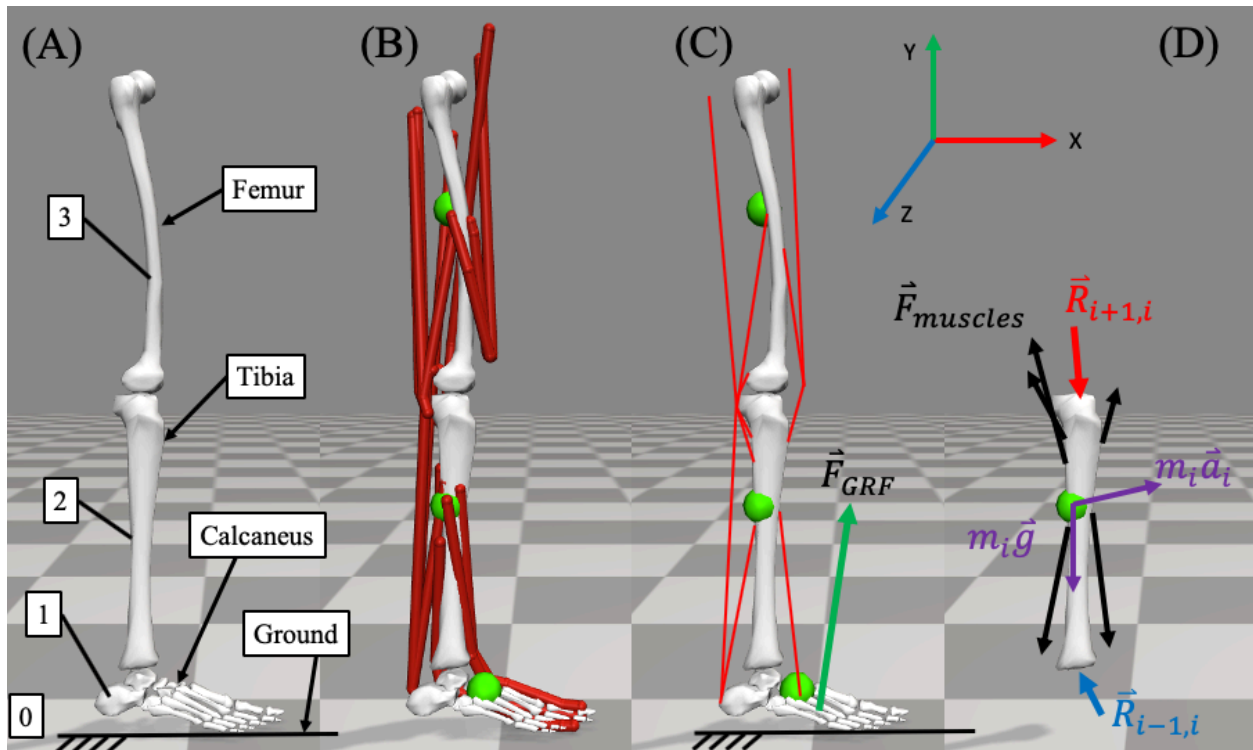


Figure 18: (a) Three link mechanism of the right leg, (b) Rendering of the virtual muscles which cause relative motion at the knee and ankle joints in OSM, (c) Simplified muscle lines if action and GRF on the right leg, (d) FBD of tibia used in joint reaction analysis.

Joint reaction loads are calculated by applying newtons laws of motion to a single body within the MSM (Steele et al.), where **Equation 16** describes the force balance of any rigid body.

$$\sum \vec{F}_{external,i} + \sum \vec{F}_{muscles,i} + \sum \vec{F}_{constraints,i} + \vec{R}_{i-1,i} + \vec{R}_{i+1,i} = m_i \vec{a}_i \quad (16)$$

Where $\vec{F}_{external,i}$ are the external forces acting on the body such as the ground reaction forces and gravity, $\vec{F}_{muscles,i}$ are the muscle forces, $\vec{F}_{constraints,i}$ are the forces due to rigid body constraints, $\vec{R}_{i-1,i}$ is the previously solved equal and opposite reaction load, $\vec{R}_{i+1,i}$ is the current unsolved reaction load of interest, and $m_i \vec{a}_i$ is the mass and acceleration of the rigid body. Starting at the most distal body segment and working up the model, the reaction loads on each body can be solved starting with the calcaneus because the external force between the calcaneus (parent body) and the ground (child body), is known by the GRFs measured by the force plates during data collection. Solving the force balance provided by **Equation 17** on the calcaneus, resolves the reaction load from the tibia, $\vec{R}_{2,1}$, at the ankle joint.

$$m_1 \vec{g} + \vec{F}_{GFR} + \sum \vec{F}_{muscles,1} + \sum \vec{F}_{constraints,1} + \vec{R}_{2,1} = m_1 \vec{a}_1 \quad (17)$$

Where $m_1 \vec{g}$ is the force due to gravity and \vec{F}_{GFR} is the ground reaction force. The equal and opposite reaction load at the ankle, $\vec{R}_{1,2}$ given by **Equation 18**, is applied to the tibia and thus the reaction force at the knee joint, $\vec{R}_{3,2}$, can be solved by, **Equation 19**.

$$\vec{R}_{1,2} = -\vec{R}_{2,1} \quad (18)$$

$$m_2 \vec{g} + \sum \vec{F}_{muscles,2} + \sum \vec{F}_{constraints,2} + \vec{R}_{1,2} + \vec{R}_{3,2} = m_2 \vec{a}_2 \quad (19)$$

An analogous set of equations exist for the summation of torques to solve for the reaction moments at each joint. Joint reaction forces and moments can be solved at each time step throughout the measured gait cycle. Time dependent functions of the joint reaction forces and moments at each

joint can be viewed with the plot tool in the OpenSim GUI. JRA gives researchers a good insight into what the reaction loads of the *in-vivo* or *in-vitro* measurements actually look like (Lerner et al.). *In-silico* approximations are good estimates into the actual joint reaction forces and moments *in-vivo*. The joint reaction forces and moments can be used as inputs for a joint contact analysis using finite element methods in a commonly used sequential approach (Hume). The JRA for MSM can serve as a primary source of forces and boundary conditions. However, complexity exists when attempting to constrain a joint because of the elastic dependence of muscle activation across a joint and muscle co-contractions through a phenomena called dynamic knee joint stability (Williams et al.). Therefore, heavy modeling assumptions are made which ameliorate an inherent limitation with *in-silico* joint constraints during FE modeling.

1.11. Computational Modeling

In recent years computational modeling has emerged as powerful tool to help bridge the gap between “real world” and theoretical experimental research (Hume). A variety of different computational modeling techniques exist, and all have their advantages and limitations (Hume). However, due to the complexity of structural representations and the lack of anatomical references to the subject specific characteristics *in-vivo*, boundary conditions are hard to quantify and mimic through simulation (Hume). *In-vitro* experimentation has aided in the boundary condition gap by understanding material properties, joint contact behavior, and the ability to examine features in the body that are not readily available through *in-vivo* experimentation. Thus, great improvements have been made in an already systemically complex field of computational modeling (Hume). The motley computational techniques across a variety of computational modeling platforms, make direct comparison of results difficult and often meaningless (Hume). Additionally, discrepancies

in MSM assumptions and subject specific boundary conditions further elucidate a need for standardization and a comprehensive software platform (Hume). No standard routine or benchmark currently exists for which to compare results. Thus, the ability to reproduce results and build on existing models is significantly hampered.

Computational modeling has traditionally separated itself in two different modeling avenues. First, there is a full body modeling approach which uses rigid links connected by joints with prescribed DOF. Full body modeling uses body scale metrics such as joint kinematics, muscle forces, and joint reaction loads. This type of modeling is good for understanding full body kinematic behavior but fails to consider the subject specific joint mechanics, because the joints are rigid and therefore do not deform in the presence of internal or externally applied forces (Hume). The second avenue of computational modeling is a joint level modeling approach, which utilized high fidelity joint models in conjunction with finite element solvers to elucidate the synergistic relationship between full body kinematics and the joint level kinematic behavior of individual joints (Hume). Joint level stresses and strains in the ligaments, muscles, and articular cartilage can be resolved which have a profound impact on the true kinematic behavior of the joint. As a result, more accurate contact behavior in the joint can be realized by joint level modeling in contrast to full body modeling of human locomotion.

More recently, a combined sequential approach to the two computational modeling avenues has emerged, which has shown promising results (Adouni and Shirazi-Adl) (Kłodowski et al.) (Adouni et al.) (Bei and Fregly). The sequential approach combines outputs from the full body modeling approach, loading conditions, muscle forces, and joint reaction loads, as inputs for the joint level

modeling approach, resulting in a finite element joint model that has boundary conditions generated from experimentally derived values in the MS model. The finite element models can then produce stresses and strains in the ligaments, cartilage, and subchondral bone of the model that resolve an accurate depiction of the contact behavior of the knee joint *in-vivo* (Hume). Although this is quite a significant accomplishment, generating an accurate FE model of the knee is extremely difficult to produce and even harder to validate *in-vivo* (Hume). One of the most difficult challenges is generating validated subject specific boundary conditions (Hume). Many of the boundary conditions such as ligament and articular cartilage material properties in previous models were retrieved from cadaveric studies, (Arnold et al.) (Delp, Anderson, et al.), which cannot be directly validated to the subject specific material properties *in-vivo*. Another boundary condition such as joint laxity plays a large role in the kinematic and contact behavior of the knee joint (Hume et al.). To make things even more complex, joint laxity is a function of muscle contraction across the joint where the time dependent parameters such as force magnitude, line of action, and moment arm of each muscle and ligament are constantly changing in time as a function of knee flexion angle throughout the stance phase of gait (Hume et al.) (Smith et al.). This makes predicting accurate boundary conditions extremely difficult with FE modeling approaches and highlights the need for simultaneous computation of muscle forces and joint mechanics in a single framework (Hume). When accurate boundary conditions of the model have been predicted, model complexity increases significantly which drives up computational cost and run time. Simulations that vary in complexity have been reported to take anywhere from a couple of hours to almost 2 weeks to run where 99.5 percent of the runtime is consumed by the FE solver (Halloran et al.). Therefore, the ability to produce accurate results from an FE model of the knee joint is challenging and time consuming.

Additionally, because no comprehensive software exists that streamlines the process of going from experimentally recorded data to an FE model, many researchers have to exercise multidisciplinary competence across many complex software platforms which is technically challenging and time consuming. As a result, more work must be done to simplify and streamline the comprehensive process of generating an accurate FE model without compromising accuracy. This would serve to advance the field biomechanical computational modeling significantly.

1.11.1. Low Fidelity Knee Models

In contrast to high fidelity knee models generated from a sequential approach, low fidelity knee models have been shown to have respectable results, despite the simplified nature of the model (Lerner et al.) (Guess et al.). Traditionally low fidelity knee models are implemented into full body musculoskeletal modeling software's such as OpenSim because for their simplified nature. The knee joint has historically been modeled as a 1 DOF revolute joint where the tibia is free to rotate about the femur in the sagittal plane (Anderson and Pandy). While this simplification is good for macroscale modeling purposes, it does a poor job in accurately simulating the true kinematic behavior of the knee. The true kinematic behavior of the knee joint is often compared to a cam and follower where the femoral condyles serve as the cam head and the tibia serves as the follower. As the knee flexes, the tibial plateau articulates around the surface of the femoral condyles generating a traditional cam and follower motion. As a result, the knee joint can be more accurately modeled with a 3 DOF planar knee model where the knee rotates and translates (anterior-posterior and superior-inferior) in the sagittal plane (Delp, Loan, et al.)(Arnold et al.), **Figure 19**. Therefore, the axis of rotation of the tibia translates in the sagittal plan as a function of knee flexion angle.

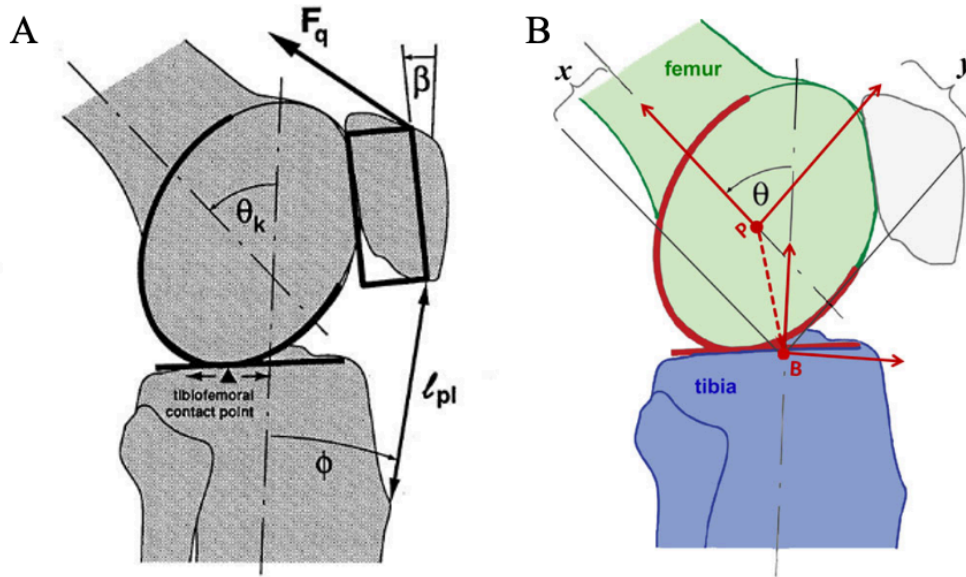


Figure 19: 3 DOF Planar Knee model were the tibia rotates and translates in the sagittal plane as a function of knee flexion angle. Photos (A) and (B) courtesy of (Delp, Loan, et al.) and (Seth, Sherman, et al.) respectively.

While a planar representation of the knee is more accurate than a simple revolute joint, there are still inherent limitations which hinder the model from accurately modeling the true kinematic and contact behavior of the knee. When trying to study joint contact at the knee, one major limitation of the planar knee model is that it only considers one point of contact in the knee, therefore it can only resolve an estimate of the total knee contact forces which can be inaccurate and inconsistent with previous studies (Lerner et al.). Additionally, the bone segments are normally modeled as rigid body segments which result in high stress environments when the contact force is concentrated at a single point in the knee. In reality, the knee has two major points of contact between the femur and the tibia where the contact force is distributed over a small area by the meniscus and the deformable nature of articular cartilage, thus reducing the peak contact stress in the cartilage (Kurosawa et al.). More recent studies have further modified the planar knee models to have two points of contact at subject specific locations of the lateral and femoral condyles (Lerner et al.) (Saxby et al.) (Gerus et al.) (Guess et al.). This model has been validated *in-vivo* for

normal walking by comparing a fully informed model of the knee to test subjects with an instrumented knee implant which can accurately measure the joint contact forces of a total knee replacement, **Figure 20** (Halder et al.) (Graichen et al.).

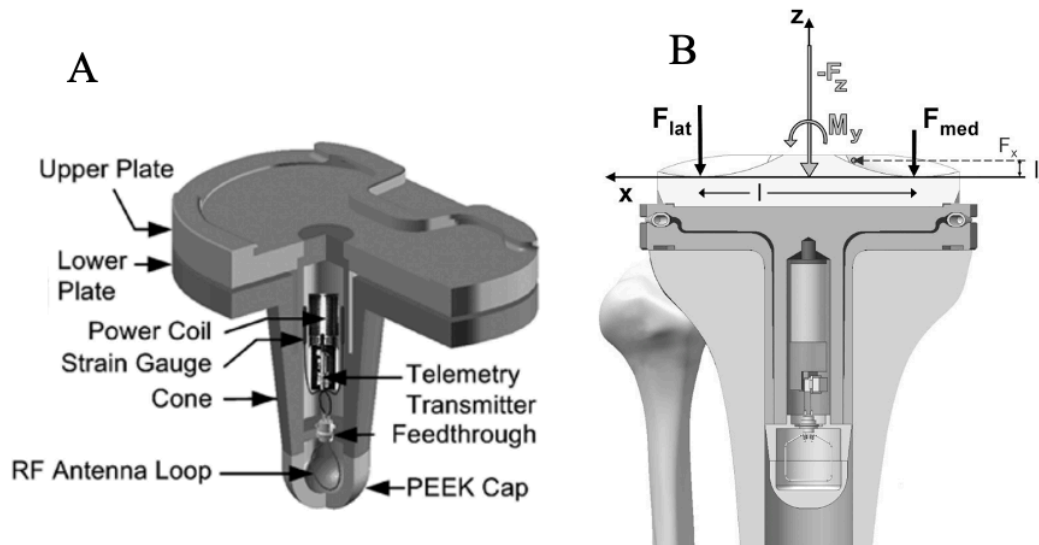


Figure 20: Instrumented Knee Implant responsible for measuring knee joint contact loads *in-vivo* for patients with total knee arthroplasty. Photos (A) and (B) adapted from (Graichen et al.) and (Halder et al.) respectively.

One study was able to effectively create and validate a fully informed model of the knee joint that resolved the compartmental loading of the knee by using subject specific tibiofemoral alignment and subject specific placement of the joint contact loads for a patient with a total knee replacement (Lerner et al.). The tibiofemoral alignment of the OpenSim model was determined by radio graphic imaging. The angle formed between the femoral head, center of the knee, and center of the ankle i.e. the tibiofemoral angle was informed in the model. Additionally, the contact locations with respect to the knee joint center were determined by radiographic imaging and was informed in the model. The result of adding these subject specific parameters is a fully informed subject specific model of the knee joint. For the fully informed model, this study predicted the error in the first peak if the medial and lateral joint contact force to be 12.4% and 11.9% respectively when

compared to *in-vivo* measurements taken from a patient with an instrumented knee implant. The study also concluded that for every degree altered in tibiofemoral alignment there was a shift in 51N ($r^2 = 0.99$) in the medial compartment knee contact force. In addition, for every mediolateral translation (1mm increments) in joint contact location, the medial compartment joint contact force changed by 41N ($r^2 = 0.99$). This study concluded that the fully informed model is a good estimate of the joint contact forces that are measured *in-vivo* for walking at self-selected speeds (Lerner et al.).

This model can be downloaded and modified for research purposes on the SimTk repository, www.simtk.org/home/med-lat-knee/. This model is referred to as the Medio-Lateral Knee (MLK) model as is discussed in detail later in this work. The MLK model is a fully validated model that can be applied to virtually any test subject measured by 3-D gait analysis, making it a good alternative to measuring the compartmental loading of the knee. Because *in-vivo* measurements of the knee joint contact forces are difficult to obtain, the MLK model is a good non-invasive alternative to estimating the compartmental loading of the knee joint through musculoskeletal modeling and 3-D gait analysis.

1.12. Conclusion and Motivation for this Research

Osteoarthritis is a common and debilitating disease that influences patients' total quality of life (Dieppe and Lohmander). Tai Chi has shown signs that it is a good exercise to help manage pain and improve patient's total quality of life who suffer from OA (Wang, Schmid, Hibberd, Kalish, Roubenoff, Roness, and McAlindon). Understanding how mediolateral compartmental load distribution behaves during stance phase of Tai Chi gait would help elucidate the potential

pathogenesis of a novel rehab exercise for patients with knee OA. Given that the external knee adduction moment, is significantly reduced during the stance phase of Tai Chi gait compared to that of Normal Walking, it is believed that there is a significant reduction in medial loading of the knee during stance phase of Tai Chi Gait as well (Liu et al.). To our knowledge, there has been no study that has measured the mediolateral compartmental loading of the knee during Tai Chi gait either *in-vivo* i.e. with an instrumented knee implant, or through a musculoskeletal modeling approach. Therefore, the aim of this study is twofold: First we would like to resolve and compare the compartmental knee contact forces of one patient performing a Normal Walking (NW) gait and a Tai Chi (TC) gait by utilizing the Medio-Lateral Knee model in OpenSim. Results from this comparative study would help elucidate the hypothesis that there is decreased loading of the medial knee compartment during stance phase TC relative to that of NW. Second, we would like, to understand how tibiofemoral alignment effect compartmental loading of the knee during stance phase TC compared to that of stance phase NW gait. The results from this study would help elucidate the hypothesis that Tai Chi is an effective rehab treatment for patients with osteoarthritis of the knee.

Chapter 2: Methods and Procedures

2.1. Introduction

The goal of this research can be divided into two main objectives. First, the medial and lateral knee compartment, joint contact forces will be resolved using a preexisting musculoskeletal model in OpenSim for two types of gait, Normal walking (NW) and Tai Chi (TC). Secondly, the effects of an altered tibiofemoral knee malalignment, varus and valgus deformity, will be analyzed to determine the change in mediolateral compartmental loading of the knee from both NW and TC gait. limitations are stated and recommendations are given based on the results of this study. A project was created for this study on the SimTK repository. Videos of each simulation, Normal walking and Tai Chi Can be view on the project page at <https://simtk.org/>. The title of the project is, “Knee Compartmental Load Distributions During Tai Chi Gait”.

2.2. Human Subject Data

The human subject chosen for this study was one 28-year-old male subject, weighing 77.11 kilograms, and a height of 1.75 meters. The subject data was reused from a previous study (Liu et al.)(Jagodinsky et al.), where subjects informed consent was given and the approval of the Auburn University Institutional Review Board was granted. Three trials of 3D gait analysis were used to conduct this study, one static trial of the subject standing in a static pose with arms abducted, one walking trail at self-selected walking speed (1.04 m/s), and one Tai Chi trial from one of the 24 Yang-style Tai Chi forms. The test subject was outfitted with retroreflective markers on bony landmarks of pelvis, thigh, shank, foot, shoulder, and trunk (Jagodinsky et al.). The gait trials were conducted barefoot, and the subject wore compression attire. A 7 camera optical motion capture

system was used to capture the trials (VICON technology, Los Angeles, CA, USA). The motion capture marker trajectories were recorded at a 100Hz capturing rate in conjunction with two imbedded force plates (Advanced mechanical Technology, Inc., Watertown, MA, USA) capturing at 1,000 Hz. The force plates were used to obtain the ground reaction force data (forces and moments about all three anatomical axes). The kinematic data was collected and post processed using Nexus software (VICON technology, Los Angeles, Ca, USA.) and Visual3D (C-Motion, Germantown, MD, USA).

2.3. Preparing Data for OpenSim Import

Synchronized marker trajectories and force plate data from Visual3D is generally produced in a single .C3D file format which cannot be directly imported into OpenSim. Therefore, the marker trajectories and force plate data were bifurcated and transformed into a file format that OpenSim can read using Matlab (The Mathworks Inc., Natick, Massachusetts, USA). OpenSim can only accept marker trajectory data in the .TRC file format. The Matlab code entitled “c3dExport.m” was used to transform the .C3D files into .TRC file formats. This code comes free with the OpenSim download. The c3dExport code not only transforms the marker trajectory data file format but also allows the data axis of the marker trajectories and force plate data to be transformed to comply with the OpenSim global coordinate reference frame given that there may be discrepancies between global reference frame definitions of the gait lab for which the data was collected and OpenSim. Upon bifurcation, the c3dExport.m code returns two files: one .trc file of the marker trajectories, and, the other, an .mot file of the ground reaction forces. The marker trajectories are X, Y, and Z coordinates of each data marker with respect to time in the global reference frame. The ground reaction forces are X, Y, and Z forces and moments at the calcaneus with respect to time.

Both files are inputs for OpenSim tools such as scaling, inverse kinematics, inverse dynamics, etc. A flow chart of the data processing to allow for the data to be imported into OpenSim can be seen in **Figure 21**.

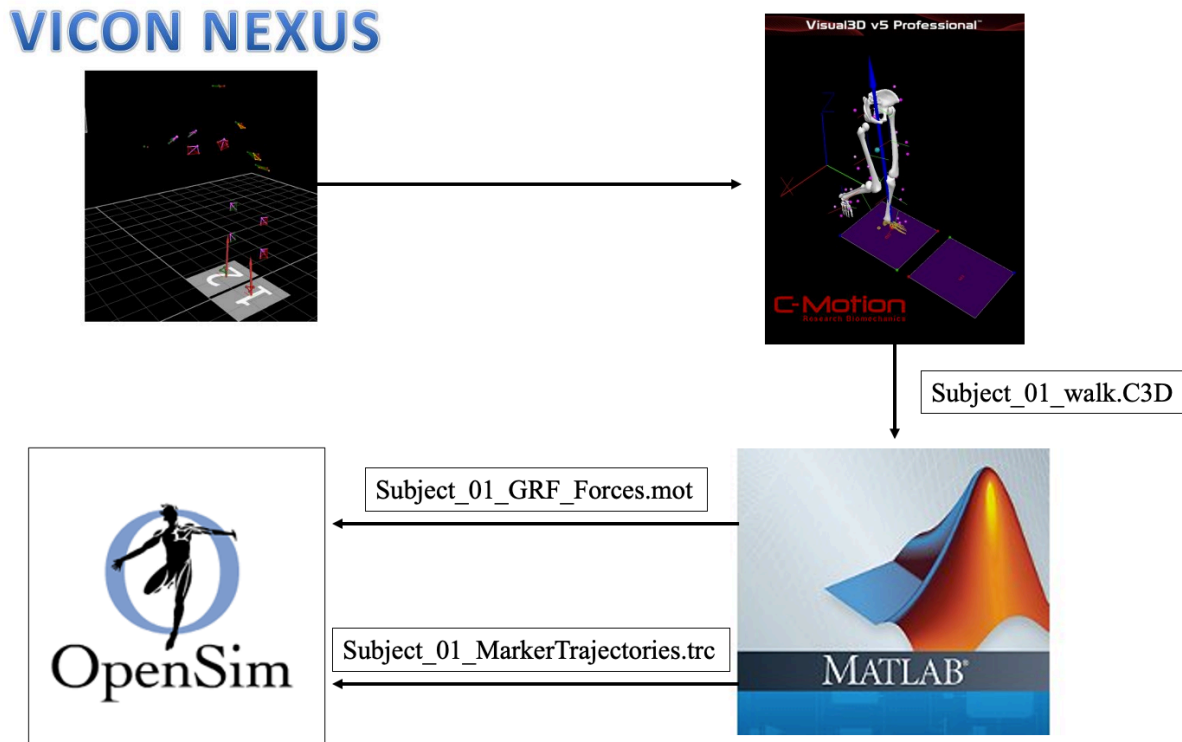


Figure 21: Flow chart of how to transform 3D gait data to be imported into OpenSim

2.4. The Musculoskeletal Model

The musculoskeletal model used for this study was developed and validated by Lerner, Delp, DeMers, and Browning (Lerner et al.). The model consists of 18 body segments, 92 muscle-tendon actuators, and 23 degrees of freedom. The body segments are linked together by joints, a ball and socket joint between the third and fourth vertebra, three translations and rotations of the pelvis with respect to the ground, ball and socket joints at each hip, sagittal plane rotational joints at each knee, and revolute joints at each ankle and subtalar joint. The sagittal plane rotation of the knee joint is defined by articulation in the sagittal plane as a function of knee flexion angle (Delp,

Loan, et al.). This allows the knee to behave in a more natural cam and follower motion compared to that of a 1 DOF revolute joint. The most novel aspect of this model is its ability to predict the compartmental joint contact forces at the medial and lateral condyles of the femur. This model is called the Medio-Lateral Knee (MLK) model. The knee joint of the MLK model is composed of seven subcomponents, **Figure 22**, the femur, femoral component, sagittal articulation frame, medial compartment, lateral compartment, tibial plateau, and the tibia.

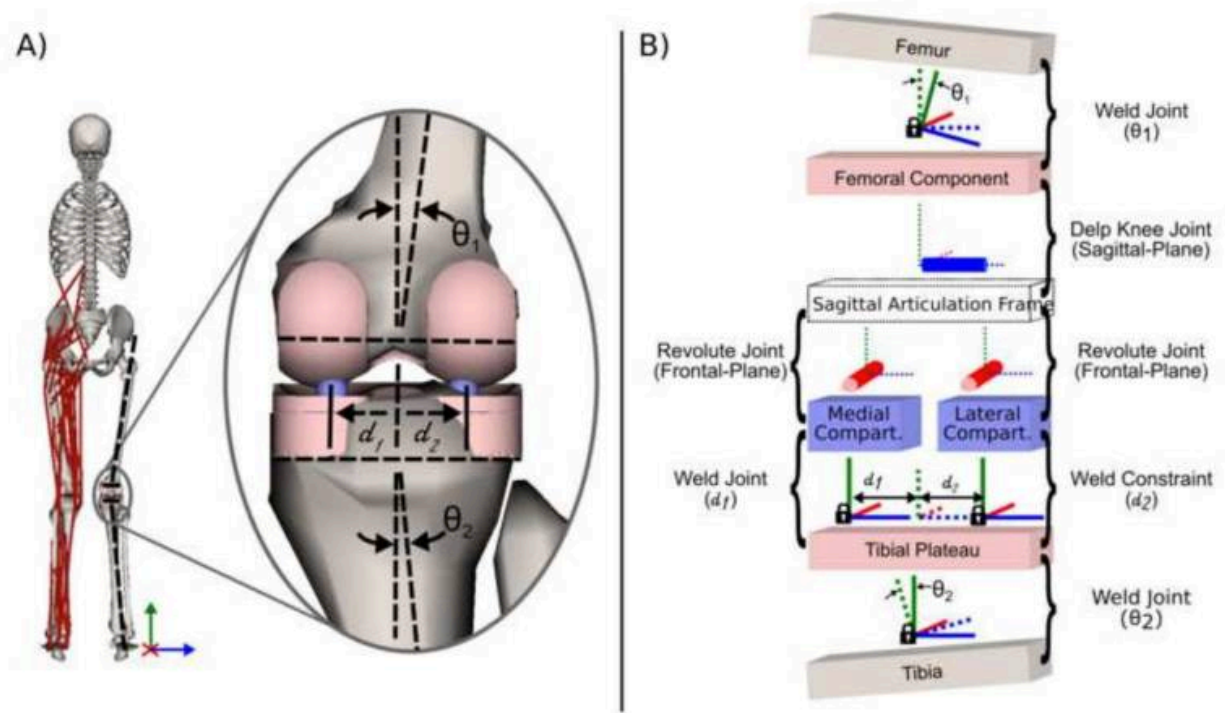


Figure 22: Knee joint decomposition if the Medio-Lateral Knee (MLK) model used for this research study. Image courtesy of (Lerner et al.).

The femoral component and the tibial plateau are fixed to the femur and the tibia respectively with an angular offset weld joint. The rotational offset is defined by θ_1 and θ_2 which comprises the tibiofemoral alignment (TFA) angle i.e. the angle formed by the segment connection of the hip knee and ankle joint centers. Therefore, the TFA angle is defined by **Equation 20**.

$$\theta_{TFA} = \theta_1 + \theta_2 \quad (20)$$

Where θ_{TFA} is the tibiofemoral alignment angle, θ_1 is the angular weld offset between the femur and the femoral component, θ_2 is the angular weld offset between the tibial plateau and the tibia. The sagittal articulation frame is a massless reference frame that translates and rotates in the sagittal plane. Its axis of rotation articulates about the femoral component as a function knee flexion angle. The medial and lateral compartments are defined by two massless spheres, **Figure 22B**. They are each attached to the sagittal articulation frame by a 1 DOF revolute joint. Each individual compartment is free to rotate in the frontal plane. However, because both the medial and lateral compartments are fixed to the tibial plateau by two weld joints, their combined effect prevents the medial and lateral compartments from rotating in the frontal plane. Thus, the tibial plateau and its successive chain are can only rotate in the sagittal plane. The locked rotation in the frontal plane allows the medial and lateral joint contact forces to be calculated between the medial and lateral compartments and the tibia plateau respectively. The horizontal distance between the medial and lateral compartments from the center of the tibial plateau in the mediolateral direction is defined by d_1 and d_2 respectively. This value can be manually adjusted in the model to allow subject specific dimensions to be defined in the model. A deconstructed MLK model of the tibia can be seen in **Figure 23**.

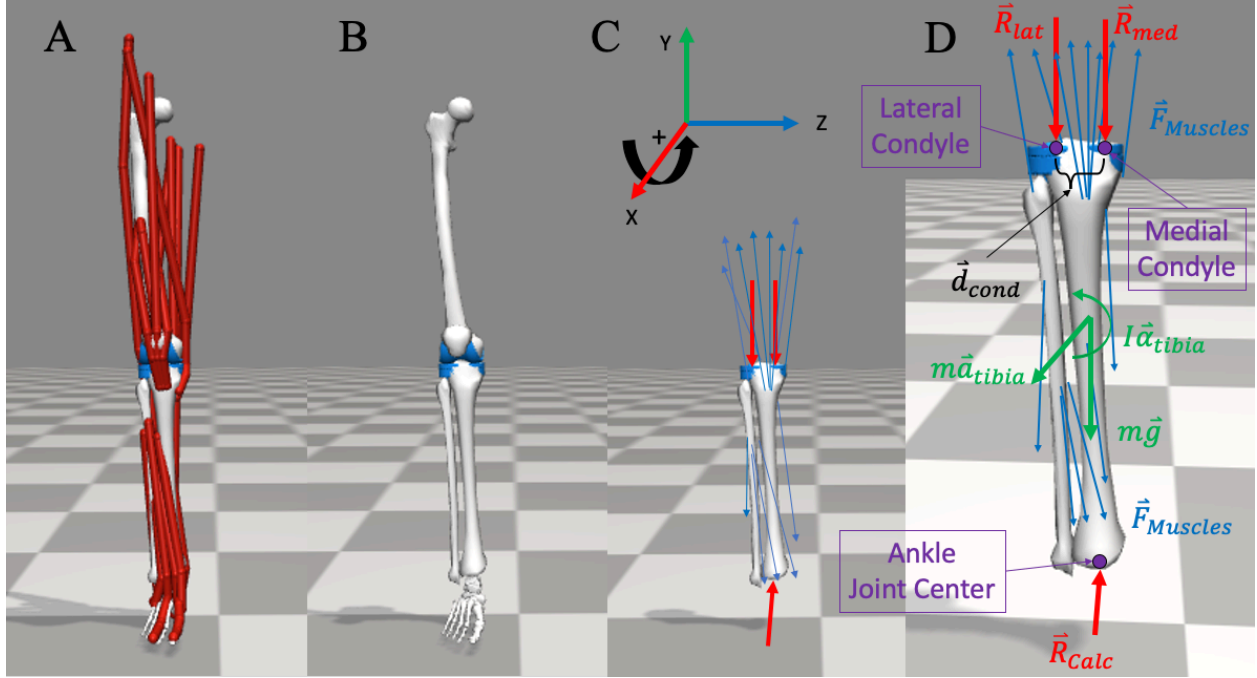


Figure 23: Decomposed tibial segment of the mediolateral knee (MLK) model. (A) shows the right lower extremity with bone segments and muscle forces acting on the tibia. (B) Shows rigid body segments of the right femur, tibia, and foot. (C) Shows the isolated muscle forces and joint reaction loads. (D) Is a 3-D Free body diagram of the tibial segment for which a moment a force balance can be conducted such that the reaction loads at the medial and lateral condyles can be solved through a joint reaction analysis in OpenSim.

Figure 23D show a 3-D Free body diagram of the right tibia where the joint reaction loads at the medial and lateral femoral condyles can be computed by applying newtons second law and summing moments about each condyle of the tibia, defined by **Equation 21** and **Equation 22** respectively.

$$\begin{aligned} \sum \vec{M}_{med} = \sum \vec{M}_{inertial} = & \left[\sum_{i=1}^n \vec{r}_{Mus,med,i} \times \vec{F}_{Muscle,i} \right] + \vec{r}_{mg,med} \times m\vec{g} \\ & + \vec{r}_{calc,med} \times \vec{R}_{calc} + \vec{d}_{cond,med} \times \vec{R}_{lat} \end{aligned} \quad (21)$$

$$\begin{aligned} \sum \bar{\mathbf{M}}_{lat} = \sum \bar{\mathbf{M}}_{inertial} = & \left[\sum_{i=1}^n \bar{\mathbf{r}}_{Mus,lat,i} \times \bar{\mathbf{F}}_{Muscle,i} \right] + \bar{\mathbf{r}}_{mg,lat} \times \mathbf{m}\bar{\mathbf{g}} \\ & + \bar{\mathbf{r}}_{calc,lat} \times \bar{\mathbf{R}}_{calc} + \bar{\mathbf{d}}_{cond,lat} \times \bar{\mathbf{R}}_{med} \end{aligned} \quad (22)$$

Where $\bar{\mathbf{M}}_{med}$ and $\bar{\mathbf{M}}_{lat}$ are the moments about the medial and lateral condyles respectively. $\sum \bar{\mathbf{M}}_{inertial}$ is the sum of all the inertial moments about the tibial segment, which includes Coriolis. $\sum_{i=1}^n \bar{\mathbf{r}}_{Mus,med} \times \bar{\mathbf{F}}_{Muscle,i}$ and $\sum_{i=1}^n \bar{\mathbf{r}}_{Mus,lat,i} \times \bar{\mathbf{F}}_{Muscle,i}$ is the sum of the moments generated by the muscle forces about the medial and lateral condyles respectively, where $\bar{\mathbf{r}}_{Mus,med,i}$ and $\bar{\mathbf{r}}_{Mus,lat,i}$ is the vector locations of each muscle insertion point to the medial and lateral condyles respectively, $\bar{\mathbf{F}}_{Muscle,i}$ is the force generated by the i^{th} muscle on the tibia, and n is the number of muscles attached to the tibia. $\bar{\mathbf{r}}_{mg,med} \times \mathbf{m}\bar{\mathbf{g}}$ and $\bar{\mathbf{r}}_{mg,lat} \times \mathbf{m}\bar{\mathbf{g}}$ are the moments generated by the force of gravity about the medial and lateral condyles respectively, where $\bar{\mathbf{r}}_{mg,med}$ and $\bar{\mathbf{r}}_{mg,lat}$ are the vector locations of the COM to the medial and lateral condyles respectively, and $\mathbf{m}\bar{\mathbf{g}}$ is the force of gravity acting at the tibial COM. $\bar{\mathbf{r}}_{calc,med} \times \bar{\mathbf{R}}_{calc}$ and $\bar{\mathbf{r}}_{calc,lat} \times \bar{\mathbf{R}}_{calc}$ are the moments generated by the reaction load of the calcaneus acting on the tibia about the medial and lateral condyles respectively, where $\bar{\mathbf{r}}_{calc,med}$ and $\bar{\mathbf{r}}_{calc,lat}$ are the vector locations of the calcaneus reaction load with respect to the medial and lateral condyles respectively, and $\bar{\mathbf{R}}_{calc}$ is the reaction load of the calcaneus acting on the distal tibia. Finally, $\bar{\mathbf{d}}_{cond,med} \times \bar{\mathbf{R}}_{lat}$ and $\bar{\mathbf{d}}_{cond,lat} \times \bar{\mathbf{R}}_{med}$ are moments generated by the lateral and medial condyle reaction loads about the medial and lateral condyles respectively, where $\bar{\mathbf{d}}_{cond,med}$ and $\bar{\mathbf{d}}_{cond,lat}$ are the vector locations of the lateral and medial reaction forces to the medial and lateral condyles respectively, and $\bar{\mathbf{R}}_{lat}$ and $\bar{\mathbf{R}}_{med}$ are the reaction loads at the medial and lateral condyles respectively. $\bar{\mathbf{R}}_{lat}$ and $\bar{\mathbf{R}}_{med}$ are the only unknowns in **Equations 21** and **22** and can be solved algebraically. This process is done by the joint reaction

analysis tool in OpenSim. Joint reaction loads at the lateral and medial condyles are solved at each time step.

Even though MLK is a low fidelity model is still a good predictor if the load distribution in the medial and lateral compartment of the knee. This model has also been validated *in-vivo* (Lerner et al.). However, limitations do exist with this model. First this model was only validated against a single individual and not across a range of individuals. Therefore, there could be unforeseen errors when applied to other individuals. However, since there are directly proportional relationships between model predictions and geometric parameter the results can seemingly be applied across a range of individuals. Secondly, the model assumes that the medial and lateral contact locations are fixed to a single point throughout knee flexion. Therefore, changes in contact locations are not possible within the MLK model. Lastly, the model was validated using a weighted least squares of muscle activations to generate the muscle forces and not against EMG therefore the muscle activations levels could be different compared to muscle activations *in-vivo*. This could present large errors in the predicted results because joint reaction loads are heavily dependent upon muscle force contractions that traverse the knee joint (Lerner et al.).

2.5. The Modeling Process and Standard Workflow

In this section a standard workflow of the modeling process was used to generate the mediolateral joint contact force in the knee. A flow chart of the workflow can be seen in **Figure 24**. Outputs from the previous analysis serve as inputs for subsequent analysis’.

Flow Chart of Analyses in OpenSim

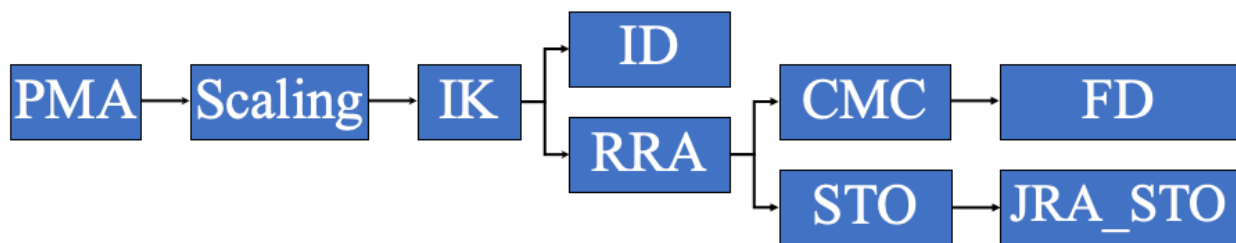


Figure 24: Flow chart of all the OpenSim Analyses to generate compartmental tibiofemoral joint contact loads. This chart also includes simulations such as ID, CMC, and FD, which were used for validation.

2.5.1. Preliminary Model Adjustments

The MLK model was used to conduct all experiments. The subject specific tibiofemoral alignment angle was manually defined in the model prior to scaling. The TFA angle was obtained using the static trial of marker trajectories. The TFA angle is the internal angle between the hip joint center, knee joint center, and ankle joint center measured medially **Figure 25**.

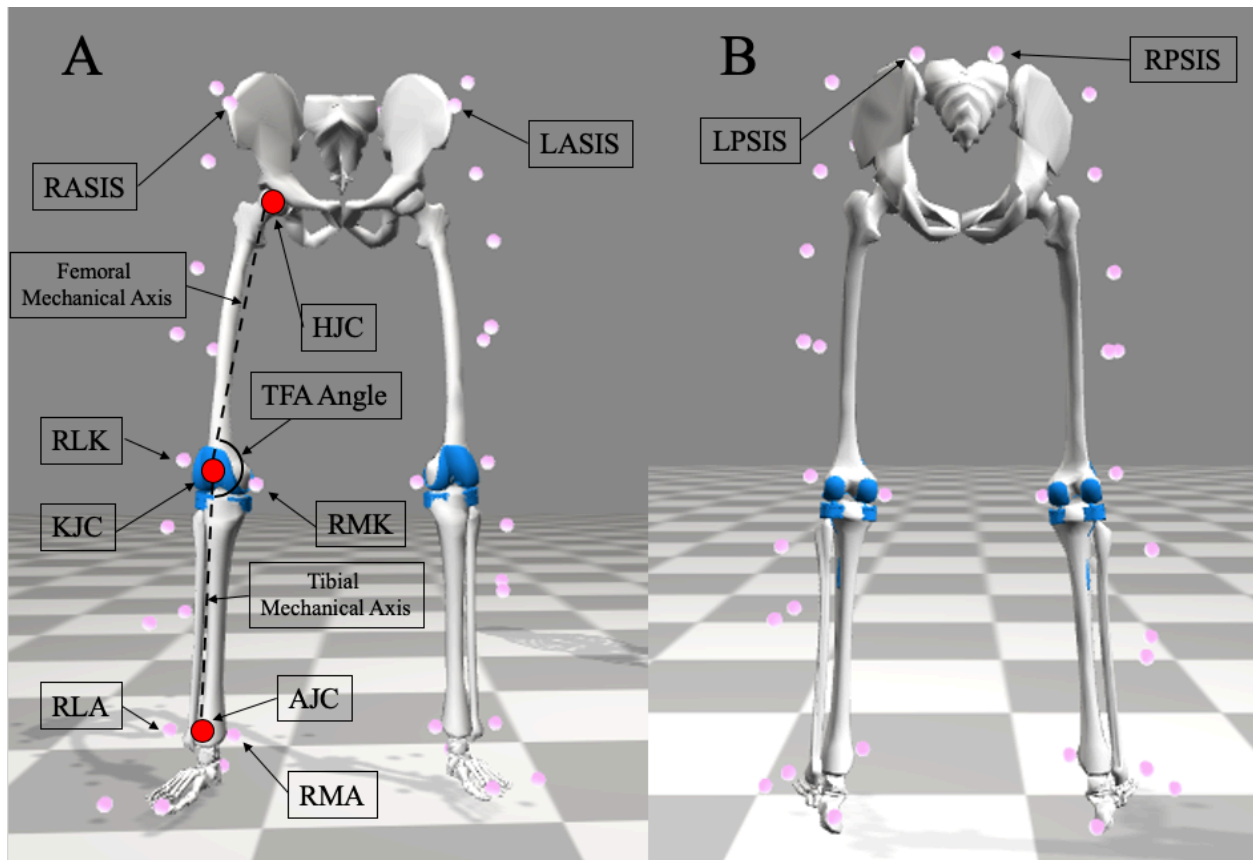


Figure 25: Markers used to calculate the right hip, knee, and ankle joint centers which from the tibiofemoral Alignment (TFA) angle. The TFA angle is the internal angle formed by the intersection of the tibial and femoral mechanical axes. Figure shows anterior (A) and posterior view (B).

The TFA angle formed by linking the hip joint center (HJC), knee joint center (KJC) and ankle joint center (AJC), was extracted from the static trial marker data and applied to the model prior to scaling. The knee and ankle joint centers were calculated by finding the midpoint of right lateral knee (RLK) and the right medial knee (RMK) markers and right lateral ankle (RLA) and the right medial ankle (RMA) markers respectively. **Equation 23** and **Equation 24** define the knee and ankle joint center calculations respectively.

$$\langle KJC \rangle = \frac{\langle RLK \rangle + \langle RMK \rangle}{2} \quad (23)$$

$$\langle AJC \rangle = \frac{\langle RLA \rangle + \langle RMA \rangle}{2} \quad (24)$$

Where, $\langle KJC \rangle$ and $\langle AJC \rangle$ are the X, Y, and Z coordinates of the right knee and ankle joint centers in the global reference frame, $\langle RLK \rangle$, $\langle RMK \rangle$, $\langle RLA \rangle$, and $\langle RMA \rangle$ are the X, Y, and Z coordinates of the markers used to calculate the right knee and ankle joint centers in the global reference frame. The right hip joint center was calculated by procedures outlined in the literature and is standard practice in Visual-3D (C-Motion, Germantown, MD, USA) when constructing a “Bell and Brand Hip Joint”, in a “V3D_Composite” coordinate system (Bell, Brand, et al.) (Bell, Pedersen, et al.). The X, Y, and Z coordinates of the right hip joint center were calculated based on **Equations 25**, **26**, and **27** respectively.

$$X_{HJC} = -0.19 * distASIS + \left[\frac{RPV_{depth}}{2} - r_{marker} \right] \quad (25)$$

$$Y_{HJC} = -0.3 * distASIS \quad (26)$$

$$Z_{HJC} = -0.36 * distASIS \quad (27)$$

Where the right hip joint center coordinates can be combined to form **Equation 28**,

$$\langle HJC \rangle = \langle X_{HJC}, Y_{HJC}, Z_{HJC} \rangle \quad (28)$$

Where, X_{HJC} , Y_{HJC} , and Z_{HJC} are the X, Y, and Z coordinates of the right hip joint center, ***distASIS*** is the distance between the RASIS and the LASIS markers, **Figure 26**, ***RPV_{depth}*** is the distance between the midpoint of the left and right anterior superior iliac spine (ASIS) and the midpoint of the left and right posterior superior iliac spine (PSIS), **Figure 26**, and ***r_{marker}*** is the radius of the marker. Markers 15mm in diameter were used for this study.

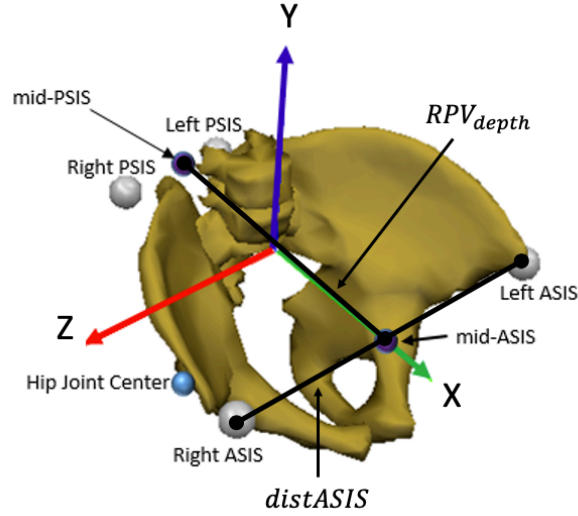


Figure 26: “Bell and Brand Pelvis” defined in V3D_Composite coordinate system in Visual-3D (C-Motion, Germantown, MD, USA). Figure modified from Visual-3D Wiki Documentation.

The TFA angle was calculated by algebraically solving for θ_{TFA} when taking the dot product of the two vectors that form tibial mechanical axis (TMA) and the femoral mechanical axis (FMA), **Equation 29**.

$$\overline{TMA} \cdot \overline{FMA} = |TMA||FMA| \cos \theta_{TFA} \quad (29)$$

Where TFA angle is the angular complement of θ_{TFA} , **Equation 30**.

$$TFA = 180 - \theta_{TFA} \quad (30)$$

Where \overline{TMA} is the vector representing the tibial mechanical axis, \overline{FMA} is the vector representing the femoral mechanical axis, $|TMA|$ is the magnitude of the tibial mechanical axis vector, $|FMA|$ is the magnitude of the femoral mechanical axis vector, θ_{TFA} is the angle between the two vectors, and TFA is the tibiofemoral alignment angle. All calculations were done in Matlab and the code can be found in **Appendix A**. The subject specific tibiofemoral alignment angle, i.e. nominal model alignment, was determined to be $TFA_{nominal} = 177.16^\circ$. Two subsequent models were generated which emphasize a varus and valgus TFA angle of the knee. The varus and valgus

tibiofemoral alignments generated TFA angles of $TFA_{varus} = 172^\circ$ and $TFA_{valgus} = 188^\circ$ respectively. **Figure 27** shows the three models used for this study and their respective tibiofemoral alignments.

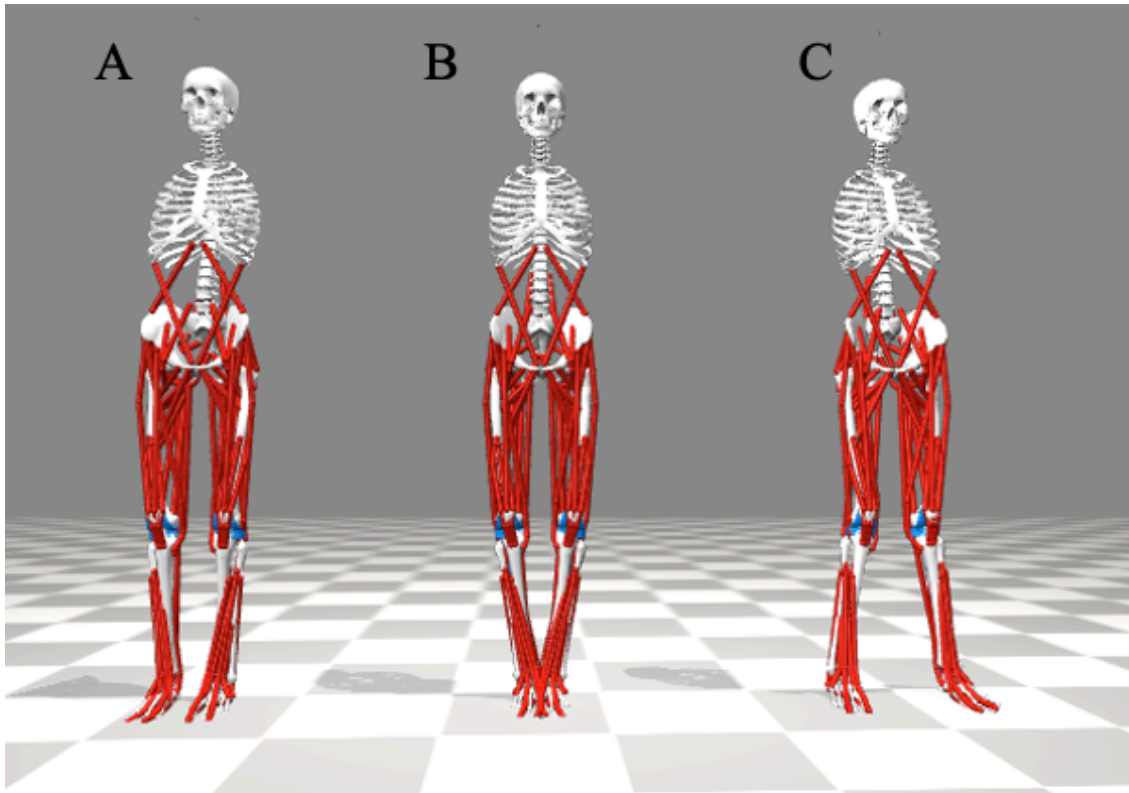


Figure 27: Three different models used for this study with varying tibiofemoral alignment, nominal TFA=177.16 degrees (A), varus TFA=172 degrees (B), and valgus TFA=188 degrees (C).

The varus and valgus malalignment angles were selected because $\pm 8^\circ$ is one standard deviation away from the mean of tibiofemoral alignment of patients with symptomatic osteoarthritis of the knee, which is consistent with the literature (Cooke et al.).

2.5.2. Scaling

The model was scaled using the scale tool in OpenSim. 37 retroreflective markers were used on the test subject during data collection; therefore, a corresponding set of 37 virtual model markers was created and appended to the model **Figure 28**.

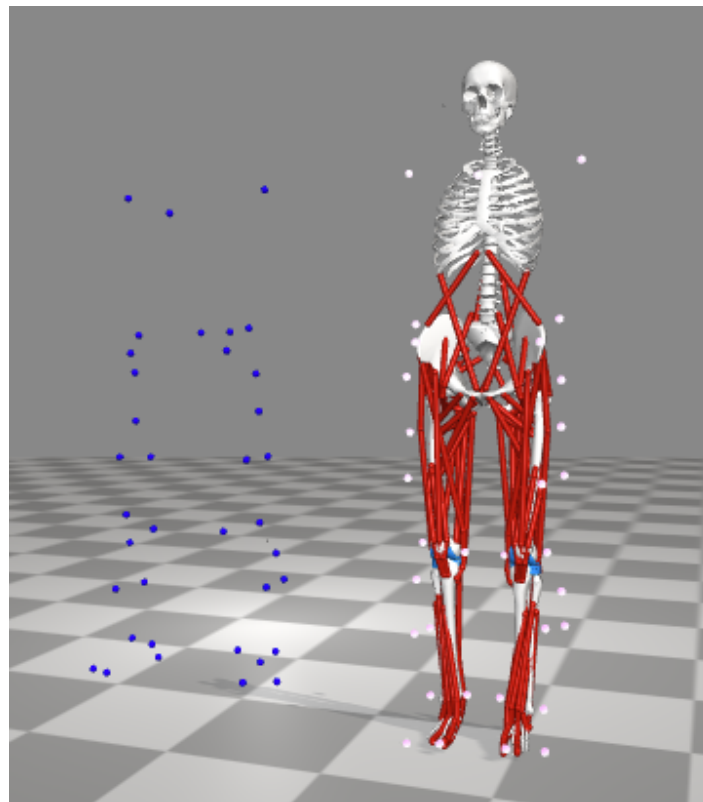


Figure 28: Nominal model with 37 virtual markers (pink) appended to the model (right). Static trial of 37 retroreflective markers (blue) measured by motion capture during data collection (left)

The static trial was used to scale the model. The mass of the subject was defined, and mass distributions were preserved. The average time measurement used to scale the model was the entire length of the static trial (0-3.25s). All scale factors were generated automatically by the scale tool. The individual scale factors can be seen in **Table 2**

Table 2: Scale factors calculated by the scale tool in OpenSim used to scale the model. Each scale factor corresponds to a specific bone segment (right and left) of the model.

Body	Scale Factor
Pelvis	1.168
thigh	0.978
shank	0.942
foot	0.728
torso	0.969

Weighting factors were also given to each virtual marker to define the degree to which the scale tool should minimize the errors between the virtual and experimental markers during scaling. Markers with higher weights were more closely tracked. The weighting factors for each marker can be seen in **Table 3**.

Table 3: Scaling marker weight factors used to scale the nominal model

Marker	Weight	Enabled	Marker	Weight	Enabled	Marker	Weight	Enabled
RTH1	1.0	yes	LTH1	1.0	yes	STN	1.0	yes
RTH2	1.0	yes	LTH2	1.0	yes	RSG	1.0	yes
RTH3	1.0	yes	LTH3	1.0	yes	LSG	1.0	yes
RLK	1000.0	yes	LLK	1000.0	yes	LPS	1.0	yes
RMK	1000.0	yes	LMK	1000.0	yes	RPS	1.0	yes
RSK1	1.0	yes	LSK1	1.0	yes	RPP	1.0	no
RSK2	1.0	yes	LSK2	1.0	yes	LPP	1.0	no
RSK3	1.0	yes	LSK3	1.0	yes	RAS	1000.0	yes
RLA	1000.0	yes	LLA	1000.0	yes	LAS	1000.0	yes
RMA	1000.0	yes	LMA	1000.0	yes	RHP	1.0	no
RFT1	1000.0	yes	LFT1	1000.0	yes	LHP	1.0	no
RFT2	1000.0	yes	LFT2	1000.0	yes			
RFT3	1.0	yes	LFT3	1.0	yes			

Some weight factors were disabled from the scaling algorithm. Inputs and out puts from the scale tool can be seen in **Figure 29**.

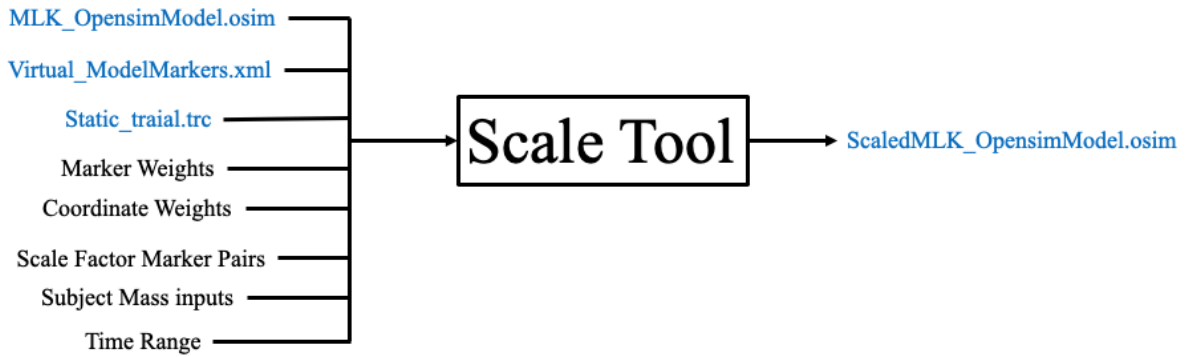


Figure 29: Inputs and outputs for the Scale Tool in OpenSim. Imported files are blue while user defined inputs are black

The scaled nominal model can be seen in **Figure 30**. The total squared error, RMS error, the maximum error and the marker associated with the maximum error can be seen in **Table 4**. The result of the scale tool is a scaled model that closely matches the anthropometry of the test subject.

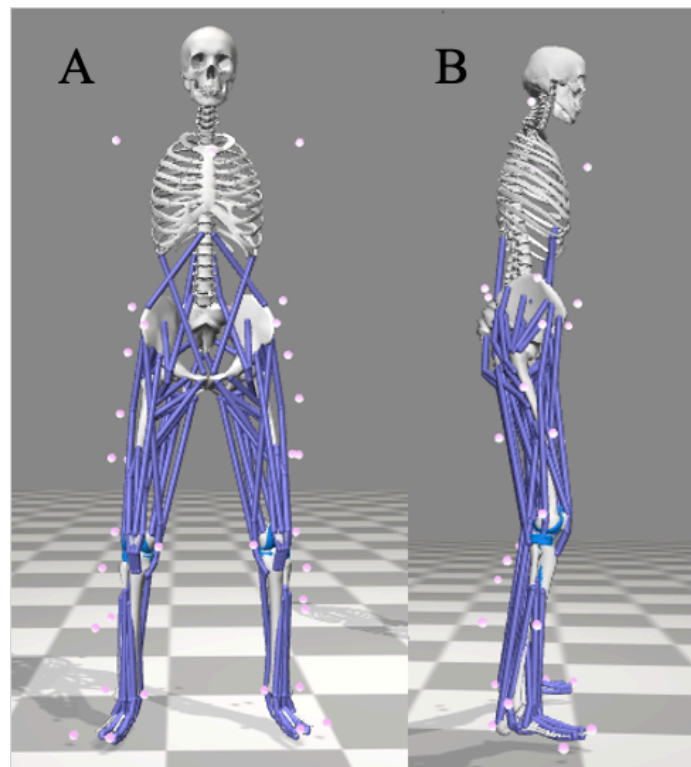


Figure 30: Rendering of the fully scaled nominal tibiofemoral alignment model used for this study.

Table 4: Scaling errors of the nominal model (TFA=177.16 deg.) used in this study

Nominal Model (TFA=177.1 Deg.)	
Parameter	Value
Total Squared Error	0.0721
Marker Error RMS	0.0467
Max Marker Error	0.0869
Max ME Name	LSG

2.5.3. Inverse Kinematics

The Inverse Kinematics Tool was used to convert the marker trajectories defined in the .TRC file into generalized coordinate positions, velocities, and accelerations using Euler angles and numerical differentiation. Inverse kinematics was used to generate coordinate kinematics for both the Normal Walking and the Tai Chi dynamic sets of marker trajectories. Coordinate tracking weights can be seen in **Table 5**. Some tracking weights were disabled from the IK Tool.

Table 5: Kinematic coordinate weights used for Normal Walking and Tai Chi trials

Coordinate Name	Weight	Enabled	Coordinate Name	Weight	Enabled	Coordinate Name	Weight	Enabled
Pelvis Tilt	1	no	Hip_flexion_r	1	no	Hip_flexion_l	1	no
Pelvis_List	1	no	Hip_adduction_r	1	no	Hip_adduction_l	1	no
Pelvis_rotation	1	no	Hip_rotation_r	1	no	Hip_rotation_l	1	no
Pelvis_tx	1	no	Knee_angle_r	1	no	Knee_angle_l	1	no
Pelvis_ty	1	no	Ankle_angle_r	1	no	Ankle_angle_l	1	no
Pelvis_tz	1	no	Subtalar_angle_r	1000	yes	Subtalar_angle_l	1000	yes
Lumbar_extension	1000	yes	Mtp_anlge_r	1000	yes	Mtp_anlge_l	1000	yes
			Lumbar_bending	1	no	Lumbar_rotation	1	no

The input time range for each trial NW and TC trials were (0-1.54s) and (0-22.74s) respectively. Inputs and outputs for the inverse kinematics tool can be seen in **Figure 31**. The results from the IK too is a set of generalized coordinate kinematics that can be used as inputs for Residual Reduction Analysis and other analyses as well.



Figure 31: Inputs and outputs for the Inverse Kinematics Tool in OpenSim. Imported files are blue while user defined inputs are black

2.5.4. Residual Reduction Analysis

Residual forces and torques were reduced for each model, TFA= 177.17, 172, and 188, and gait trail, NW and TC. The residuals were reduced using an iterative process of adjusting mass parameters and coordinate tracking weights. The mass parameters were no longer adjusted when the total mass change recommended by the software was less than 1% difference. The residuals were further reduced by adjusting tracking weights of the translational and rotational coordinates of the pelvis with respect to the ground. These residuals are considered “hand of god” forces and must be reduced to minimize large muscle redundancy and errors in the model (Hicks et al.). The residuals were reduced iteratively until the residual forces and torque parameters at the pelvis fell within the given thresholds displayed in **Table 6**.

Table 6: Threshold for residual forces, torques and coordinate errors about the pelvis for reducing residuals during residual reduction analysis

Threshold	Sufficient	Tolerable	Innsufficient
Max Residual Force	0-10 N	10-25 N	> 25 N
RMS Residual Force	0-5 N	5-10 N	> 10 N
Max Residual Moment	0-50 Nm	50-75 Nm	> 75 N
RMS Residual moment	0-30 Nm	30-50 Nm	> 50 N
Max Coordinate Error (Translation)	0-2 cm	2-5 cm	> 5 cm
RMS Coordinate Error (Translation)	0-2 cm	2-4 cm	> 4 cm
Max Coordinate Error (Rotation)	0-2 deg	2-5 deg	> 5 deg
RMS Coordinate Error (Rotation)	0-2 deg	2-5 deg	> 5 deg

The ideal reduction is to have all residual forces, torques, and coordinate errors fall within the “Sufficient” range of **Table 6**. However, that was often not achievable. Therefore, the residuals were reduced until they could no longer be reduced any further. This was often indicated by having corresponding residual forces and errors fall in the “tolerable” or “insufficient” zone. The “give and take” nature of reducing residuals creates a limit for which the residuals could no longer be reduced. Tables for each residual reduction trial, six total, can be seen in **Appendix B**. The final residuals for the Normal Walking trial and the Tai Chi trial of the nominal tibiofemoral alignment can be seen in **Table 7** and **Table 8** respectively.

Table 7: Final residual “hand of god” forces, moments, and coordinate errors about the pelvis in the ground reference frame for the nominal model for Normal Walking trail. Green values are sufficient, yellow values are “Tolerable”, and red values are “Insufficient”

Exp_Normal_Walking Nominal Model TFA=177.16 deg.							
Residual Force (N)		Residual Moment (Nm)		Translational Error (m)		Rotational Error (Deg.)	
FX_Max	14.96	MX_Max	-28.85	tx_Max	0.0478	rx_Max	-0.0200
FX_RMS	9.01	MX_RMS	11.52	tx_RMS	0.0274	rx_RMS	0.0089
FY_Max	8.99	MY_Max	11.61	ty_Max	0.0041	ry_Max	-0.0449
FY_RMS	3.52	MY_RMS	4.18	ty_RMS	0.0020	ry_RMS	0.0136
FZ_Max	-5.09	MZ_Max	-65.83	tz_Max	-0.0089	rz_Max	-0.6719
FZ_RMS	1.75	MZ_RMS	26.25	tz_RMS	0.0047	rz_RMS	0.2563

Table 8: Final residual “hand of god” forces, moments, and coordinate errors about the pelvis in the ground reference frame for the nominal model for Tai Chi trail. Green values are sufficient, yellow values are “Tolerable”, and red values are “Insufficient”

Exp_TaiChi Nominal Model TFA=177.16 deg.							
Residual Force (N)		Residual Moment (Nm)		Translational Error (m)		Rotational Error (Deg.)	
FX_Max	19.6961	MX_Max	18.2997	tx_Max	0.034	rx_Max	-0.0505
FX_RMS	10.6603	MX_RMS	7.6817	tx_RMS	0.017	rx_RMS	0.0268
FY_Max	-8.4876	MY_Max	6.7037	ty_Max	0.0308	ry_Max	0.0556
FY_RMS	2.6788	MY_RMS	2.319	ty_RMS	0.013	ry_RMS	0.0255
FZ_Max	-6.9639	MZ_Max	24.4643	tz_Max	-0.026	rz_Max	-0.0347
FZ_RMS	3.3227	MZ_RMS	9.8322	tz_RMS	0.0128	rz_RMS	0.0167

Inputs and outputs for RRA can be seen in **Figure 32**. A Matlab code was used to extract the residual forces, torques, and coordinate errors from the output files of RRA and can be seen in

Appendix A. A flow chart for the inputs and outputs for the Matlab data extraction can be seen in **Figure 33.**



Figure 32: Inputs and outputs for the Residual Reduction Analysis (RRA) Tool in OpenSim. Imported files are blue while user defined inputs are black

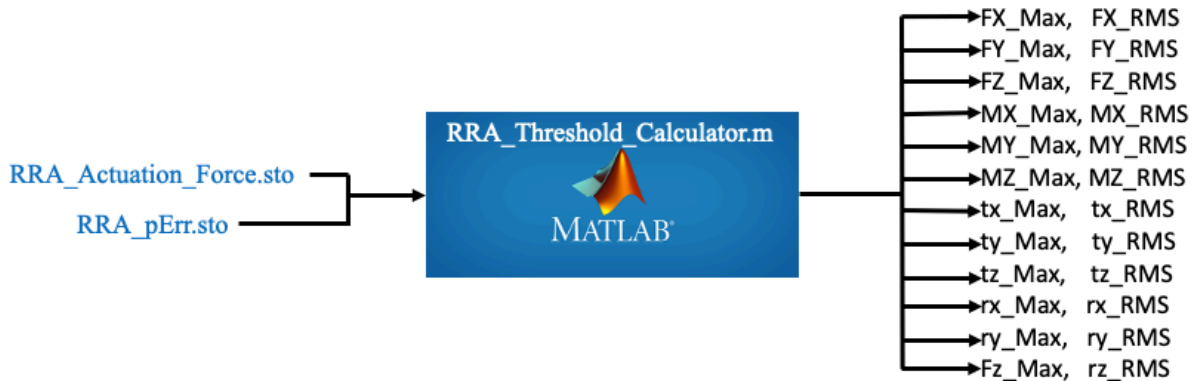


Figure 33: Inputs and outputs for residual forces, moments, and coordinate errors data extraction using Matlab. This code extracts data from two files (blue) generated by each RRA iteration

The input kinematics from IK were used and filtered with a 6Hz lowpass Butterworth filter. RRA tracking tasks, control constraints, actuators, and external loads were added to the model. All integrator settings were set to the default condition. The “Time range to process” was determined by the window of time where all external forces were known. The instances of time where either foot was in contact with the ground and not a force plate were removed from the “time range to

process”. Time instances of (0.4s-1.35s) and (6.84s-16.15s) were used for NW and TC respectively. These windows of time were also used for all subsequent analyses. The mtp_angle_r, mtp_angle_l, subtalar_angle_r, and subtalar_angle_l joints were locked to avoid noise stack up error during differentiation. The result of the residual reduction analysis is a new model with adjusted mass properties and a new set of kinematics that were used as inputs for static optimization and computed muscle control.

2.5.5. Computed Muscle Control

The computed muscle control tool was used to generate a set of muscle forces and activations that were used to drive a model forward in time with a forward dynamic simulation. The inputs and outputs for CMC can be seen in **Figure 34**.

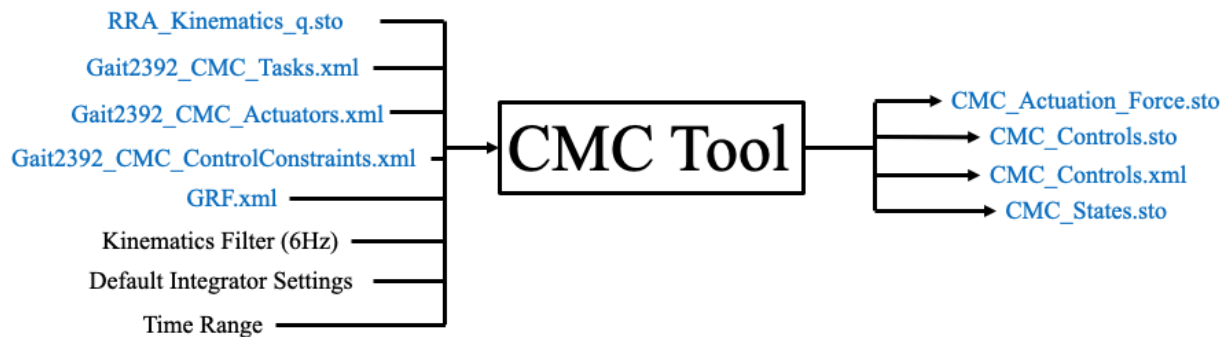


Figure 34: Inputs and outputs for the Computed Muscle Control (CMC) Tool in OpenSim. Imported files are blue while user defined inputs are black

CMC tracking tasks, control constraints, actuators, and external loads were added to the model. The kinematics file computed during RRA, “RRA_Kinematics_q.sto”, for each model and condition were used as the “Desired Kinematics”. The Kinematics were not filtered. Time instances of (0.4s-1.35s) and (6.84s-16.15s) were used for NW and TC respectively. The “CMC look ahead window” was set to (0.01). Integrator settings were set to default conditions for all

trials. Muscle activations, muscle forces and controls were generated as a result of CMC. The results from CMC were used as inputs for Forward dynamics during model calibration.

2.5.6. Static Optimization

The static optimization tool served as the primary tool for calculating muscle forces and served as inputs for joint reaction analysis. Input kinematics from RRA were used, and no filtering was applied. Time instances of (0.4s-1.35s) and (6.84s-16.15s) were used for NW and TC respectively. The step interval was set to 10 and CMC actuators and external loads were applied to the model. Inputs and outputs for the static optimization tool can be seen in **Figure 35**. The results from the static optimization tool are a set of muscle forces and activations along with a set if actuator controls.



Figure 35:Inputs and outputs for the Static Optimization (STO) Tool in OpenSim. Imported files are in blue while user defined inputs are in black

2.5.7. Joint Reaction Analysis

A joint reaction analysis was used to calculate the reaction loads between selected bodies in the MLK model using the Analyze Tool in OpenSim. Kinematics from RRA were used to track the model. Filtering was not applied to the RRA kinematics. CMC actuators and external loads were added to the model. The step interval was set to 10 and muscle forces from static optimization were applied to the model. Joint contact definitions were defined at each condyle with the tibia

plateau being the parent body and the medial and lateral compartments being the child bodies. The joint contact loads were defined in the tibial reference frame with positive y direction directed superior and normal to the tibial plateau. Another joint contact definition was defined between the sagittal articulation frame and the femoral component, where the sagittal articulation frame is was the parent body and the femoral component was the child body. The contact forces and moments were also defined in the tibial reference frame. This definition resolved the sum total of both contact forces at each condyle. These contact definitions were calculated for the right and left knee.

The joint reaction analysis can use muscle forces generated by CMC instead of STO. However, CMC is more computationally expensive, and static optimization is the standard routine outlined in the literature (Lerner et al.). Some studies have shown no difference between joint reaction forces calculated by CMC vs STO (Anderson and Pandy). The inputs and outputs for the joint reaction analysis can be seen in **Figure 36**.

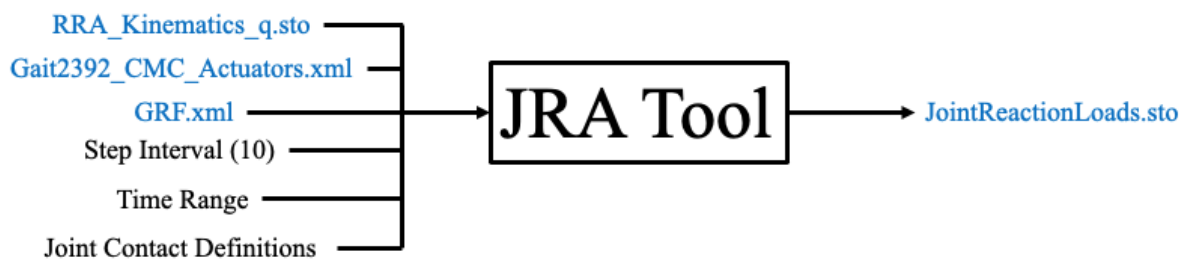


Figure 36: Inputs and outputs for the Joint reaction Analysis (JRA) Tool in OpenSim. Imported files are in blue while user defined inputs are in black

Contact forces and reaction moments were calculated at each definition in all three Cartesian directions in the tibial reference frame. The Y component of the joint contact force, i.e. the force normal to the tibial plateau, was considered to be the joint reaction load at the knee joint.

2.5.8. Forward Dynamics

The forward dynamics tool was used for model calibration and is talked about later in this work. However, inputs to the forward dynamics tool were calculated from computed muscle control. The controls file calculated by CMC is a set of muscle activations and residual actuator controls that are used to drive the model forward in time. Initial states calculated from CMC were added to the model along with CMC actuators and external loads. A kinematic analysis was added to the forward dynamics tool in order to record the joint coordinates that are produced by the forward muscle driven model. Comparing the forward kinematics to the inverse kinematics can be used to determine if the model forces are sufficient to produce the desired motion of the model. This will be discussed later in the calibration section. Inputs and outputs from the forward dynamic analysis can be seen in **Figure 37**.

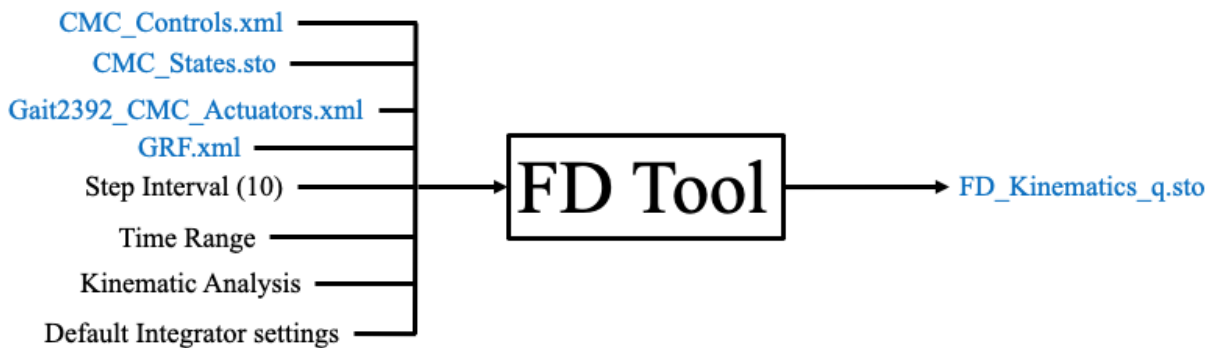


Figure 37: Inputs and outputs for the Forward Dynamics (FD) Tool in OpenSim. Imported files are in blue while user defined inputs are in black

2.6. Gait Characteristics

Results from the joint reaction analysis for Normal Walking and Tai Chi of the right knee during right leg stance phase of gait were analyzed. Stance phase for both walking and Tai Chi is defined by the portion of the gait cycle where the foot is in contact with the ground (Chris Kirtly). The

stance phase of normal walking gait is characterized by the double peak ground reaction force in the superior direction **Figure 38**. The first peak comes from weight acceptance phase just after heel strike. The second peak comes from the push off of the toes just before toe off. This phase of the gait is called push off.

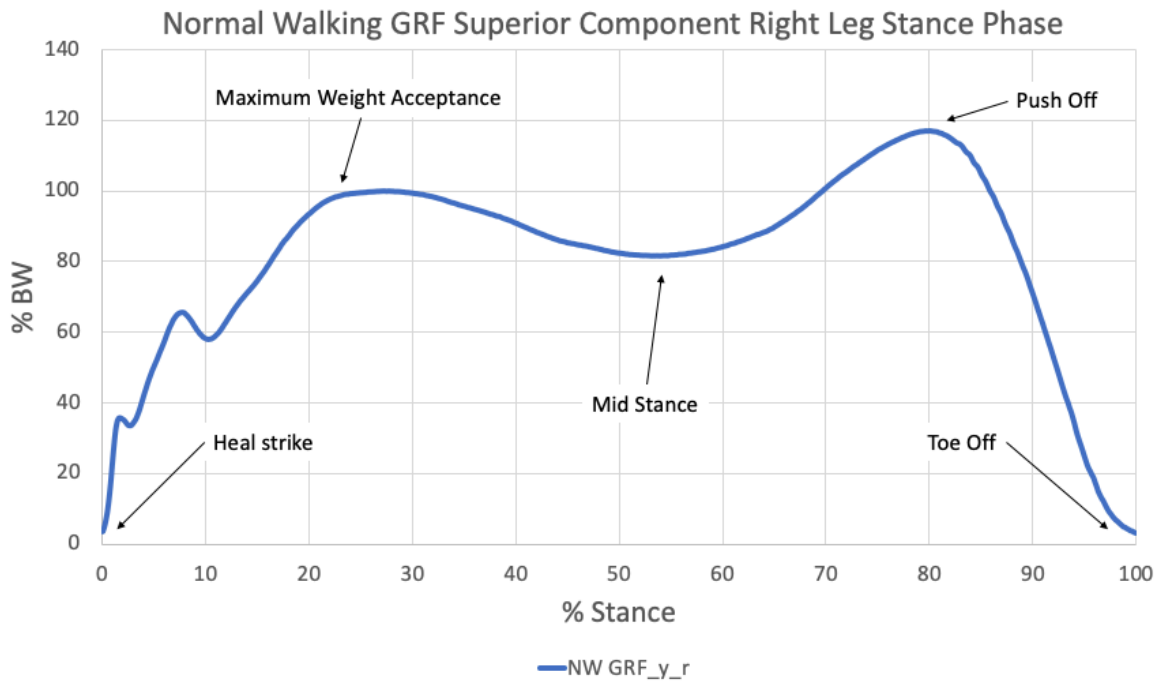


Figure 38: Break down of the classic M-Shape of the vertical ground reaction force for right leg stance phase of Normal Walking. This GRF data comes from the Normal Walking trial used for this study.

The gait cycle of the Tai Chi used in this study can be subdivided into 4 different phases: Double support I, Single Support, Double support II, and Swing, **Figure 39**, (Liu et al.).

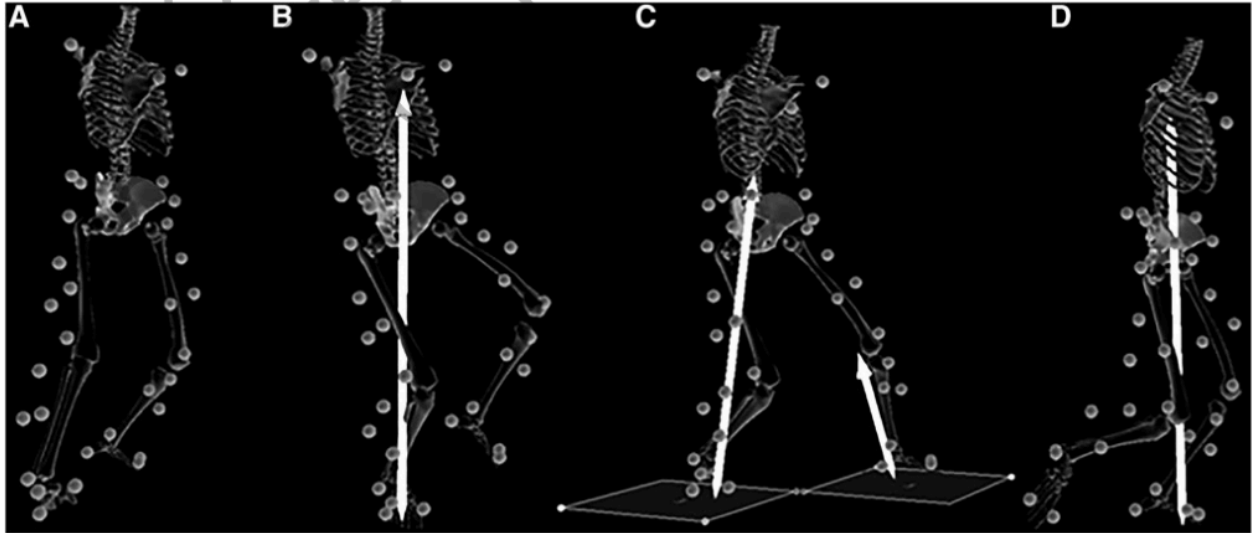


Figure 39: Subphases of the Tai Chi Gait Cycle used for this study: Double support I (A), Single support (B), Double support II (C), Swing (D). Photo courtesy of (Liu et al.).

However, Tai Chi stance phase consist of the first 3 phases of gait cycle, double support I, single support, double support II. As it pertains to the superior component of the ground reaction force, each phase can be seen as a function of right leg stance phase in **Figure 40**.

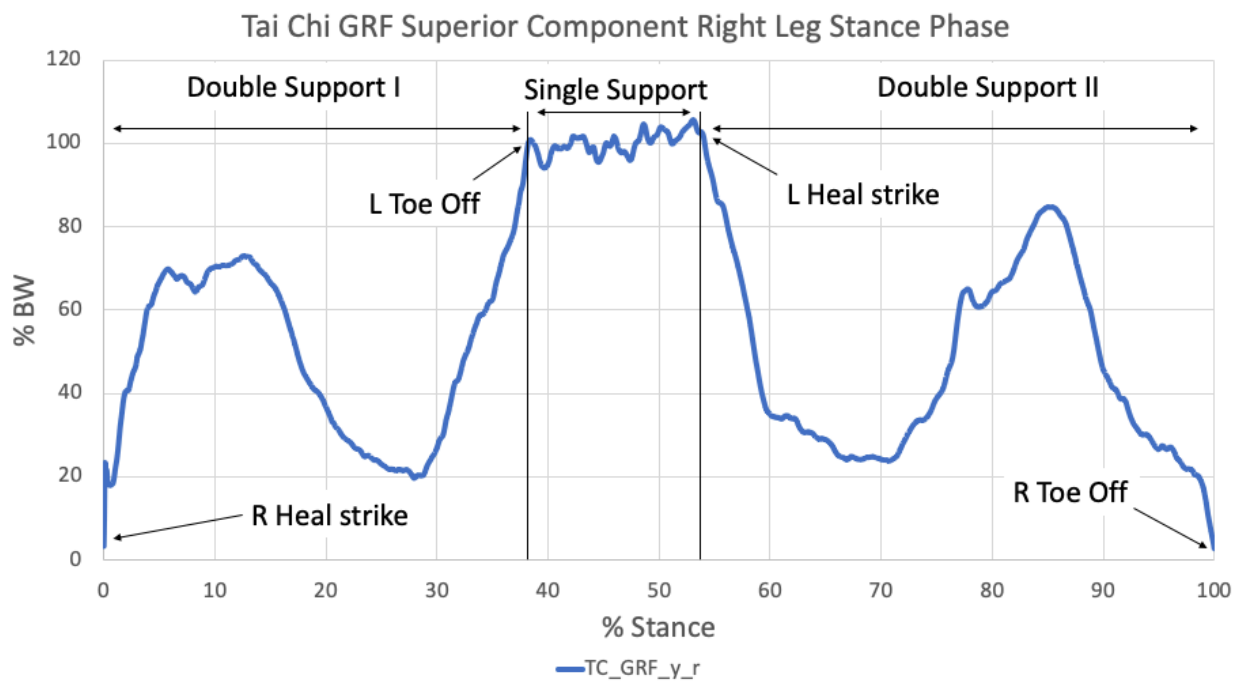


Figure 40: Break down of the of the vertical ground reaction force for right leg stance phase of Tai Chi. This GRF data comes from the Tai Chi trial used for this study.

2.7. Data Analyses

Joint reaction forces at the right knee during stance phase of gait for both trials, Normal Walking and Tai Chi, were used to generate most of the data analysis. Joint reaction loads at each condyle were calculated along with the total joint reaction load at the knee. Joint reaction force data was collected using the OpenSim Analyze tool and imported into Microsoft Excel for data manipulation. The forces were normalized by the body weight (BW) of the subject, **Equation 31**, and analyzed during right leg stance phase of gait for both Tai Chi and Normal Walking.

$$F_{normalized} = \frac{F_{contact}}{m_{subject} * g} * 100 \quad (31)$$

Where $F_{normalized}$ is the percentage of body weight the contact force exhibits, $F_{contact}$ is the joint reaction forces calculated by OpenSim., $m_{subject}$ is the virtual mass of the model, g is the acceleration of gravity. Force normalization was done for the joint contact forces of medial and lateral joint contact force as well as the total joint contact force. As a result, all joint contact forces were plotted as a function of % BW and % stance phase of gait for the right leg. Both the medial and lateral normalized contact loads were divided by the total normalized load at each time step to resolve the percentage of total load that each condyle accepts during gait. Those percentages were then averaged across the stance phase of gait to resolve the mean % total load that each knee compartment accepts during gait, **Equation 32**.

$$Mean_ \% TotalLoad_ med = \frac{\sum_{i=1}^{n_{time\ steps}} \frac{F_{total,i}}{F_{med,i}} + \dots \frac{F_{total,n}}{F_{med,1n}}}{n_{time\ steps}} * 100 \quad (32)$$

Where $n_{time\ steps}$ are the total number of time steps in the stance phase, $F_{total,i}$ it the normalized total contact force at each time step, and $F_{med,i}$ is the normalized contact force at the medial

compartment. A synonymous calculation was performed for the lateral side. The amount of time that each condyle accepts the majority of the total load was determined by dividing the amount of amount of time steps that a respective condyle accepts the majority of the load by the total amount of timesteps record during the stance phase of gait **Equation 33** . This was done for the medial and lateral sides of the right knee for Tai Chi and Normal Walking.

$$Time_MLA_med = \frac{T_{majority}}{T_{total}} * 100 \quad (33)$$

Where ***Time_MLA_med*** is the percentage of time that the medial condyle accepts the majority of the load, ***T_{majority}*** are the number of time steps where the medial condyle accepts over 50% of the total load, and ***T_{total}*** is the total amount of time steps recorded during stance phase for which there is data (note: the capture window for OpenSim is smaller than time window for stance phase). Max and mean normalized forces were calculated for total, medial, and lateral contact forces of the right leg during stance phase of TC and NW gaits. All the previously described calculations were performed for each gait cycle and for subsequent altered TFA angles.

Other plots were generated in Excel from the data collected from the other OpenSim analyses. Muscle forces were collected and normalized with the same process, **Equation 31**, as previously described and plotted as a function of % Stance phase of the right leg. This was done to help characterize the efficacy of the contact loads in the model. OpenSim muscle activations and EMG muscle activations were plotted as a function of % Stance phase of the right leg as well. Muscle activation and EMG plots were used to independently validate the model. This is expounded upon in the validation section.

2.8. Statistical Analyses

Two sample t-test were used to compare the joint contact forces (total, medial % total load, lateral % total load) to test for significant difference of the two mean contact load values of Tai Chi vs Normal Walking. The null and alternate hypothesis were used for each one sided two sample t-test defined by **Equations 34** and **Equation 35** respectively.

$$H_0: \mu_1 = \mu_2 \quad (34)$$

$$H_a: \mu_1 > \mu_2 \quad (35)$$

Subsequent paired t-test were used to test for significance in compartmental knee joint loading as a function of tibiofemoral alignment angle. The normalized force at each time step were used as the sample pair for the paired t-test calculation. This was done for all trials of varied tibiofemoral alignment angle to test for significance difference in contact force at each time step. A Bessel spline function was used in excel to interpolate data that did not have corresponding time step values. This was done so that each data pair in the paired t-test would be at equivalent time steps. The null and alternative hypothesis were used for the one sided paired t-test between two sample means defined by **Equations 36** and **37** respectively

$$H_0: \mu_{diff} = 0 \quad (36)$$

$$H_a: \mu_{diff} > 0 \quad (37)$$

Where μ_{diff} is the mean difference between each joint contact force at a given time step defined by **Equation 38**.

$$\mu_{diff} = \frac{\sum_{i=0}^n x_{1,1} - x_{2,1} + \dots x_{1,n} - x_{2,n}}{n} \quad (38)$$

All statistical analyses were conducted with $\alpha = 0.005$. All statistical calculations were performed in excel. Descriptive statistics were calculated for each parameter of each trail and can be found in **Appendix C** and **Appendix D**.

Chapter 3: Results

3.1. Introduction

Normalized joint reaction loads for each trial, Normal Walking and Tai Chi of the nominal model, TFA=177.16 deg., were compared and tested for the significant difference of means for each parameter of each trail. Subsequently, the TFA angle of each model was altered for each trial, varus alignment (TFA=172 Deg.) and valgus alignment (TFA= 188deg.). The routine was redone for each trail at each altered TFA angle. Normalized joint reaction loads of each trial, NW and TC, with all three TFA angles (177.16deg., 172 deg., and 188 deg.) were directly compared. Two sample t-tests and paired t-tests were used to determine significant differences of mean contact loads of the various trials. All contact forces were calculated with muscles from static optimization.

3.2. Joint Contact Forces of Tai Chi and Normal Walking for the Nominal Model

3.2.1. Nominal Normal Walking

Normalized joint contact forces for the Normal Walking nominal model can be seen in **Figure 41**.

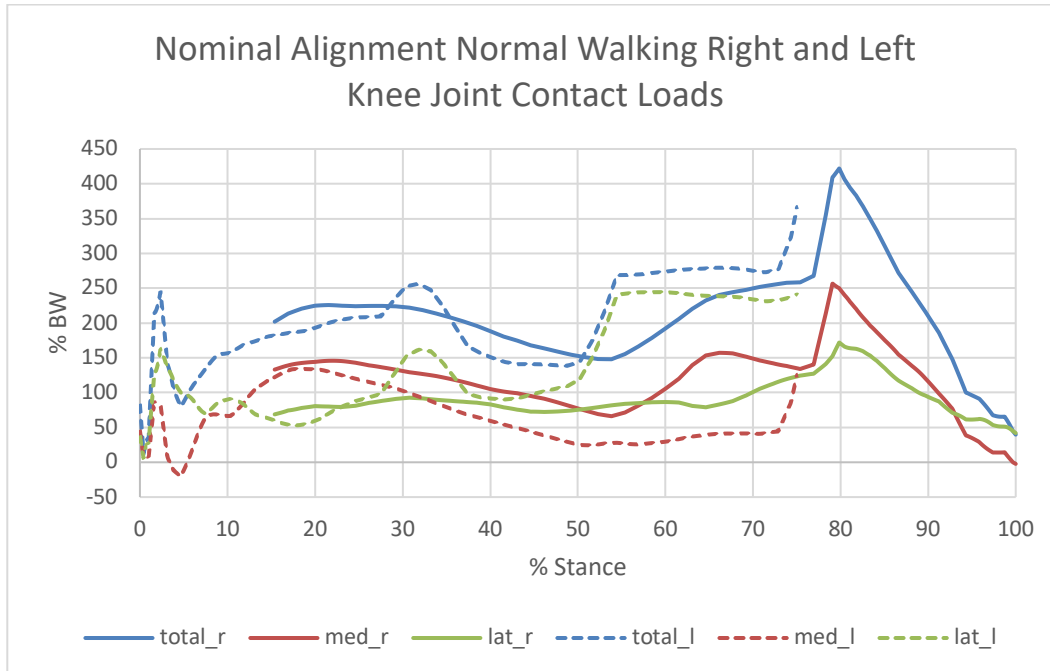


Figure 41: Normalized joint contact loads of the total, medial, and lateral left and right knee compartments during stance phase of Normal Walking gait with nominal alignment, TFA=177.16 degrees.

The total joint contact force of the nominal Normal Walking trial experienced a peak total load of 417 % BW at about 80% stance phase. The medial and lateral condyles experienced maximum loads of 247.45% BW and 170.53 % BW, respectively, at about 80 % stance phase. The average medial, lateral and total normalized contact loads throughout stance phase were 120.23 % BW, 91.06 % BW, and 211.29 % BW respectively. The medial compartment accepted about 54.35 % of the total load on average and the time of the majority load accepted (MLA) was 82.14% of the stance time (ST). In other words, the medial compartment accepts a majority of the load 82.14% of the time during stance phase. Conversely, the lateral compartment accepted 45.65% of the total load on average and accepted a majority of the load 17.86 % of the stance time. Contact force as a percentage of body weight and as a percent of total contact load can be seen easily in **Figure 42** and **Figure 43** respectively. Similar plots for the left leg can be seen in **Appendix C**. A table of

all meaningful results of the nominal Normal Walking trail can be seen in **Table 9**. A similar table of the left leg results can be seen in **Appendix C**.

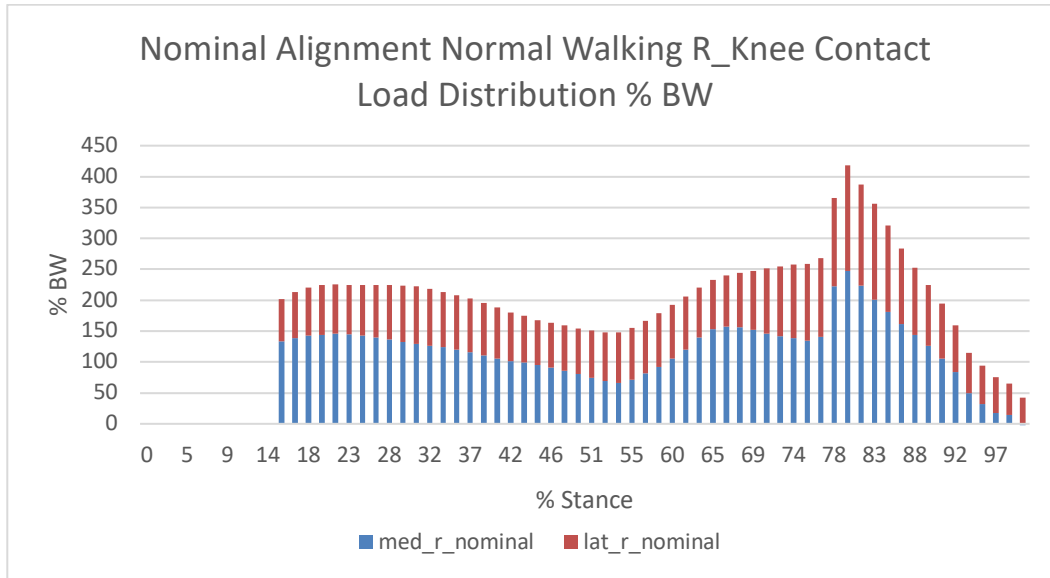


Figure 42: Right Medial and lateral normalized joint contact loads summed to show the total contact loads as a percentage of body weight during stance phase of Normal Walking gait with nominal alignment, TFA=177.16 degrees.

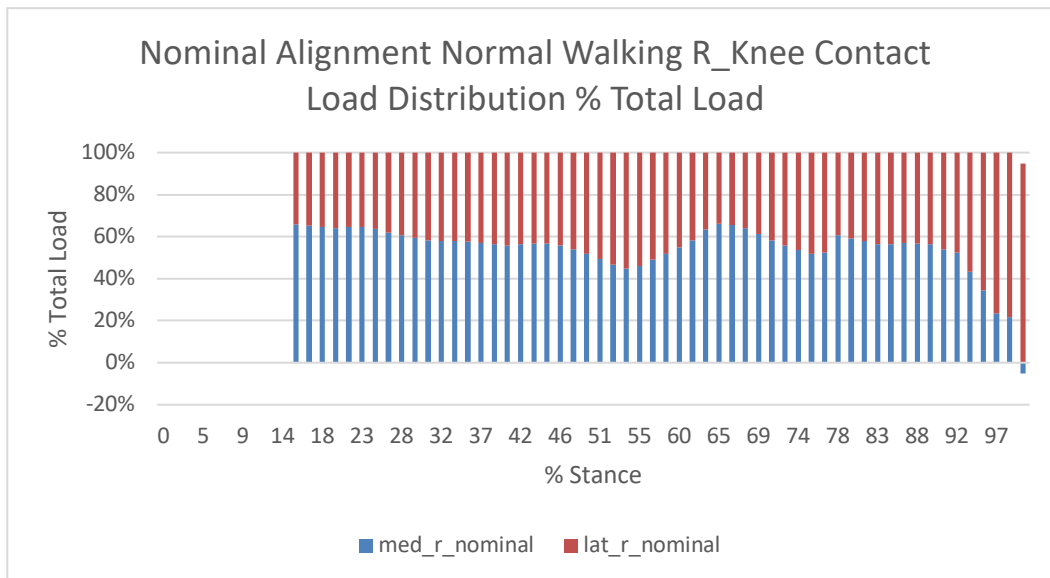


Figure 43: Right Medial and lateral normalized joint contact load distribution as a percentage of the total contact load during stance phase of Normal Walking gait with nominal alignment, TFA=177.16 degrees.

Table 9: Statistical results calculated for the Normal Walking, right and left knee, stance phase, nominal tibiofemoral alignment, TFA=177.16 degrees.

Nominal Normal Walking Joint Contact Load Data			
Parameter	Right	Left	Unit
Max_total	417.98	321.80	%BW
Max_med	247.45	86.48	%BW
Max_lat	170.53	357.07	%BW
Mean_total	211.29	179.12	%BW
Mean_med	120.23	-17.06	%BW
Mean_lat	91.06	196.18	%BW
Mean_%TotalLoad_med	54.35	-7.54	%TL
Mean_%TotalLoad_lat	45.65	107.54	%TL
Time_MLA_med	82.14	5.36	%ST
Time_MLA_lat	17.86	94.64	%ST

3.2.2. Nominal Tai Chi

Normalized joint contact forces for Nominal Tai Chi trial can be seen in **Figure 44**.

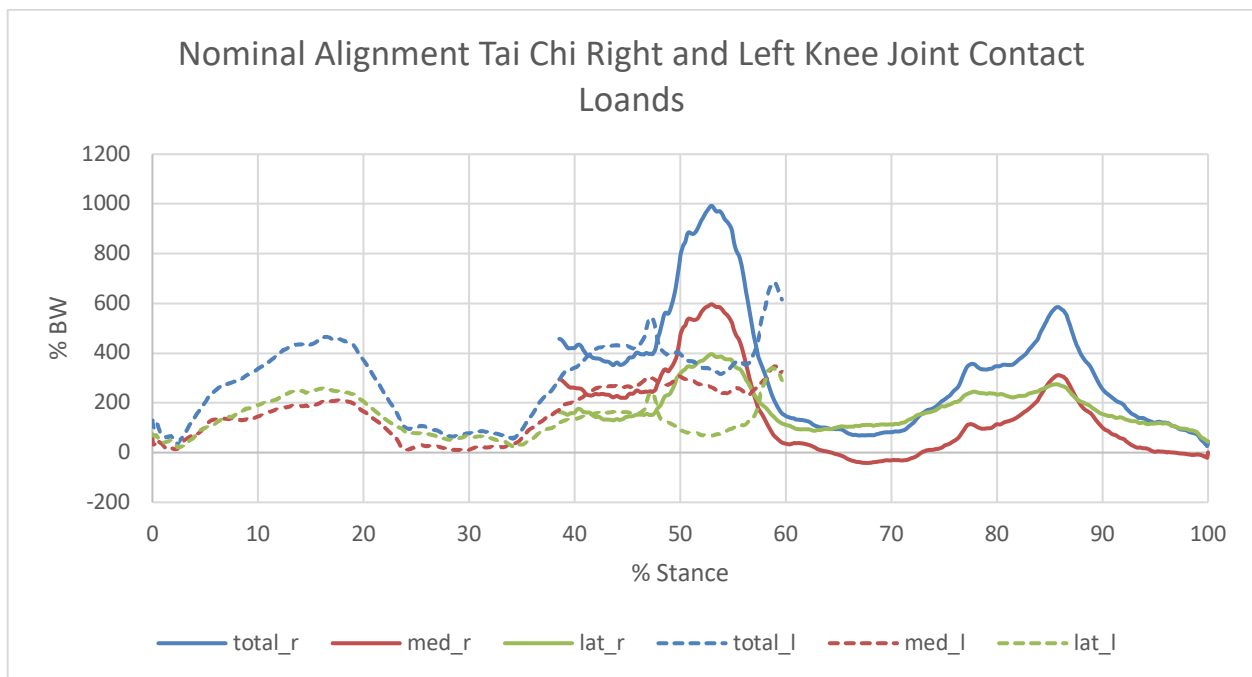


Figure 44: Normalized joint contact loads of the total, medial, and lateral right and left knee compartments during stance phase of Tai Chi gait with nominal alignment, TFA=177.16 degrees.

The total joint contact load for the nominal Tai Chi trial experienced peak load of 992.43 % BW at about 54% of stance phase during single support phase of Tai Chi gait. A second peak of 585.02

% BW occurs about 85.72 % stance phase during double support phase II of Tai Chi gait. The medial and lateral compartments experienced maximum loads of 596.42 % BW and 396% B, respectively at about 54% stance phase. The average medial, lateral and total normalized contact loads throughout stance phase were 152.23%BW, 181.54%BW and 333.77%BW respectively. The medial compartment accepted about 27.72% of the total load on average and accepted the majority of the load 34.8% of the stance time. Conversely, the lateral compartment accepted 72.65% of the total load on average and accepted a majority of the load 65.2 % of the stance time. Joint contact forces as a percentage of body weight and as a percent of total contact load can be seen easily in **Figure 45** and **Figure 46** respectively. Similar plots for the left leg can be seen in **Appendix C**. A table of all meaningful results of the Nominal Tai Chi trail can be seen in **Table 10**. A similar table of the left leg results can be seen in **Appendix C**.

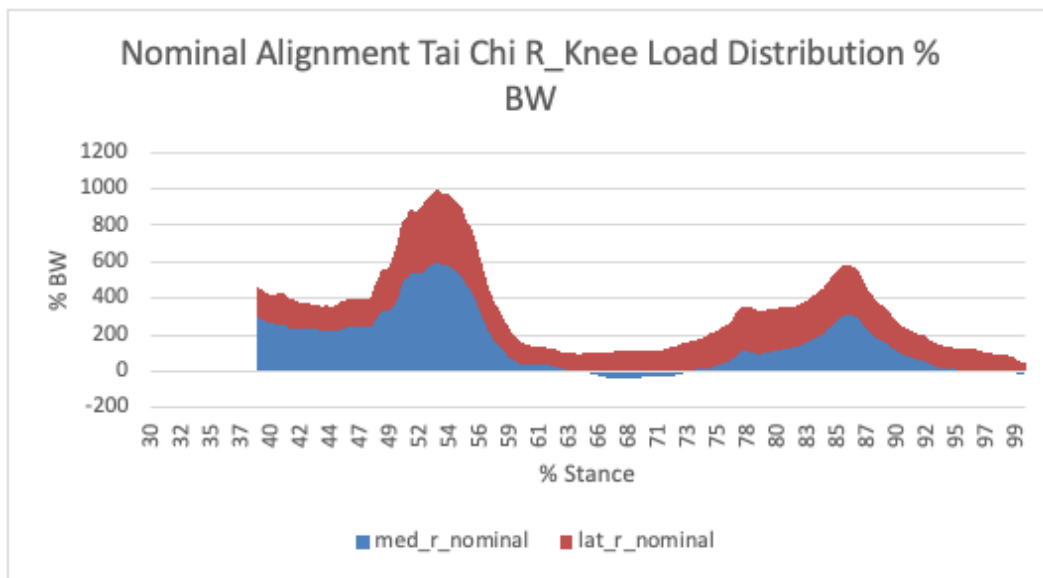


Figure 45: Medial and lateral normalized joint contact loads summed to show the total contact loads as a percentage of body weight during stance phase of Tai Chi gait with nominal alignment, TFA=177.16 degrees.

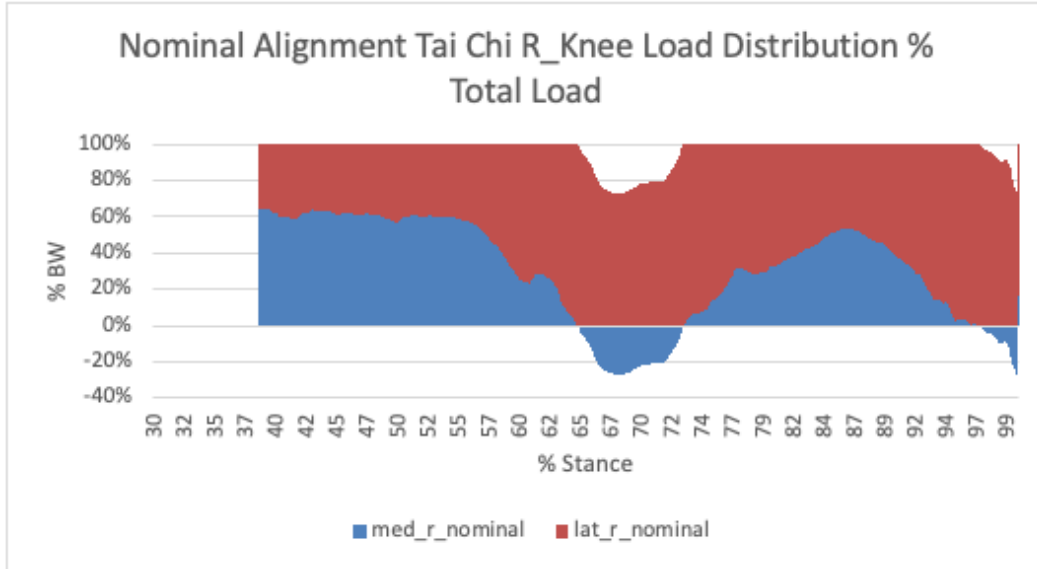


Figure 46: Medial and lateral normalized joint contact load distribution as a percentage of the total contact load during stance phase of Tai Chi gait with nominal alignment, TFA=177.16 degrees.

Table 10: Statistical results calculated for the Tai Chi, right and left knee, stance phase, nominal tibiofemoral alignment, TFA=177.16 degrees.

Nominal Tai Chi Joint Contact Load Data			
Parameter	Right	Left	Unit
Max_total	992.43	685.66	%BW
Max_med	596.42	347.17	%BW
Max_lat	396.00	340.36	%BW
Mean_total	333.77	291.72	%BW
Mean_med	152.23	158.20	%BW
Mean_lat	181.54	133.52	%BW
Mean_%TotalLoad_med	27.35	49.74	%TL
Mean_%TotalLoad_lat	72.65	50.26	%TL
Time_MLA_med	34.8	48.58	%ST
Time_MLA_lat	65.2	51.42	%ST

3.2.3. Varus Normal Walking

Normalized joint contact forces for the Varus Normal Walking trial can be seen in **Figure 47**. A similar plot of the left knee joint contact forces can be seen in **Appendix C**.

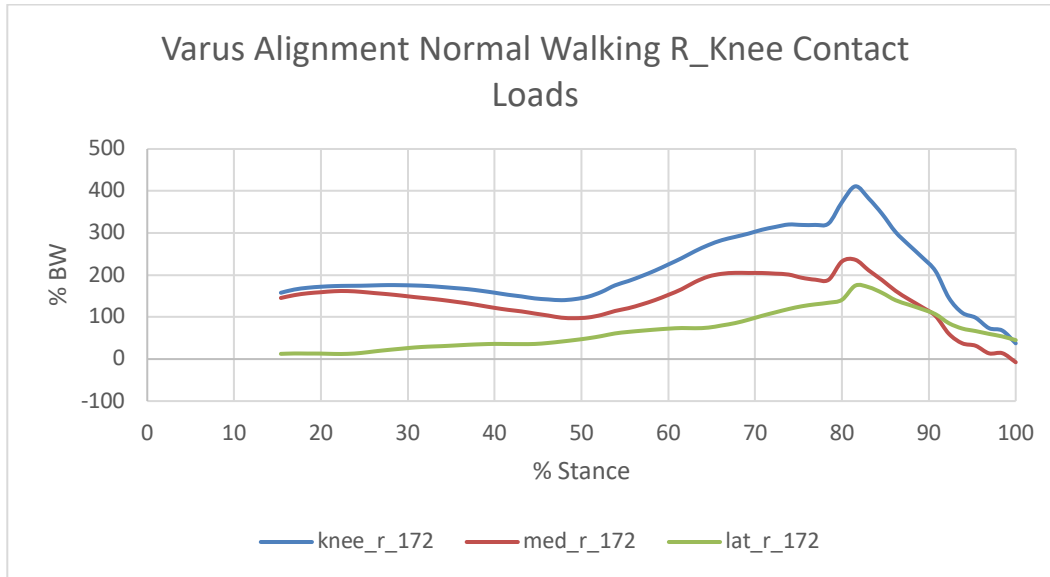


Figure 47: Normalized joint contact loads of the total, medial, and lateral right knee compartments during stance phase of Normal Walking gait with varus alignment, TFA=172 degrees.

The total normalized joint contact load for the Varus Normal Walking trial experienced peak loads of 411.4%BW at about 82% of stance phase. The medial and lateral condyles experienced maximum loads of 236.25%BW and 174.76%BW, respectively, at about 82% stance phase. The average medial, lateral, and total normalized contact loads throughout stance phase were 141.05%BW, 67.53%BW and 208.58%BW, respectively. The medial compartment accepted about 66.70 % of the total load on average and accepted the majority of the load 87.5 % of the time during stance phase. Conversely, the lateral compartment accepted 33.30% of the total load on average and accepted a majority of the load 12.5 % of the stance time. Contact forces as a percentage of body weight and as a percent of total contact load can be seen easily in **Figure 48** and **Figure 49** respectively. Similar plots for the left leg can be seen in **Appendix C**. A table of all meaningful results of the Varus Normal Walking trail can be seen in **Table 11**. A similar table of the left leg results can be seen in **Appendix C**.

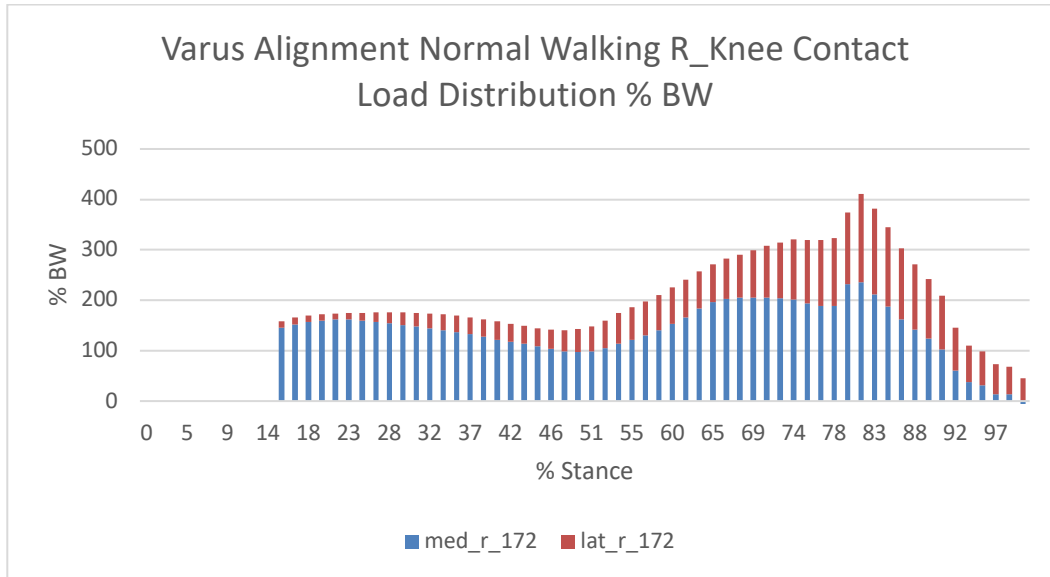


Figure 48: Medial and lateral normalized joint contact loads summed to show the total contact loads as a percentage of body weight during stance phase of Normal Walking gait with varus alignment, TFA=172 degrees.

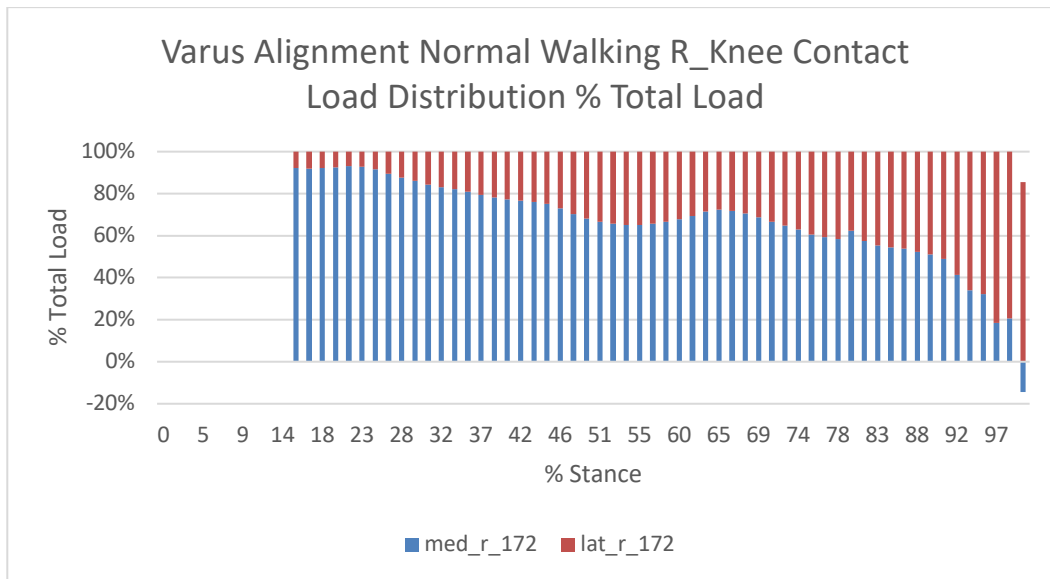


Figure 49: Medial and lateral normalized joint contact load distribution as a percentage of the total contact load during stance phase of Normal Walking gait with varus alignment, TFA=172 degrees.

Table 11: Statistical results calculated for the Normal Walking, right and left knee, stance phase, varus tibiofemoral alignment, TFA=172 degrees.

Varus Normal Walking Joint Contact Load Data			
Parameter	Right	Left	Unit
Max_total	411.14	344.12	%BW
Max_med	236.25	352.12	%BW
Max_lat	174.89	113.22	%BW
Mean_total	208.58	175.12	%BW
Mean_med	141.05	180.56	%BW
Mean_lat	67.53	-5.44	%BW
Mean_%TotalLoad_med	66.70	118.44	%TL
Mean_%TotalLoad_lat	33.30	-18.44	%TL
Time_MLA_med	87.5	91.07	%ST
Time_MLA_lat	12.5	8.93	%ST

3.2.4. Varus Tai Chi

Normalized joint contact forces for Varus Tai Chi trial can be seen in **Figure 50**. A similar plot of the left knee joint contact forces can be seen in **Appendix C**.

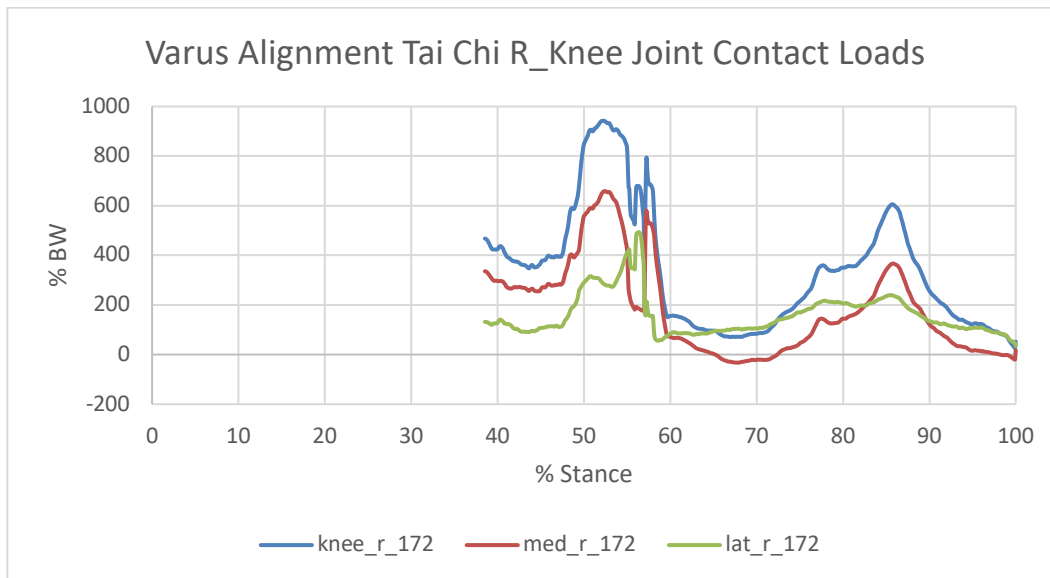


Figure 50: Normalized joint contact loads of the total, medial, and lateral right knee compartments during stance phase of Tai Chi gait with varus alignment, TFA=172 degrees.

The total normalized joint contact load for the Varus Tai Chi trial experienced a peak contact load of 942.33%BW at about 54% of stance phase during single support phase of Tai Chi gait. A second peak of 604.84%BW occurs about 85.82% of stance phase during double support phase II of Tai

Chi gait. The medial and lateral compartments experienced maximum loads of 659.16%BW and 493.70%BW respectively at about 54% stance phase. The average medial, lateral and total normalized contact loads throughout stance phase were 182.80%BW, 159.62%BW and 342.43%BW, respectively. The medial compartment accepted 39.91% of the total load on average and accepted the majority of the load 42.56% of the stance time. Conversely, the lateral compartment accepted 63.09% of the total load on average and accepted a majority of the load 57.44 % of the stance time. Contact forces as a percentage of body weight and as a percent of total contact load can be seen easily in **Figure 51** and **Figure 52**, respectively. Similar plots for the left leg can be seen in **Appendix C**. A table of all meaningful results of the Varus Normal Walking trail can be seen in **Table 12**. A similar table of the left leg results can be seen in **Appendix C**.

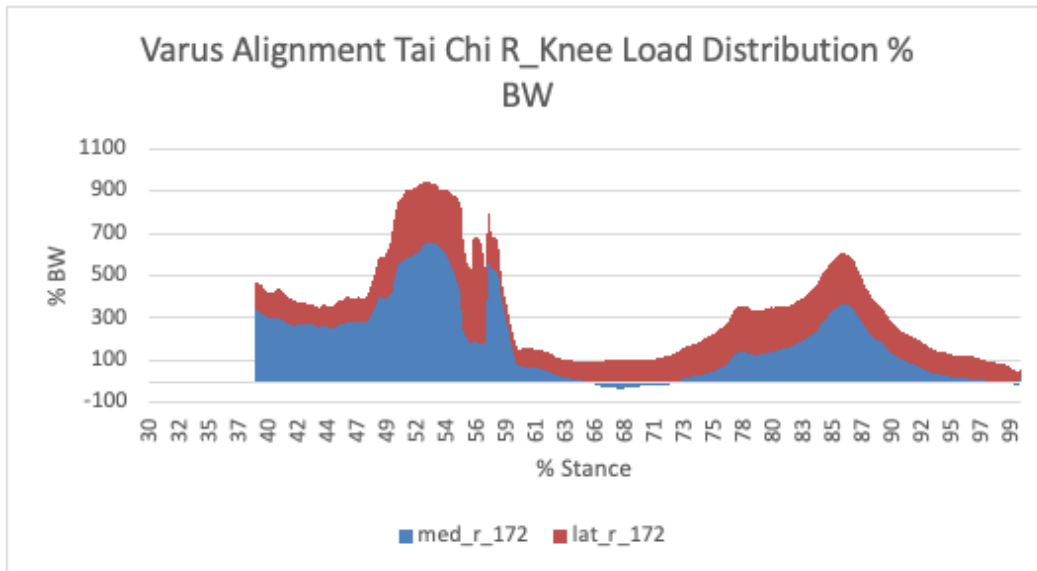


Figure 51: Medial and lateral normalized joint contact loads summed to show the total contact loads as a percentage of body weight during stance phase of Tai Chi gait with varus alignment, TFA=172 degrees.

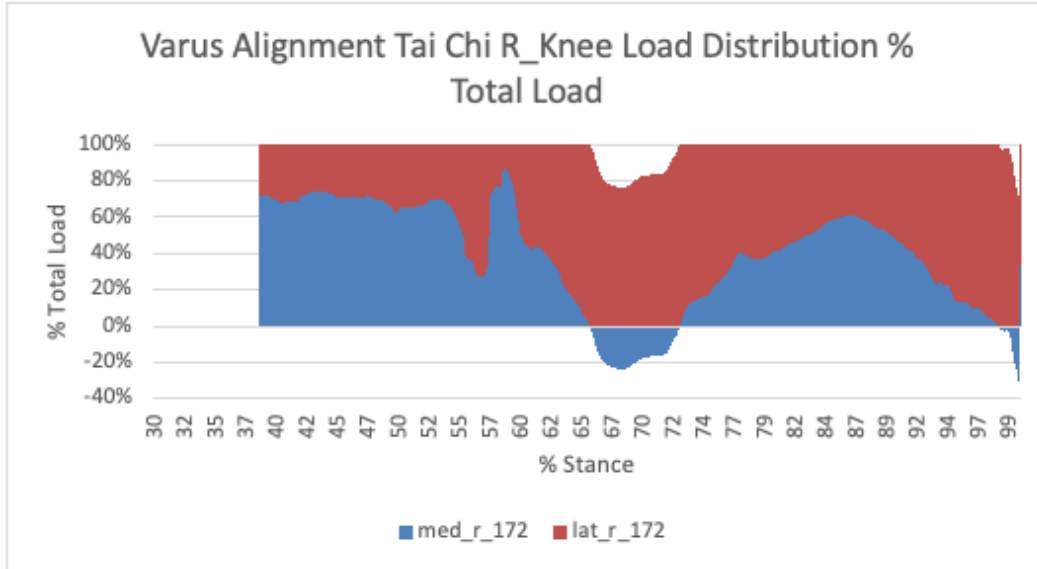


Figure 52: Medial and lateral normalized joint contact load distribution as a percentage of the total contact load during stance phase of Tai Chi gait with varus alignment, TFA=172 degrees.

Table 12: Statistical results calculated for the Tai Chi, right and left knee, stance phase, varus tibiofemoral alignment, TFA=172 degrees.

Varus Tai Chi Joint Contact Load Data			
Parameter	Right	Left	Unit
Max_total	942.33	679.43	%BW
Max_med	659.19	393.78	%BW
Max_lat	493.70	287.45	%BW
Mean_total	342.43	291.50	%BW
Mean_med	182.80	183.81	%BW
Mean_lat	159.62	107.69	%BW
Mean_%TotalLoad_med	36.91	59.93	%TL
Mean_%TotalLoad_lat	63.09	40.07	%TL
Time_MLA_med	42.56	78.95	%ST
Time_MLA_lat	57.44	21.05	%ST

3.2.5. Valgus Normal Walking

Normalized joint contact forces for the Valgus Normal Walking trial can be seen in **Figure 53**. A similar plot of the left knee joint contact forces can be seen in **Appendix C**.

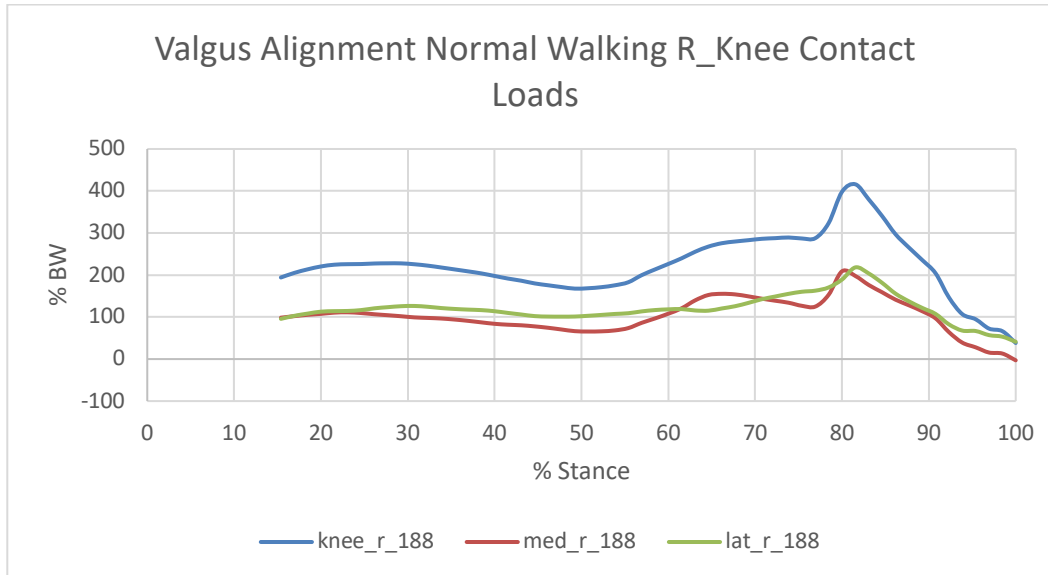


Figure 53: Normalized joint contact loads of the total, medial, and lateral right knee compartments during stance phase of Normal Walking gait with valgus alignment, TFA=188 degrees.

The total normalized joint contact load for the Valgus Normal Walking trial experienced a peak contact load of 415.92%BW at about 82% of stance phase. The medial and lateral compartments experienced maximum loads of 208.98%BW and 218.20%BW, respectively, at about 82% stance phase. The average medial, lateral and total normalized contact loads throughout stance phase were 103.50%BW, 120.05%BW, and 223.55%BW, respectively. The medial compartment accepted 44.06% of the total load on average and accepted the majority of the load for 16.07% of the stance phase. Conversely, the lateral compartment accepted 55.94% of the load on average and accepted a majority of the load 83.93% of the stance time. Contact forces as a percentage of body weight and as a percent of total contact load can be seen easily in **Figure 54** and **Figure 55**, respectively. Similar plots for the left leg can be seen in **Appendix C**. A table of all meaningful results of the Valgus Normal Walking trail can be seen in **Table 13**. A similar table of the left leg results can be seen in **Appendix C**.

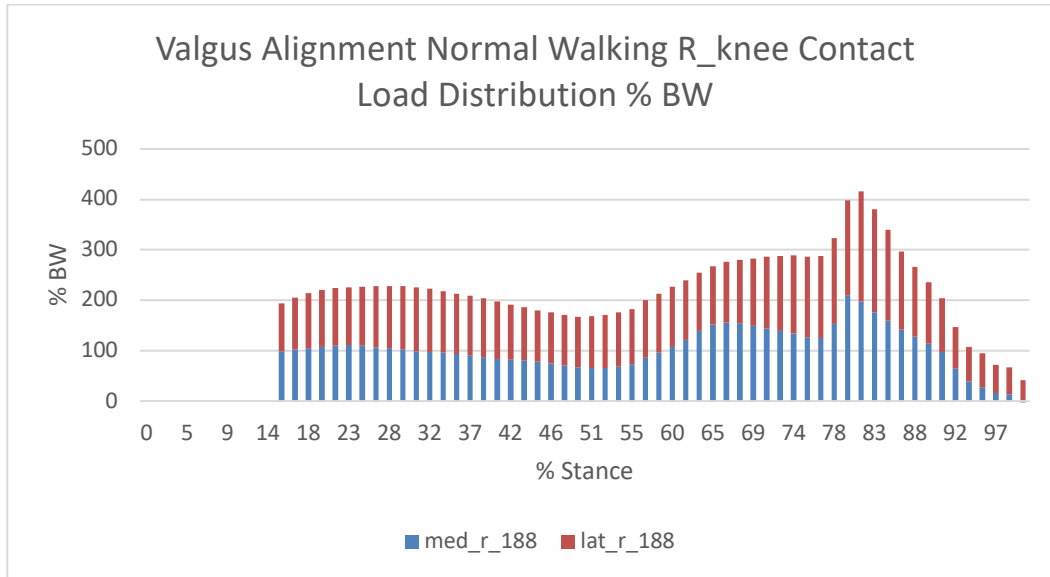


Figure 54: Medial and lateral normalized joint contact loads summed to show the total contact loads as a percentage of body weight during stance phase of Normal Walking gait with valgus alignment, TFA=188 degrees.

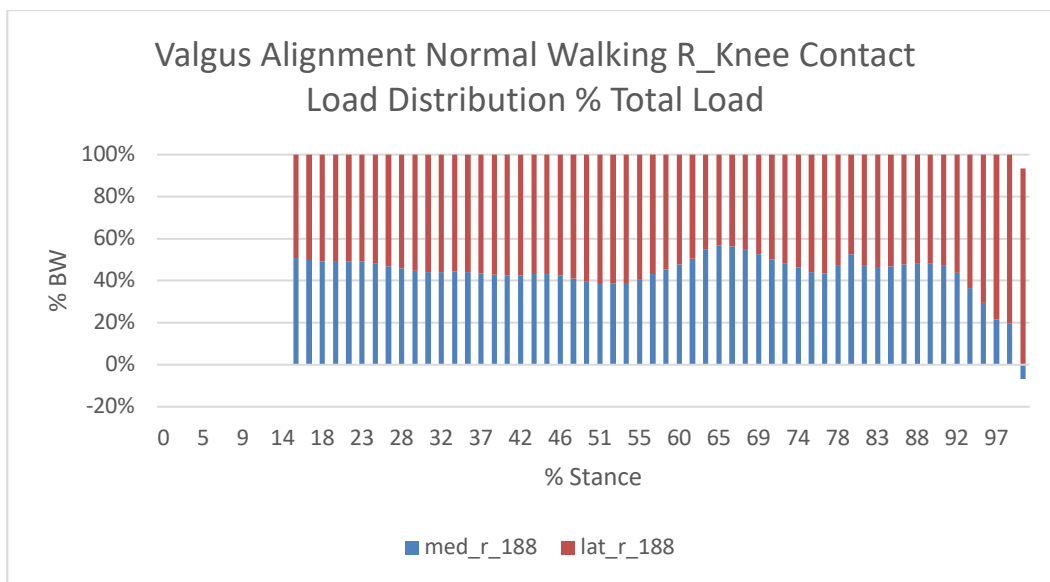


Figure 55: Medial and lateral normalized joint contact load distribution as a percentage of the total contact load during stance phase of Normal Walking gait with valgus alignment, TFA=188 degrees.

Table 13: Statistical results calculated for the Normal Walking, right and left knee, stance phase, valgus tibiofemoral alignment, TFA=188 degrees.

Valgus Normal Walking Joint Contact Load Data			
Parameter	Right	Left	Unit
Max_total	415.92	430.56	%BW
Max_med	208.98	196.54	%BW
Max_lat	218.20	234.01	%BW
Mean_total	223.55	197.69	%BW
Mean_med	103.50	70.80	%BW
Mean_lat	120.05	126.89	%BW
Mean %TotalLoad_med	44.06	33.58	%TL
Mean %TotalLoad_lat	55.94	66.42	%TL
Time_MLA_med	16.07	3.57	%ST
Time_MLA_lat	83.93	96.43	%ST

3.2.6. Valgus Tai Chi

Normalized joint contact forces for the Valgus Tai Chi trial can be seen in **Figure 56**. A similar plot of the left knee joint contact forces can be seen in **Appendix C**.

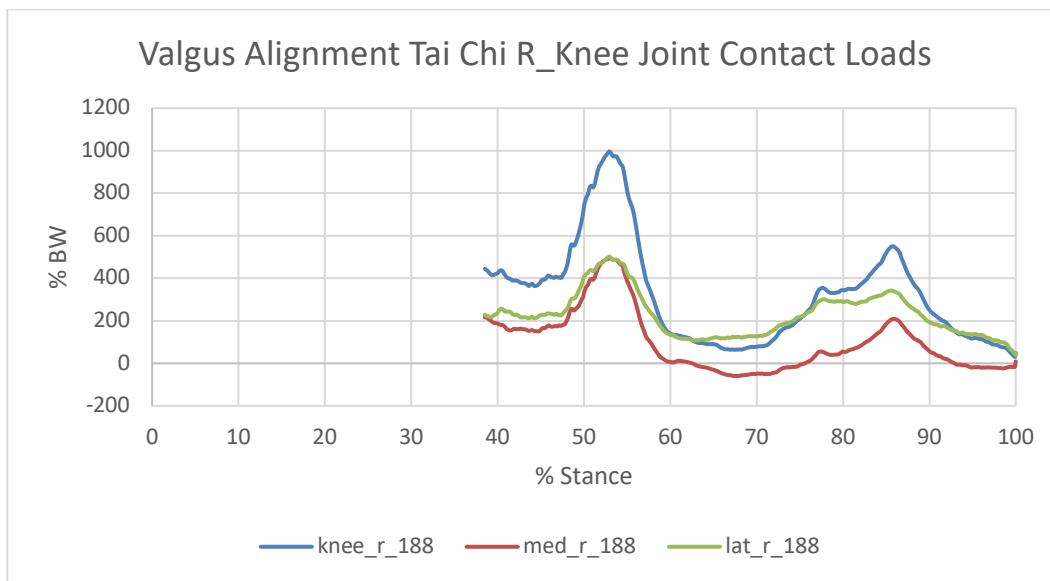


Figure 56: Normalized joint contact loads of the total, medial, and lateral right knee compartments during stance phase of Tai Chi gait with valgus alignment, TFA=188 degrees.

The total normalized joint contact load for the Valgus Tai Chi trial experienced a peak contact load of 995.87 % BW at about 53% of stance phase during single support phase of Tai Chi gait. A

second peak of 550.19 % BW occurs about 86% stance phase during double support phase II of Tai Chi gait. The medial and lateral condyles experienced maximum loads of 494.45%BW and 501.42%BW, respectively, at about 53% stance phase. The average medial, lateral and total normalized contact loads throughout stance phase were 97.80%BW, 228.86%BW, and 326.66%BW, respectively. The medial compartment accepted 9.22% of the total load on average and accepted the majority of the load 1.16% of the stance time. Conversely, the lateral compartment accepted 90.78% of the total load on average and accepted a majority of the load 98.84 % of the stance time. Contact forces as a percentage of body weight and as a percent of total contact load can be seen easily in **Figure 57** and **Figure 58**, respectively. Similar plots for the left leg can be seen in **Appendix C**. A table of all meaningful results of the Valgus Tai Chi trail can be seen in **Table 14**. A similar table of the left leg results can be seen in **Appendix C**.

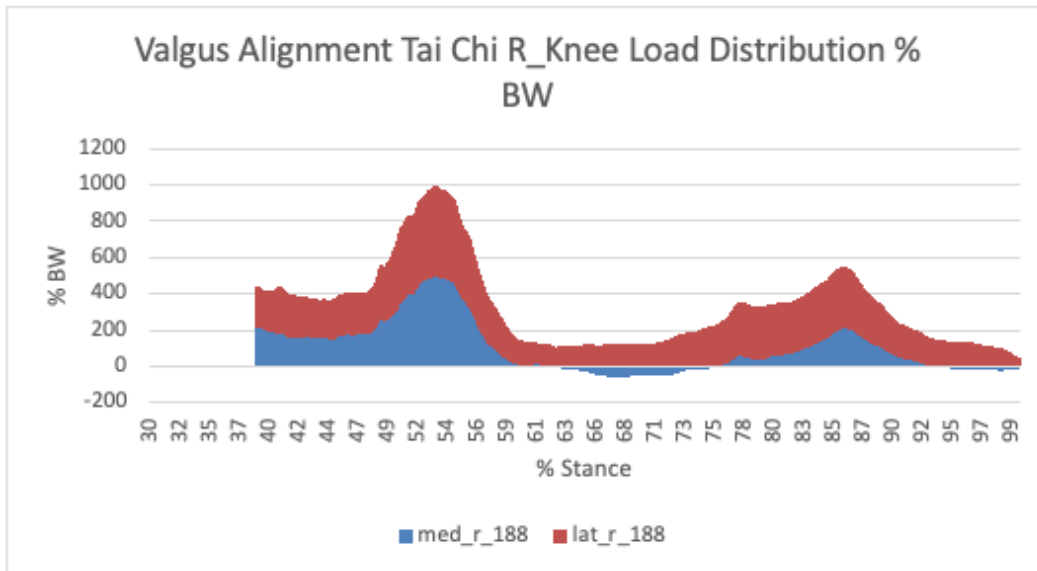


Figure 57: Medial and lateral normalized joint contact loads summed to show the total contact loads as a percentage of body weight during stance phase of Tai Chi gait with valgus alignment, TFA=188 degrees.

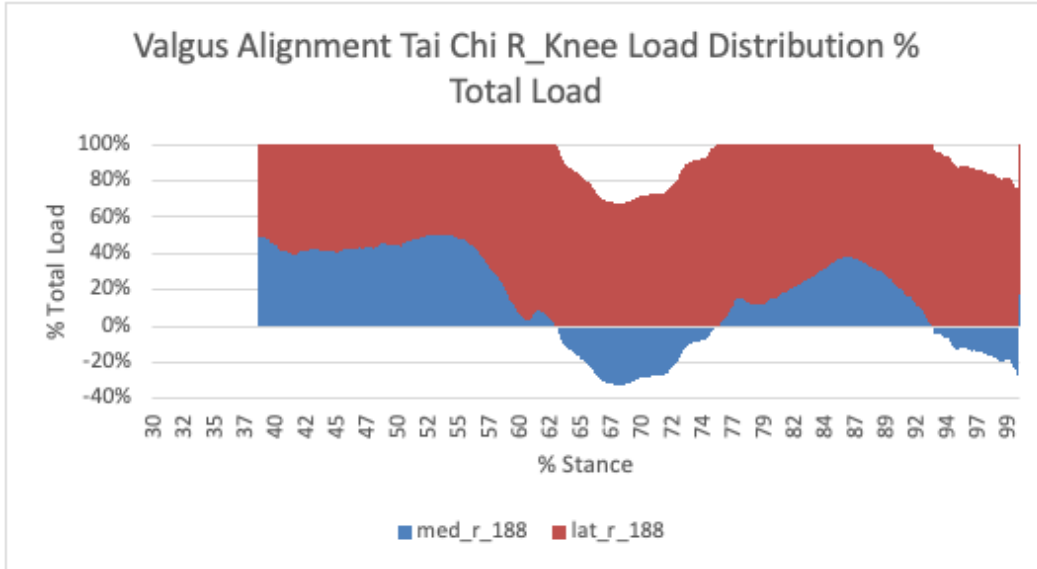


Figure 58: Medial and lateral normalized joint contact load distribution as a percentage of the total contact load during stance phase of Tai Chi gait with Valgus alignment, TFA=188 degrees.

Table 14: Statistical results calculated for the Normal Walking, right and left knee, stance phase, valgus tibiofemoral alignment, TFA=188 degrees.

Valgus Tai Chi Joint Contact Load Data			
Parameter	Right	Left	Unit
Max_total	995.87	723.84	%BW
Max_med	494.45	271.10	%BW
Max_lat	501.42	455.09	%BW
Mean_total	326.66	292.97	%BW
Mean_med	97.80	106.29	%BW
Mean_lat	228.86	186.68	%BW
Mean_%TotalLoad_med	9.22	28.52	%TL
Mean_%TotalLoad_lat	90.78	71.48	%TL
Time_MLA_med	1.16	0	%ST
Time_MLA_lat	98.84	100	%ST

3.3. Comparing Results

3.3.1. Nominal Normal Walking Vs. Nominal Tai Chi

When comparing Tai Chi to Normal Walking, the max total load increased by 574.45 %BW, while the mean total load increased by 122.48 %BW. When looking at the medial compartment the max load increased by 348.98 %BW, mean medial load increased by 32 %BW when comparing Tai

Chi to Normal Walking. For the medial compartment the percentage of total accepted decreased by 27 %TL, and the time of majority load accepted decreased by 47.34 %ST. All mean differences were significant (P-value<0.005). Conversely, when looking at the lateral component, the max load increased by 225.47 % BW while the mean load increased by 90.48 % BW. When looking at the load distribution, the percentage of total load for the lateral component increased by 27 %TL, and the time that lateral load accepts the majority of the load increased by 47.34 %ST. All mean differences were significant (P-value<0.005). A comparison of Tai Chi data to Normal Walking data for the right knee can be seen in **Table 15**. A similar table of the left knee results can be seen in **Appendix D**.

Table 15: Statistical comparisons of normalized joint contact forces for the right knee nominal alignment of Tai Chi and Normal Walking.

Nominal Tai Chi Vs. Normal Walking Right Knee Comparative Statistics					
	NW	TC	Diff (TC-NW)		P-Value
Max_total	417.98	992.43	574.45	%BW	
Max_med	247.45	596.42	348.98	%BW	
Max_lat	170.53	396.00	225.47	%BW	
Mean_total	211.29	333.77	122.48	%BW	p<0.005
Mean_med	120.23	152.23	32.00	%BW	p<0.005
Mean_lat	91.06	181.54	90.48	%BW	p<0.005
Mean_%TotalLoad_med	54.35	27.35	-27.00	%TL	p<0.005
Mean_%TotalLoad_lat	45.65	72.65	27.00	%TL	p<0.005
Time_MLA_med	82.14	34.8	-47.34	%ST	
Time_MLA_lat	17.86	65.2	47.34	%ST	

3.3.2. Normal Walking Altered Tibiofemoral Alignment

When comparing how tibiofemoral alignment effect compartmental loading of the knee for Normal Walking there are a number of changes. When there is a varus shift of 5.16 degrees (TFA=172 deg.) from nominal alignment (TFA=177.16), the max load decreased by 6.84 %BW. The mean total load is decreased by 2.71 %BW; however, it was not significant (P-value=0.2955).

Therefore, on average there is no difference between the mean total loads of varus (TFA=172 deg.) and nominal alignment (TFA=177.16 deg.). When looking at the medial compartment loading, the max load decreased by 11.2 %BW, the mean load increased by 20.82 %BW, the mean percentage of total load increased by 12.35 %TL, and the time of majority load accepted decreased by 5.36 %ST. All mean differences were significant (P-value<0.005). Conversely, the lateral compartment max load increased by 4.36 %BW, the mean load decreased by 23.53 %BW, the mean percentage of total load decreased by 12.35 %BW, and the time of majority load accepted decreased by 5.36 %ST. All Mean differences were significant (P-value<0.005).

When there is a valgus deformity of 10.84 degrees (TFA=188 deg.) from nominal alignment (TFA=177.16), the max load decreased by 2.06 % BW. The mean total load is increased significantly by 12.26 % BW (P-value<0.005). When looking at the medial compartment loading, the max load decreased by 38 %BW, the mean load decreased by 16.73 %BW, the mean percentage of total load decreased by 10.29 %TL, and the time of majority load accepted decreased by 66.07 %ST. All mean differences were significant (P-value<0.005). Conversely, the lateral compartment max load increased by 47.53 %BW, the mean load increased by 28.99 %BW, the mean percentage of total load increased by 10.29 %BW, and the time of majority load accepted increased by 66.07 %ST. All Mean differences were significant (P-value<0.005). Normalized joint contact force plots of the total, medial and lateral compartment load of altered tibiofemoral alignment for Tai Chi can be seen in **Figure 59**, **Figure 60**, and **Figure 61** respectively. Similar force plots for the left knee compartmental loads can be seen in **Appendix D**. A table of

comparative data for altered tibiofemoral alignment for Normal Walking can be seen in **Table 16**.

A similar table of the left knee can be seen in **Appendix D**.

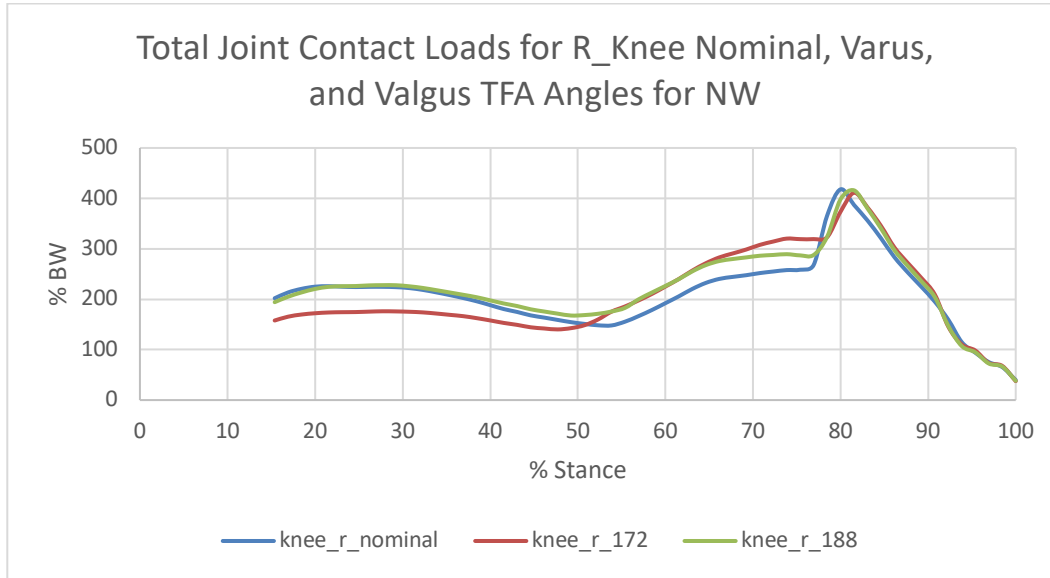


Figure 59: Normalized, right knee, stance phase, total joint contact loads of Normal Walking gait for nominal (TFA=177.16 deg.), varus (TFA=172 deg.), and valgus (TFA=188 deg.) tibiofemoral alignments.

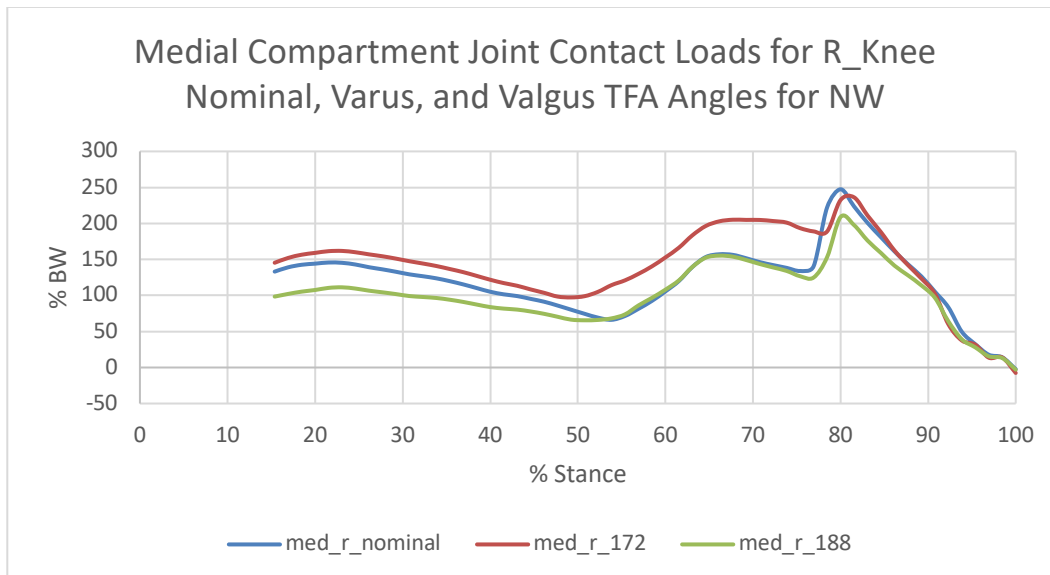


Figure 60: Normalized, right knee, stance phase, medial compartment joint contact loads of Normal Walking gait for nominal (TFA=177.16 deg.), varus (TFA=172 deg.), and valgus (TFA=188 deg.) tibiofemoral alignments

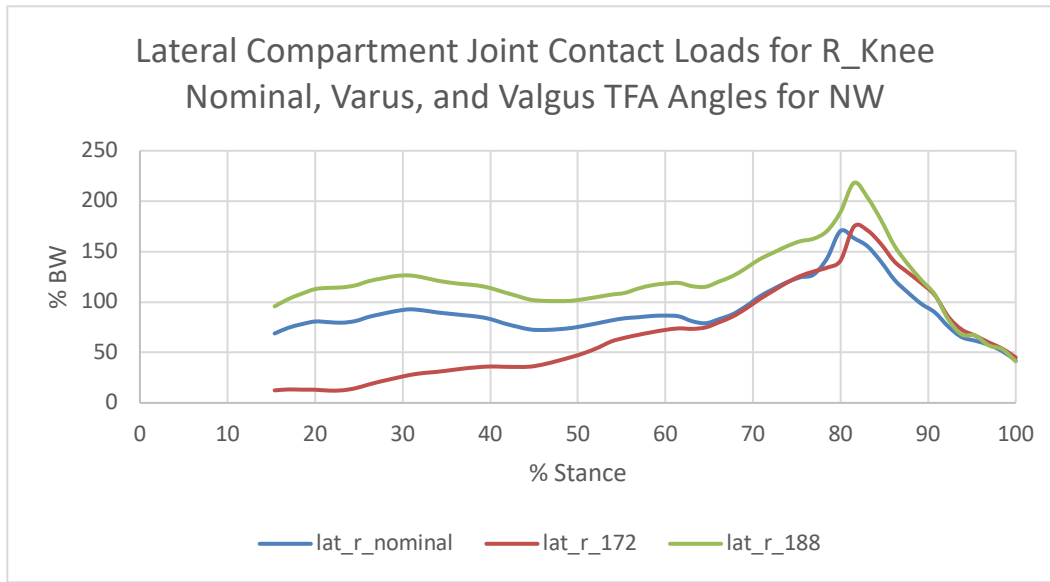


Figure 61: Normalized, right knee, stance phase, lateral compartment joint contact loads of Normal Walking gait for nominal (TFA=177.16 deg.), varus (TFA=172 deg.), and valgus (TFA=188 deg.) tibiofemoral alignments

Table 16: Statistical comparisons of normalized joint contact forces for the right knee altered tibiofemoral alignment of Normal Walking.

	Normal Walking Right Knee Comparative Statistics for Altered TFA								P-Value One-Sided		
	Nominal	Varus	Valgus	Diff (Vr-N)	Diff (Vg-N)	Units	% Diff (Vr-N)	% Diff (Vg-N)	Vr-N	Vg-N	Vr-Vg
Max_total	417.98	411.14	415.92	-6.83	-2.05	%BW	-1.64	-0.49			
Max_med	247.45	236.25	208.98	-11.19	-38.47	%BW	-4.52	-15.55			
Max_lat	170.53	174.89	218.20	4.36	47.67	%BW	2.56	27.95			
Mean_total	211.29	208.58	223.55	-2.71	12.27	%BW	-1.28	5.81	0.2955	p<0.005	p<0.005
Mean_med	120.23	141.05	103.50	20.82	-16.73	%BW	17.32	-13.91	p<0.005	p<0.005	p<0.005
Mean_lat	91.06	67.53	120.05	-23.53	28.99	%BW	-25.84	31.84	p<0.005	p<0.005	p<0.005
Mean_%TotalLoad_med	54.35	66.70	44.06	12.35	-10.30	%TL	22.72	-18.94	p<0.005	p<0.005	p<0.005
Mean_%TotalLoad_lat	45.65	33.30	55.94	-12.35	10.30	%TL	-27.05	22.56	p<0.005	p<0.005	p<0.005
Time_MLA_med	82.14	87.5	16.07	5.36	-66.07	%ST	6.53	-80.44			
Time_MLA_lat	17.86	12.5	83.93	-5.36	66.07	%ST	-30.01	369.93			

3.3.3. Tai Chi Altered Tibiofemoral Alignment

When comparing how tibiofemoral alignment effects compartmental loading of the knee for Tai Chi there are a number of changes. When there is a varus shift of 5.16 degrees (TFA=172 deg.) from nominal alignment (TFA=177.16), the max load decreased by 50.10 %BW. The mean total load is decreased by 8.66 %BW, (P-value<0.005). Therefore, on average there is a significant difference between the mean total load of varus (TFA=172 deg.) and nominal alignment

(TFA=177.16 deg.) during Tai Chi gait. When looking at the medial compartment loading, the max load increased by 62.77 %BW, the mean load increased by 30.57 %BW, the mean percentage of total load increased by 9.56 %TL, and the time of majority load accepted increased by 7.76 %ST. All mean differences were significant (P-value<0.005). Conversely, the lateral compartment max load increased by 97.70 %BW, the mean load decreased by 21.92 %BW, the mean percentage of total load decreased by 9.56 %BW, and the time of majority load accepted decreased by 7.76 %ST. All Mean differences were significant (P-value<0.005).

When there is a valgus shift of 10.84 degrees (TFA=188 deg.) from nominal alignment (TFA=177.16) for Tai Chi gait, the max load increased by 3.44%BW while the mean total load decreased significantly by 7.12 %BW (P-value<0.005). When looking at the medial compartment loading, the max load decreased by 101.97 %BW, the mean load decreased by 54.43 %BW, the mean percentage of total load decreased by 18.13 %TL, and the time of majority load accepted decreased by 33.64 %ST. All mean differences were significant (P-value<0.005). Conversely, the lateral compartment max load increased by 105.42 %BW, the mean load increased by 47.32 %BW, the mean percentage of total load increased by 18.13 %BW, and the time of majority load accepted increased by 33.64 %ST. All mean differences were significant (P-value<0.005). Normalized joint contact force plots for the total, medial and lateral compartment loads of altered tibiofemoral alignment for Tai Chi can be seen in **Figure 62**, **Figure 63**, and **Figure 64** respectively. Similar force plots for the left knee compartmental loads can be seen in **Appendix D**. A table of values for altered tibiofemoral alignment for Tai Chi can be seen in

Table 17. A similar table of the left knee can be seen in **Appendix D**.

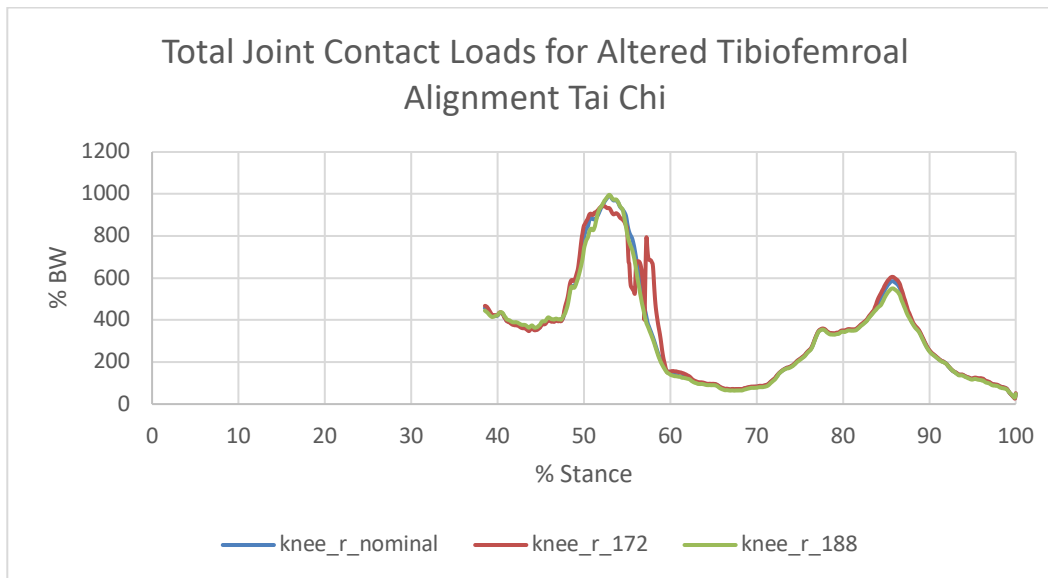


Figure 62: Normalized, right knee, stance phase, total joint contact loads of Tai Chi gait for nominal (TFA=177.16 deg.), varus (TFA=172 deg.), and valgus (TFA=188 deg.) tibiofemoral alignments.

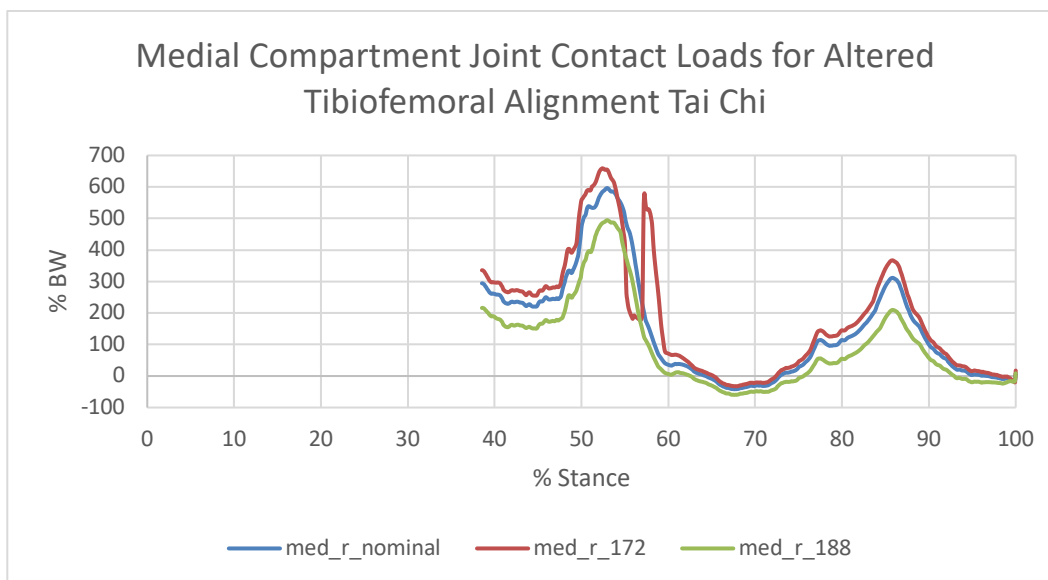


Figure 63: Normalized, right knee, stance phase, medial compartment joint contact loads of Tai Chi gait for nominal (TFA=177.16 deg.), varus (TFA=172 deg.), and valgus (TFA=188 deg.) tibiofemoral alignments.

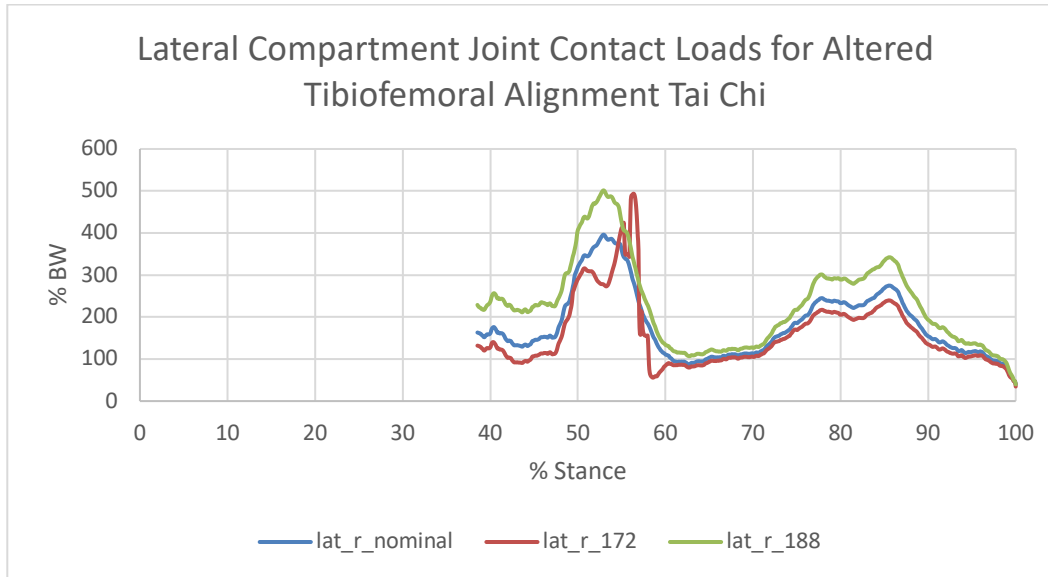


Figure 64: Normalized, right knee, stance phase, lateral compartment joint contact loads of Tai Chi gait for nominal (TFA=177.16 deg.), varus (TFA=172 deg.), and valgus (TFA=188 deg.) tibiofemoral alignments.

Table 17: Statistical comparisons of normalized joint contact forces for right knee altered tibiofemoral alignment of Tai Chi.

	Tai Chi Right Knee Comparitive Statistics for Altered TFA								P-Value One-Sided		
	Nominal	Varus	Valgus	Diff (Vr-N)	Diff (Vg-N)	Units	% Diff (Vr-N)	% Diff (Vg-N)	Vr-N	Vg-N	Vr-Vg
Max_total	992.43	942.33	995.87	-50.10	3.44	%BW	-5.05	0.35			
Max_med	596.42	659.19	494.45	62.77	-101.97	%BW	10.52	-17.10			
Max_lat	396.00	493.70	501.42	97.70	105.42	%BW	24.67	26.62			
Mean_total	333.77	342.43	326.66	8.66	-7.12	%BW	2.59	-2.13	p<0.005	p<0.005	p<0.005
Mean_med	152.23	182.80	97.80	30.57	-54.43	%BW	20.08	-35.76	p<0.005	p<0.005	p<0.005
Mean_lat	181.54	159.62	228.86	-21.92	47.32	%BW	-12.07	26.06	p<0.005	p<0.005	p<0.005
Mean_%TotalLoad_med	27.35	36.91	9.22	9.56	-18.13	%TL	34.93	-66.30	p<0.005	p<0.005	p<0.005
Mean_%TotalLoad_lat	72.65	63.09	90.78	-9.56	18.13	%TL	-13.15	24.96	p<0.005	p<0.005	p<0.005
Time_MLA_med	34.8	42.56	1.16	7.76	-33.64	%ST	22.30	-96.67			
Time_MLA_lat	65.2	57.44	98.84	-7.76	33.64	%ST	-11.90	51.60			

3.3.4. Normal Walking Altered TFA Vs. Tai Chi Altered TFA

When comparing the altered tibiofemoral alignment for Normal Walking and Tai chi, there are some significant points to highlight. In terms of percent difference in mean total loads for a varus shift for Tai Chi vs. Normal Walking, the mean medial load and the mean medial percent total load showed a greater change for Tai Chi than for Normal walking **Table 18**. However, the mean lateral load and the mean lateral percent total load showed a smaller change for Tai Chi than for Normal

Walking. These results and more can be found in **Table 18**. A similar table of the left knee results can be seen in **Appendix D**.

Table 18: Percent difference of normalized joint contact force data comparisons of right knee varus and valgus tibiofemoral alignment for Tai Chi and Normal Walking.

Tai Chi and Normal Walking Right Knee Comparitive Statistics for Altered TFA				
	TC % Diff (Vr-N)	NW % Diff (Vr-N)	TC % Diff (Vg-N)	NW % Diff (Vg-N)
Max_total	-5.05	-1.64	0.35	-0.49
Max_med	10.52	-4.52	-17.10	-15.55
Max_lat	24.67	2.56	26.62	27.95
Mean_total	2.59	-1.28	-2.13	5.81
Mean_med	20.08	17.32	-35.76	-13.91
Mean_lat	-12.07	-25.84	26.06	31.84
Mean_%TotalLoad_med	34.93	22.72	-66.30	-18.94
Mean_%TotalLoad_lat	-13.15	-27.05	24.96	22.56
Time_MLA_med	22.30	6.53	-96.67	-80.44
Time_MLA_lat	-11.90	-30.01	51.60	369.93

All percent differences of means were larger for valgus alignment than for the varus alignment for both Tai Chi and Normal Walking when compared to nominal alignment except for the percent difference in mean total load. However, it is important to note that there is a greater shift in tibiofemoral alignment for the valgus alignment than for the varus alignment when compared to nominal tibiofemoral alignment. There is was 5.17 degree change in TFA angle for varus alignment from nominal, while there was a 10.84 degree change in TFA angle for a valgus alignment form nominal. Therefore, after normalizing the percent difference for the degree of shift, i.e. the diving the % difference by the change in degree of malalignment for varus and valgus shift, the following results were found **Table 19**. A similar table of the left knee results can be seen in **Appendix D**.

Table 19: Normalized percent difference per degree of malalignment of normalized joint contact force data comparisons of right knee varus and valgus tibiofemoral alignment for Tai Chi and Normal Walking.

Tai Chi and Normal Walking Right Knee Comparative Statistics for Altered TFA Normalized Per Degree TFA				
	TC %Diff(Vr-N)/deg.	NW %Diff(Vr-N)/deg.	TC %Diff(Vg-N)/deg.	NW %Diff(Vg-N)/deg.
Max_total	-0.98	-0.32	0.03	-0.05
Max_med	2.04	-0.88	-1.58	-1.43
Max_lat	4.78	0.50	2.46	2.58
Mean_total	0.50	-0.25	-0.20	0.54
Mean_med	3.89	3.36	-3.30	-1.28
Mean_lat	-2.34	-5.01	2.40	2.94
Mean_%TotalLoad_med	6.77	4.40	-6.12	-1.75
Mean_%TotalLoad_lat	-2.55	-5.24	2.30	2.08

In terms of normalized percent difference, the change in mean loads and the change mean percent total load is greater for the medial compartment than the lateral compartment for Tai Chi when a tibiofemoral malalignment is present, regardless of malalignment of direction. However, the reciprocal is true for Normal Walking. In terms of percent difference, the change in mean load and mean percent total load is greater for the lateral compartment than for the medial compartment for Normal Walking. This trend is independent of malalignment direction; therefore, it holds true regardless of varus or valgus malalignment. This trend also holds true when comparing the raw difference, percent difference, and the normalized percent difference. Therefore, the medial compartment is more sensitive to change in load per change in degree of malalignment for Tai Chi than for Normal walking. The reciprocal holds true for lateral compartment.

Chapter 4: Discussion of the Results

4.1. Nominal Normal Walking Vs. Nominal Tai Chi

Based on the results from the nominal TFA model, peak normalized contact forces and average normalized contact forces were significantly higher for the total, medial, and lateral compartment loads for Tai Chi and then for Normal Walking, with mean differences of 122.48%BW for the total load, 32%BW for medial load, and 90%BW for lateral loads. Therefore, it can be concluded that joint contact forces generated by Tai Chi are significantly greater than joint contact forces produced by Normal Walking. This suggests that there could be more articular cartilage degradation during Tai Chi as opposed to Normal Walking strictly because the joint contact forces are higher.

4.1.1. Influence of Muscle Forces on Joint Contact Loading

In order to determine the efficacy of the high joint contact loads, it is important to look at the muscles forces that traverse the knee joint which produce moments about the knee to cause locomotion. There are 13 linear actuators that serve as muscles in the MLK model that traverse the knee joint, and when activated, they contribute to the joint reaction force in the knee. Those muscle actuators are the semimembranosus, semitendinosus, biceps femoris long head, biceps femoris short head, sartorius, tensor fasciae latae, gracilis, rectus femoris, vastus medialis, vastus lateralis, vastus intermedius, medial gastrocnemius, and the lateral gastrocnemius. A plot of the normalized muscle forces that traverses the right knee can be seen as a function of the right leg stance phase in **Figure 65** and **Figure 66** for Normal Walking and Tai Chi, respectively. Synonymous plots of the left side muscle forces for NW and TC can be seen in **Appendix E**.

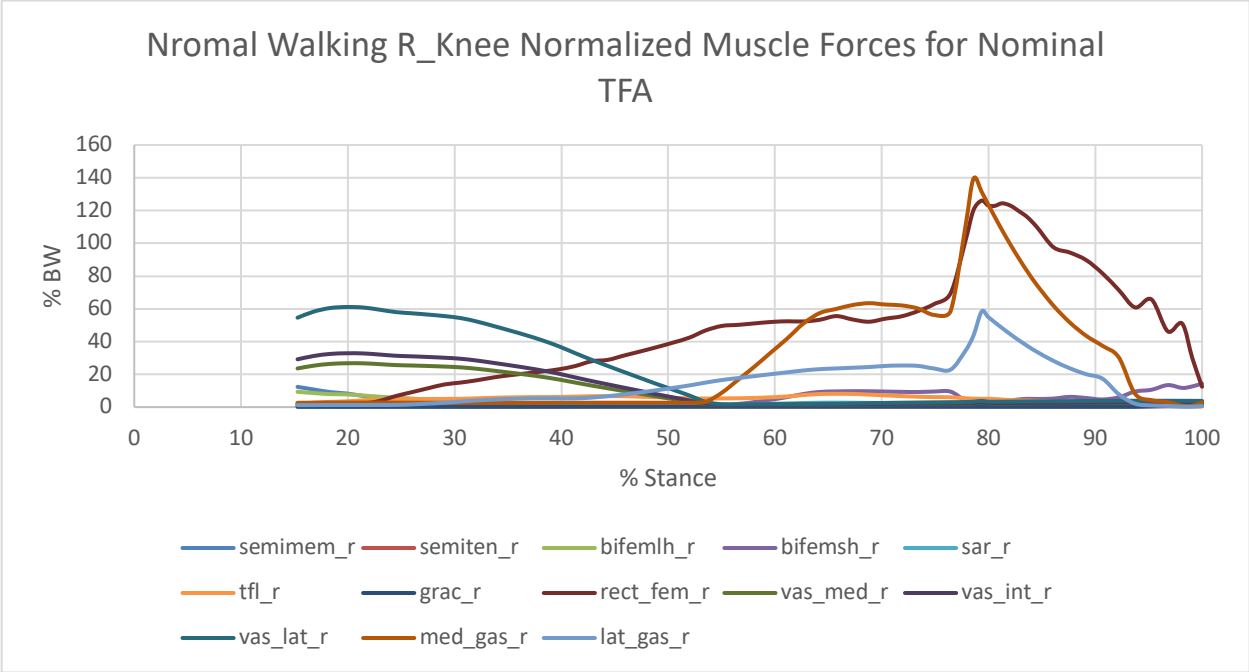


Figure 65: Normalized muscle forces that traverse the right knee during stance phase for Normal Walking, nominal tibiofemoral alignment (TFA=177.16deg.)

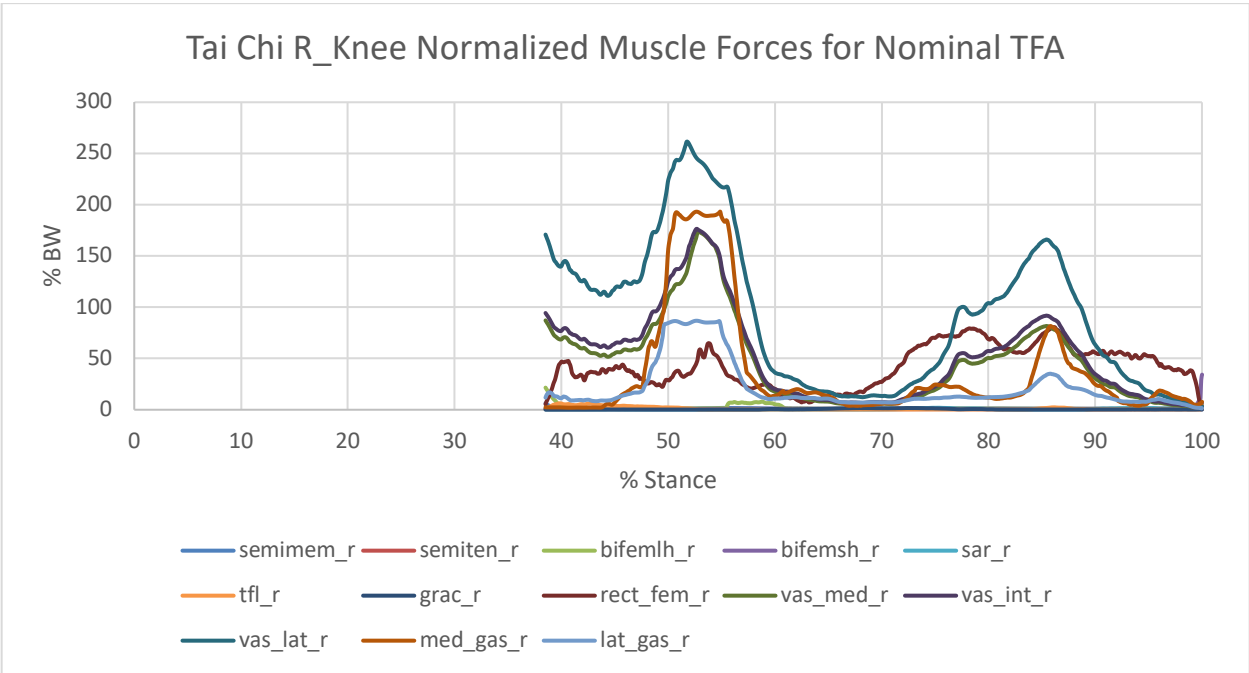


Figure 66: Normalized muscle forces that traverse the right knee during stance phase for Tai Chi, nominal tibiofemoral alignment (TFA=177.16deg.)

As seen in **Figure 65**, for Normal Walking, it is evident that the Rectus Femoris (RF), Lateral Gastrocnemius (LG), and Medial Gastrocnemius (MG) generate the most muscle force throughout stance phase of gait, particularly in late stance phase. When compared to the normalized total joint contact load throughout stance phase, the RF, LG, MG muscles appear to have a profound effect on total joint contact load. **Figure 67** shows the normalized total joint contact forces for right leg stance phase of Normal Walking compared to the sum of the three most influential muscles forces (Sum Isolated Muscle Forces) as well as the sum of total muscle forces across the knee joint. The “Sum Isolated Muscle Forces” is the sum of the FR, LG and MG muscles. The “Sum Total Muscle Forces” is the sum of all 13 muscle forces that traverse the knee joint. When comparing the sum of total normalized muscle forces to the total normalized joint contact load, the summed muscle force profile is nearly identical only shifted below the total joint contact force curve, **Figure 67**.

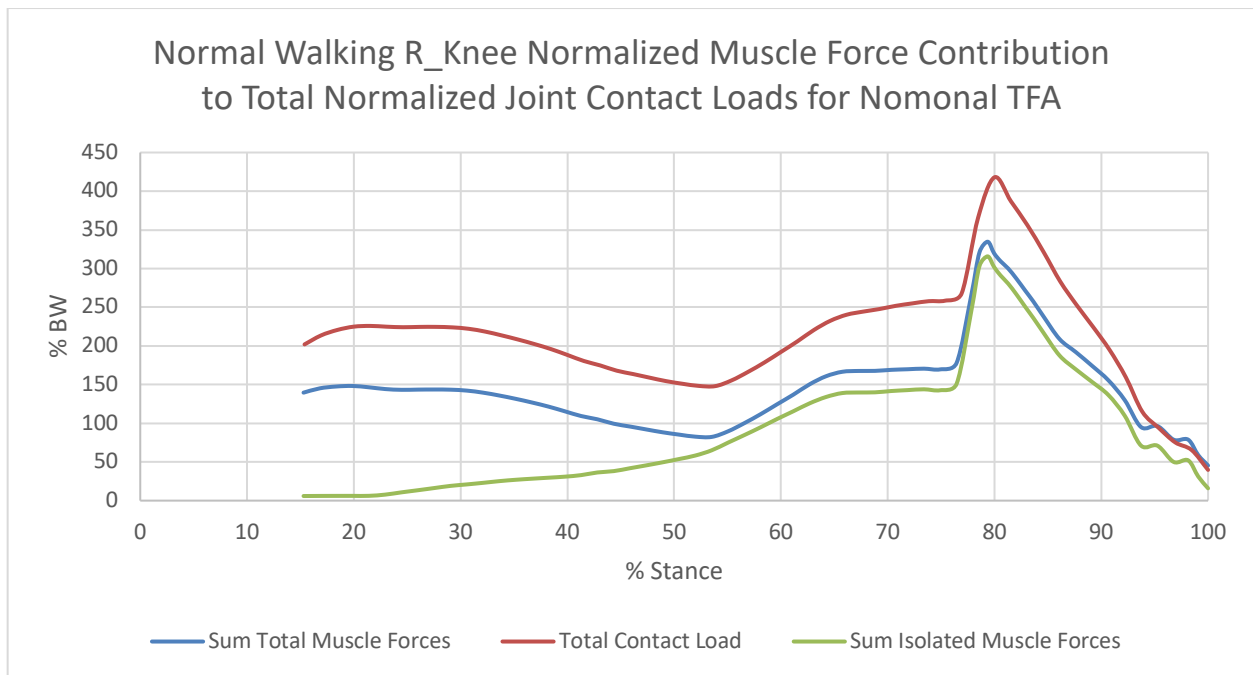


Figure 67: Normalized joint contact forces compared to the sum of the three most influential muscle forces (Sum Isolated Muscle Forces), rectus femoris, lateral gastrocnemius, medial gastrocnemius and the total muscle forces that traverse the right knee, stance phase, Normal Walking, nominal tibiofemoral alignment (TFA=177.16)

A similar observation is true for Tai Chi, **Figure 68**. The sum of total normalized muscle forces closely follows the total joint contact force profile for Tai Chi when compared to Normal Walking. The muscle force contributions for Tai Chi were more evenly distributed throughout the quadriceps muscle than for Normal Walking, **Figure 66**. Therefore, the most influential muscles were the Rectus Femoris, Vastus Medialis, Vastus Intermedius, and the Vastus Lateralis muscles, as well as the Medial Gastrocnemius and the Lateral Gastrocnemius muscles. It is clear that the muscle forces have a profound impact on the total joint contact load because the force profiles are nearly identical and similar in magnitude for TC and NW. Muscle force contributions for the left leg of NW and TC can be seen in **Appendix E**.

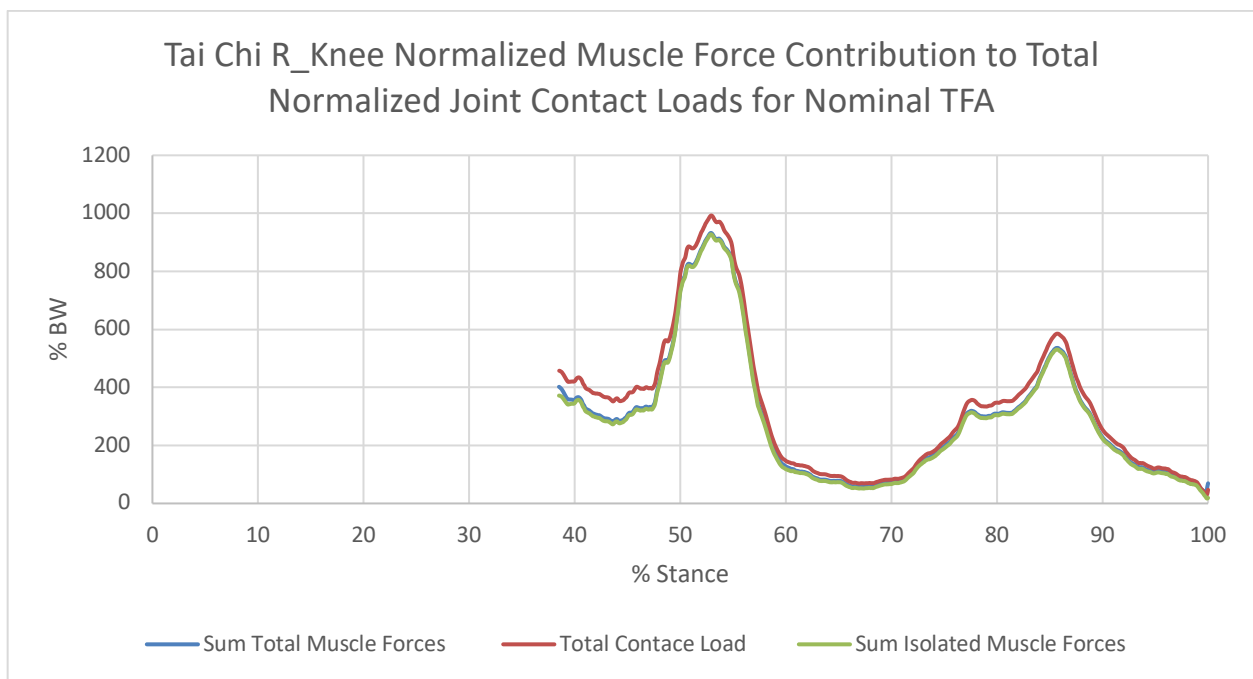


Figure 68: Normalized joint contact forces compared to the sum of the three most influential muscle forces (Sum Isolated Muscle Forces), medial and lateral gastrocnemius, vastus medialis, vastus lateralis, vastus intermedius, rectus femoris, muscle forces that traverse the right knee, stance phase, Tai Chi, nominal tibiofemoral alignment (TFA=177.16)

While these force comparisons are helpful, they fail to determine the actual individual muscle force contributions because the component of the muscle acting along the mechanical axis of the tibia

could not be extracted from the software. The summation of muscle forces used in comparison to total joint contact, is the summation of the individual muscle force magnitude. Therefore, the summation of magnitudes is higher than the summation of contributing muscle force components used to pull the tibia into femur. As a result, a limitation exists when using the muscle force comparative plots. However, not only do the muscle forces contribute significantly to the joint contact forces, but the muscle forces for Tai Chi are significantly greater than the muscle forces for Normal Walking which would explain why the joint contact forces are higher for Tai Chi than for normal walking. One justification as to why the muscle forces are greater for Tai Chi is that both the right and left knees are more flexed throughout stance phase of gait, which lowers the COM of the pelvis and ultimately causes larger muscle contractions in the quadriceps in order to maintain ambulation. More specifically, the vastus lateralis muscle generated a peak muscle contraction force of 252%BW during single support phase of TC gait while a peak muscle contraction of only 60%BW was generated during early stance phase for NW gait. This would explain why the total, medial, and lateral joint contact loads are higher for Tai Chi than for Normal Walking.

4.1.2. Influence of Medial and Lateral Muscle Forces on Compartmental Load Distribution

When comparing medio-lateral load distribution, this study showed that there was a significant shift in load distribution from the medial compartment to the lateral compartment for TC gait when compared to NW. For TC, the medial compartment accepted 27.35% of the total load on average, while the medial compartment for NW accepted about 54.35% of the total load on average. The inverse is true for the lateral compartment. There are a number of explanations for the shift in load distribution for TC gait. The first explanation is to consider the muscle force contributions for each

compartment for each case. The muscle forces that generated the most medial load were compared to the muscle forces that generated the most lateral load. The muscle forces for both cases that generated the most medial load were the medial gastrocnemius in the calf and the vastus medialis muscle in the quadricep. Conversely, the muscles that contributed to the most lateral load were the lateral gastrocnemius and the vastus lateralis muscles. A diagram of where these muscles are located with respect the knee joint can be seen in below **Figure 69**.

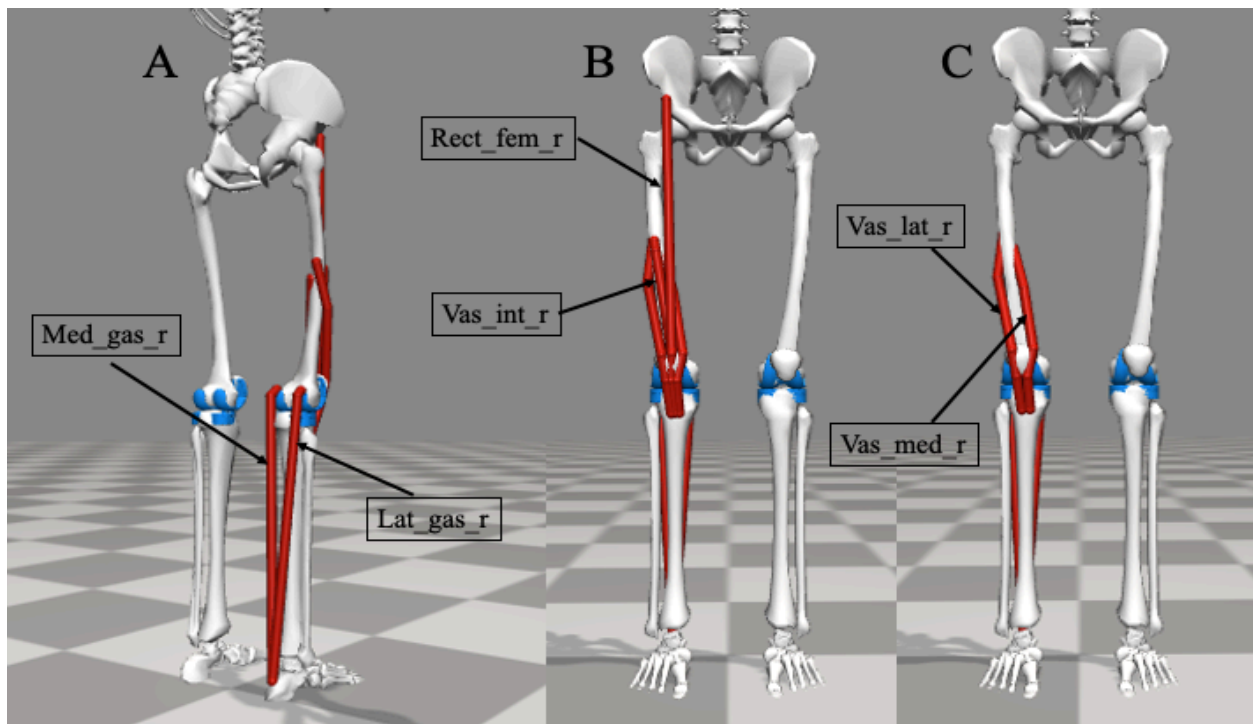


Figure 69: Diagram of the anatomical locations of most influential muscles that contribute to the joint contact load of the right knee. (A) Shows the location of the medial and lateral gastrocnemius muscles in the calf. (B) Shows the rectus femoris and the vastus intermedius muscles in the quadricep. (C) Shows the vastus medialis and the vastus lateralis in the quadricep.

The sum of the medial forces ($\text{med_gas_r} + \text{vas_med_r}$) was compared to the sum of the lateral muscle forces ($\text{lat_gas_r} + \text{vas_lat_r}$) for Tai Chi and Normal Walking and can be seen in **Figure 70** and **Figure 71**, respectively. Synonymous plots of the left leg muscle forces for NW and TC can be seen in **Appendix E**.

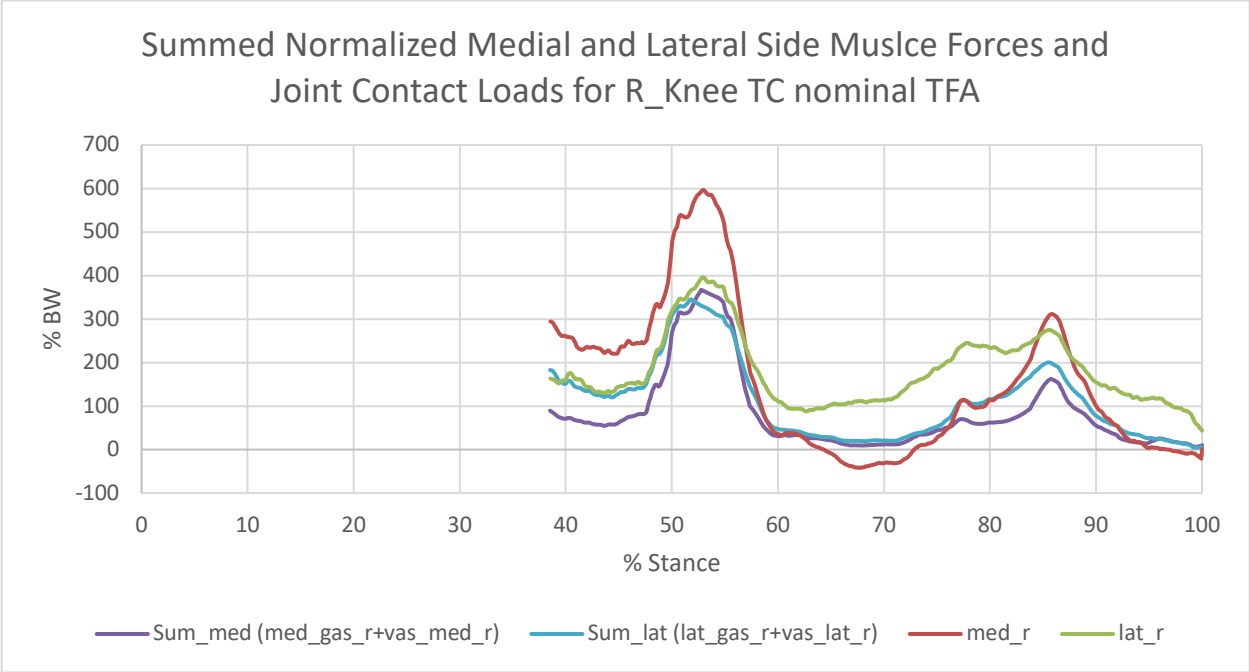


Figure 70: Summed normalized muscle forces for the medial and the lateral sides compared to the medial and lateral joint contact forces of the right knee during stance phase of Tai Chi gait.

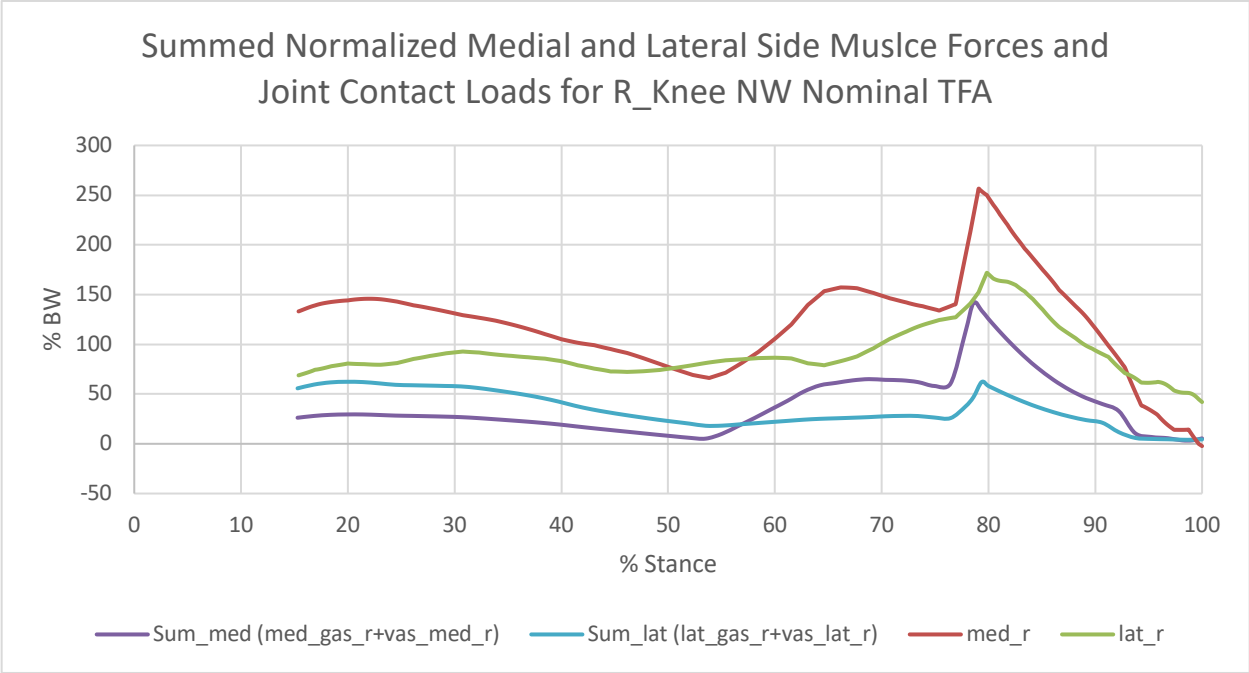


Figure 71: Summed normalized muscle forces for the medial and the lateral sides compared to the medial and lateral joint contact forces of the right knee during stance phase of Normal Walking gait.

By looking at the force plots in **Figure 70** and **Figure 71**, it is clear the lateral muscles generate a higher load for a longer period of time across the stance phase of gait than the medial muscle forces for Tai Chi. On average, the sum of the medial muscle forces (84.4%BW) is lower than the sum of the lateral muscle forces (112.78%BW) for Tai Chi, **Table 20**. For Normal Walking, on average, the sum of the medial muscle forces (42.89%BW) is higher than the sum of the lateral muscle forces (35.36%BW), **Table 20**. This could explain why there is a significant medial to lateral shift of load distribution of the knee for Tai Chi compared to normal Walking. A synonymous table for the left side can be found in **Appendix E**

Table 20: Mean sum medial side muscle force and lateral side muscle forces that contribute the medio-lateral compartmental joint contact loads in the right knee.

Mean Sum Normalized Influential Right Medial and Lateral Muscle Forces			
	Tai Chi	Normal Walking	
Mean_Sum_Med	84.4	42.89	%BW
Mean_Sum_Lat	112.78	35.36	%BW

4.1.3. Influence of EKAM on Compartmental Load Distribution

Another explanation for the shift in compartmental loading has to do with influence of the external knee adduction moment (EKAM). It is believed that there is a reduction in external knee adduction moment for TC during the double support phase I compared to NW, **Figure 72B** (Liu et al.).

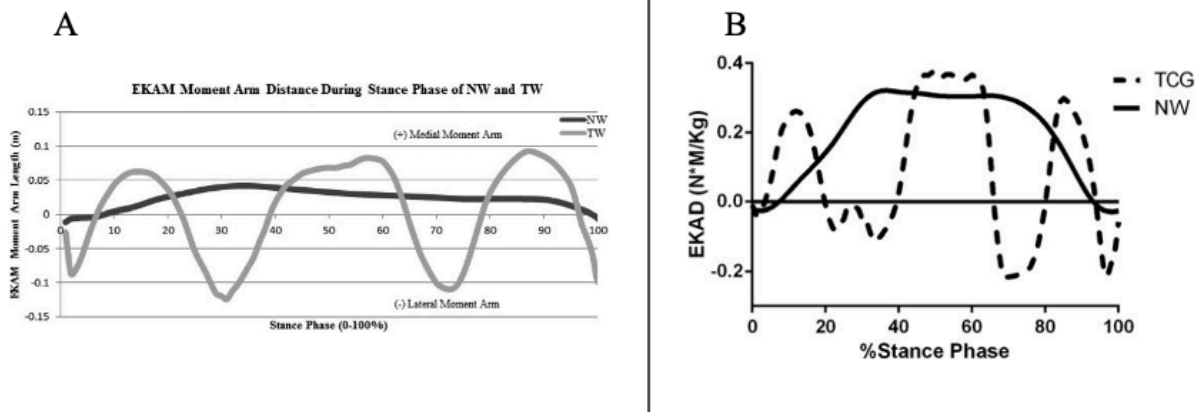


Figure 72: External Knee adduction moment (EKAM) arm as a function of stance phase (A) and the EKAM as a function of stance phase (B). Measurements were taken from the same data set but calculated in another study (Jagodinsky et al.) and (Liu et al.) respectively.

Figure 72B shows the dramatic change in EKAM in magnitude and direction throughout the entire stance phase of gait. When the EKAM is positive, an external knee adduction is achieved. Conversely, when the EKAM is negative, an external knee abduction moment is achieved. The EKAM appears to behave cyclically transitioning from the positive to the negative regions and vice versa 5 times throughout stance phase of gait **Figure 72B**.

The simulated EKAM of Tai Chi and Normal Walking gait was calculated for this study. A body kinematic analysis was performed in OpenSim on the left and right tibial plateaus which resolved the position and orientation of the tibial reference frame, i.e. the tibial origin, with respect to global reference frame. Those orientation angles, i.e. Euler angles, were then used to transform the magnitude and position of the ground reaction force into the tibial reference frame. A Cardan x-y-z sequence rotation matrix, $[R_o]$, was used to transform the GRF vector position and orientation into the tibial reference frame as was consistent with the literature (Winter), **Equation 39**. The

EKAM is the moment about the knee in the frontal plane generated by the GRF. Therefore, the EKAM is the x component of the cross product of the GRF vector and its position vector with respect to the knee joint center, **Equation 42** and **Equation 43**, where the knee joint center is the same point as the tibial origin in OpenSim. The EKAM was calculated in Matlab using Equations 39, 40, 41, 42, and 43. The Matlab the code can be found in **Appendix A**.

$$[R_o] = \begin{bmatrix} C_2 C_3 & S_3 C_1 + S_1 S_2 C_3 & S_1 S_3 - C_1 S_2 C_3 \\ -C_2 S_3 & C_1 C_3 - S_1 S_2 S_3 & S_1 C_3 + C_1 S_2 S_3 \\ S_2 & -S_1 C_2 & C_1 C_2 \end{bmatrix} \quad (39)$$

$$\overline{rGRF}_{tibial} = [R_o]^T * \overline{rGRF}_{global} - \overline{H} \quad (40)$$

$$\overline{GRF}_{tibail} = [R_o] * \overline{GRF}_{global} \quad (41)$$

$$\overline{M}_{knee} = \overline{rGRF}_{tibial} \times \overline{GRF}_{tibial} \quad (42)$$

$$EKAM = M_{knee,x} \quad (43)$$

Where $[R_o]$ is the Cardan rotation matrix that transforms vectors from global to tibial reference frame, C_1 , C_2 , and C_3 are $\cos \theta_x$, $\cos \theta_y$, and $\cos \theta_z$ of the x-y-z Euler angles, and S_1 , S_2 , and S_3 are $\sin \theta_x$, $\sin \theta_y$, and $\sin \theta_z$ of the x-y-z Euler angles. \overline{rGRF}_{tibial} is the position of the GRF in the tibial reference frame, \overline{rGRF}_{global} is the position of the GRF in the global reference frame, and \overline{H} is the location of the knee joint center, i.e. tibial origin, in the global reference frame. \overline{GRF}_{tibail} is the ground reaction force in the tibial reference frame, \overline{GRF}_{global} is the GRF in the global reference frame, \overline{M}_{knee} is the moment about the knee joint center caused by the GRF, EKAM is the external knee adduction moment, $M_{knee,x}$ is the x component if the knee joint moment, \overline{M}_{knee} , which is equal to the EKAM.

The EKAM was calculated for the left and right knees for of stance phase Tai Chi and Normal Walking and can be seen in **Figure 73**. Statistical Data of the EKAM for the left and right knees of the nominal model can be seen in **Table 21**. Subsequently, the EKAM was calculated for the altered TFA and was compared for the left and right knees of stance phase Tai Chi and Normal walking **Figure 74** and **Figure 75** respectively.

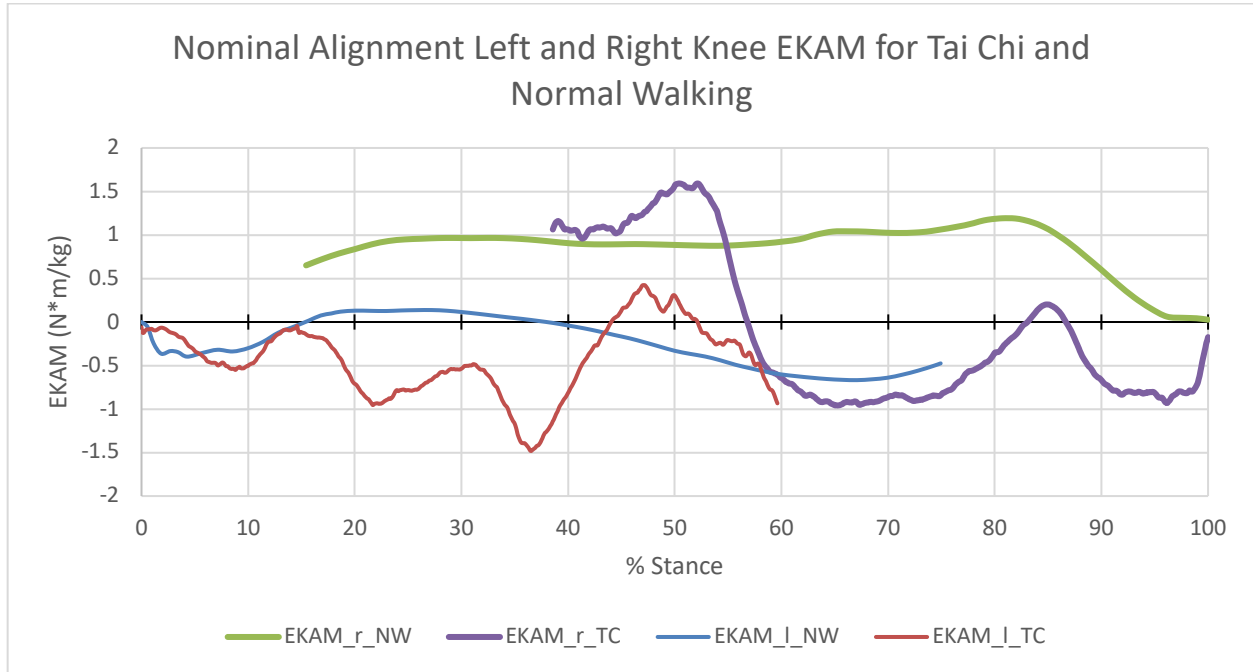


Figure 73: External knee adduction moment normalized by body mass of the left and right knees for stance phase of Tai Chi and Normal Walking

Table 21: Statistical data for the EKAM calculated about the left and right knees of stance phase for Normal Walking and Tai Chi gait.

EKAM Statistics for Right and Left Knee Stance Phase NW and TC					
Parameter	TC_r	NW_r	TC_l	NW_l	Unit
Peak EKAM	1.59	1.19	-1.48	-0.67	Nm/kg
Mean EKAM	-0.087	0.87	-0.43	-0.23	Nm/kg
Range EKAM	2.55	1.17	1.91	0.81	Nm/kg

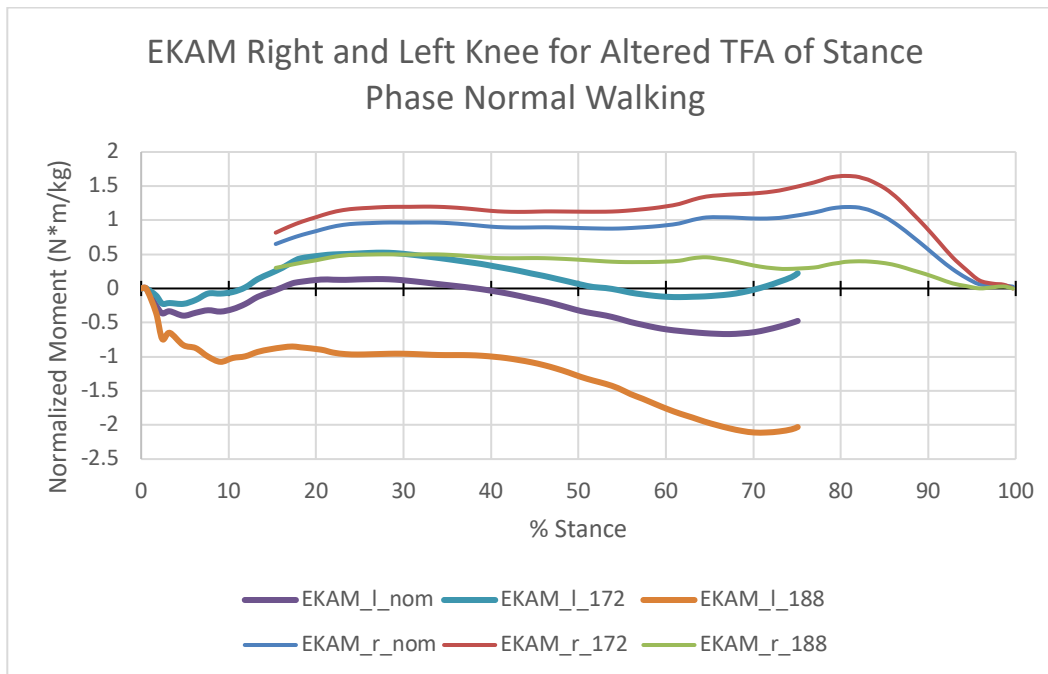


Figure 74: External knee adduction moment for altered tibiofemoral alignment, nominal TFA=177.16, varus TFA=172, and valgus TFA=188, about the left and right knees for stance phase of Normal Walking gait.

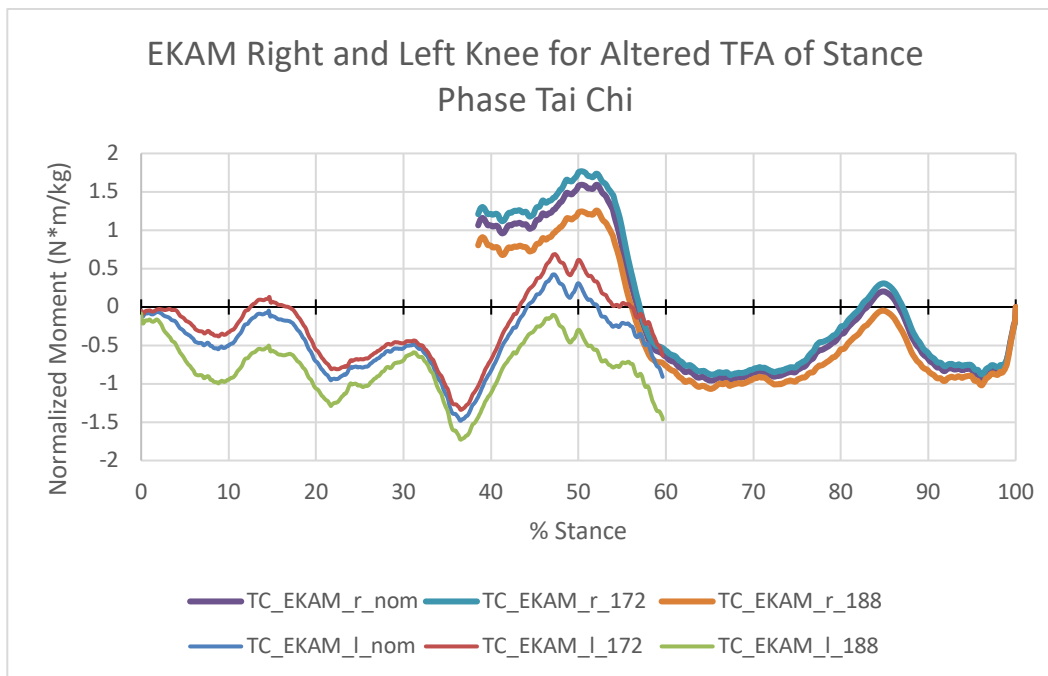


Figure 75: External knee adduction moment for altered tibiofemoral alignment, nominal TFA=177.16, varus TFA=172, and valgus TFA=188, about the left and right knees for stance phase of Tai Chi gait.

A comparison of the simulated EKAM and the compartmental joint contact loads of stance phase Tai Chi for the right and left knees can be seen in **Figure 76** and **Figure 77** respectively.

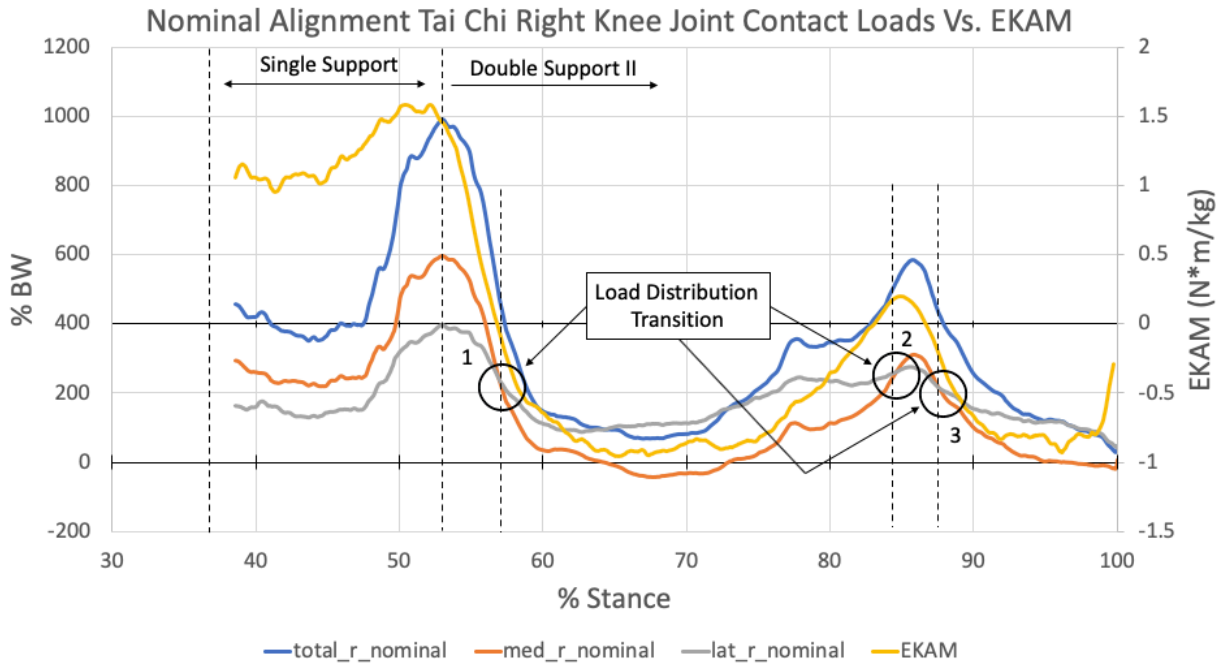


Figure 76: Simulated EKAM for right leg stance phase of Tai Chi overlaid against the Nominal Tai Chi joint contact loads.

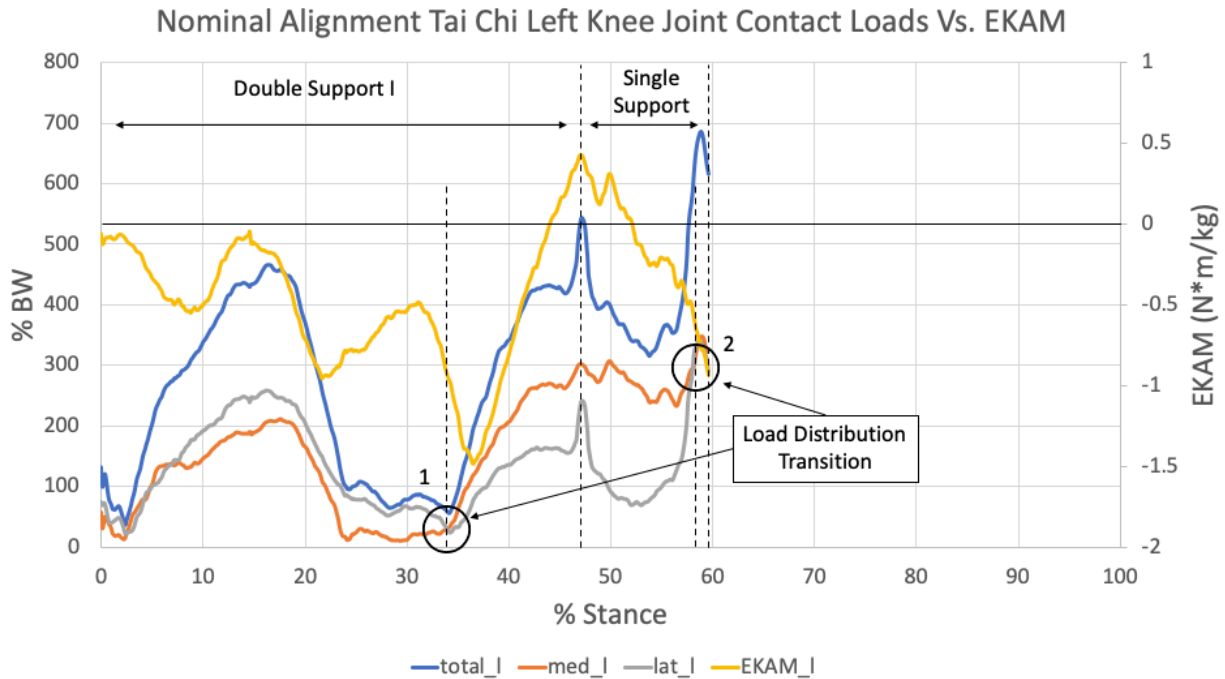


Figure 77: Simulated EKAM for left leg stance phase of Tai Chi overlaid against the Nominal Tai Chi joint contact loads

When comparing the EKAM to the joint contact loads of right leg stance phase of Tai Chi, the EKAM transitions into the negative region during right leg double support II phase, at about 57% Stance Phase, load transition 1 of **Figure 76**. Three transitions in compartmental load distributions were observed. The first transition occurs at the same moment that the EKAM transitions from positive, i.e. knee adduction moment, to negative, i.e. knee abduction moment, at 57% stance phase. Additionally, the medial joint contact load shifts into the negative region while the EKAM is in the negative region, **Figure 76**. Given that muscles can only contract, compressive contact forces in joints can only be achieved from muscle contraction. The fact that the medial contact load transitions into the negative region suggests that, the EKAM is generating a large knee abduction moment about the knee which would help explain why compartmental unloading (i.e. negative contact load) is observed in the medial compartment of the knee. The EKAM also

behaved appears to behave cyclically and transition from the positive to negative and vice versa throughout stance phase of Tai Chi gait. This is a dramatic change in EKAM during stance phase for Tai Chi gait compared to Normal Walking gait, which could explain why there is such a dramatic shift of the mean percent total load from the medial compartment to the lateral compartment during Tai Chi compared to that of Normal Walking. In addition, there is a dramatic change in the EKAM moment arm throughout stance phase of Tai Chi Gait which would help explain why the EKAM transitions from the positive to negative region cyclically **Figure 72A**, and ultimately causes a shift in the compartmental loading of the knee. Nevertheless, there is a dramatic shift in total contact load distribution from medial to lateral compartments for Tai Chi compared to Normal Walking. However, more research needs to be done to further explain this phenomenon.

When looking at the left knee contact loads and the EKAM as a function of stance phase Tai Chi, **Figure 77**, a transition in compartmental load distribution occurs at about 35% of stance phase, during double support I. The EKAM does not transition from a positive to negative simultaneously with the transition in joint contact load distribution like it does for the first load transition of right knee stance phase, **Figure 76**. Therefore, EKAM direction, i.e. positive or negative EKAM, does not exclusively dictate when a compartmental load distribution transition will occur. However, the EKAM does appear to behave cyclically like it does for the right knee. Additionally, the right and left knee plots confirm the observation that when the EKAM is positive, the medial compartment tends to accept a majority of the total contact load, and when the EKAM is negative, the lateral compartment tends to accept a majority of the load.

The simulated EKAM was calculated and compared to the joint contact loads for the right and left knees of Normal Walking and can be seen in **Figure 78** and **Figure 79** respectively.

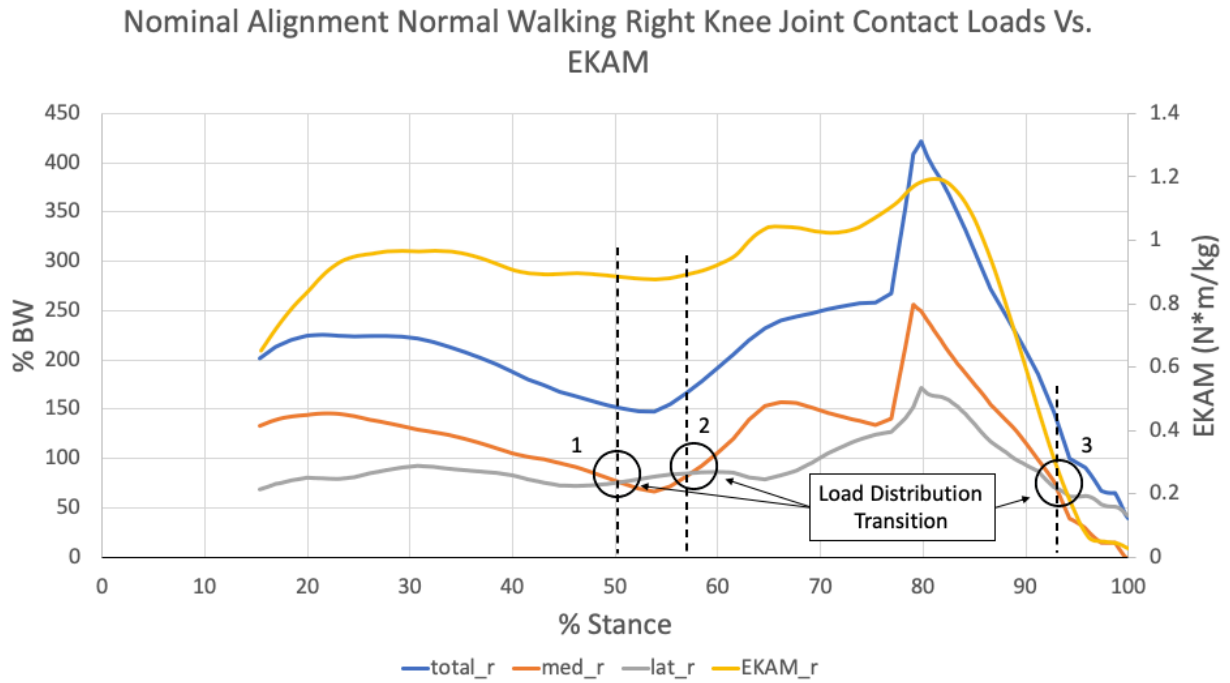


Figure 78: Simulated EKAM for right leg stance phase of Normal Walking overlaid against the Nominal Normal Walking joint contact loads.

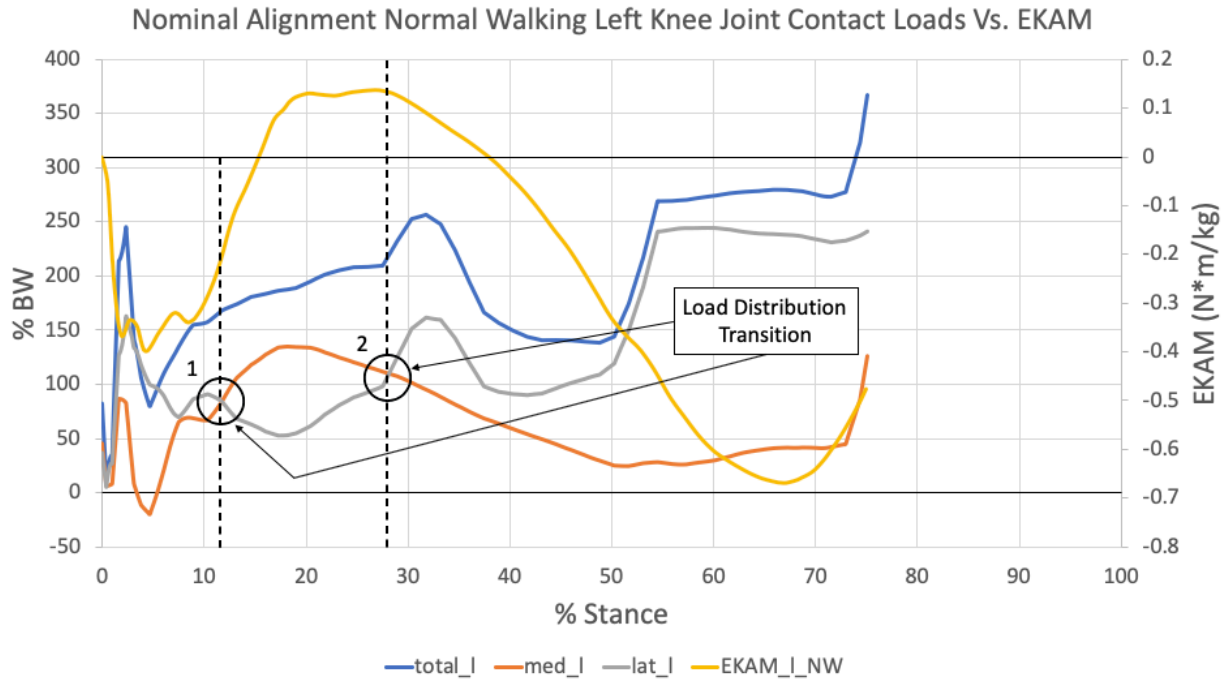


Figure 79: Simulated EKAM for left leg stance phase of Normal Walking overlaid against the Nominal Normal Walking joint contact loads.

For right leg stance phase of Normal Walking, the EKAM remains fully in the positive region which promotes more medial compartment loading in the knee **Figure 78**. This could explain why the medial compartment experiences a higher mean percentage of the total load compared to right leg stance phase of Tai Chi gait. There were three load distribution transition points throughout right leg stance phase. Transition points 1 and 2 occur during mid stance between heel strike and toe off, **Figure 78**. The EKAM shows a slight dip, i.e. a trough, during mid stance phase but is still high relative to the rest of stance phase. This suggests that the transition in compartmental loading from medial to lateral during mid stance phase is not attributed to the EKAM but some other factor. The medial and lateral muscle forces could better explain the shift in contact loading for right leg stance phase, **Figure 71**. There is a transition point between the sum of the medial muscle forces and the sum of the lateral muscle forces for the right leg of stance phase. The medial muscle forces

become greater than the lateral forces around the same time the first and second contact load transitions occur, at between 50-60 %stance for the right leg. As the medial muscle forces increase, **Figure 71**, the medial joint contact load tends to increase, **Figure 78**. Therefore, the transition in muscle forces better explains the midstance transitions in compartmental load distribution for the right leg of Normal Walking.

When looking at the joint contact loads compared to the EKAM for the left leg of stance phase for normal walking, there are two transitions in early stance **Figure 79**. The EKAM is predominantly in the negative region throughout stance phase but has a crest in the positive region which could explain the compartmental load distribution. For left leg stance phase of Normal Walking, the lateral compartment tends to accept a majority of the load for a longer time. The fact that the EKAM is in the negative region would explain why the lateral compartment accepts a greater portion of the total load than the medial compartment for Normal Walking of left leg stance phase. When looking at the medial and lateral muscle forces for the left leg of stance phase, **Figure 125** found in **Appendix E**, the lateral muscle forces are higher, mean force of 57.72%BW, than the medial muscle forces, mean force 13.75 %BW,

Table 39 found in **Appendix E**. Therefore, the muscle forces tend to have a greater effect on the compartmental joint contact loads than the EKAM for Normal Walking compared to Tai Chi. As a result, it can be concluded that the EKAM has a greater influence on the medial and lateral knee joint contact loads for Tai Chi than for Normal Walking.

This dramatic shift in compartmental loads for Tai Chi could promote healthy mechanical loading of the knee by shifting the load distribution from one compartment to another within the articular

cartilage of the knee. This shift in mechanical loading could promote healthy intermittent hydrostatic stress which would be an effective technique to mechanically simulate chondrocyte synthesis, promote ECM remodeling, and ultimately promote cartilage maintenance and total joint health. In addition to the significant shift in compartmental loading, there was a dramatic shift of 47% in total time that the medial compartment accepts the majority of the total contact load for Tai Chi vs. Normal Walking. Therefore, the medial compartment accepts majority of the load for a much shorter amount of time for Tai Chi than for Normal Walking, which could lead to greater pain reduction in the medial compartment for patients with medial knee osteoarthritis.

In summary, there was a dramatic shift in compartmental loading of the knee for Tai Chi compared to that of Normal Walking in terms of percentage that each compartment accepts the total contact load. This can be attributed to the cyclic nature of the EKAM for Tai Chi. The EKAM showed to be more influential in explaining the compartmental load distribution in the knee for Tai Chi compared to Normal Walking. Conversely, the compartmental load distribution for Normal Walking can best be explained by the medial and lateral muscle force contributions in the knee. This suggests that Tai Chi could be an alternative treatment to patients with knee OA because there are signs of cyclically altered compartmental loads throughout stance phase of Tai Chi gait. However, due to high muscle forces generated during Tai Chi gait the magnitude of the medial, lateral, and total joint contact loads were all greater than that of Normal Walking. Therefore, more degradation of the articular cartilage in the knee could be present because of the significantly higher loads.

4.2. Normal Walking Altered TFA Vs. Tai Chi Altered Tai Chi

When comparing the results for altered tibiofemoral alignment there was one common trend. In terms of percent difference, the change in mean loads and mean percent total load is greater for the medial compartment than the lateral compartment for Tai Chi when a tibiofemoral malalignment is present. However, the reciprocal is true for Normal Walking. In terms of percent difference, the change in mean load and mean percent total load is greater for the lateral compartment than for the medial compartment. This trend is independent of malalignment direction; therefore, it holds true regardless of varus or valgus malalignment. As a result, the medial compartment loading is more sensitive to tibiofemoral malalignment than the lateral compartment for Tai Chi. This means that there is a greater change in medial compartment loading per degree alteration in tibiofemoral alignment compared to the change in lateral loads in terms of percent difference. The reciprocal is true for Normal Walking. The lateral compartmental loading is more sensitive to tibiofemoral malalignment than the medial compartment. The only explanation for this trend must be in the muscle coordination for Tai Chi vs. Normal Walking. One explanation could be that the muscles on the medial side or the right leg are more sensitive to change in tibiofemoral alignment than the lateral side muscles. This trend could lead to further pathogenesis of why Tai Chi seemingly improves balance and helps prevent falls in older adults (Yang and Liu). However, further research needs to be done in order to make this claim. When looking at the EKAM for altered tibiofemoral alignment, the shifts are intuitive. For a varus malalignment the EKAM was shifted up relative to the nominal EKAM, **Figure 74** and **Figure 75**, signifying an increase in knee adduction moment in the positive regions and a reduction in the abduction moment in the negative regions across stance phase for the left and right knees of Normal Walking and Tai Chi gait. For a valgus malalignment, the EKAM was shifted down relative to the nominal EKAM, signifying a

reduction in the knee adduction moment in the positive regions and an increase in the knee abduction moment in the negative regions across stance phase for the left and right knees of Normal Walking and Tai Chi gait. The results garnered from this study support the fact that the EKAM helped lower the medial compartmental load distribution of the knee. Thus, there is a legitimate reason to continue to investigate the hypothesis that Tai Chi is an effective rehab exercise for patients with osteoarthritis of the knee.

4.3. Discussion Summary

In summary, the following results and conclusions can be made from the results that were found:

1. Higher total knee contact loads for Tai Chi than for Normal Walking
2. Shift in joint contact load distribution for from medial to lateral compartment for Tai Chi relative to Normal walking. Reduced medial joint contact load distribution for Tai Chi.
3. Medial compartment unloading during stance phase Tai Chi
4. Medial compartment loading is more sensitive to malalignment than the lateral compartment for Tai Chi. The reciprocal is true for Normal Walking.
5. The cyclic nature of the EKAM effects compartmental loading of Tai Chi, ultimately promoting cartilage health.
6. Therefore, there is a good reason to believe that Tai Chi could be an effective alternative for OA mitigation and prevention.

Chapter 5: Validation

5.1. Intro to Model Validation Process

Every researcher and computational modeler must ask two fundamental questions: How do we know the results are correct? And subsequently, how do we quantify the error in our results? From a musculoskeletal modeling standpoint, the answer to these questions are not straight forward because *in-vivo* data is not easily obtained. However, there are a number of ways to validate musculoskeletal modeling results (Hicks et al.). Biomechanical researchers from Stanford University and the developers of OpenSim have published a pragmatic comprehensive resource on the best practices to validate musculoskeletal models and simulation results called, “Is My Model Good Enough? Best Practices for Verification and Validation of Musculoskeletal Models and Simulations of Movement”(Hicks et al.). They outline many practical techniques for model validation specific to OpenSim, but the same practices can be broadly applied across other musculoskeletal software platforms.

It is important to first define the common terms used for model validation practices that are relevant in the context of the current study. First, validation is “the process of determining the degree to which a model is an accurate representation of the real world from the perspective of the intended uses of the model” (Thacker). Calibration is “the process of choosing model and simulation parameters that provide the best match to experimental or other reference data” (Hicks et al.). Error is “the difference between a measured or estimated value of a parameter and its true value” (Hicks et al.). Uncertainty is “the potential source of error which can arise from a gap in knowledge about a biological or physical system under study or from inherent variability in the subject or

phenomenon being measured” (Hicks et al.). Credibility is “the degree of trust placed in a particular model or simulation answering a specific research question” (Hicks et al.). These terms and definitions are the foundation on which a legitimate verification plan can be implemented to garner the best understanding of the model results and their legitimacy.

The most obvious way to validate results to directly compare results from a subject specific model to an *in-vivo* measurement of the same subject being modeled. However, access to that data is often difficult to measure and thus is not easily obtained. Therefore, the most common way to validate results is to compare model and simulation results to independent experiments and other models. For example, one could compare muscle activation to the EMG signal of an anthropometrically similar model to determine the degree of accuracy of the muscle activations in the model. Other independent model parameters that can be compared include, joint contact forces from a patient with an instrumented knee implant, and ultrasound data to compare muscle tendon parameters. This data is often freely available for a common gait such as normal walking and can be used to independently validate the model (Fregly et al.). Another way to independently validate the model, is to compare model parameters and simulation results to other validated models outlined in the literature. This often includes comparing kinematic joint angles for models of similar gaits, joint moments from inverse dynamic analysis, ground reaction force magnitudes and profiles, muscle activations and corresponding muscle forces, internal joint loads i.e. joint contact forces, and finally muscle fiber and tendon velocities (Hicks et al.).

After independent validation, a test for robustness in the model results is often used to evaluate the sensitivity of the simulation results to input errors and model parameters. Musculoskeletal

modeling simulations are often interdependent, and a cascading sequence of simulations are often required to produce a desired result. Therefore it is important to identify the sensitivity of modeling outputs to experimental inputs and model parameters in order to eliminate error propagation in the final results (Hicks et al.). By systematically changing the input parameters, a quantifiable range of possible outcomes or confidence intervals can be determined. When the output range is small the parameter is less sensitive compared to when the output range is large. Sensitivity analyses are typically performed iteratively and range in complexity with a Monte Carlo analysis being the “gold standard” for sensitivity analyses (Reinbolt et al.). It is important to understand the sensitivity of possible outcomes to input parameters in order to quantify the uncertainty and possible experimental error which could perniciously exist in the input data.

Validating a musculoskeletal model is not straight forward and often difficult. Many iterations are needed to fully quantify the uncertainty in the model to satisfy the credibility of the model results. One of the biggest hindrances to model validation is obtaining access to accurate and relevant independent data such as EMG signals and other validated model data. Therefore, researchers are often limited in their ability to quantify the credibility of their results.

5.2. Current Validation Process

The validation process used for this study was threefold: Calibration, Internal Validation, and Independent validation. Simply put, calibration involves the comparison of results from an inverse dynamic modeling approach to the results generated by a forward dynamic modeling approach for the same model. Internal validation compares the moments generated by the muscle forces to the total joint moment about a particular generalized coordinate. Independent validation involves the

comparison model results to an existing set of validated model results generated from an independent subject of similar anthropometric parameters. A work workflow of the validation process used for this study can be seen in **Figure 80**.

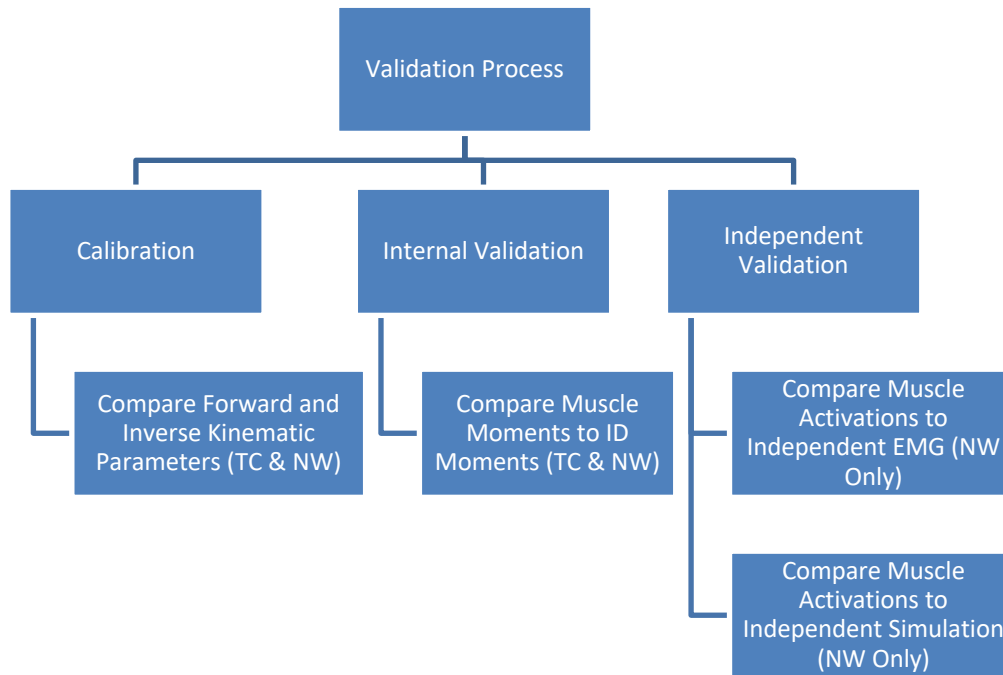


Figure 80: Workflow of the validation process used for this study to validate the kinematic and muscle force results for Tai Chi and Normal Walking.

5.2.1. Calibration Process

One of the biggest contributors to the joint contact forces in the knee are the muscle forces generated by the muscles that traverse the knee joint (Guess et al.). Therefore, joint contact forces are sensitive to muscle contractions. As a result, it is important that the muscle activations model the correct set of muscle activations in order to produce accurate results. One way to verify that the muscle force results are correct is by performing a calibration analysis. A calibration analysis uses the muscle force outputs generated from an inverse analysis, as inputs for a forward analysis, and the results are compared. A forward dynamic (FD) analysis in OpenSim, was used to perform the calibration analysis. The forward dynamics tool used the activations and controls generated

my computed muscle control to drive the model forward in time. As the muscles moved the model forward in time, a set of joint kinematics was produced which were compared to the original joint kinematics generated from inverse kinematics. The errors in the two joint kinematics elucidate the error form the muscle forces in the MSM. A workflow of the calibration analysis can be seen in **Figure 81**.

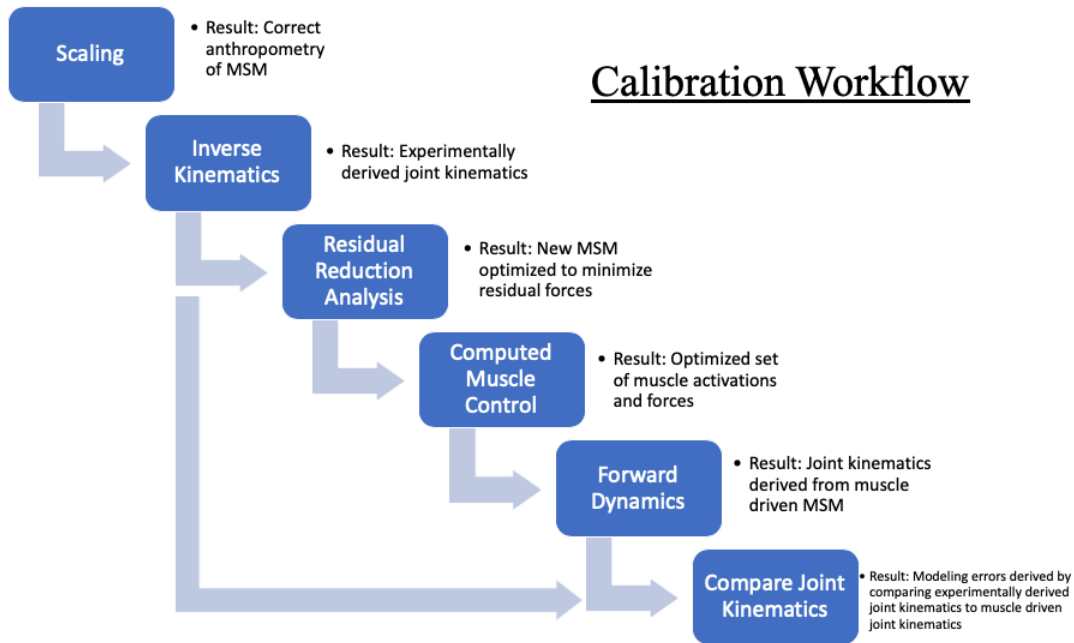


Figure 81: The following OpenSim simulations compose the calibration analysis workflow. Results from each simulation serve as inputs for the next

The error between forward and inverse kinematic results is called forward-inverse error (FIE). If the errors are small, i.e. the average percent difference in values at each time step are small, $\text{Mean_ \%Diff} < 5\%$, and the p-value of a paired t-test comparing kinematic mean differences of designated coordinates of interest is greater than alpha, $\alpha = 0.005$, then it is safe to assume that the muscle forces generated no kinematic error for a forward solution compared to an inverse solution. Thus, the set of muscle forces generated by CMC was adequate to produce the desired kinematics. A paired t-test was used to compare the kinematic mean differences of designated

coordinates. Paired values are the inverse and forward kinematic coordinate values at a given time step. The null and alternate hypothesis are defined by **Equation 44** and **Equation 45**, respectively.

$$H_0: \mu_{diff} = 0 \quad (44)$$

$$H_a: \mu_{diff} \neq 0 \quad (45)$$

Where μ_{diff} is the mean difference between forward and inverse kinematic coordinates at a given time step defined by **Equation 46**.

$$\mu_{diff} = \frac{\sum_{i=0}^n x_{1,1} - x_{2,1} + \dots x_{1,n} - x_{2,n}}{n} \quad (46)$$

Paired t-tests were used to calibrate the Normal Walking model and the Tai Chi model for the following kinematic coordinates: pelvis translation_x, pelvis translation_y, pelvis translation_z, hip flexion angle, knee flexion angle, and ankle angle. These kinematic coordinates were selected because they are mostly influenced by the muscle forces that traverse the knee joint. The translational coordinates help determine if and when the center of mass of body begins to diverge translationally during the muscle driven simulation. If the muscles are weak, then the translational coordinates of the forward simulation will show a divergence indicating that the COM is not sufficiently supported by the muscle forces in the legs. Similarly, the rotations about the hip, knee, and ankle joints will diverge if insufficient muscle forces were calculated. If insufficient muscle force were calculated, then divergence in the rotational displacement about the hip, knee, and ankle joints can be seen during the forward simulation.

A paired t-test is an effective way to compare the kinematic coordinate errors for errors that are relatively small. However, if the kinematic FIE's are too large then the model can become unstable and the muscle forces produce a motion that is unachievable during gait, **Figure 82**, and therefore

the kinematic coordinate errors cannot be statistically compared as was the case for the Tia Chi Model.

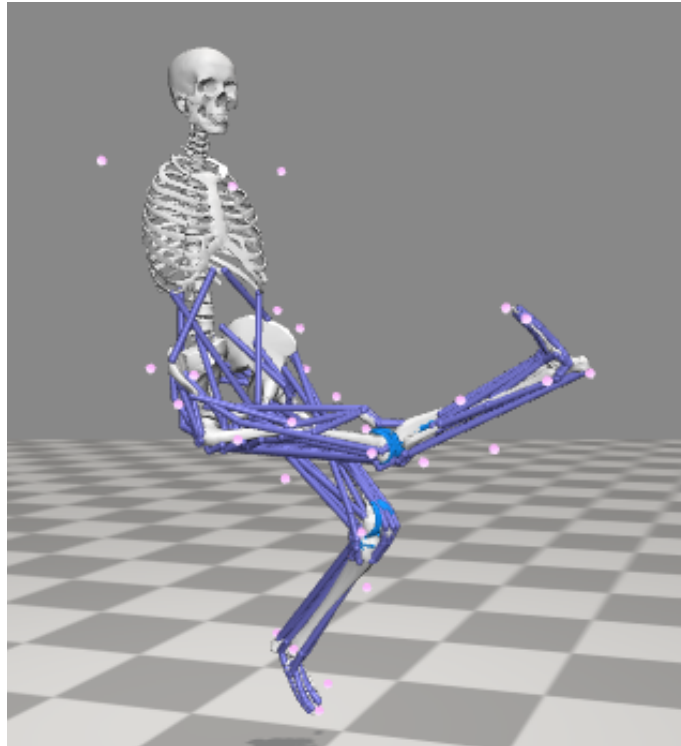


Figure 82: Unstable forward dynamic simulation that results in abnormal model motion during gait

After the calibration results have been analyzed, precaution must be considered before moving forward, because limitations exist with calibration. Just because there is insignificant difference in FIE of kinematic coordinates, does not guarantee the set of computed muscle activations are synonymous with the *in-vivo* muscle activations. Therefore, independent validation is needed to further validate the *in-vivo* muscle activations generated by the simulation. On the other hand, calibration analysis confirms that the set of computed muscle activations is sufficient to produce the desired gait kinematics measured during data collection. Therefore, a high level of confidence can be placed in the muscle force and thus in the joint reaction analysis results.

5.2.2. Internal validation

Internal validation involves the application of newtons second law, by directly comparing the summation of the torques generated by the muscle forces that cause rotation of a specific joint, with the total joint torque produced during inverse dynamics, **Equation 47**.

$$\left[\sum_{i=0}^{n_{muscles}} \mathbf{F}_{i,j} \mathbf{r}_{i,j} \right] - \boldsymbol{\tau}_{ID,j} = \boldsymbol{\tau}_{error,j} \quad (47)$$

Where, $\mathbf{F}_{i,j}$ is the i^{th} muscle force that generates rotation about the j^{th} coordinate, $\mathbf{r}_{i,j}$ is the corresponding i^{th} muscle moment arm about the j^{th} coordinate, $\boldsymbol{\tau}_{ID,j}$ is the j^{th} joint torque calculated by inverse dynamics, and $\boldsymbol{\tau}_{error,j}$ is the torque error in the j^{th} coordinate manifested by the errors in the muscle forces. For this study, only the right knee flexion coordinate was analyzed, because only the right knee joint contact forces were calculated. If the torque errors are small, i.e. the average % difference between the muscle moments and the inverse dynamic moments is less than 5% difference, then the error in the muscle forces are minimal and higher confidence in the joint reaction analysis results can be concluded.

Much like the limitations with calibration, there are inherent limitations with the internal validations process. Just because errors are small, does not guarantee that the muscle force are the same muscle forces that are being observed in-vivo. Further validation is needed to determine if the correct muscle coordination is being modeled. Therefore, independent validation will help elucidate the credibility of the simulated muscle activations.

5.2.3. Independent Validation

In order to further validate the muscle activations, an independent validation procedure was used to directly compare the muscle activations with an independent reference. This involves comparing the results from each simulation to validated results outlined in the literature. For this study, two independent references were used to independently validate the simulated muscle force results. First, the muscle forces and activations were compared to other independent muscle forces generated by OpenSim. The data files that came with the OpenSim download served as a “gold standard” reference with which to compare muscle activation results. This was done by comparing corresponding “gold standard” muscle activations of the most influential muscles that contribute to joint contact at the knee for Normal Walking, with activations generated by the test subject. Those muscles were the rectus femoris, medial gastrocnemius, and lateral gastrocnemius. If the muscle activation profiles are similar, the confidence in the results are increased. Secondly, the influential muscle activations were then compared to EMG data of an independent subject. Freely available EMG data of an anthropometrically similar subject (Female, Height=1.67m, Weight=78.4kg) was downloaded and used for independent validation, **Figure 83**. EMG data for the rectus femoris, medial gastrocnemius and the lateral gastrocnemius was rectified and normalized by dividing the muscle activations by the maximum voluntary contraction (MVC) **Figure 84**, **Figure 85** and **Figure 86**, respectively. Therefore, the activation level of each muscle was calculated in terms of percent maximum voluntary contraction (%MVC). The maximum voluntary contraction value was determined by taking the 95-percentile value of the maximum voluntary contraction data for each muscle, as was consistent with the literature (Sousa and Tavares). The normalized EMG data was then plotted as a function of stance phase for Normal Walking.

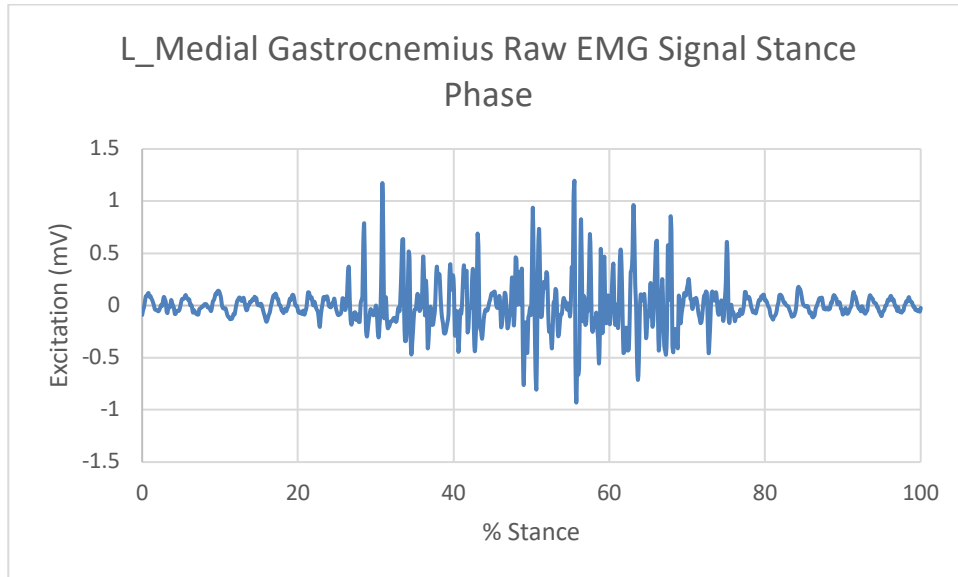


Figure 83: Raw EMG signal for medial gastrocnemius of the left leg, stance phase of the independent test subject from the grand challenge study.

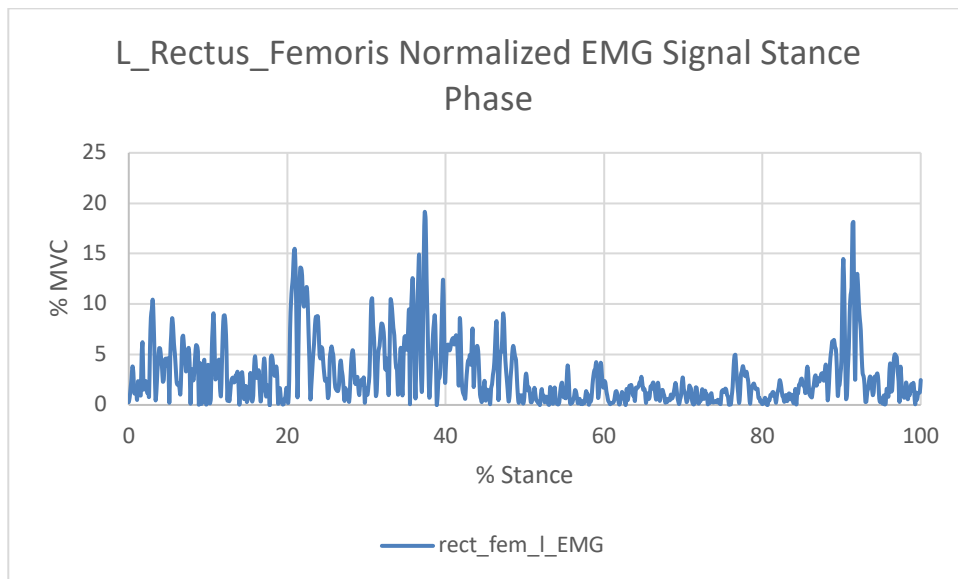


Figure 84: Left rectus femoris EMG signal rectified and normalized for percent maximum voluntary contraction for stance phase of the independent test subject from the grand challenge study.

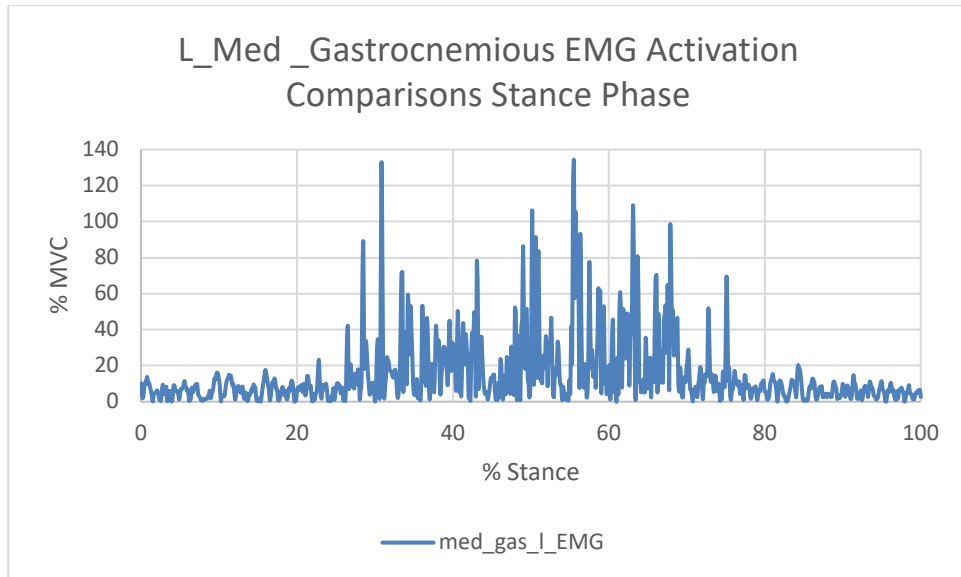


Figure 85: Left medial gastrocnemius EMG signal rectified and normalized for percent maximum voluntary contraction for stance phase of the independent test subject from the grand challenge study.

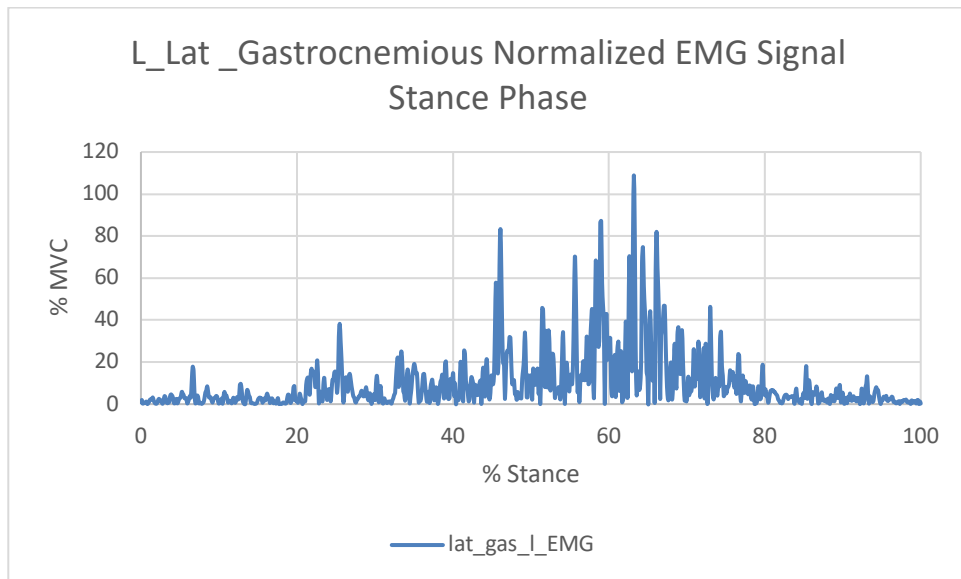


Figure 86: Left lateral gastrocnemius EMG signal rectified and normalized for percent maximum voluntary contraction for stance phase of the independent test subject from the grand challenge study.

The muscle activations were generated by static optimization for the Normal Walking trial and the OpenSim reference. The Normal walking and OpenSim reference muscle activations were compared and plotted against the normalized EMG data for each corresponding muscle as a function of stance phase. The paired t-tests for the difference of means were used to compare the muscle activations from the OpenSim reference data to the Normal Walking muscle activations throughout stance phase.

Limitations exist when comparing muscle activations from independent studies. First there is really no effective way to statistically compare the EMG data to the activations in the muscles because there is simply too much noise in the EMG data. Therefore, visual inspection could only be used. Also, there are many conflicting views on how EMG data can be normalized and compared within subjects. Therefore, uncertainty in the EMG data exists and is difficult to quantify (Sousa and Tavares). Therefore, the degree of error cannot be quantified through independent validation of EMG alone. However, a visual inspection of the activation data can elucidate whether the simulated results are credible. Obviously, given the inherent patient specificity among studies, large variability will be present. Therefore, the results will not closely match the results in the literature. This is to be expected. However, a direct comparison to the literature will at least elucidate the credibility of simulated results by comparing kinematic profiles. In other words, if simulated kinematic profiles are similar in contour and magnitude to those outlined in the literature, the results can be deemed credible. However, precaution must be taken when this independent validation method is used because the justifications are somewhat arbitrary and quantifiable uncertainty cannot be obtained. Therefore, direct *in-vivo* validation must be used before any significant clinical or research conclusions can be made from these results.

5.3. Validation Results and Discussion

5.3.1. Calibration Results

Two calibration trials were conducted for this study, one for the Normal Walking, and one for Tai Chi. For Normal Walking, a comparison of the forward and inverse kinematic parameters of pelvis can be seen in **Figure 87** and **Figure 88**, while kinematic coordinates at the right hip, knee, and ankle can be seen in **Figure 89**. Kinematic coordinates of the Left hip, knee, and ankle can be seen in **Appendix** for Normal Walking of the nominal TFA.

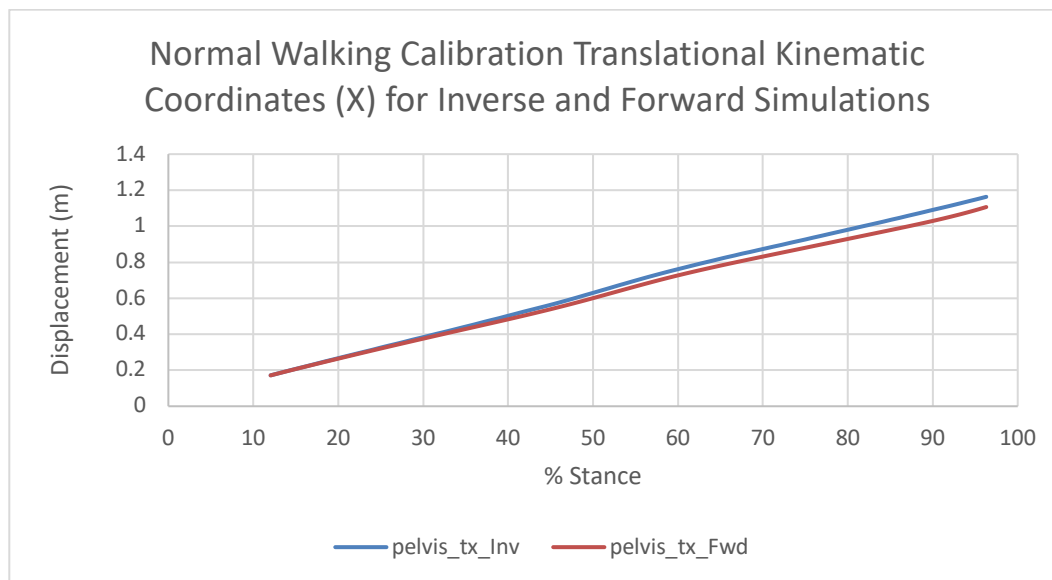


Figure 87: Calibration results for the Normal Walking trial of the nominal model. A comparison of the inverse kinematic and forward dynamic X translational coordinate of the pelvis for right leg, stance phase.

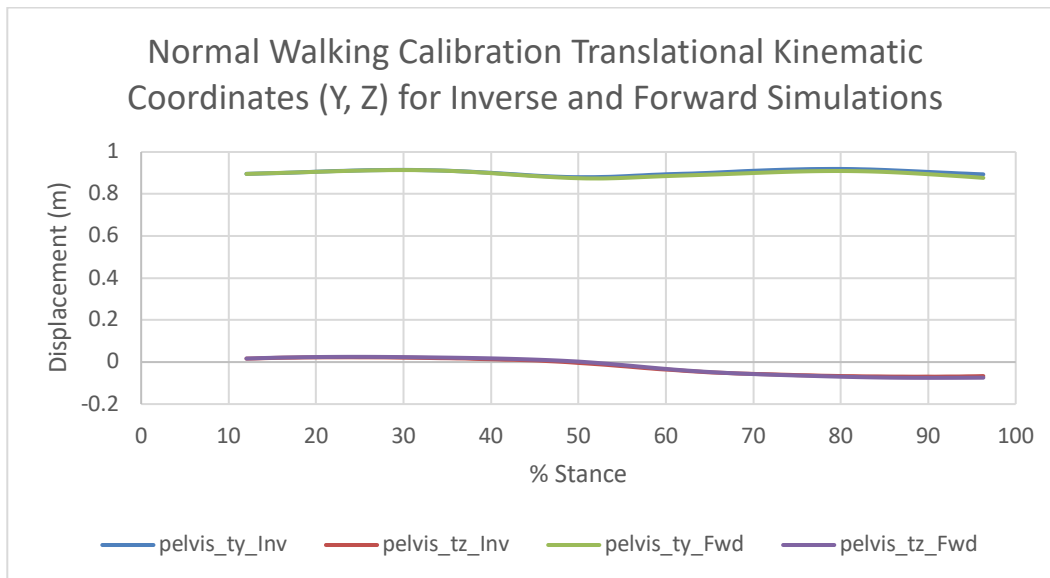


Figure 88: Calibration results for the Normal Walking trial of the nominal model. A comparison of the inverse kinematic and forward dynamic Y & Z translational coordinates of the pelvis for right leg, stance phase.

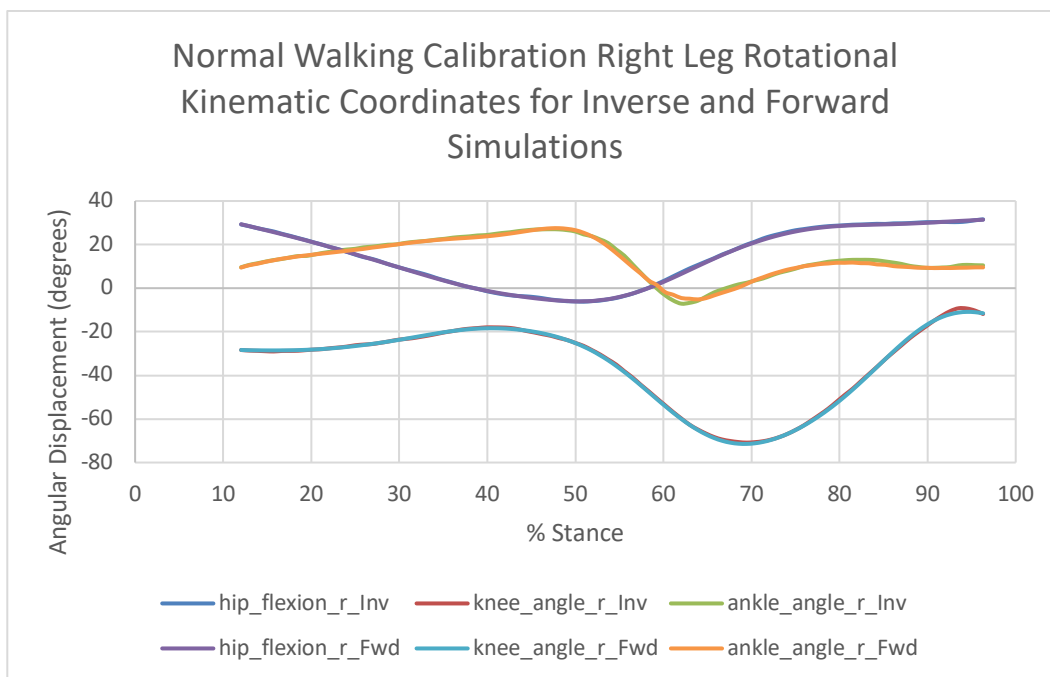


Figure 89: Calibration results for the Normal Walking trial of the nominal model. A comparison of the inverse kinematic and forward dynamic rotations of the hip, knee, and ankle coordinates for right leg, stance phase.

Paired t-tests were used to determine statistical differences between the inverse kinematic and the forward kinematic coordinates. Of the 6 coordinates tested, only one coordinate, pelvis_z translation, was found to not have significant difference between coordinate values from inverse kinematic vs. forward dynamics, **Table 22**. However, when looking at the mean % difference in coordinates values all time steps during stance phase, the following was observed: -3.82 %Diff for the X translational coordinate of the pelvis, -0.64 %Diff for the Y translational coordinate of the pelvis, 4.95 %Diff for the Z translational coordinate of the pelvis, -1.55 %Diff for hip flexion, 0.81 %Diff for knee rotation, and -14.05 %Diff for the rotation of the ankle, **Table 23**. The Mean % difference of coordinate values was calculated by taking the percent different between inverse kinematic coordinate values and forward dynamic values at each individual time step. The percent differences were then averaged across all time step to give the average percent difference between the inverse and forward values across the entire stance phase of gait.

Table 22: Statistical results of paired t-tests for the difference of means for kinematic coordinates calculated by inverse dynamics and forward dynamics. All values are for the right leg stance phase of the Normal Walking trial.

Normal Walking Calibration Statistical Results Right Leg				
Coordinate	Inv_Mean	Fwd_Mean	Diff_Mean	P-Value
Pelvis_tx	0.676	0.645	-0.0302	p<0.005
Pelvis_ty	0.903	0.897	-0.00578	p<0.005
Pelvis_tz	-0.0211	-0.0205	0.000646	0.100
Hip_flexion_r	14.364	14.212	-0.152	p<0.005
Knee_angle_r	-35.089	-35.260	-0.171	p<0.005
Ankle_angle_r	13.704	13.375	-0.328	p<0.005

Table 23: The mean the percent differences in kinematic coordinate values at all time steps for inverse kinematics and forward dynamics throughout right leg stance phase of gait for the Normal Walking trial.

Mean % Differences of Normal Walking Kinematic Coordinates Right Leg		
Coordinate	Mean_%Diff	Unit
Pelvis_tx	-3.82	%
Pelvis_ty	-0.64	%
Pelvis_tz	4.95	%
Hip_flexion_r	-1.55	%
Knee_angle_r	0.81	%
Ankle_angle_r	-14.05	%

The calibration analysis for the Tai Chi model became unstable at T=7.1sec around 40.6 % of stance phase, **Figure 82**. Therefore, the results from the calibration analysis cannot be statistically compared. However, forward and inverse kinematic calibration plots of the Tai Chi stance phase can be seen in **Appendix** .

5.3.2. Calibration Discussion

The following conclusions can be made for the calibration results for both Normal walking. All but 1 kinematic coordinate showed a significant difference when comparing results from the inverse kinematics and forward dynamics. This would assume that the kinematic coordinates are significantly different and thus there is a significant amount of error in the muscle forces used to drive the model forward in time. Therefore, the confidence in the muscle forces are low strictly based on the statistical observation. However, upon visual inspection of the coordinates as a function of stance phase, **Figure 87**, **Figure 88**, and **Figure 89**, very little error appears to be present when comparing inverse and forward kinematic coordinate values. In addition, the mean percent difference in inverse values compared to forward values appear to be small. All values are

less than 5% difference, except for the ankle angle coordinate which showed an average percent difference of -14.05 % difference. This would indicate that there is significant error in the medial and lateral gastrocnemius muscles because they are most influential in causing rotation about the ankle joint, plantar dorsiflexion. The ankle joint error does not point to errors in the medial and lateral gastrocnemius exclusively. The ankle error could be caused by the error in the soleus muscle which was not analyzed. Therefore, further investigation into the medial and lateral gastrocnemius muscle activations are necessary in order to gain confidence in the current muscle forces for Normal Walking.

The results from the Tai Chi calibration analysis could not be analyzed because the model became unusable early on during right leg stance phase. However, calibration plots of the right leg for stance phase Tai Chi can be seen in **Appendix** . As the model became unstable, the right foot appears to slip out anteriorly with respect to the ground. This would indicate that there is a weak ground reaction force in the posterior direction. Therefore, there is a potential error in the X component ground reaction force which is applied to the right calcaneus. When looking at the X component ground reaction force in **Figure 90**, there appears to be a significant amount of noise which would point to errors in the force plates during data collection. The noise could be residual noise coming from the ground or some other form of inaccuracy in the force plate when measuring horizontal GRF.

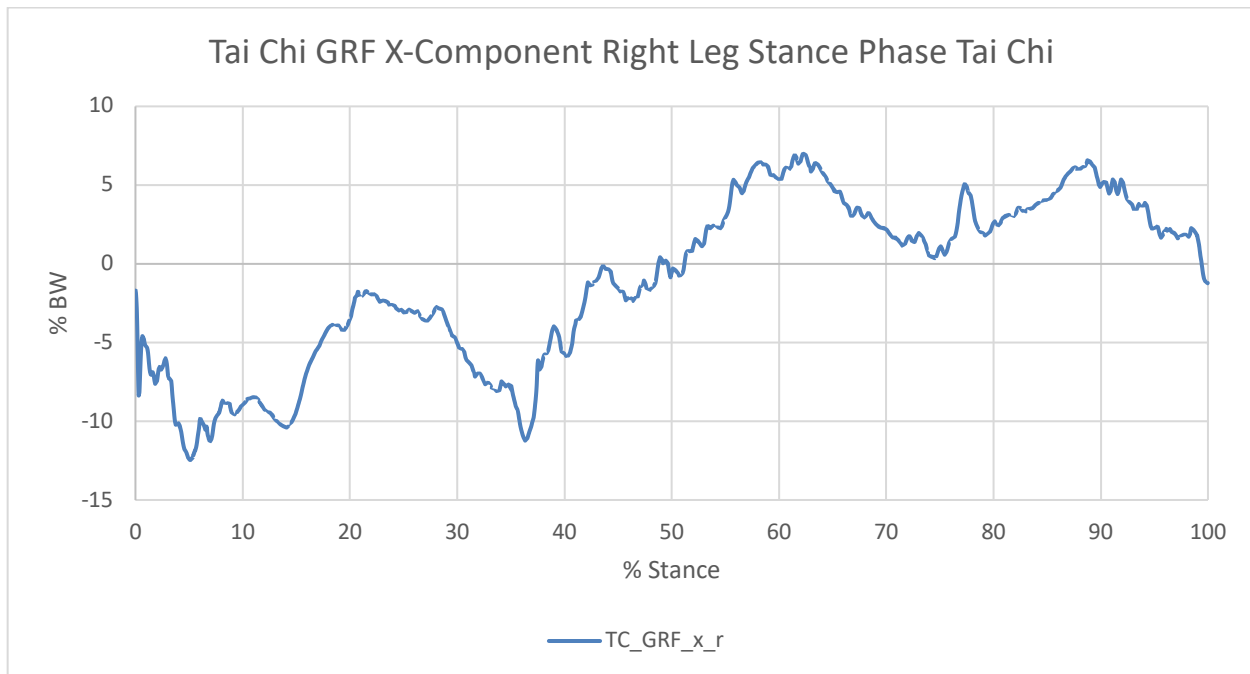


Figure 90: Anteroposterior, X-component, ground reaction force measured at the right calcaneus by the force plate for stance phase of Tai Chi gait

5.3.3. Internal Validation Results

An internal validation approach was conducted for the flexion/extension moments generated by the muscle forces about the left and right knees for Normal Walking and Tai Chi. The muscle force moment and inverse dynamic moment were normalized for body mass. The sum of the muscle force moments and the inverse dynamics moment can be seen as function of right and left leg stance phase for Normal Walking and Tai Chis in **Figure 91** and **Figure 92** respectively. A table of the moment definitions from the internal validation can be seen in

Table 24.

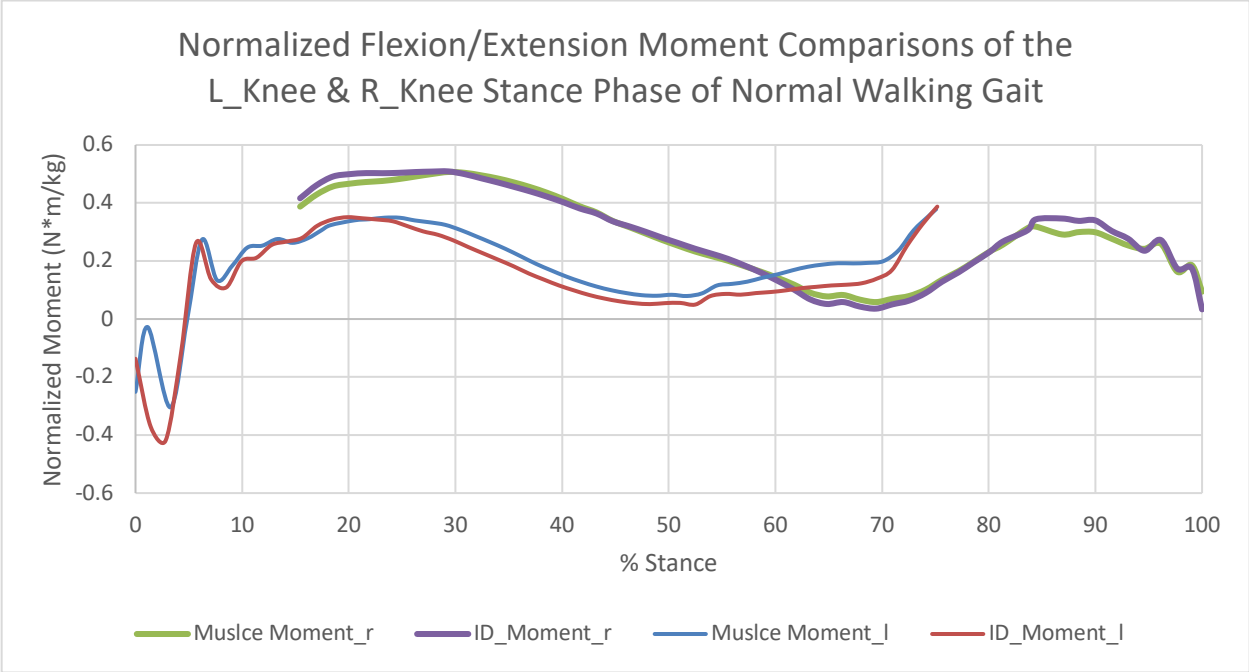


Figure 91: Normalized moment comparisons used for internal validation of the right and left knee stance phase for Normal Walking gait

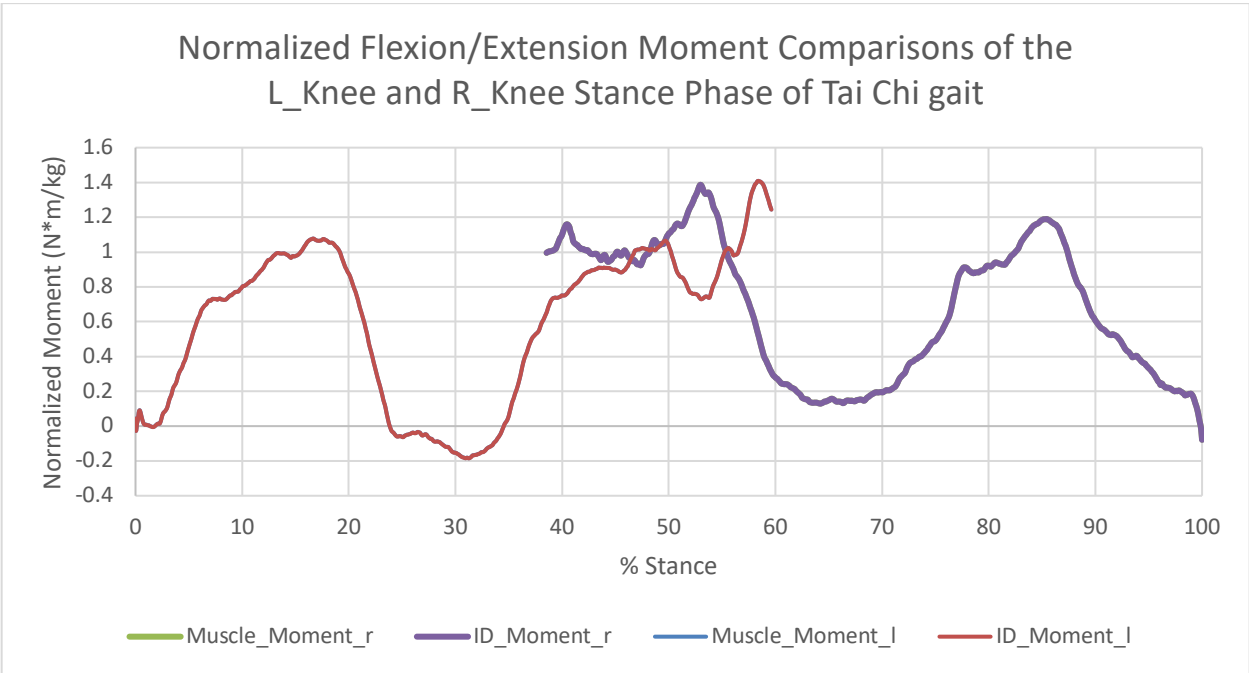


Figure 92: Normalized moment comparisons used for internal validation of the right and left knee stance phase for Tai Chi gait

Table 24: Defines each moment calculation, Figure 91, about the right knee used for internally validating the muscle forces calculations for Tai Chi gai.

Name	Definition
Muscle_Moment	Sum of all moments generated by the 13 muscles that traverse the knee joint that generate the flexion/extension moment about the knee. Those muscles include: the semimembranosus, semitendinosus, biceps femoris long head, biceps femoris short head, sartorius, tensor fasciae latae, gracilis, rectus femoris, vastus medialis, vastus lateralis, vastus intermedius, medial gastrocnemius, and the lateral gastrocnemius
ID_Moment	Total Knee flexion/ extension torque about the knee required to generate the desired locomotion calculated by inverse dynamics

Upon visual inspection of the Normal Walking internal validation results for the left and right knees, there is an obvious amount of error between the muscle moment and the ID moment. The average error between the muscle moments and ID moment was -0.00247 Nm/kg and 0.0391 Nm/kg for the left and right knees of normal walking respectively. The average percent error across right and left stance phase of gait were 7.58% and 25.315% Error respectively. When looking at the moment errors for the left and right knees for Tai Chi, the errors were much smaller compared to normal walking for the left and right knees. The average moment error for the right and left knees were 0.000718 Nm/kg and -0.000365 Nm/kg , respectively. The average percent error between the muscle force moment and inverse dynamics moments for the right and left flexion/extension moments of stance phase Tai Chi were -0.0632% and 0.347% Error, respectively. Error and percent error plots of the left and right knee flexion/extension moments as a function of right and left stance phase can be seen in **Figure 134** and **Figure 135** in **Appendix** . All values for the internal validation for the Tai Chi gait can be seen in **Table 25**.

Table 25: Internal validation results of moments calculated about the right and left knee joints for stance phase of Normal walking and Tai Chi gait, where the errors are the difference in inverse dynamic flexion/extension moment and the muscle force flexion/extension moment about the left and right knees.

Internal Validation Results for Normal Walking and Tai Chi			
Parameter	Normal Walking	Tai Chi	Unit
Mean_Moment_r_Error	-0.00247	0.000178	Nm/kg
Mean_Moment_l_Error	0.0391	-0.000365	Nm/kg
Mean_Moment_r_%Error	7.580	-0.0632	%
Mean_Moment_l_%Error	25.315	0.347	%

5.3.4. Internal Validation Discussion

The average errors and percent errors between the left and right knee flexion/extension moments were significantly smaller for Tai Chi than for Normal Walking. The left and right percent errors for Tai Chi were both less than 1 % error. Therefore, the muscle forces generated about the left and right knees are consistent with the moments generated from inverse dynamics with minimal error between the two. This suggests that the muscle forces generated about the left and right knees are sufficient to produce the desired locomotion with minimal modeling errors. As a result, greater confidence can be placed in the muscle forces that traverse the knee joint for Tai Chi. The low errors generated during internal validation for Tai Chi ultimately increase the confidence in the joint contact force results. It is important to point out that the percent error for the right leg is nearly 5 times smaller than for the left leg. Therefore, it is safe to assume that the results for the right leg are more reliable than the results for the left leg of Tai Chi gait.

The average errors and percent errors between the left and right knee flexion/extension moments were much larger for Normal Walking than for Tai Chi. The percent error for the right and left knees were both greater than 5% error, with the left side experiencing an average percent error of over 25%. This is a significantly large error and ultimately decreases the confidence in the muscle

forces that traverse the left knee for Normal Walking. The average percent error for the right knee is much smaller, 7.58%, compared to the left knee. As a result, it is safe to assume that the confidence level in the muscle forces that traverse the right knee joint is greater than confidence level in the muscle forces that traverse the left knee. It is also safe to assume that the confidence in the muscle forces for Tai Chi is greater than the confidence in the muscle forces for Normal Walking. As a result, less confidence can be placed in the Normal walking joint contact forces than for the joint contact forces for Tai Chi, especially for the left knee of Normal Walking.

Based on the internal validation results, a high confidence can be placed in the muscle forces generated for Tai Chi. Conversely a lower confidence can be placed in the muscles generated for Normal Walking. Therefore, a significant amount of error exists in the muscle forces for Normal Walking, especially in the left side. As a result, higher confidence can be placed in the muscle forces generated for the Tai Chi than for Normal walking gait. However, this does not mean that the simulated muscle activations for Tai Chi are equivalent to the muscle activations *in-vivo*, which is a limitation of the internal validation method. Therefore, a direct comparison of the muscle activations must be done in order to further validate the muscle model. Another limitation is that the internal validation moment comparison does not account for residual torques that are added to the knee joint during RRA for dynamic consistency. Nevertheless, the residual torques have little to no bearing on the accuracy of the joint contact forces in the knee.

5.3.5. Independent Validation Results

Independent validation was used to directly compare the muscle model activations to EMG data of an independent subject and to compare model activations to another independently validated

OpenSim model which is referred to as the “OpenSim Reference”. Independent validation could only be performed for the Normal Walking trial because neither EMG data nor an existing OpenSim reference of Tai Chi gait was readily available for comparison. EMG data of the rectus femoris, medial gastrocnemius, and lateral gastrocnemius of the left leg of an independent sample was compared to the muscle activations of the Normal Walking trail along with the activations from the OpenSim reference, which can be seen in **Figure 93**, **Figure 94**, and **Figure 95**.

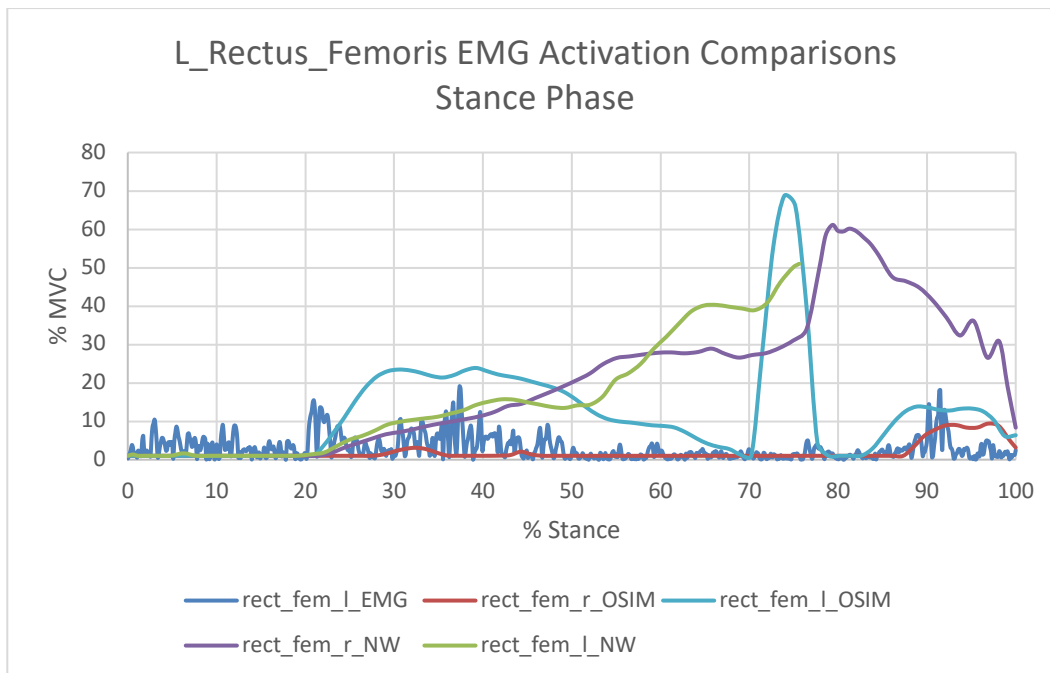


Figure 93: Rectus femoris muscle activation comparisons of EMG, Normal Walking, and the OpenSim reference models. The EMG data is the normalized muscle activation of the left rectus femoris from an independent subject. Right and left muscle activations are shown for the Normal Walking and OpenSim reference models. All activations are a function stance phase.

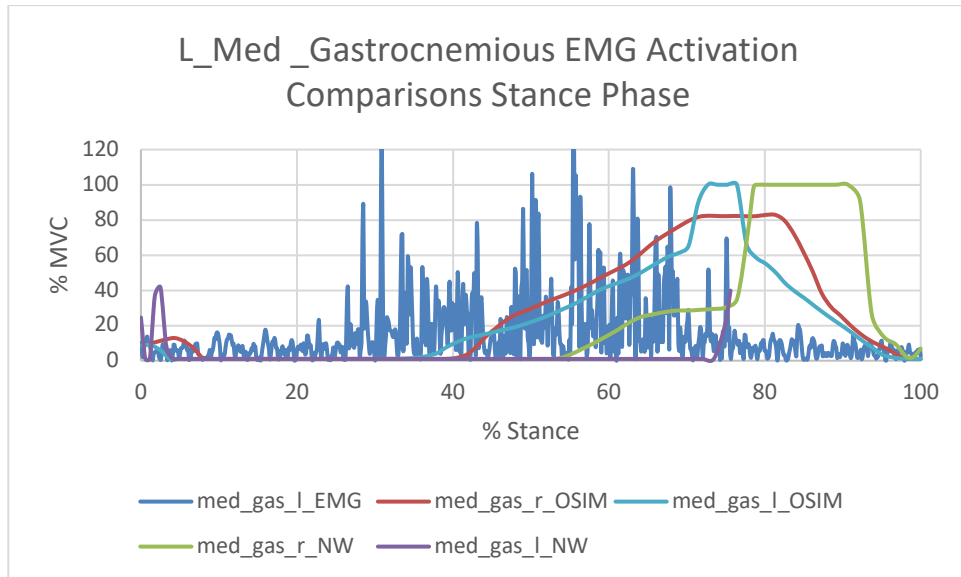


Figure 94: Medial gastrocnemius muscle activation comparisons of EMG, Normal Walking, the OpenSim reference models. The EMG data is the normalized muscle activation of the left medial gastrocnemius from an independent subject. Right and left muscle activations are shown for the Normal Walking and OpenSim reference models. All activations are a function stance phase.

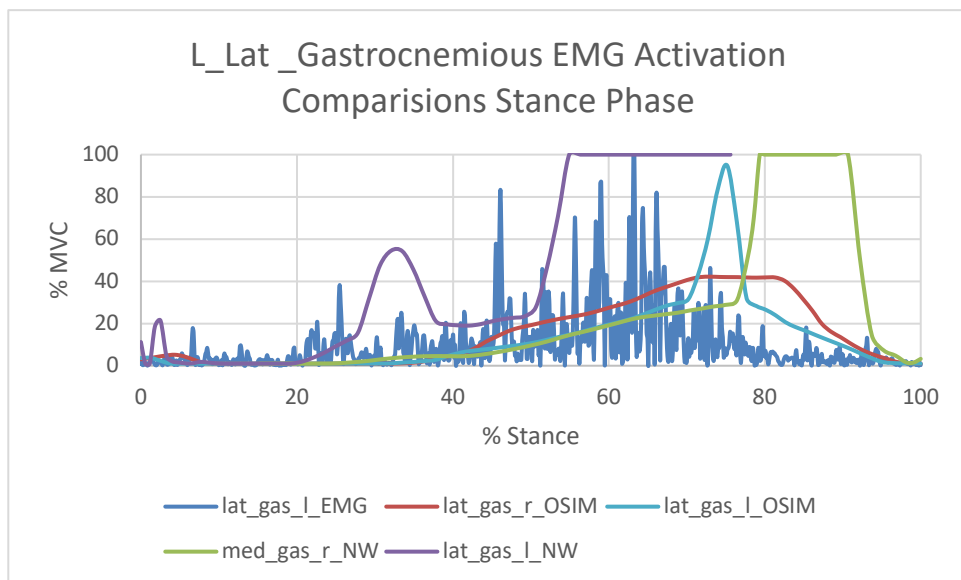


Figure 95: Lateral gastrocnemius muscle activation comparisons of EMG, Normal Walking, the OpenSim reference models. The EMG data is the normalized muscle activation of the left lateral gastrocnemius from an independent subject. Right and left muscle activations are

shown for the Normal Walking and OpenSim reference models. All activations are a function of stance phase.

The activation of the rectus femoris for the Normal Walking model appears to show peak activation of about 60% during late stance phase, **Figure 93**. There appears to be symmetry between the right and left muscle activations for Normal Walking. When compared to the EMG activation, the Normal Walking activation is much higher in late stance phase with peak activations of 60 %MVC for Normal Walking compared to 18 %MVC for EMG. The activation for EMG is much lower on average, 3.01%MVC than the Normal Walking, 14.81%MVC, data with a peak activation of 19.11%MVC, occurring in during mid stance, relative to the 51%MVC peak in late stance for Normal Walking. When comparing the Normal Walking activation to the OpenSim reference, there appears to be more activation in early stance for the OpenSim reference than for Normal Walking. The muscle activation for the OpenSim reference are smaller on average, 12.34 %MVC, compared to Normal Walking, 14.18 %MVC.

The activation of the medial gastrocnemius for the right leg of the Normal Walking model appears to show peak activation of 100% during late stance phase, **Figure 94**. Late stance phase of the left medial gastrocnemius could not be captured and therefore the peak could not be determined. However, it does appear that it will approach maximum voluntary contraction based on the profile at 75 % stance phase. The right and left activations appear to show symmetry for the Normal Walking model. When comparing the Normal Walking activations of the medial gastrocnemius, the EMG shows a peak activation, 133.53 %MVC, during mid stance while peak activation occurs in late stance for Normal Walking. When comparing the activations of the OpenSim reference to the normal walking model, the peaks occur in late stance phase similar to that of the Normal Walking model.

The activation of the lateral gastrocnemius for the left leg of the Normal Walking model appears to show peak activation of 100% during late mid stance phase, **Figure 95**. The activations for the left leg reached a peak activation during late mid stance phase while the peak activation for the right leg occurred during late stance phase. When comparing the EMG activations and the Normal Walking activation, both the peak activations occurred during late mid stance for the left leg. When comparing the activations of the Normal Walking model to the OpenSim reference the peak activations were 100%MVC and 94.77 %MVC for the right and left leg respectively. The peak activation for the OpenSim reference occurred during late stance phase and had a short peak, while the activation for Normal Walking occurred earlier during late midstance and the peak remained at 100 %MVC for longer period of time. On average the Normal Walking activation level, 39.35 %MVC, was higher than the EMG, 10.13 %MVC, and the OpenSim reference, 12.75 %MVC, for the left leg. A comparison of the mean and maximum activations that were compared can be found in **Table 26**.

Table 26: Statistical values for muscle activations from independent validation, EMG activations, OpenSim reference activations, and the activations from the Normal Walking trial in this study.

Statistical Values of Muslce Activations for Independent Validation			
	Mean	Max	Unit
Rect_fem_l_EMG	3.01	19.11	%MVC
Rect_fem_r_OSIM	1.90	9.39	%MVC
Rect_fem_l_OSIM	12.34	68.76	%MVC
Rect_fem_r_NW	26.18	61.14	%MVC
Rect_fem_l_NW	14.81	51.01	%MVC
Med_gas_l_EMG	15.10	133.53	%MVC
Med_gas_r_OSIM	27.24	82.87	%MVC
Med_gas_l_OSIM	23.19	100.00	%MVC
Med_gas_r_NW	30.37	100.00	%MVC
Med_gas_l_NW	3.79	41.60	%MVC
Lat_gas_l_EMG	10.13	108.87	%MVC
Lat_gas_r_OSIM	14.94	42.19	%MVC
Lat_gas_l_OSIM	12.75	94.77	%MVC
Lat_gas_r_NW	30.07	100.00	%MVC
Lat_gas_l_NW	39.35	100.00	%MVC

5.3.6. Independent Validation Discussion

Given that the muscle activation level in the rectus femoris is much higher than both the EMG and OpenSim reference, it can be concluded that there is a significant difference between the model activations and the independent reference. Therefore, the credibility of the rectus femoris muscle activation is not likely; thus, the confidence level is low. The high activation will generate a higher than expected joint contact force thus skewing the results. The high activation level could be the result of redundant muscle co-contraction between the rectus femoris and the hamstring muscles. Another explanation for the high muscle activation in the rectus femoris for Normal Walking could be because the activation in the quadriceps are more concentrated in the rectus femoris whereas the activation in the independent subject could be more evenly distributed throughout the quadricep muscles. More investigation is needed to explain this phenomenon. As a result, there is very little confidence in the muscle force accuracy for the Normal Walking model thus generating a significant amount of uncertainty in the joint contact force in the knee joint.

Based on the activation comparison of the medial gastrocnemius, the credibility is reasonable. The magnitudes and profiles appear to be similar whereas the timing is different for EMG compared to the rest of the activations. The peak EMG occurs earlier in the stance phase compared to Normal Walking and the OpenSim reference. One possible explanation for the later activation has to do with the posture of the individual during gait. The model seemed to be hunched forward which could result in large muscle contraction in later stance phase. However, despite the differences, the muscle activations for Normal Walking appears to be reasonably credible for the medial gastrocnemius muscle. As a result, there is a reasonable amount of confidence medial gastrocnemius.

Based on the activation comparison of the lateral gastrocnemius, the credibility is reasonable as well. Much like the medial gastrocnemius the magnitude and profiles are similar to the EMG data. The timing of the peak activation seems to occur around the same time during late mid stance phase. However, the activation for the left lateral gastrocnemius of Normal Walking is much later. In fact, the actuator is 100% activated for a significant amount of time. This suggests that there is a disproportionate amount muscle activation in the gastrocnemius relative to force that it is producing. Therefore, if the medial gastrocnemius could activate more, it would in order to achieve the desired output force. This indicates that there is some error in the muscle model. One explanation for the over activation of the medial gastrocnemius muscle could be the error in the tendon slack length. This error can cause the muscle force generation to not operate in the optimal region of the force-length-velocity relationship curve ultimately producing weak muscle forces. Therefore, this would cause the model to “over actuate” or even “max out” as it attempts to generate the force required for locomotion. Therefore, more investigation should be done in order increase the confidence in the lateral gastrocnemius muscle activation. However, based on the current results, it can be concluded that there is a reasonable amount of confidence in the lateral gastrocnemius activation. Thus, a reasonable amount of confidence can be placed in the lateral gastrocnemius force for the Normal Walking trial. An overview of the confidence levels of each influential muscle in the Normal Walking trial can be seen in **Table 27**.

Table 27: Influential muscle force confidence levels based on calibration and independent validation results for normal walking of the nominal TFA model

Muscle	Confidence level	Justification
Rectus Femoris	Low	<ul style="list-style-type: none"> - Weak activation correlation between EMG reference (Peak magnitude and location are significantly different) - Weak activation correlation between OpenSim reference (Peak magnitude and location are significantly different)
Medial Gastrocnemius	Reasonable	<ul style="list-style-type: none"> - Reasonable activation correlation between EMG reference (peak magnitude is similar, but location is different) - Good activation correlation between OpenSim reference (Peak magnitude and location are reasonably similar)
Lateral Gastrocnemius	Reasonable	<ul style="list-style-type: none"> - Good activation correlation between EMG reference (peak magnitude and location are reasonably similar) - Reasonable activation correlation between OpenSim reference (Peak location is similar, but magnitude is different)

There are a number of limitations associated with the independent validation method used. The first limitation is that the EMG data could only be obtained for the left leg. Ideally, EMG data for the right leg would be more advantageous given that the joint contact forces are calculated for the right leg. Therefore, the right muscle activations were assumed to be symmetrical with the left. The reality is that the muscle activations are not always symmetrical. Secondly, the EMG data was taken from an independent subject. Therefore, there is some inherent variability and error that could not be seen in this comparison. Lastly, and perhaps the most obvious limitation is that the independent validation could not be done for the Tai Chi muscle activations because there was no independent EMG or OpenSim reference data available with which to compare activations. Therefore, it can be concluded that the muscle activation for Tai Chi cannot be trusted until fully validated. Thus, more research must be done in order to trust the joint reaction results for Tai Chi.

5.4. Validation Conclusion

There are many conclusions that can be made regarding the validation of the Normal Walking and Tai Chi trials. First the Normal walking model showed stability and produced seeming reasonable results with visual inspection during the calibration analysis. However, the majority of kinematic parameters showed a significance of mean difference for inverse results compared to forward results. On the contrary, the percent differences in the kinematic parameters were small except for the ankle joint angle. This is seemingly contradictory and, therefore, a low level of confidence was placed in the muscle forces for Normal Walking. The calibration results from Tai Chi yielded a low confidence because the model became unstable during the Forward simulation. Thus, the results could not be compared. When looking at the results for internal validation small errors were shown between the muscle force and the inverse dynamic flexion/extension moments for Tai Chi. However, there were large errors seen in the internal validation results for Normal Walking. Therefore, a greater confidence can be placed in the muscle forces for Tai Chi relative to Normal Walking. When, looking at the independent validation results for Normal Walking, it was concluded the muscle activations for the lateral and medial gastrocnemius muscles are credible but still a low level of confidence was placed in those muscle because of the uncertainty in the EMG data with which it was compared to. The rectus femoris muscle was shown to have a dramatically different activation profile compared to that of the EMG and the OpenSim reference. Therefore, the activation of the rectus femoris cannot be trusted. Since the joint reaction forces are so highly dependent on the muscle forces, and because there is a low level of confidence in the accuracy of those forces, it can be concluded that the joint reaction results from Normal Walking have a high degree of uncertainty and cannot be trusted unless more extensive validation is conducted.

The calibration analysis for Tai Chi was unsuccessful because the model became unstable in early stance phase. The reason is probably due to the noise and errors in the ground reaction force in the X-direction during data collection. The results from the internal validation analysis show minimal errors between the inverse dynamic torque and muscle force moments about the knee joint. This suggests that the muscle forces about the knee are sufficient to achieve the desired gait. However, this does not directly prove that the muscle forces are comparable to the *in-vivo* muscle forces. An independent validation could not be performed because independent Tai Chi data could not be obtained.

5.5. Validation Future Recommendations

Given the current limitations of the entire validation process, it is abundantly clear that there is a significant amount of uncertainty in the muscle forces and thus the joint contact force in the knee. As a result, further investigation must be done in order to validate the joint contact results. Therefore, the following recommendations are necessary to validate the results for this study. First it would be best to restart this study with a new patient. Ideally, it would be best to recruit a patient with an instrumented knee implant. During data collection the subject should perform 3 trials: static, Normal Walking, and Tai Chi. Real time synchronized EMG data along with synchronize knee implant contact data should be collected while the subject performs the Normal Walking and Tai Chi Trials. Along with the synchronized EMG data, maximum voluntary contraction data should be collected on the muscle forces that are most influential to the knee joint contact forces. Those muscles are the rectus femoris, vastus medialis, vastus lateralis, vastus intermedius, medial gastrocnemius, the lateral gastrocnemius, the biceps femoris, the semimembranosus, and the semitendinosus. EMG data that is subject specific would allow the muscle forces in each gait trial

to be directly validated because the *in-vivo* muscle activations would be known. Validated muscle activations are absolutely imperative to garnering accurate joint contact results. Not only will the model be directly validated, but the joint contact forces could be directly validated *in-vivo* by comparing the simulated joint contact forces to the forces measured with the knee implant. In addition to a fully validated model, the error and uncertainty in the joint contact results can be numerically quantified. As it stands with the current study, the error and uncertainty cannot be numerically resolved. Thus, the uncertainty is subjective and somewhat arbitrary. The results from the new study could more reliably elucidate the hypothesis that Tai Chi is an effective counter measure for patients with knee osteoarthritis.

Chapter 6: Conclusion

6.1. Limitations

Many evident limitations exist with this study. The first and perhaps the most obvious is the fact that there was not enough data to capture the full right leg stance phase of gait and therefore many of the numbers could be skewed. The entire double support phase I of Tai Chi was not capturable, **Figure 96**, because the ground reaction force of the left leg during double support phase I was not measured by a force plate. Therefore, the dynamic simulations used for this study could not be analyzed for early stance phase of Tai chi gait.

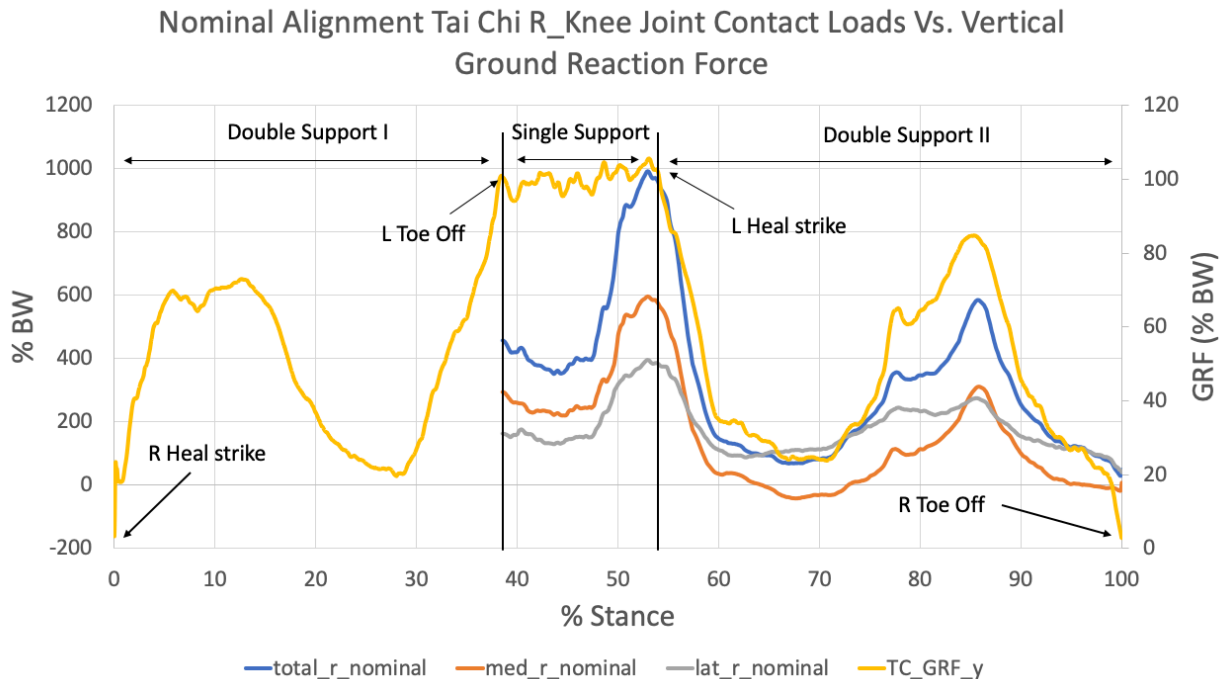


Figure 96: Normalized joint contact loads for the right knee, stance phase, nominal tibiofemoral alignment compared against the respective vertical component ground reaction force.

A minimum of 3 force plates must be used in order capture the full stance phase of gait. Only two force plates were used for this study. The second limitation is present because direct validation through *in-vivo* tibiofemoral contact loads could not be achieved because this patient did have an

instrumented knee implant that could measure the contact loads *in-vivo*. This comparison must be made in order fully validate the joint contact results. To our knowledge, no freely available *in-vivo* joint contact data for Tai Chi currently exists like it does for Normal Walking (Fregly et al.). Additionally, no freely available EMG data for Tai Chi was able to be obtained which results in significant uncertainty in the muscle force activations. lastly, there was an obvious limitation at the calibration step because the model became unstable during the muscle driven forward dynamic simulation. Therefore, there is very little confidence in the Tai Chi muscle forces for this study. The muscle forces in the simulation are also heavily dependent in muscle tendon slack length (Hicks et al.)(Ackland et al.). Tendon slack length effects the range for which the muscle actuators operate in the force length velocity curve. If this is not set correctly, then the muscle force could be over actuated therefore skewing the joint contact results. Iterative solutions exist to help improve the accuracy of the muscle activations, however no reference data with which to compare, i.e. synchronized Tai Chi EMG data, could be obtained. Thus, no iterative muscle force solutions were conducted. Given that joint contact forces are so sensitive to muscle force magnitudes, there is very little confidence in the muscle forces generated for Tai Chi gait during this study.

6.2. Future Recommendations

In leu of the significant limitation of this study, many recommendations can be made to improve the results garnered from this study. Fist it would be best to restart this study with a new patient. Ideally, it would be best to recruit a patient with an instrumented knee implant. During data collection the subject should preform 3 trials: static, Normal Walking, and Tai Chi. Real time synchronized EMG data along with synchronize knee implant contact data should be collected while the subject preforms the Normal Walking and Tai Chi Trials. Along with the synchronized

EMG data, maximum voluntary contraction data should be collected on the muscle that are most influential to the knee joint contact forces. Those muscles are the rectus femoris, vastus medialis, vastus lateralis, vastus intermedius, medial gastrocnemius, the lateral gastrocnemius, the biceps femoris, the semimembranosus, and the semitendinosus. EMG data that is subject specific would allow the muscle forces in each gait trial to be directly validated because the *in-vivo* muscle activations would be known. Validated muscle activations are absolutely imperative to garnering accurate joint contact results. Not only will the model be directly validated, but the joint contact forces could be directly validated *in-vivo* by comparing the simulated joint contact forces to the forces measured with the knee implant. In addition to a fully validated model, the error and uncertainty in the joint contact results can be numerically quantified.

Additionally, three force plates must be used in order to capture the full stance phase of gait. Other subject specific model parameters such muscle physiological cross-sectional area and tendon slack length can be obtained and manually defined in the model which would garner better muscle activation results. When more accurate muscle force activations are obtained, the more confidence in the joint reaction force results will be achieved. The EMG data could be used to drive the musculoskeletal model forward in time which would ultimately garner better results.

6.3. Conclusion

Osteoarthritis is one of the leading causes of disability among older individuals (March and Bachmeier). OA is degenerative and no cure currently exists to reverse the degenerative process. In severe cases, the degenerative nature of the disease often leads to total knee arthroplasty (Rönn et al.). Due to the high risk and long recovery time of TKA, alternative forms of non-invasive

rehab have been sought after to avoid invasive surgeries. One of those rehab exercises under investigation is Tai Chi, an ancient martial art recently turned therapeutic exercise (Barnes et al.). Tai Chi has been shown to increase joint stability, balance, and help manage pain in patients with OA (Wang, Schmid, Hibberd, Kalish, Roubenoff, Rones, and McAlindon). It is believed that moderate mechanical loading of the knee joint can stimulate cell synthesis and help maintain cartilage homeostasis and total joint health (M. Christopher). The aim of this study was to take a closer look at the mechanical behavior of knee joint loading during Tai Chi gait relative to Normal Walking through a musculoskeletal modeling approach. One 28-year-old male subject, weighing 77.11 kilograms, and a height of 1.75 meters was used to conduct this study. One yang style Tai Chi gait and one Normal Walking gait was measured with 3D gait analysis. That data was then used to generate a musculoskeletal model in OpenSim with a subject specific tibiofemoral alignment. The model used for this was study was a previously validated OpenSim model that resolves the medial and lateral knee compartment loads to two user defined contact point locations in the knee. A standard joint reaction analysis in OpenSim was used to compare the mediolateral compartmental contact loads for Tai Chi and Normal Walking. Subsequent joint reaction analyses were then conducted to analyze the effects of tibiofemoral malalignment, $\pm 8^\circ$ varus-valgus, on compartmental loading for both Tai Chi and Normal walking. This study found that the total, medial and lateral joint contact loads were all significantly higher for Tai Chi (333.77% BW, 152.23%BW, and 181.54%BW respectively) than for Normal Walking (211.29% BW, 120.23%BW, and 91.06%BW, respectively). However, in terms of average load distribution, the medial compartment accepted a significantly smaller percentage of the total load for Tai Chi, 27.35%TL, than for Normal Walking, 54.35%TL. Medial compartmental unloading of the knee was also observed in late stance phase of Tai Chi gait. This observation is consistent with the

hypothesis that a reduced external knee adduction moment will reduce medial compartment loading in the knee joint for Tai Chi. This dramatic shift in compartmental load distribution could help generate cell synthesis and maintain cartilage health. Finally, when analyzing the medial and lateral joint contact loads for a varus and valgus tibiofemoral malalignment, the medial compartment showed a higher sensitivity to change in medial load per degree malalignment than the lateral load of the lateral compartment for Tai Chi. For Normal Walking, the reciprocal was observed. These findings show that altered mechanical loading patterns are achieved during Tai Chi gait compared to that of Normal Walking. This change in mechanical loading could help generate cell synthesis in the cartilage ECM, thus stimulating healthy cartilage growth. Therefore, from a musculoskeletal modeling standpoint, there is strong evidence to support the hypothesis that Tai Chi is a good rehab exercise for patients with osteoarthritis of the knee. However, more research should be conducted to support the efficacy of this claim. (Fregly et al.)

References

- Abulhasan, Jawad F., and Michael J. Grey. "Anatomy and Physiology of Knee Stability." *Journal of Functional Morphology and Kinesiology*, vol. 2, no. 4, MDPI Multidisciplinary Digital Publishing Institute, 1 Dec. 2017, doi:10.3390/jfmk2040034.
- Ackland, David C., et al. "Sensitivity of Model Predictions of Muscle Function to Changes in Moment Arms and Muscle-Tendon Properties: A Monte-Carlo Analysis." *Journal of Biomechanics*, 2012, doi:10.1016/j.jbiomech.2012.02.023.
- Adouni, M., et al. "Computational Biodynamics of Human Knee Joint in Gait: From Muscle Forces to Cartilage Stresses." *Journal of Biomechanics*, vol. 45, no. 12, Elsevier, 2012, pp. 2149–56, doi:10.1016/j.jbiomech.2012.05.040.
- Adouni, M., and A. Shirazi-Adl. "Consideration of Equilibrium Equations at the Hip Joint alongside Those at the Knee and Ankle Joints Has Mixed Effects on Knee Joint Response during Gait." *Journal of Biomechanics*, vol. 46, no. 3, Elsevier, 2013, pp. 619–24, doi:10.1016/j.jbiomech.2012.09.035.
- Altman, R. D., et al. "Atlas of Individual Radiographic Features in Osteoarthritis." *Osteoarthritis and Cartilage*, vol. 3, no. SUPPL. A, 1995, doi:10.1016/j.joca.2006.11.009.
- Anderson, Frank C., et al. "SimTrack: Software for Rapidly Generating Muscle-Actuated Simulations of Long-Duration Movement." *International Symposium on Biomedical Engineering*, 2006, pp. 3–6.
- Anderson, Frank C., and Marcus G. Pandy. "Static and Dynamic Optimization Solutions for Gait Are Practically Equivalent." *Journal of Biomechanics*, 2001, doi:10.1016/S0021-9290(00)00155-X.
- Andriacchi, T. P. "Dynamics of Knee Malalignment." *Orthopedic Clinics of North America*, 1994.
- Andriacchi, Thomas P., et al. "Gait Mechanics Influence Healthy Cartilage Morphology and Osteoarthritis of the Knee." *Journal of Bone and Joint Surgery - Series A*, vol. 91, no. SUPPL. 1, 2009, pp. 95–101, doi:10.2106/JBJS.H.01408.
- Andriacchi, Thomas P., and Annegret Mündermann. "The Role of Ambulatory Mechanics in the Initiation and Progression of Knee Osteoarthritis." *Current Opinion in Rheumatology*, 2006, doi:10.1097/01.bor.0000240365.16842.4e.
- Apuzzo, Nicola D. "Motion Capture by Least Squares Matching Tracking Algorithm." *Proceedings of the Avatars 2000 Workshop*, 2000.
- Arnold, Edith M., et al. "A Model of the Lower Limb for Analysis of Human Movement." *Annals of Biomedical Engineering*, vol. 38, no. 2, 2010, pp. 269–79, doi:10.1007/s10439-009-9852-5.
- Barnes, Patricia M., et al. "Complementary and Alternative Medicine Use among Adults: United States, 2002." *Advance Data*, no. 343, 2004, pp. 1–19, doi:10.1016/j.sigm.2004.07.003.
- Bei, Yanhong, and Benjamin J. Fregly. "Multibody Dynamic Simulation of Knee Contact

- Mechanics.” *Medical Engineering and Physics*, vol. 26, no. 9 SPEC.ISS., 2004, pp. 777–89, doi:10.1016/j.medengphy.2004.07.004.
- Bell, Alexander L., Douglas R. Pedersen, et al. “A Comparison of the Accuracy of Several Hip Center Location Prediction Methods.” *Journal of Biomechanics*, 1990, doi:10.1016/0021-9290(90)90054-7.
- Bell, Alexander L., Richard A. Brand, et al. “Prediction of Hip Joint Centre Location from External Landmarks.” *Human Movement Science*, 1989, doi:10.1016/0167-9457(89)90020-1.
- Bennell, Kim L., et al. “Management of Osteoarthritis of the Knee.” *BMJ (Online)*, 2012, doi:10.1136/bmj.e4934.
- Blemker, Silvia S., et al. “Image-Based Musculoskeletal Modeling: Applications, Advances, and Future Opportunities.” *Journal of Magnetic Resonance Imaging*, vol. 25, no. 2, 2007, pp. 441–51, doi:10.1002/jmri.20805.
- Cappozzo, A., et al. “Position and Orientation in Space of Bones during Movement: Anatomical Frame Definition and Determination.” *Clinical Biomechanics*, 1995, doi:10.1016/0268-0033(95)91394-T.
- Chris Kirtly. “Clinical Gait Analysis: Theory and Practice.” *Elsevier*, 2006, doi:10.1016/B978-0-7506-3560-8.50001-9.
- Cohen, Nathaniel P., et al. “Composition and Dynamics of Articular Cartilage: Structure, Function, and Maintaining Healthy State.” *Journal of Orthopaedic and Sports Physical Therapy*, vol. 28, no. 4, 1998, pp. 203–15, doi:10.2519/jospt.1998.28.4.203.
- Colyer, Steffi L., et al. “A Review of the Evolution of Vision-Based Motion Analysis and the Integration of Advanced Computer Vision Methods Towards Developing a Markerless System.” *Sports Medicine - Open*, vol. 4, no. 1, Sports Medicine - Open, 2018, doi:10.1186/s40798-018-0139-y.
- Cooke, D., et al. “Axial Lower-Limb Alignment: Comparison of Knee Geometry in Normal Volunteers and Osteoarthritis Patients.” *Osteoarthritis and Cartilage*, 1997, doi:10.1016/S1063-4584(97)80030-1.
- Cox, Chandler F., and John B. Hubbard. “Anatomy, Bony Pelvis and Lower Limb, Knee Patella.” *StatPearls*, 2018.
- Dan, Cristian. *Articular Cartilage Segmentation and Tracking In*. 2005.
- Delp, Scott L., J. Peter Loan, et al. “An Interactive Graphics-Based Model of the Lower Extremity to Study Orthopaedic Surgical Procedures.” *IEEE Transactions on Biomedical Engineering*, vol. 37, no. 8, 1990, pp. 757–67, doi:10.1109/10.102791.
- Delp, Scott L., Frank C. Anderson, et al. “OpenSim: Open-Source Software to Create and Analyze Dynamic Simulations of Movement.” *IEEE Transactions on Biomedical Engineering*, 2007, doi:10.1109/TBME.2007.901024.
- Dieppe, Paul A., and L. Stefan Lohmander. “Pathogenesis and Management of Pain in Osteoarthritis.” *Lancet*, vol. 365, no. 9463, 2005, pp. 965–73, doi:10.1016/S0140-6736(05)71086-2.

- Donati, Marco, et al. "Anatomical Frame Identification and Reconstruction for Repeatable Lower Limb Joint Kinematics Estimates." *Journal of Biomechanics*, vol. 41, no. 10, 2008, pp. 2219–26, doi:10.1016/j.jbiomech.2008.04.018.
- Ebnezar, John, et al. "Effects of an Integrated Approach of Hatha Yoga Therapy on Functional Disability, Pain, and Flexibility in Osteoarthritis of the Knee Joint: A Randomized Controlled Study." *Journal of Alternative and Complementary Medicine*, vol. 18, no. 5, 2012, pp. 463–72, doi:10.1089/acm.2010.0320.
- Fithian, D. C., et al. "Material Properties and Structure-Function Relationships in the Menisci." *Clinical Orthopaedics and Related Research*, no. 252, 1990, pp. 19–31, doi:10.1097/00003086-199003000-00004.
- Fransen, Marlene, et al. "Physical Activity for Osteoarthritis Management: A Randomized Controlled Clinical Trial Evaluating Hydrotherapy or Tai Chi Classes." *Arthritis Care and Research*, vol. 57, no. 3, 2007, pp. 407–14, doi:10.1002/art.22621.
- Fregly, Benjamin J. "Gait Modification to Treat Knee Osteoarthritis." *HSS Journal*, vol. 8, no. 1, 2012, pp. 45–48, doi:10.1007/s11420-011-9229-9.
- . "Grand Challenge Competition to Predict in Vivo Knee Loads." *Journal of Orthopaedic Research*, vol. 30, no. 4, 2012, pp. 503–13, doi:10.1002/jor.22023.
- Fujisawa, Takuo, et al. "Cyclic Mechanical Stress Induces Extracellular Matrix Degradation in Cultured Chondrocytes via Gene Expression of Matrix Metalloproteinases and Interleukin-1." *Journal of Biochemistry*, vol. 125, no. 5, 1999, pp. 966–75, doi:10.1093/oxfordjournals.jbchem.a022376.
- Geneen, Louise J., et al. "Physical Activity and Exercise for Chronic Pain in Adults." *Journal of Sociology*, no. 1, 2017, pp. 135–39, doi:10.1002/14651858.CD011279.pub3.www.cochranelibrary.com.
- Gerus, Pauline, et al. "Subject-Specific Knee Joint Geometry Improves Predictions of Medial Tibiofemoral Contact Forces." *Journal of Biomechanics*, 2013, doi:10.1016/j.jbiomech.2013.09.005.
- Graichen, Friedmar, et al. "Implantable 9-Channel Telemetry System for in Vivo Load Measurements with Orthopedic Implants." *IEEE Transactions on Biomedical Engineering*, vol. 54, no. 2, 2007, pp. 253–61, doi:10.1109/TBME.2006.886857.
- Griffin, Timothy M., and Farshid Guilak. "The Role of Mechanical Loading in the Onset and Progression of Osteoarthritis." *Exercise and Sport Sciences Reviews*, vol. 33, no. 4, 2005, pp. 195–200, doi:10.1097/00003677-200510000-00008.
- Gudmann, Natasja Stæhr, et al. "Cartilage Turnover Reflected by Metabolic Processing of Type II Collagen: A Novel Marker of Anabolic Function in Chondrocytes." *International Journal of Molecular Sciences*, vol. 15, no. 10, 2014, pp. 18789–803, doi:10.3390/ijms151018789.
- Guess, Trent M., et al. "Concurrent Prediction of Muscle and Tibiofemoral Contact Forces during Treadmill Gait." *Journal of Biomechanical Engineering*, vol. 136, no. 2, 2014, doi:10.1115/1.4026359.
- Halder, Andreas, et al. "Influence of Limb Alignment on Mediolateral." *Journal of Bone and Joint Surgery*, vol. 94, 2014, pp. 1023–29.

- Halloran, Jason P., et al. “Concurrent Musculoskeletal Dynamics and Finite Element Analysis Predicts Altered Gait Patterns to Reduce Foot Tissue Loading.” *Journal of Biomechanics*, vol. 43, no. 14, Elsevier Ltd, 2010, pp. 2810–15, doi:10.1016/j.jbiomech.2010.05.036.
- Harrington, M. E., et al. “Prediction of the Hip Joint Centre in Adults, Children, and Patients with Cerebral Palsy Based on Magnetic Resonance Imaging.” *Journal of Biomechanics*, vol. 40, no. 3, 2007, pp. 595–602, doi:10.1016/j.jbiomech.2006.02.003.
- Hast, Michael W., et al. “Simulating Contact Using the Elastic Foundation Algorithm in OpenSim.” *Journal of Biomechanics*, vol. 82, Elsevier Ltd, 2019, pp. 392–96, doi:10.1016/j.jbiomech.2018.11.025.
- Hicks, Jennifer L., et al. “Is My Model Good Enough? Best Practices for Verification and Validation of Musculoskeletal Models and Simulations of Movement.” *Journal of Biomechanical Engineering*, vol. 137, no. 2, 2015, p. 020905, doi:10.1115/1.4029304.
- Hiligsmann, Mickaël, et al. “Health Economics in the Field of Osteoarthritis: An Expert’s Consensus Paper from the European Society for Clinical and Economic Aspects of Osteoporosis and Osteoarthritis (ESCEO).” *Seminars in Arthritis and Rheumatism*, vol. 43, no. 3, Elsevier, 2013, pp. 303–13, doi:10.1016/j.semarthrit.2013.07.003.
- Houard, Xavier, et al. “Homeostatic Mechanisms in Articular Cartilage and Role of Inflammation in Osteoarthritis.” *Current Rheumatology Reports*, vol. 15, no. 11, 2013, doi:10.1007/s11926-013-0375-6.
- Hsu, R. W. W., et al. “Normal Axial Alignment of the Lower Extremity and Load-Bearing Distribution at the Knee.” *Clinical Orthopaedics and Related Research*, no. 255, 1990, pp. 215–27, doi:10.1097/00003086-199006000-00029.
- Hume, Donald R., et al. “The Interaction of Muscle Moment Arm, Knee Laxity, and Torque in a Multi-Scale Musculoskeletal Model of the Lower Limb.” *Journal of Biomechanics*, vol. 76, Elsevier Ltd, 2018, pp. 173–80, doi:10.1016/j.jbiomech.2018.05.030.
- Hume, Donald R. *Translating Data from the Laboratory into Simulation: A Computational Framework for Subject-Specific Finite Element Musculoskeletal Simulation Recommended Citation* "Translating Data from the Laboratory into Simulation: A Computational Framework for S. 2018, <https://digitalcommons.du.edu/cgi/viewcontent.cgi?article=2499&context=etd>.
- Ikenoue, Takashi, et al. “Mechanoregulation of Human Articular Chondrocyte Aggrecan and Type II Collagen Expression by Intermittent Hydrostatic Pressure in Vitro.” *Journal of Orthopaedic Research*, vol. 21, no. 1, 2003, pp. 110–16, doi:10.1016/S0736-0266(02)00091-8.
- Jagodinsky, Adam, et al. “Biomechanical Comparison of Frontal Plane Knee Joint Moment Arms during Normal and Tai Chi Walking.” *Journal of Physical Therapy Science*, vol. 27, no. 9, 2015, pp. 2959–61, doi:10.1589/jpts.27.2959.
- Johnson, F. ; Leidl, S; Waugh, W. “The Distribution of Load Across the Knee.” *The Journal of Bone and Joint Surgery*, vol. 62-B, no. 3, 1980, pp. 346–49.
- Kan, H. S., et al. “Non-Surgical Treatment of Knee Osteoarthritis.” *Hong Kong Medical Journal*, vol. 25, no. 2, 2019, pp. 127–33, doi:10.12809/hkmj187600.

- Kim, Hyung J., et al. "Evaluation of Predicted Knee-Joint Muscle Forces during Gait Using an Instrumented Knee Implant." *Journal of Orthopaedic Research*, vol. 27, no. 10, 2009, pp. 1326–31, doi:10.1002/jor.20876.
- Kłodowski, Adam, et al. "Merge of Motion Analysis, Multibody Dynamics and Finite Element Method for the Subject-Specific Analysis of Cartilage Loading Patterns during Gait: Differences between Rotation and Moment-Driven Models of Human Knee Joint." *Multibody System Dynamics*, vol. 37, no. 3, Springer Science+Business Media Dordrecht, 2016, pp. 271–90, doi:10.1007/s11044-015-9470-y.
- Krackow, K. A. "The Measurement and Analysis of Axial Deformity at the Knee." *Home Strv*, 2008, pp. 1–14, <http://www.ubortho.buffalo.edu/axialdeformity.pdf>.
- Kuo, Arthur D. *A Least Squares Estimation Approach to Improving the Precision of Inverse Dynamics Computations*. 1995.
- Kurosawa, H., et al. "Load-Bearing Mode of the Knee Joint: Physical Behavior of the Knee Joint with or without Menisci." *Clinical Orthopaedics and Related Research*, vol. NO 149, 1980, pp. 283–90, doi:10.1097/00003086-198006000-00039.
- Kwan, Michael K., et al. "Fundamentals of Fluid Transport through Cartilage in Compression." *Annals of Biomedical Engineering*, vol. 12, no. 6, 1984, pp. 537–58, doi:10.1007/BF02371448.
- Lai, W. M., et al. "A Triphasic Theory for the Swelling and Deformation Behaviors of Articular Cartilage." *Journal of Biomechanical Engineering*, 1991, doi:10.1115/1.2894880.
- Lance, R. H., and D. N. Robinson. "A Maximum Shear Stress Theory of Plastic Failure of Fiber-Reinforced Materials." *Journal of the Mechanics and Physics of Solids*, vol. 19, no. 2, 1971, pp. 49–60, doi:10.1016/0022-5096(71)90017-2.
- Lane Smith, R., et al. "Effects of Shear Stress on Articular Chondrocyte Metabolism." *Biorheology*, vol. 37, no. 1–2, 2000, pp. 95–107.
- Lathrop, Rebecca L., et al. "Comparative Assessment of Bone Pose Estimation Using Point Cluster Technique and Opensim." *Journal of Biomechanical Engineering*, vol. 133, no. 11, 2011, pp. 1–6, doi:10.1115/1.4005409.
- Lauche, R., et al. "A Systematic Review and Meta-Analysis of Tai Chi for Osteoarthritis of the Knee." *Complementary Therapies in Medicine*, 2013, doi:10.1016/j.ctim.2013.06.001.
- Lawrence, Reva C. "Estimates of Pre." *Arthritis Rheum*, vol. 58, no. 1, 2008, pp. 26–35, doi:10.1002/art.23176.Estimates.
- Lee, Myeong Soo, et al. "Tai Chi for Osteoarthritis: A Systematic Review." *Clinical Rheumatology*, vol. 27, no. 2, 2008, pp. 211–18, doi:10.1007/s10067-007-0700-4.
- Lerner, Zachary F., et al. "How Tibiofemoral Alignment and Contact Locations Affect Predictions of Medial and Lateral Tibiofemoral Contact Forces." *Journal of Biomechanics*, 2015, doi:10.1016/j.jbiomech.2014.12.049.
- Li, Yefu, and Lin Xu. "Advances in Understanding Cartilage Remodeling." *F1000Research*, vol. 4, 2015, pp. 2–7, doi:10.12688/f1000research.6514.1.
- Linn, Frank C., and Leon Sokoloff. "Movement and Composition of Interstitial Fluid of

- Cartilage.” *Arthritis & Rheumatism*, 1965, doi:10.1002/art.1780080402.
- Liu, Wei, et al. “Does T'ai Chi Gait Reduce External Knee Adduction Moment?” *Journal of Alternative and Complementary Medicine*, vol. 22, no. 10, 2016, pp. 818–23, doi:10.1089/acm.2014.0174.
- Lluna, E., et al. “Velocity Vector (3D) Measurement for Spherical Objects Using an Electro-Optical Device.” *Measurement: Journal of the International Measurement Confederation*, vol. 44, no. 9, Elsevier Ltd, 2011, pp. 1723–29, doi:10.1016/j.measurement.2011.07.006.
- Loeser, Richard F., et al. “Osteoarthritis: A Disease of the Joint as an Organ.” *Arthritis and Rheumatism*, 2012, doi:10.1002/art.34453.
- Lu, Xin L., and Van C. Mow. “Biomechanics of Articular Cartilage and Determination of Material Properties.” *Medicine and Science in Sports and Exercise*, vol. 40, no. 2, 2008, pp. 193–99, doi:10.1249/mss.0b013e31815cb1fc.
- Lundblad, H., et al. “Prediction of Persistent Pain after Total Knee Replacement for Osteoarthritis.” *Journal of Bone and Joint Surgery - Series B*, vol. 90, no. 2, 2008, pp. 166–71, doi:10.1302/0301-620X.90B2.19640.
- M. Christopher, A. Melnick L. Sheng. “Mechanical Loading: Potential and Therapeutic Strategy for Osteoarthritis, HHS Public Access.” *Physiology & Behavior*, vol. 176, no. 1, 2016, pp. 100–106, doi:10.1016/j.gde.2016.03.011.
- Magalhães, Claudio Marcos Bedran de, and Renata Noce Kirkwood. “Strategies to Reduce Joint Load in the Medial Compartment of the Knee during Gait in Individuals with Osteoarthritis: A Review of the Literature.” *Fisioterapia Em Movimento*, vol. 29, no. 4, 2016, pp. 831–42, doi:10.1590/1980-5918.029.004.ao20.
- Maini, Lalit, et al. “Radiographic Analysis of the Axial Alignment of the Lower Extremity in Indian Adult Males.” *Journal of Arthroscopy and Joint Surgery*, vol. 2, no. 3, International Society for Knowledge for Surgeons on Arthroscopy and Arthroplasty, 2015, pp. 128–31, doi:10.1016/j.jajs.2015.11.010.
- Maiwald, Christian, et al. “The Effect of Intracortical Bone Pin Application on Kinetics and Tibiocalcaneal Kinematics of Walking Gait.” *Gait and Posture*, vol. 52, Elsevier B.V., 2017, pp. 129–34, doi:10.1016/j.gaitpost.2016.10.023.
- Maletsky, Lorin P., et al. “Accuracy of an Optical Active-Marker System to Track the Relative Motion of Rigid Bodies.” *Journal of Biomechanics*, vol. 40, no. 3, 2007, pp. 682–85, doi:10.1016/j.jbiomech.2006.01.017.
- Manolagas, Stavros C. “Birth and Death of Bone Cells: Basic Regulatory Mechanisms and Implications for the Pathogenesis and Treatment of Osteoporosis.” *Endocrine Reviews*, vol. 21, no. 2, 2000, pp. 115–37, doi:10.1210/er.21.2.115.
- March, L. M., and C. J. M. Bachmeier. “Economics of Osteoarthritis: A Global Perspective.” *Bailliere's Clinical Rheumatology*, vol. 11, no. 4, 1997, pp. 817–34, doi:10.1016/S0950-3579(97)80011-8.
- Millard, Matthew, et al. “Flexing Computational Muscle: Modeling and Simulation of Musculotendon Dynamics.” *Journal of Biomechanical Engineering*, 2013, doi:10.1115/1.4023390.

- Miyazaki, T., et al. “Dynamic Load at Baseline Can Predict Radiographic Disease Progression in Medial Compartment Knee Osteoarthritis.” *Annals of the Rheumatic Diseases*, vol. 61, no. 7, 2002, pp. 617–22, doi:10.1136/ard.61.7.617.
- Mow, V. C., et al. “Biphasic Creep and Stress Relaxation of Articular Cartilage in Compression: Theory and Experiments.” *Journal of Biomechanical Engineering*, 1980, doi:10.1115/1.3138202.
- Mow, Van C., et al. “Cartilage and Diarthrodial Joints as Paradigms for Hierarchical Materials and Structures.” *Biomaterials*, vol. 13, no. 2, 1992, pp. 67–97, doi:10.1016/0142-9612(92)90001-5.
- Mündermann, Lars, et al. “The Evolution of Methods for the Capture of Human Movement Leading to Markerless Motion Capture for Biomechanical Applications.” *Journal of NeuroEngineering and Rehabilitation*, vol. 3, 2006, pp. 1–11, doi:10.1186/1743-0003-3-6.
- Murray, Christopher J. ..., and Alan D. Lopez. “Global Burden of Disease and Injur Y Series the Global Burden of Disease.” *Oms*, 1996, pp. 1–46, doi:10.1088/1742-6596/707/1/012025.
- Musumeci, Giuseppe. “The Effect of Mechanical Loading on Articular Cartilage.” *Journal of Functional Morphology and Kinesiology*, vol. 1, no. 2, MDPI Multidisciplinary Digital Publishing Institute, 1 June 2016, pp. 154–61, doi:10.3390/jfmk1020154.
- Nie, Yong, et al. “The Relationship between Knee Adduction Moment and Knee Osteoarthritis Symptoms According to Static Alignment and Pelvic Drop.” *BioMed Research International*, vol. 2019, 2019, doi:10.1155/2019/7603249.
- Pasdar, Arefeh, et al. “A Comparison between Computed Muscle Control Method and Static Optimization Technique to Determine Muscle Forces during a Weight Training Exercise with a Dumbbell.” *2012 19th Iranian Conference of Biomedical Engineering, ICBME 2012*, no. December, IEEE, 2012, pp. 85–90, doi:10.1109/ICBME.2012.6519663.
- Paul, J. P. “The History of Musculoskeletal Modelling in Human Gait.” *Theoretical Issues in Ergonomics Science*, vol. 6, no. 3–4, 2005, pp. 217–24, doi:10.1080/14639220512331329464.
- Péloquin, Lucie, et al. “Effects of a Cross-Training Exercise Program in Persons with Osteoarthritis of the Knee. A Randomized Controlled Trial.” *Journal of Clinical Rheumatology*, 1999, doi:10.1097/00124743-199906000-00004.
- Peungsuwan, Punnee, et al. “The Effectiveness of Thai Exercise with Traditional Massage on the Pain, Walking Ability and QOL of Older People with Knee Osteoarthritis: A Randomized Controlled Trial in the Community.” *Journal of Physical Therapy Science*, vol. 26, no. 1, 2014, pp. 139–44, doi:10.1589/jpts.26.139.
- Plotnikoff, Ronald, et al. “Osteoarthritis Prevalence and Modifiable Factors: A Population Study Chronic Disease Epidemiology.” *BMC Public Health*, vol. 15, no. 1, BMC Public Health, 2015, pp. 1–10, doi:10.1186/s12889-015-2529-0.
- Raikova, R. “About Weight Factors in the Non-Linear Objective Functions Used for Solving Indeterminate Problems in Biomechanics.” *Journal of Biomechanics*, vol. 32, no. 7, 1999, pp. 689–94, doi:10.1016/S0021-9290(99)00037-8.
- Reinbolt, Jeffrey A., et al. “Determination of Patient-Specific Multi-Joint Kinematic Models

- through Two-Level Optimization.” *Journal of Biomechanics*, 2005, doi:10.1016/j.jbiomech.2004.03.031.
- Richards, James G. “The Measurement of Human Motion: A Comparison of Commercially Available Systems.” *Human Movement Science*, vol. 18, no. 5, 1999, pp. 589–602, doi:10.1016/S0167-9457(99)00023-8.
- Roddy, Edward, et al. “Evidence-Based Recommendations for the Role of Exercise in the Management of Osteoarthritis of the Hip or Knee - The MOVE Concensus.” *Rheumatology*, 2005, doi:10.1093/rheumatology/keh399.
- Rönn, Karolin, et al. “Current Surgical Treatment of Knee Osteoarthritis.” *Arthritis*, vol. 2011, 2011, pp. 1–9, doi:10.1155/2011/454873.
- Saxby, David J., et al. “Tibiofemoral Contact Forces during Walking, Running and Sidestepping.” *Gait and Posture*, vol. 49, Elsevier B.V., 2016, pp. 78–85, doi:10.1016/j.gaitpost.2016.06.014.
- Schreven, Sander, et al. “Optimising Filtering Parameters for a 3D Motion Analysis System.” *Journal of Electromyography and Kinesiology*, vol. 25, no. 5, Elsevier Ltd, 2015, pp. 808–14, doi:10.1016/j.jelekin.2015.06.004.
- Scorza, A., et al. “A Review on Methods and Devices for Force Platforms Calibration in Medical Applications.” *Journal of Engineering Science and Technology Review*, vol. 11, no. 1, 2018, pp. 10–18, doi:10.25103/jestr.111.02.
- Seedhom, B. B. “Conditioning of Cartilage during Normal Activities Is an Important Factor in the Development of Osteoarthritis.” *Rheumatology*, vol. 45, no. 2, 2006, pp. 146–49, doi:10.1093/rheumatology/kei197.
- . “Transmission of the Load in the Knee Joint with Special Reference to the Role of the Menisci. Part I. Anatomy, Analysis and Apparatus.” *Engineering in Medicine*, vol. 8, no. 4, 1979, pp. 207–19.
- Seth, Ajay, Michael Sherman, et al. “Minimal Formulation of Joint Motion for Biomechanisms.” *Nonlinear Dynamics*, vol. 62, no. 1, 2010, pp. 291–303, doi:10.1007/s11071-010-9717-3.
- Seth, Ajay, Jennifer L. Hicks, et al. “OpenSim: Simulating Musculoskeletal Dynamics and Neuromuscular Control to Study Human and Animal Movement.” *PLoS Computational Biology*, 2018, doi:10.1371/journal.pcbi.1006223.
- Sharma, Leena, et al. “The Role of Knee Alignment in Disease Progression and Functional Decline in Knee Osteoarthritis.” *Journal of the American Medical Association*, vol. 286, no. 2, 2001, pp. 188–95, doi:10.1001/jama.286.2.188.
- Smith, Colin R., et al. “Influence of Ligament Properties on Knee Mechanics in Walking.” *Journal of Knee Surgery*, vol. 29, no. 2, 2016, pp. 99–106, doi:10.1055/s-0035-1558858.Influence.
- Sophia Fox, Alice J., et al. “The Basic Science of Articular Cartilage: Structure, Composition, and Function.” *Sports Health*, vol. 1, no. 6, Nov. 2009, pp. 461–68, doi:10.1177/1941738109350438.
- Sousa, Andreia S. P., and João Manuel R. S. Tavares. “Surface Electromyographic Amplitude

- Normalization Methods: A Review.” *Electromyography: New Developments, Procedures and Applications*, 2012, pp. 85–102.
- Steele, Katherine M., et al. “Compressive Tibiofemoral Force during Crouch Gait.” *Gait and Posture*, 2012, doi:10.1016/j.gaitpost.2011.11.023.
- Tchetina, Elena V., et al. “Increased Type II Collagen Degradation and Very Early Focal Cartilage Degeneration Is Associated with Upregulation of Chondrocyte Differentiation Related Genes in Early Human Articular Cartilage Lesions.” *Journal of Rheumatology*, vol. 32, no. 5, 2005, pp. 876–86.
- Thacker, Ben H. “ASME Standards Committee on Verification and Validation in Computational Solid Mechanics.” *Conference Proceedings of the Society for Experimental Mechanics Series*, 2005.
- Thambyah, A., et al. “Mechanical Properties of Articular Cartilage Covered by the Meniscus.” *Osteoarthritis and Cartilage*, vol. 14, no. 6, 2006, pp. 580–88, doi:10.1016/j.joca.2006.01.015.
- Thelen, Darryl G. “Adjustment of Muscle Mechanics Model Parameters to Simulate Dynamic Contractions in Older Adults.” *Journal of Biomechanical Engineering*, vol. 125, no. 1, 2003, pp. 70–77, doi:10.1115/1.1531112.
- . “Generating Dynamic Simulations of Movement Using Computed Muscle Control.” *Journal of Biomechanics*, vol. 36, no. 3, 2003, pp. 321–28, doi:10.1016/S0021-9290(02)00432-3.
- Thelen, Darryl G., and Frank C. Anderson. “Using Computed Muscle Control to Generate Forward Dynamic Simulations of Human Walking from Experimental Data.” *Journal of Biomechanics*, vol. 39, no. 6, 2006, pp. 1107–15, doi:10.1016/j.jbiomech.2005.02.010.
- van der Kruk, Eline, and Marco M. Reijne. “Accuracy of Human Motion Capture Systems for Sport Applications; State-of-the-Art Review.” *European Journal of Sport Science*, vol. 18, no. 6, Taylor & Francis, 2018, pp. 806–19, doi:10.1080/17461391.2018.1463397.
- Verzijl, Nicole, et al. “Effect of Collagen Turnover on the Accumulation of Advanced Glycation End Products.” *Journal of Biological Chemistry*, vol. 275, no. 50, 2000, pp. 39027–31, doi:10.1074/jbc.M006700200.
- Wang, Chenchen, Christopher H. Schmid, Maura D. Iversen, William F. Harvey, Roger A. Fielding, Jeffrey B. Driban, Lori Lyn Price, et al. “Comparative Effectiveness of Tai Chi versus Physical Therapy for Knee Osteoarthritis: A Randomized Trial.” *Annals of Internal Medicine*, vol. 165, no. 2, 2016, pp. 77–86, doi:10.7326/M15-2143.
- Wang, Chenchen, Christopher H. Schmid, Patricia L. Hibberd, Robert Kalish, Ronenn Roubenoff, Ramel Ronés, Aghogho Okparavero, et al. “Tai Chi for Treating Knee Osteoarthritis: Designing a Long-Term Follow up Randomized Controlled Trial.” *BMC Musculoskeletal Disorders*, vol. 9, 2008, pp. 1–9, doi:10.1186/1471-2474-9-108.
- Wang, Chenchen, Christopher H. Schmid, Patricia L. Hibberd, Robert Kalish, Ronenn Roubenoff, Ramel Ronés, and Timothy McAlindon. “Tai Chi Is Effective in Treating Knee Osteoarthritis: A Randomized Controlled Trial.” *Arthritis Care and Research*, vol. 61, no. 11, 2009, pp. 1545–53, doi:10.1002/art.24832.
- Wayne, Peter M., and Ted J. Kaptchuk. “Challenges Inherent to T’ai Chi Research: Part I - T’ai

- Chi as a Complex Multicomponent Intervention.” *Journal of Alternative and Complementary Medicine*, vol. 14, no. 1, 2008, pp. 95–102, doi:10.1089/acm.2007.7170A.
- Whitman, Walt. “Articular Cartilage.” *Lancet*, vol. 2, no. 7715, 1971, p. 81.
- Williams, G. N., et al. “Dynamic Knee Stability: Current Theory and Implications for Clinicians and Scientists.” *Journal of Orthopaedic and Sports Physical Therapy*, vol. 31, no. 10, 2001, pp. 546–66, doi:10.2519/jospt.2001.31.10.546.
- Winter, David A. “Biomechanics and Motor Control of Human Movement: Fourth Edition.” *Biomechanics and Motor Control of Human Movement: Fourth Edition*, 2009, doi:10.1002/9780470549148.
- Woltring, Herman J. “A Fortran Package for Generalized, Cross-Validatory Spline Smoothing and Differentiation.” *Advances in Engineering Software (1978)*, 1986, doi:10.1016/0141-1195(86)90098-7.
- Yan, Jun Hong, et al. “Efficacy of Tai Chi on Pain, Stiffness and Function in Patients with Osteoarthritis: A Meta-Analysis.” *PLoS ONE*, vol. 8, no. 4, 2013, doi:10.1371/journal.pone.0061672.
- Yang, Feng, and Wei Liu. “Biomechanical Mechanism of Tai-Chi Gait for Preventing Falls: A Pilot Study.” *Journal of Biomechanics*, no. xxxx, Elsevier Ltd, 2020, p. 109769, doi:10.1016/j.jbiomech.2020.109769.
- Yang, Nicholas H., et al. “Effect of Frontal Plane Tibiofemoral Angle on the Stress and Strain at the Knee Cartilage during the Stance Phase of Gait.” *Journal of Orthopaedic Research*, vol. 28, no. 12, 2010, pp. 1539–47, doi:10.1002/jor.21174.
- Yildiz, Necmettin, et al. “Health-Related Quality of Life (Nottingham Health Profile) in Knee Osteoarthritis: Correlation with Clinical Variables and Self-Reported Disability.” *Rheumatology International*, vol. 30, no. 12, 2010, pp. 1595–600, doi:10.1007/s00296-009-1195-x.
- Yuqing Zhang, D.Sc and Joanne M. Jordan, MD, MPH. “Epidemiology of Osteoarthritis Yuqing.” *Clin Geriatr Med.*, vol. 26, no. 3, 2011, pp. 355–69, doi:10.1016/j.cger.2010.03.001.Epidemiology.

Appendix

Appendix A: Matlab Codes

A.1. Joint Center Calculation

```
% Code calculated the hip joint center of the left and right hips in the
% global reference frame
% This Code will also return the tibiofemoral alignment of the left and
% right lower extremities from the marker file that is selected.

[filename1,filepath1]=uigetfile('*.trc','please select static calibration marker'); % Select the
marker file used to scale the model
selectedfile1=fullfile(filepath1,filename1);
%data=uiimport(selectedfile1);
data1=importTRCfile(selectedfile1);% generates a "struct" matrix of vectors with column headers
from data in "selectedfile"

%% Extract Marker data

LPSIS_xv=data1.X4;
LPSIS_yv=data1.Y4;
LPSIS_zv=data1.Z4;

RPSIS_xv=data1.X5;
RPSIS_yv=data1.Y5;
RPSIS_zv=data1.Z5;

LASIS_xv=data1.X10;
LASIS_yv=data1.Y10;
LASIS_zv=data1.Z10;

RASIS_xv=data1.X7;
RASIS_yv=data1.Y7;
RASIS_zv=data1.Z7;

RFT_xv=data1.X8;
RFT_yv=data1.Y8;
RFT_zv=data1.Z8;

LFT_xv=data1.X11;
LFT_yv=data1.Y11;
LFT_zv=data1.Z11;

RLK_xv=data1.X15;
RLK_yv=data1.Y15;
RLK_zv=data1.Z15;

LLK_xv=data1.X28;
LLK_yv=data1.Y28;
LLK_zv=data1.Z28;

RMK_xv=data1.X16;
RMK_yv=data1.Y16;
RMK_zv=data1.Z16;

LMK_xv=data1.X29;
LMK_yv=data1.Y29;
LMK_zv=data1.Z29;

RLA_xv=data1.X20;
RLA_yv=data1.Y20;
RLA_zv=data1.Z20;

RMA_xv=data1.X21;
RMA_yv=data1.Y21;
```

```

RMA_zv=data1.Z21;

LLA_xv=data1.X33;
LLA_yv=data1.Y33;
LLA_zv=data1.Z33;

LMA_xv=data1.X34;
LMA_yv=data1.Y34;
LMA_zv=data1.Z34;

% compute the average coordinates over all time steps

LPSIS_x=mean(LPSIS_xv);
LPSIS_y=mean(LPSIS_yv);
LPSIS_z=mean(LPSIS_zv);

RPSIS_x=mean(RPSIS_xv);
RPSIS_y=mean(RPSIS_yv);
RPSIS_z=mean(RPSIS_zv);

LASIS_x=mean(LASIS_xv);
LASIS_y=mean(LASIS_yv);
LASIS_z=mean(LASIS_zv);

RASIS_x=mean(RASIS_xv);
RASIS_y=mean(RASIS_yv);
RASIS_z=mean(RASIS_zv);

RFT_x=mean(RFT_xv);
RFT_y=mean(RFT_yv);
RFT_z=mean(RFT_zv);

LFT_x=mean(LFT_xv);
LFT_y=mean(LFT_yv);
LFT_z=mean(LFT_zv);

RLK_x=mean(RLK_xv);
RLK_y=mean(RLK_yv);
RLK_z=mean(RLK_zv);

LLK_x=mean(LLK_xv);
LLK_y=mean(LLK_yv);
LLK_z=mean(LLK_zv);

RMK_x=mean(RMK_xv);
RMK_y=mean(RMK_yv);
RMK_z=mean(RMK_zv);

LMK_x=mean(LMK_xv);
LMK_y=mean(LMK_yv);
LMK_z=mean(LMK_zv);

RLA_x=mean(RLA_xv);
RLA_y=mean(RLA_yv);
RLA_z=mean(RLA_zv);

RMA_x=mean(RMA_xv);
RMA_y=mean(RMA_yv);
RMA_z=mean(RMA_zv);

LLA_x=mean(LLA_xv);
LLA_y=mean(LLA_yv);
LLA_z=mean(LLA_zv);

LMA_x=mean(LMA_xv);
LMA_y=mean(LMA_yv);
LMA_z=mean(LMA_zv);

% put coordinates in vector notation

format short
LPSIS=[LPSIS_x, LPSIS_y, LPSIS_z];

```

```

RPSIS=[RPSIS_x, RPSIS_y, RPSIS_z];
LASIS=[LASIS_x, LASIS_y, LASIS_z];
RASIS=[RASIS_x, RASIS_y, RASIS_z];
RFT=[RFT_x, RFT_y, RFT_z];
LFT=[LFT_x, LFT_y, LFT_z];
RLK=[RLK_x, RLK_y, RLK_z];
LLK=[LLK_x, LLK_y, LLK_z];
RMK=[RMK_x, RMK_y, RMK_z];
LMK=[LMK_x, LMK_y, LMK_z];
RLA=[RLA_x, RLA_y, RLA_z];
RMA=[RMA_x, RMA_y, RMA_z];
LLA=[LLA_x, LLA_y, LLA_z];
LMA=[LMA_x, LMA_y, LMA_z];

% calculate Distances and midpoints

midPSIS=(RPSIS+LPSIS)/2;
midASIS=(RASIS+LASIS)/2;
distASIS=sqrt((RASIS(1)-LASIS(1))^2+(RASIS(2)-LASIS(2))^2+(RASIS(3)-LASIS(3))^2);
RPV_Depth=sqrt((midPSIS(1)-midASIS(1))^2+(midPSIS(2)-midASIS(2))^2+(midPSIS(3)-midASIS(3))^2);
target_radius=7.5; % Radius of the marker in millimeters
pelvis_origin=(midASIS+midPSIS)/2;

% Calculate the HJC

RHJC_x=-.19*distASIS+(0.5*RPV_Depth-target_radius);
RHJC_y=-0.3*distASIS;
RHJC_z=0.36*distASIS;

LHJC_x=-.19*distASIS+(0.5*RPV_Depth-target_radius);
LHJC_y=-0.3*distASIS;
LHJC_z=-0.36*distASIS;

RHJC=pelvis_origin+[RHJC_x RHJC_y RHJC_z];
LHJC=pelvis_origin+[LHJC_x LHJC_y LHJC_z];

% Calculate the joint centers Knee and ankle

RKJC=(RMK+RLK)/2;
LKJC=(LMK+LLK)/2;
RAJC=(RMA+RLA)/2;
LAJC=(LMA+LLA)/2;

labels={'LPSIS' 'RPSIS' 'LASIS' 'RASIS' 'RFT' 'LFT' 'RLK' 'LLK' 'RMK' 'LMK' 'RLA' 'RMA' 'LLA'
'LMA' 'midPSIS' 'midASIS' 'Po' 'LHJC' 'RHJC' 'RKJC' 'LKJC' 'RAJC' 'LAJC'};
points3d=[LPSIS; RPSIS; LASIS; RASIS; RFT; LFT; RLK; LLK; RMK; LMK; RLA; RMA; LLA; LMA; midPSIS;
midASIS; pelvis_origin; LHJC; RHJC; RKJC; LKJC; RAJC; LAJC];
plot3(points3d(:,1),points3d(:,2),points3d(:,3),'o');
axis equal
xlabel('X')
ylabel('Y')
zlabel('Z')
text(points3d(:,1),points3d(:,2),points3d(:,3),labels)

% Extract 2d Joint centers

RHJC2d=[RHJC(3) RHJC(2)];
LHJC2d=[LHJC(3) LHJC(2)];
RKJC2d=[RKJC(3) RKJC(2)];
LKJC2d=[LKJC(3) LKJC(2)];
RAJC2d=[RAJC(3) RAJC(2)];
LAJC2d=[LAJC(3) LAJC(2)];

points2d=[RHJC2d; LHJC2d; RKJC2d; LKJC2d; RAJC2d; LAJC2d];
hold on
plot(points2d(:,1),points2d(:,2),'o');
xlabel('X');
ylabel('Y');

line([points2d(1,1) points2d(3,1) points2d(5,1)],[points2d(1,2),points2d(3,2),points2d(5,2)]);
line([points2d(2,1) points2d(4,1) points2d(6,1)],[points2d(2,2),points2d(4,2),points2d(6,2)]);

```

```

% Create vectors of bone segments

R_shank=RKJC2d-RAJC2d;
R_thigh=RHJC2d-RKJC2d;
L_shank=LKJC2d-LAJC2d;
L_thigh=LHJC2d-LKJC2d;

R_dot=dot(R_shank,R_thigh);
L_dot=dot(L_shank,L_thigh);

Mag_r_shank=sqrt((R_shank(1)^2)+(R_shank(2)^2));
Mag_r_thigh=sqrt((R_thigh(1)^2)+(R_thigh(2)^2));
Mag_l_shank=sqrt((L_shank(1)^2)+(L_shank(2)^2));
Mag_l_thigh=sqrt((L_thigh(1)^2)+(L_thigh(2)^2));

R_theta=acos(R_dot/(Mag_r_shank*Mag_r_thigh));
L_theta=acos(L_dot/(Mag_l_shank*Mag_l_thigh));

R_theta_deg=R_theta*180/pi;
L_theta_deg=L_theta*180/pi;

R_tibiofemoral_alignment=180-R_theta_deg;
L_tibiofemoral_alignment=180-L_theta_deg;

R_weld_offset=R_theta_deg/2;
L_weld_offset=L_theta_deg/2;

ave_theta=(R_theta_deg+L_theta_deg)/2;
ave_TF_Alignment=(R_tibiofemoral_alignment+L_tibiofemoral_alignment)/2;
ave_weld_offset=(R_weld_offset+L_weld_offset)/2;
ave_weld_offset_rad=ave_weld_offset*pi/180

% Calculate varus and valgus angle adjustment valuse

% Nominal
theta_180d=180
theta_180r=theta_180d*pi/180;
theta_180_WO=(pi-theta_180r)/2

% Varus
theta_176d=176
theta_176r=theta_176d*pi/180;
theta_176_WO=(pi-theta_176r)/2

theta_172d=172
theta_172r=theta_172d*pi/180;
theta_172_WO=(pi-theta_172r)/2

% Valgus

theta_184d=184
theta_184r=theta_184d*pi/180;
theta_184_WO=(pi-theta_184r)/2

theta_188d=188
theta_188r=theta_188d*pi/180;
theta_188_WO=(pi-theta_188r)/2

```

A.2. RRA Parameter Extraction and Reduction Code

```
% This Code allows the specific RRA parameters: forces, moments, and
% coordinate errors that are used to reduce the residuals to be extracted
% from the residual output files after running an RRA simulation.
% This will help in reducing residuals to the proper threshold during the
% iterative process. The inputs for this code are the residual forces files
% and the kinematic errors files produced during each RRA simulation. This
% code will tell you which threshold each parameter is in and which parameters
% need to be further reduced.

% Import Data

[filename1,filepath1]=uigetfile('*.sto','please select Residuals force file');
selectedfile1=fullfile(filepath1,filename1);
%data=uiimport(selectedfile);
datal=importfile(selectedfile1); % generates a "struct" matrix of vectors with column headers
from data in "selectedfile"

[filename2,filepath2]=uigetfile('*.sto','please select Kinimatic Error file');
selectedfile2=fullfile(filepath2,filename2);
%data=uiimport(selectedfile);
data2=importfile(selectedfile2);

%Extracted kinematic joints from chosen file "selectedfile"

time=datal.time;
FX=datal.FX;
FY=datal.FY;
FZ=datal.FZ;
MX=datal.MX;
MY=datal.MY;
MZ=datal.MZ;

time=data2.time;
pelvis_tx=data2.pelvis_tx;
pelvis_ty=data2.pelvis_ty;
pelvis_tz=data2.pelvis_tz;
pelvis_rz_rad=data2.pelvis_tilt;
pelvis_rx_rad=data2.pelvis_list;
pelvis_ry_rad=data2.pelvis_rotation;

% Convert Rotational error from radians to degrees
pelvis_rz=pelvis_rz_rad*(180/pi);
pelvis_rx=pelvis_rx_rad*(180/pi);
pelvis_ry=pelvis_ry_rad*(180/pi);

% Extract Data For FX
FX_Avg=mean(FX);
FX_RMS=rms(FX);
FX_Max=max(FX);
FX_Min=min(FX);
FX_Max_Abs=sqrt((FX_Max)^2);
FX_Min_Abs=sqrt((FX_Min)^2);

if FX_Max_Abs<FX_Min_Abs;

    FX_Mag=FX_Min;
else
    FX_Mag=FX_Max;
end

% Extract Data For FY
FY_Avg=mean(FY);
FY_RMS=rms(FY);
FY_Max=max(FY);
FY_Min=min(FY);
FY_Max_Abs=sqrt((FY_Max)^2);
FY_Min_Abs=sqrt((FY_Min)^2);

if FY_Max_Abs<FY_Min_Abs;
```

```

        FY_Mag=FY_Min;
else
        FY_Mag=FY_Max;
end

% Extract Data For FZ
FZ_Avg=mean(FZ);
FZ_RMS=rms(FZ);
FZ_Max=max(FZ);
FZ_Min=min(FZ);
FZ_Max_Abs=sqrt((FZ_Max)^2);
FZ_Min_Abs=sqrt((FZ_Min)^2);

if FZ_Max_Abs<FZ_Min_Abs;

        FZ_Mag=FZ_Min;
else
        FZ_Mag=FZ_Max;
end

% Extract Data For MX
MX_Avg=mean(MX);
MX_RMS=rms(MX);
MX_Max=max(MX);
MX_Min=min(MX);
MX_Max_Abs=sqrt((MX_Max)^2);
MX_Min_Abs=sqrt((MX_Min)^2);

if MX_Max_Abs<MX_Min_Abs;

        MX_Mag=MX_Min;
else
        MX_Mag=MX_Max;
end

% Extract Data For MY
MY_Avg=mean(MY);
MY_RMS=rms(MY);
MY_Max=max(MY);
MY_Min=min(MY);
MY_Max_Abs=sqrt((MY_Max)^2);
MY_Min_Abs=sqrt((MY_Min)^2);

if MY_Max_Abs<MY_Min_Abs;

        MY_Mag=MY_Min;
else
        MY_Mag=MY_Max;
end

% Extract Data For MZ
MZ_Avg=mean(MZ);
MZ_RMS=rms(MZ);
MZ_Max=max(MZ);
MZ_Min=min(MZ);
MZ_Max_Abs=sqrt((MZ_Max)^2);
MZ_Min_Abs=sqrt((MZ_Min)^2);

if MZ_Max_Abs<MZ_Min_Abs
        MZ_Mag=MZ_Min;
else
        MZ_Mag=MZ_Max;
end

% Extract Data For pelvis_tx
pelvis_tx_Avg=mean(pelvis_tx);
pelvis_tx_RMS=rms(pelvis_tx);
pelvis_tx_Max=max(pelvis_tx);
pelvis_tx_Min=min(pelvis_tx);
pelvis_tx_Max_Abs=sqrt((pelvis_tx_Max)^2);
pelvis_tx_Min_Abs=sqrt((pelvis_tx_Min)^2);

```

```

if pelvis_tx_Max_Abs<pelvis_tx_Min_Abs;

    pelvis_tx_Mag=pelvis_tx_Min;
else
    pelvis_tx_Mag=pelvis_tx_Max;
end

% Extract Data For pelvis_ty
pelvis_ty_Avg=mean(pelvis_ty);
pelvis_ty_RMS=rms(pelvis_ty);
pelvis_ty_Max=max(pelvis_ty);
pelvis_ty_Min=min(pelvis_ty);
pelvis_ty_Max_Abs=sqrt((pelvis_ty_Max)^2);
pelvis_ty_Min_Abs=sqrt((pelvis_ty_Min)^2);

if pelvis_ty_Max_Abs<pelvis_ty_Min_Abs;

    pelvis_ty_Mag=pelvis_ty_Min;
else
    pelvis_ty_Mag=pelvis_ty_Max;
end

% Extract Data For pelvis_tz
pelvis_tz_Avg=mean(pelvis_tz);
pelvis_tz_RMS=rms(pelvis_tz);
pelvis_tz_Max=max(pelvis_tz);
pelvis_tz_Min=min(pelvis_tz);
pelvis_tz_Max_Abs=sqrt((pelvis_tz_Max)^2);
pelvis_tz_Min_Abs=sqrt((pelvis_tz_Min)^2);

if pelvis_tz_Max_Abs<pelvis_tz_Min_Abs;

    pelvis_tz_Mag=pelvis_tz_Min;
else
    pelvis_tz_Mag=pelvis_tz_Max;
end

% Extract Data For pelvis_rx
pelvis_rx_Avg=mean(pelvis_rx);
pelvis_rx_RMS=rms(pelvis_rx);
pelvis_rx_Max=max(pelvis_rx);
pelvis_rx_Min=min(pelvis_rx);
pelvis_rx_Max_Abs=sqrt((pelvis_rx_Max)^2);
pelvis_rx_Min_Abs=sqrt((pelvis_rx_Min)^2);

if pelvis_rx_Max_Abs<pelvis_rx_Min_Abs;

    pelvis_rx_Mag=pelvis_rx_Min;
else
    pelvis_rx_Mag=pelvis_rx_Max;
end

% Extract Data For pelvis_ry
pelvis_ry_Avg=mean(pelvis_ry);
pelvis_ry_RMS=rms(pelvis_ry);
pelvis_ry_Max=max(pelvis_ry);
pelvis_ry_Min=min(pelvis_ry);
pelvis_ry_Max_Abs=sqrt((pelvis_ry_Max)^2);
pelvis_ry_Min_Abs=sqrt((pelvis_ry_Min)^2);

if pelvis_ry_Max_Abs<pelvis_ry_Min_Abs;

    pelvis_ry_Mag=pelvis_ry_Min;
else
    pelvis_ry_Mag=pelvis_ry_Max;
end

% Extract Data For pelvis_rz
pelvis_rz_Avg=mean(pelvis_rz);
pelvis_rz_RMS=rms(pelvis_rz);
pelvis_rz_Max=max(pelvis_rz);
pelvis_rz_Min=min(pelvis_rz);
pelvis_rz_Max_Abs=sqrt((pelvis_rz_Max)^2);

```

```

pelvis_rz_Min_Abs=sqrt((pelvis_rz_Min)^2);
if pelvis_rz_Max_Abs<pelvis_rz_Min_Abs;
    pelvis_rz_Mag=pelvis_rz_Min;
else
    pelvis_rz_Mag=pelvis_rz_Max;
end

% Define status
good='good';
okay='okay';
bad='bad';

%% Create Thresholds

% Force Thresholds FX, FY, FZ
%FX Threshold
if abs(FX_Mag)<10
    status1s=good;
    status1n=1;
elseif abs(FX_Mag)>10 && abs(FX_Mag)<25
    status1s=okay;
    status1n=2;
else
    status1s=bad;
    status1n=3;
end

if FX_RMS<5
    status2s=good;
    status2n=1;
elseif FX_RMS>5 && FX_RMS<10
    status2s=okay;
    status2n=2;
else
    status2s=bad;
    status2n=3;
end

% FY Threshold
if abs(FY_Mag)<10
    status3s=good;
    status3n=1;
elseif abs(FY_Mag)>10 && abs(FY_Mag)<25
    status3s=okay;
    status3n=2;
else
    status3s=bad;
    status3n=3;
end

if FY_RMS<5
    status4s=good;
    status4n=1;
elseif FY_RMS>5 && FY_RMS<10
    status4s=okay;
    status4n=2;
else
    status4s=bad;
    status4n=3;
end

% FZ Threshold
if abs(FZ_Mag)<10
    status5s=good;
    status5n=1;
elseif abs(FZ_Mag)>10 && abs(FZ_Mag)<25
    status5s=okay;
    status5n=2;
else
    status5s=bad;

```

```

        status5n=3;
    end

    if FZ_RMS<5
        status6s=good;
        status6n=1;
    elseif FZ_RMS>5 && FZ_RMS<10
        status6s=okay;
        status6n=2;
    else
        status6s=bad;
        status6n=3;
    end

    % Moment Thresholds MX, MY, MZ
    % MX Threshold
    if abs(MX_Mag)<50
        status7s=good;
        status7n=1;
    elseif abs(MX_Mag)>50 && abs(MX_Mag)<75
        status7s=okay;
        status7n=2;
    else
        status7s=bad;
        status7n=3;
    end

    if MX_RMS<30
        status8s=good;
        status8n=1;
    elseif MX_RMS>30 && MX_RMS<50
        status8s=okay;
        status8n=2;
    else
        status8s=bad;
        status8n=3;
    end

    % MY Threshold
    if abs(MY_Mag)<50
        status9s=good;
        status9n=1;
    elseif abs(MY_Mag)>50 && abs(MY_Mag)<75
        status9s=okay;
        status9n=2;
    else
        status9s=bad;
        status9n=3;
    end

    if MY_RMS<30
        status10s=good;
        status10n=1;
    elseif MY_RMS>30 && MY_RMS<50
        status10s=okay;
        status10n=2;
    else
        status10s=bad;
        status10n=3;
    end

    % MZ Threshold
    if abs(MZ_Mag)<50
        status11s=good;
        status11n=1;
    elseif abs(MZ_Mag)>50 && abs(MZ_Mag)<75
        status11s=okay;
        status11n=2;
    else
        status11s=bad;
    end

```

```

        status11n=3;
    end

    if MZ_RMS<30
        status12s=good;
        status12n=1;
    elseif MZ_RMS>30 && MZ_RMS<50
        status12s=okay;
        status12n=2;
    else
        status12s=bad;
        status12n=3;
    end

    % Translational Error Thresholds tx, ty, tz
    % pelvis_tx Threshold
    if abs(pelvis_tx_Mag)<.02
        status13s=good;
        status13n=1;
    elseif abs(pelvis_tx_Mag)>.02 && abs(pelvis_tx_Mag)<.05
        status13s=okay;
        status13n=2;
    else
        status13s=bad;
        status13n=3;
    end

    if pelvis_tx_RMS<.02
        status14s=good;
        status14n=1;
    elseif pelvis_tx_RMS>.02 && pelvis_tx_RMS<.04
        status14s=okay;
        status14n=2;
    else
        status14s=bad;
        status14n=3;
    end

    % pelvis_ty Threshold
    if abs(pelvis_ty_Mag)<.02
        status15s=good;
        status15n=1;
    elseif abs(pelvis_ty_Mag)>.02 && abs(pelvis_ty_Mag)<.05
        status15s=okay;
        status15n=2;
    else
        status15s=bad;
        status15n=3;
    end

    if pelvis_ty_RMS<.02
        status16s=good;
        status16n=1;
    elseif pelvis_ty_RMS>.02 && pelvis_ty_RMS<.04
        status16s=okay;
        status16n=2;
    else
        status16s=bad;
        status16n=3;
    end

    % pelvis_tz Threshold
    if abs(pelvis_tz_Mag)<.02
        status17s=good;
        status17n=1;
    elseif abs(pelvis_tz_Mag)>.02 && abs(pelvis_tz_Mag)<.05
        status17s=okay;
        status17n=2;
    else
        status17s=bad;
        status17n=3;
    end
end

```

```

if pelvis_tz_RMS<.02
    status18s=good;
    status18n=1;
elseif pelvis_tz_RMS>.02 && pelvis_tz_RMS<.04
    status18s=okay;
    status18n=2;
else
    status18s=bad;
    status18n=3;
end

% Rotational Error Thresholds MX, MY, MZ
% pelvis_rx Threshold
if abs(pelvis_rx_Mag)<2
    status19s=good;
    status19n=1;
elseif abs(pelvis_rx_Mag)>2 && abs(pelvis_rx_Mag)<5
    status19s=okay;
    status19n=2;
else
    status19s=bad;
    status19n=3;
end

if pelvis_rx_RMS<2
    status20s=good;
    status20n=1;
elseif pelvis_rx_RMS>2 && pelvis_rx_RMS<5
    status20s=okay;
    status20n=2;
else
    status20s=bad;
    status20n=3;
end

% pelvis_ry Threshold
if abs(pelvis_ry_Mag)<2
    status21s=good;
    status21n=1;
elseif abs(pelvis_ry_Mag)>2 && abs(pelvis_ry_Mag)<5
    status21s=okay;
    status21n=2;
else
    status21s=bad;
    status21n=3;
end

if pelvis_ry_RMS<2
    status22s=good;
    status22n=1;
elseif pelvis_ry_RMS>2 && pelvis_ry_RMS<5
    status22s=okay;
    status22n=2;
else
    status22s=bad;
    status22n=3;
end

% pelvis_rz Threshold
if abs(pelvis_rz_Mag)<2
    status23s=good;
    status23n=1;
elseif abs(pelvis_rz_Mag)>2 && abs(pelvis_rz_Mag)<5
    status23s=okay;
    status23n=2;
else
    status23s=bad;
    status23n=3;
end

```

```

if pelvis_rz_RMS<2
    status24s=good;
    status24n=1;
elseif pelvis_rz_RMS>2 && pelvis_rz_RMS<5
    status24s=okay;
    status24n=2;
else
    status24s=bad;
    status24n=3;
end

status_n1=[status1n status2n status3n status4n status5n status6n status7n status8n status9n
status10n status11n status12n...
    status13n status14n status15n status16n status17n status18n status19n status20n status21n
status22n status23n status24n];

status_s1={status1s status2s status3s status4s status5s status6s status7s status8s status9s
status10s status11s status12s...
    status13s status14s status15s status16s status17s status18s status19s status20s status21s
status22s status23s status24s};

values1=[FX_Mag FX_RMS FY_Mag FY_RMS FZ_Mag FZ_RMS MX_Mag MX_RMS MY_Mag MY_RMS MZ_Mag MZ_RMS...
    pelvis_tx_Mag pelvis_tx_RMS pelvis_ty_Mag pelvis_ty_RMS pelvis_tz_Mag pelvis_tz_RMS ...
    pelvis_rx_Mag pelvis_rx_RMS pelvis_ry_Mag pelvis_ry_RMS pelvis_rz_Mag pelvis_rz_RMS];

names1={'FX_Max' 'FX_RMS' 'FY_Max' 'FY_RMS' 'FZ_Max' 'FZ_RMS' 'MX_Max' 'MX_RMS' 'MY_Max' 'MY_RMS'
'MZ_Max' 'MZ_RMS'...
    'pelvis_tx_Max' 'pelvis_tx_RMS' 'pelvis_ty_Max' 'pelvis_ty_RMS' 'pelvis_tz_Max'
'pelvis_tz_RMS' 'pelvis_rx_Max'...
    'pelvis_rx_RMS' 'pelvis_ry_Max' 'pelvis_ry_RMS' 'pelvis_rz_Max' 'pelvis_rz_RMS'};

status_n=status_n1'
status_s=status_s1';
values=values1'
names=names1';

fprintf('\n')
fprintf('FX_Max=%4f %s\n',FX_Mag,status1s) % 1
fprintf('FX_RMS=%4f %s\n\n',FX_RMS,status2s) % 2

fprintf('FY_Max=%4f %s\n',FY_Mag,status3s) % 3
fprintf('FY_RMS=%4f %s\n\n',FY_RMS,status4s) % 4

fprintf('FZ_Max=%4f %s\n',FZ_Mag,status5s) % 5
fprintf('FZ_RMS=%4f %s\n\n',FZ_RMS,status5s) % 6

fprintf('MX_Max=%4f %s\n',MX_Mag,status7s) % 7
fprintf('MX_RMS=%4f %s\n\n',MX_RMS,status8s) % 8

fprintf('MY_Max=%4f %s\n',MY_Mag,status9s) % 9
fprintf('MY_RMS=%4f %s\n\n',MY_RMS,status10s) % 10

fprintf('MZ_Max=%4f %s\n',MZ_Mag,status11s) % 11
fprintf('MZ_RMS=%4f %s\n\n',MZ_RMS,status12s) % 12

fprintf('pelvis_tx_Max=%4f %s\n',pelvis_tx_Mag,status13s) % 13
fprintf('pelvis_tx_RMS=%4f %s\n\n',pelvis_tx_RMS,status14s) % 14

fprintf('pelvis_ty_Max=%4f %s\n',pelvis_ty_Mag,status15s) % 15
fprintf('pelvis_ty_RMS=%4f %s\n\n',pelvis_ty_RMS,status16s) % 16

fprintf('pelvis_tz_Max=%4f %s\n',pelvis_tz_Mag,status17s) % 17
fprintf('pelvis_tz_RMS=%4f %s\n\n',pelvis_tz_RMS,status18s) % 18

fprintf('pelvis_rx_Max=%4f %s\n',pelvis_rx_Mag,status19s) % 19
fprintf('pelvis_rx_RMS=%4f %s\n\n',pelvis_rx_RMS,status20s) % 20

fprintf('pelvis_ry_Max=%4f %s\n',pelvis_ry_Mag,status21s) % 21
fprintf('pelvis_ry_RMS=%4f %s\n\n',pelvis_ry_RMS,status22s) % 22

fprintf('pelvis_rz_Max=%4f %s\n',pelvis_rz_Mag,status23s) % 23
fprintf('pelvis_rz_RMS=%4f %s\n\n',pelvis_rz_RMS,status24s) % 24

```

```
n=24;
%s=1;

fprintf('\nNeeds Adjustment \n')
for s=1:n
    if status_n(s)~=1
        fprintf('%s=%4f %s\n',names{s},values(s),status_s{s});
    end
end
```

A.3. Internal validation Code

```
% This Code Calculates the moments generated by the 13 muscles that traverse
% the knee joint that contribute to the knee flexion and extension moments.
% Moments are calculated about the left and right knees for all time steps.

% Right knee Moment arm File
[filename1,filepath1]=uigetfile('*.sto','please select r_knee moment arm file'); % select the
Right knee angle moment arm file
selectedfile1=fullfile(filepath1,filename1);
%data=uiimport(selectedfile);
data1=importfile(selectedfile1); % generates a "struct" matrix of vectors with column headers
from data in "selectedfile"

% left knee Moment arm File
[filename1,filepath1]=uigetfile('*.sto','please select l_knee moment file'); % select the left
knee angle moment arm file
selectedfile1=fullfile(filepath1,filename1);
%data=uiimport(selectedfile);
data3=importfile(selectedfile1); % generates a "struct" matrix of vectors with column headers
from data in "selectedfile"

% select Muscle force file
[filename2,filepath2]=uigetfile('*.sto','please select muscle force file'); % Select the muscle
force file
selectedfile2=fullfile(filepath2,filename2);
%data=uiimport(selectedfile);
data2=importfile(selectedfile2);

% % select Muscle force file
% [filename2,filepath2]=uigetfile('*.sto','please select muscle force file'); % Select the
muscle force file
% selectedfile2=fullfile(filepath2,filename2);
% %data=uiimport(selectedfile);
% data4=importfile(selectedfile2);
%
% time4=data4.time
% ID_knee_r=data4.knee_angle_r_moment;
% ID_knee_l=data4.knee_angle_l_moment;
%
% dim=102;
% ID_knee_r_zeros=zeros(dim,1);
% ID_knee_l_zeros=zeros(dim,1);
% time4_zeros=zeros(dim,1);
%
% a=1;
% b=1;
%
% while b<=102
%     if abs(time3(a)-time4(b))<.0009
%         ID_knee_r_zeros(b,1)=ID_knee_r(a);
%         ID_knee_l_zeros(b,1)=ID_knee_l(a);
%
%         time4_zeros(b,1)=time4(a);
%
%         b=b+1;
%         a=1;
%     else
%         a=a+1;
%     end
%     b=b;
% end
%
% ID_knee_r=ID_knee_r_zeros;
% ID_knee_l=ID_knee_l_zeros;
%
% time4=time4_zeros;

%Extracted kinematic joints from chosen file "selectedfile"

time1=data1.time;
semimem_arm_r=data1.semimem_r;
```

```

semiten_arm_r=data1.semiten_r;
bifemlh_arm_r=data1.bifemlh_r;
bifemsh_arm_r=data1.bifemsh_r;
sar_arm_r=data1.sar_r;
tfl_arm_r=data1.tfl_r;
grac_arm_r=data1.grac_r;
rect_fem_arm_r=data1.rect_fem_r;
vas_med_arm_r=data1.vas_med_r;
vas_int_arm_r=data1.vas_int_r;
vas_lat_arm_r=data1.vas_lat_r;
med_gas_arm_r=data1.med_gas_r;
lat_gas_arm_r=data1.lat_gas_r;

time3=data3.time;
semimem_arm_l=data3.semimem_l;
semiten_arm_l=data3.semiten_l;
bifemlh_arm_l=data3.bifemlh_l;
bifemsh_arm_l=data3.bifemsh_l;
sar_arm_l=data3.sar_l;
tfl_arm_l=data3.tfl_l;
grac_arm_l=data3.grac_l;
rect_fem_arm_l=data3.rect_fem_l;
vas_med_arm_l=data3.vas_med_l;
vas_int_arm_l=data3.vas_int_l;
vas_lat_arm_l=data3.vas_lat_l;
med_gas_arm_l=data3.med_gas_l;
lat_gas_arm_l=data3.lat_gas_l;

% Extract right and left Muscle forces
time2=data2.time;
semimem_F_r=data2.semimem_r;
semiten_F_r=data2.semiten_r;
bifemlh_F_r=data2.bifemlh_r;
bifemsh_F_r=data2.bifemsh_r;
sar_F_r=data2.sar_r;
tfl_F_r=data2.tfl_r;
grac_F_r=data2.grac_r;
rect_fem_F_r=data2.rect_fem_r;
vas_med_F_r=data2.vas_med_r;
vas_int_F_r=data2.vas_int_r;
vas_lat_F_r=data2.vas_lat_r;
med_gas_F_r=data2.med_gas_r;
lat_gas_F_r=data2.lat_gas_r;

semimem_F_l=data2.semimem_l;
semiten_F_l=data2.semiten_l;
bifemlh_F_l=data2.bifemlh_l;
bifemsh_F_l=data2.bifemsh_l;
sar_F_l=data2.sar_l;
tfl_F_l=data2.tfl_l;
grac_F_l=data2.grac_l;
rect_fem_F_l=data2.rect_fem_l;
vas_med_F_l=data2.vas_med_l;
vas_int_F_l=data2.vas_int_l;
vas_lat_F_l=data2.vas_lat_l;
med_gas_F_l=data2.med_gas_l;
lat_gas_F_l=data2.lat_gas_l;

% ID_knee_reserve_r=data2.knee_angle_r_reserve;
% ID_knee_reserve_l=data2.knee_angle_l_reserve;

% Compute right and left Muscle Moments
semimem_m_r=semimem_arm_r.*semimem_F_r;
semiten_m_r=semiten_arm_r.*semiten_F_r;
bifemlh_m_r=bifemlh_arm_r.*bifemlh_F_r;
bifemsh_m_r=bifemsh_arm_r.*bifemsh_F_r;
sar_m_r=sar_arm_r.*sar_F_r;
tfl_m_r=tfl_arm_r.*tfl_F_r;
grac_m_r=grac_arm_r.*grac_F_r;
rect_fem_m_r=rect_fem_arm_r.*rect_fem_F_r;
vas_med_m_r=vas_med_arm_r.*vas_med_F_r;
vas_int_m_r=vas_int_arm_r.*vas_int_F_r;
vas_lat_m_r=vas_lat_arm_r.*vas_lat_F_r;

```

```

med_gas_m_r=med_gas_arm_r.*med_gas_F_r;
lat_gas_m_r=lat_gas_arm_r.*lat_gas_F_r;

semimem_m_l=semimem_arm_l.*semimem_F_l;
semiten_m_l=semiten_arm_l.*semiten_F_l;
bifemlh_m_l=bifemlh_arm_l.*bifemlh_F_l;
bifemsh_m_l=bifemsh_arm_l.*bifemsh_F_l;
sar_m_l=sar_arm_l.*sar_F_l;
tfl_m_l=tfl_arm_l.*tfl_F_l;
grac_m_l=grac_arm_l.*grac_F_l;
rect_fem_m_l=rect_fem_arm_l.*rect_fem_F_l;
vas_med_m_l=vas_med_arm_l.*vas_med_F_l;
vas_int_m_l=vas_int_arm_l.*vas_int_F_l;
vas_lat_m_l=vas_lat_arm_l.*vas_lat_F_l;
med_gas_m_l=med_gas_arm_l.*med_gas_F_l;
lat_gas_m_l=lat_gas_arm_l.*lat_gas_F_l;

% sum the right and left muscle moments
sum_m_r=semimem_m_r+semiten_m_r+bifemlh_m_r+bifemsh_m_r+sar_m_r+tfl_m_r+grac_m_r+rect_fem_m_r+vas
_med_m_r+vas_int_m_r+vas_lat_m_r+med_gas_m_r+lat_gas_m_r;
sum_m_l=semimem_m_l+semiten_m_l+bifemlh_m_l+bifemsh_m_l+sar_m_l+tfl_m_l+grac_m_l+rect_fem_m_l+vas
_med_m_l+vas_int_m_l+vas_lat_m_l+med_gas_m_l+lat_gas_m_l;

```

A.4. EKAM Calculation Code

```
% file computes the external knee adduction moment about the right and
% left knees for Normal Walking gait

% Import Data
% Import GRF data
[filename1,filepath1]=uigetfile('*.mot','please select GRF force file'); % select Ground reaction
force file
selectedfile1=fullfile(filepath1,filename1);
%data=uiimport(selectedfile);
data1=importfile(selectedfile1); % generates a "struct" matrix of vectors with column headers
from data in "selectedfile"

% Import Body kinematics file
[filename2,filepath2]=uigetfile('*.sto','please select Body kinematics file'); % select body
kinematics file
selectedfile2=fullfile(filepath2,filename2);
%data=uiimport(selectedfile);
data2=importfile(selectedfile2);

% Extract Ground reaction force data. Right leg Force comonents and location in global coordinate
frame.

time1_=data1.time;
GRFxr_=data1.ground_force_1_vx;
GRFyr_=data1.ground_force_1_vy;
GRFzr_=data1.ground_force_1_vz;
Rx_GRFr_=data1.ground_force_1_px;
Ry_GRFr_=data1.ground_force_1_py;
Rz_GRFr_=data1.ground_force_1_pz;

GRFx1_=data1.ground_force_2_vx;
GRFy1_=data1.ground_force_2_vy;
GRFz1_=data1.ground_force_2_vz;
Rx_GRF1_=data1.ground_force_2_px;
Ry_GRF1_=data1.ground_force_2_py;
Rz_GRF1_=data1.ground_force_2_pz;

% Extract positon and orientation of tibia ie knee joint enter in Global reference
% frame

time2=data2.time;
Rx_KJCr=data2.tibial_plat_r_X;
Ry_KJCr=data2.tibial_plat_r_Y;
Rz_KJCr=data2.tibial_plat_r_Z;

Rx_KJCl=data2.tibial_plat_l_X;
Ry_KJCl=data2.tibial_plat_l_Y;
Rz_KJCl=data2.tibial_plat_l_Z;

theta_xr=data2.tibial_plat_r_Ox;
theta_yr=data2.tibial_plat_r_Oy;
theta_zr=data2.tibial_plat_r_Oz;

theta_xl=data2.tibial_plat_l_Ox;
theta_yl=data2.tibial_plat_l_Oy;
theta_zl=data2.tibial_plat_l_Oz;

% filter the ground reaction force data

dim=139;
i=40;
j=0;

GRFxr_zeros=zeros(dim-i,1);
GRFyr_zeros=zeros(dim-i,1);
GRFzr_zeros=zeros(dim-i,1);

GRFx1_zeros=zeros(dim-i,1);
GRFy1_zeros=zeros(dim-i,1);
```

```

GRFzl_zeros=zeros(dim-i,1);

Rx_GRFr_zeros=zeros(dim-i,1);
Ry_GRFr_zeros=zeros(dim-i,1);
Rz_GRFr_zeros=zeros(dim-i,1);

Rx_GRF1_zeros=zeros(dim-i,1);
Ry_GRF1_zeros=zeros(dim-i,1);
Rz_GRF1_zeros=zeros(dim-i,1);

time1_zeros=zeros(dim-i,1);

a=1;
b=1;
while b<=99
    if abs(time1_(a)-time2(b))<.0009
        GRFxr_zeros(b,1)=GRFxr_(a);
        GRFyr_zeros(b,1)=GRFyr_(a);
        GRFzr_zeros(b,1)=GRFzr_(a);
        GRFxl_zeros(b,1)=GRFxl_(a);
        GRFyl_zeros(b,1)=GRFyl_(a);
        GRFzl_zeros(b,1)=GRFzl_(a);
        Rx_GRFr_zeros(b,1)=Rx_GRFr_(a);
        Ry_GRFr_zeros(b,1)=Ry_GRFr_(a);
        Rz_GRFr_zeros(b,1)=Rz_GRFr_(a);

        Rx_GRF1_zeros(b,1)=Rx_GRF1_(a);
        Ry_GRF1_zeros(b,1)=Ry_GRF1_(a);
        Rz_GRF1_zeros(b,1)=Rz_GRF1_(a);

        time1_zeros(b,1)=time1_(a);

        b=b+1;
        a=1;
    else
        a=a+1;
    end
    b=b;
end

GRFxr=GRFxr_zeros;
GRFyr=GRFyr_zeros;
GRFzr=GRFzr_zeros;

GRFxl=GRFxl_zeros;
GRFyl=GRFyl_zeros;
GRFzl=GRFzl_zeros;

Rx_GRFr=Rx_GRFr_zeros;
Ry_GRFr=Ry_GRFr_zeros;
Rz_GRFr=Rz_GRFr_zeros;

Rx_GRF1=Rx_GRF1_zeros;
Ry_GRF1=Ry_GRF1_zeros;
Rz_GRF1=Rz_GRF1_zeros;

time1=time1_zeros;

for k=1:99
    % define sine and cosine terms 1, 2, 3 corresponds to theta_x, theta_y, theta_z

C1r=cosd(theta_xr(k));
C2r=cosd(theta_yr(k));
C3r=cosd(theta_zr(k));
S1r=sind(theta_xr(k));
S2r=sind(theta_yr(k));
S3r=sind(theta_zr(k));

```

```

C1l=cosd(theta_xl(k));
C2l=cosd(theta_yl(k));
C3l=cosd(theta_zl(k));
S1l=sind(theta_xl(k));
S2l=sind(theta_yl(k));
S3l=sind(theta_zl(k));

% define rotation matrix. Transforms coordinates from the global reference
% frame to the tibial reference frame

RCr=[C2r*C3r S3r*C1r+S1r*S2r*C3r S1r*S3r-C1r*S2r*C3r;-C2r*S3r C1r*C3r-S1r*S2r*S3r
S1r*C3r+C1r*S2r*S3r; S2r -S1r*C2r C1r*C2r]; % Cardan Transformation matrix
RCl=[C2l*C3l S3l*C1l+S1l*S2l*C3l S1l*S3l-C1l*S2l*C3l;-C2l*S3l C1l*C3l-S1l*S2l*S3l
S1l*C3l+C1l*S2l*S3l; S2l -S1l*C2l C1l*C2l];
% REr=[C2r*C3r -C2r*S3r S2r; C1r*S3r+S1r*S2r*C3r C1r*C3r-S1r*S2r*S3r -S1r*C2r; S1r*S3r-
C1r*S2r*C3r S1r*C3r+C1r*S2r*S3r C1r*C2r]; % Euler Transformation Matrix
% REEr=[C2r*C3r S1r*S2r*C3r-S3r*C1r S1r*S3r+C1r*S2r*C3r;C2r*S3r C1r*C3r+S1r*S2r*S3r C1r*S2r*S3r-
S1r*C3r; -S2r S1r*C2r C1r*C2r];
% transform ground reaction forces from global to Tibial GRF_global to
% GRF_Tibial

GRF_globalr=[GRFxr(k) GRFyr(k) GRFzr(k)]; % GRF vector in the global reference frame
GRF_tibialr=RCr*GRF_globalr'; % Transformed GRF Vector to the Tibial reference frame

GRF_globall=[GRFxl(k) GRFyl(k) GRFzl(k)]; % GRF vector in the global reference frame
GRF_tibiall=RCl*GRF_globall'; % Transformed GRF Vector to the Tibial reference frame

% Transform location of GRF

R_GRFr=[Rx_GRFr(k) Ry_GRFr(k) Rz_GRFr(k)]; % Ground Reaction Force location vector in global
reference
R_KJCr=[Rx_KJCr(k) Ry_KJCr(k) Rz_KJCr(k)]; % position vector of the tibial reference in the Global
reference frame.

R_GRFl=[Rx_GRFl(k) Ry_GRFl(k) Rz_GRFl(k)]; % Ground Reaction Force location vector in global
reference
R_KJCl=[Rx_KJCl(k) Ry_KJCl(k) Rz_KJCl(k)]; % position vector of the tibial reference in the Global
reference frame.

Tr=-R_KJCr; % inverse position vector of the tibial reference in the Global reference frame.
Tl=-R_KJCl;

r_GRFr=RCr'*R_GRFr'+Tr'; % Position vector of the ground reaction force in the tibial reference
frame.
r_GRFl=RCl'*R_GRFl'+Tl'; % Position vector of the ground reaction force in the tibial reference
frame.

GRF_momentr=cross(r_GRFr,GRF_tibialr); % Calculates the moment about the knee joint center in the
tibial reference frame induced by the knee GRF
GRF_momentl=cross(r_GRFl,GRF_tibiall);

EKAMr(k)=GRF_momentr(1); % Store x component values as the EKAM
rx_GRFr(k)=(r_GRFr(1));

EKAMl(k)=GRF_momentl(1); % Store x component values as the EKAM
rx_GRFl(k)=(r_GRFl(1));
end

timel;
EKAMr';
EKAMl';

% plot(timel,EKAM')
% plot(timel,rx_GRF')

```

Appendix B: RRA Data

Table 28: RRA iterative residual “hand of god” forces and moments on the pelvis for Nominal Normal Walking TFA=177.16. All parameters shown were minimized until they could not be minimized any further. Green= sufficient value, yellow=tolerable value, and red=insufficient value. Threshold values can be found in Table 6.

	Iteration	FX_Max	FX_RMS	FY_Max	FY_RMS	FZ_Max	FZ_RMS	MX_Max	MX_RMS	MY_Max	MY_RMS	MZ_Max	MZ_RMS	tx_Max	tx_RMS	ty_Max	ty_RMS	tz_Max	tz_RMS	rx_Max	rx_RMS	ry_Max	ry_RMS	rz_Max	rz_RMS
Status	1	2	3	2	2	1	1	2	1	1	1	1	1	2	1	2	1	1	1	1	1	1	1	1	1
Valus	1	21.134	13.343	-12.538	5.5134	-8.1857	3.3058	57.9303	23.0262	9.3511	3.2966	37.2573	13.2888	0.025	0.0174	-0.0209	0.0083	0.0091	0.0043	0.2137	0.1265	0.0469	0.0276	-0.1594	0.0861
Status	2	2	3	1	1	1	1	2	1	1	1	1	1	2	1	1	1	1	1	1	1	1	1	1	1
Valus	2	20.691	13.132	9.0455	4.8459	-8.0981	3.2441	57.0338	22.7642	9.8224	3.3328	39.4732	13.7887	0.0244	0.017	0.015	0.0093	0.007	0.0038	0.2087	0.1235	0.0461	0.0271	0.1879	0.1051
Status	3	1	1	2	2	1	1	2	1	1	1	2	1	3	3	1	1	1	1	1	1	1	1	1	1
Valus	3	8.0052	2.6364	-13.235	5.641	-8.7085	3.6204	57.8089	24.449	8.963	3.7493	55.327	16.6974	0.082	0.041	0.0153	0.0093	0.0115	0.005	1.1506	0.7191	0.0676	0.0408	0.0188	0.0108
Status	4	1	1	2	2	2	1	2	1	1	1	2	1	3	2	2	1	1	1	1	1	1	1	1	1
Valus	4	8.6017	3.3349	-16.827	6.8074	-10.571	4.4816	59.0844	27.2533	10.0992	4.2328	53.7595	16.4042	0.0779	0.0395	0.0215	0.0121	0.0167	0.0066	1.683	1.0899	0.0908	0.0574	0.0404	0.0228
Status	5	1	1	2	2	2	1	2	1	1	1	2	1	3	3	2	1	1	1	1	1	1	1	1	1
Valus	5	7.7437	2.6265	-16.239	7.0306	-10.562	4.4774	59.0257	27.214	10.112	4.2344	53.6932	16.3954	0.0819	0.041	0.0279	0.0145	0.0166	0.0066	1.6798	1.0878	0.0909	0.0575	0.0406	0.0229
Status	6	1	1	2	2	2	1	2	1	1	1	2	1	3	2	1	1	1	1	1	1	1	1	1	1
Valus	6	9.6629	4.0703	12.4101	6.1474	10.2958	4.1926	57.2164	22.7569	10.2422	3.3997	54.6896	16.6219	0.0744	0.0382	0.0133	0.0086	0.0089	0.0042	0.1	0.0592	0.0599	0.0349	0.0177	0.0103
Status	7	1	1	1	1	1	1	2	1	1	1	2	1	3	2	1	1	1	1	1	1	1	1	1	1
Valus	7	9.6338	4.0578	8.5005	4.0306	-8.5762	3.474	57.4367	22.6613	10.5404	3.4133	54.3942	16.6077	0.0745	0.0382	0.0103	0.0066	0.0065	0.0036	0.0765	0.0452	0.0485	0.0281	0.0173	0.0102
Status	8	1	1	2	2	1	1	1	1	1	1	3	2	3	3	1	1	1	1	1	1	1	1	1	1
Valus	8	-8.5488	2.5426	12.9243	5.7371	-5.1249	1.7597	28.87	11.4573	11.7586	4.4071	-90.074	36.6458	0.0836	0.0412	-0.0076	0.0025	-0.0089	0.0047	-0.0245	0.0132	-0.0525	0.0149	-0.098	0.0379
Status	9	1	1	2	2	1	1	1	1	1	1	3	2	3	3	1	1	1	1	1	1	1	1	1	1
Valus	9	-8.5797	2.5396	15.497	6.8986	-5.0983	1.7586	-28.842	11.509	11.7306	4.4056	-90.297	36.7222	0.0837	0.0413	-0.0099	0.0031	-0.0089	0.0047	-0.0253	0.0133	-0.0525	0.0149	-0.0982	0.038
Status	10	1	1	2	2	1	1	1	1	1	1	3	2	3	3	1	1	1	1	1	1	1	1	1	1
Valus	10	-8.3655	2.4881	17.7813	7.3756	-6.0396	2.0257	28.8144	11.3149	11.7086	4.4223	-89.751	36.4424	0.0836	0.0412	-0.0102	0.0031	-0.0084	0.0043	-0.0249	0.0135	-0.0507	0.0146	-0.1944	0.0728
Status	11	1	1	2	2	1	1	1	1	1	1	3	2	3	3	1	1	1	1	1	1	1	1	1	1
Valus	11	-8.3656	2.4881	17.7811	7.3755	-6.0399	2.0257	28.8168	11.3144	11.7088	4.4223	-89.752	36.4429	0.0836	0.0412	-0.0102	0.0031	-0.0084	0.0042	-0.0249	0.0135	-0.0507	0.0146	-0.1944	0.0728
Status	12	1	1	2	2	1	1	1	1	1	1	3	2	3	3	1	1	1	1	1	1	1	1	1	1
Valus	12	-8.3669	2.4875	14.406	5.9553	-6.0395	2.0279	28.8151	11.334	11.7081	4.422	-89.707	36.4538	0.0836	0.0412	-0.0075	0.0025	-0.0084	0.0043	-0.0249	0.0134	-0.0508	0.0146	-0.1946	0.073
Status	13	1	1	2	1	1	1	1	1	1	1	3	2	3	3	1	1	1	1	1	1	1	1	1	1
Valus	13	-8.3682	2.4938	11.1509	4.5702	-6.0391	2.0343	28.8125	11.3773	11.7074	4.4142	-89.665	36.312	0.0836	0.0412	-0.005	0.0021	-0.0084	0.0043	-0.0249	0.0134	-0.051	0.0147	-0.1948	0.0731
Status	14	3	3	1	1	1	1	1	1	1	1	2	1	1	1	1	1	1	1	1	1	1	1	1	1
Valus	14	25.04	13.671	9.2084	2.7156	-5.0799	1.7416	-28.956	11.5739	11.8639	4.0236	-68.899	20.796	0.016	0.0116	0.0044	0.0021	-0.0089	0.0047	-0.0307	0.012	-0.0339	0.0112	-0.035	0.0137
Status	15	2	3	1	1	1	1	1	1	1	1	2	1	2	1	1	1	1	1	1	1	1	1	1	1
Valus	15	19.759	12.432	9.6591	3.1314	-5.0858	1.7456	-28.933	11.5597	11.7705	4.0557	-73.33	23.5943	0.027	0.018	0.0044	0.002	-0.0089	0.0047	-0.025	0.0112	-0.0398	0.0126	-0.0494	0.0191
Status	16	2	2	1	1	1	1	1	1	1	1	2	1	2	2	1	1	1	1	1	1	1	1	1	1
Valus	16	14.961	9.0065	8.9912	3.5216	-5.0883	1.749	-28.846	11.5198	11.613	4.1775	-65.825	26.2491	0.0478	0.0274	0.0041	0.002	-0.0089	0.0047	-0.02	0.0089	-0.0449	0.0136	-0.6719	0.2563

Table 29: RRA iterative residual “hand of god” forces and moments on the pelvis for Varus Normal Walking TFA=172. All parameters shown were minimized until they could not be minimized any further. Green= sufficient value, yellow=tolerable value, and red=insufficient value. Threshold values can be found in Table 6.

	Iteration	FX_Max	FX_RMS	FY_Max	FY_RMS	FZ_Max	FZ_RMS	MX_Max	MX_RMS	MY_Max	MY_RMS	MZ_Max	MZ_RMS	tx_Max	tx_RMS	ty_Max	ty_RMS	tz_Max	tz_RMS	rx_Max	rx_RMS	ry_Max	ry_RMS	rz_Max	rz_RMS
Status	1	2	3	1	1	1	1	1	1	1	1	1	1	2	2	2	1	1	1	1	1	1	1	1	1
Value		16.4206	10.4815	-4.1365	1.502	-6.5608	2.1472	40.0195	13.1317	13.3843	4.4799	41.394	14.0888	0.0419	0.0253	-0.0442	0.0188	-0.0076	0.0038	0.0268	0.0145	0.0272	0.0142	0.1806	0.0986
Status	2	2	3	1	1	1	1	1	1	1	1	1	1	2	2	1	1	1	1	1	1	1	1	1	1
Value		15.9594	10.3001	-3.2481	1.1881	-6.4212	2.0959	38.3492	12.8618	13.9786	4.5689	43.6353	14.6649	0.0405	0.0245	0.0071	0.0045	-0.0087	0.0043	0.0218	0.0111	0.0276	0.0143	0.23	0.124
Status	3	2	3	1	1	1	1	1	1	1	1	1	1	2	2	1	1	1	1	1	1	1	1	1	1
Value		15.9408	10.2794	-3.1764	1.1485	-6.3979	2.0353	38.1255	12.4672	13.9922	4.4606	43.5468	14.5141	0.0405	0.0245	0.0071	0.0045	-0.0087	0.0044	0.0246	0.0124	0.027	0.0138	0.2271	0.1223
Status	4																								
Value																									
Status	5																								
Value																									
Status	6																								
Value																									

Table 30: RRA iterative residual “hand of god” forces and moments on the pelvis for Valgus Normal Walking TFA=188. All parameters shown were minimized until they could not be minimized any further. Green= sufficient value, yellow=tolerable value, and red=insufficient value. Threshold values can be found in Table 6.

	Iteration	FX_Max	FX_RMS	FY_Max	FY_RMS	FZ_Max	FZ_RMS	MX_Max	MX_RMS	MY_Max	MY_RMS	MZ_Max	MZ_RMS	tx_Max	tx_RMS	ty_Max	ty_RMS	tz_Max	tz_RMS	rx_Max	rx_RMS	ry_Max	ry_RMS	rz_Max	rz_RMS
Status	1	2	3	1	1	1	1	1	1	1	1	1	1	2	2	2	2	1	1	1	1	1	1	1	1
Value		17.558	11.117	-4.1518	2.0625	-5.8103	1.8706	35.9585	12.0134	11.6572	3.9425	40.5461	15.4368	0.0443	0.027	-0.0482	0.0209	-0.0074	0.0036	0.0225	0.0116	0.0297	0.0161	0.1811	0.1019
Status	2	2	3	1	1	1	1	1	1	1	1	1	1	2	2	1	1	1	1	1	1	1	1	1	1
Value		17.126	10.924	4.1865	1.9973	-5.7568	1.851	35.2033	11.9344	12.0771	4.0081	42.4827	15.9266	0.0431	0.0263	0.0076	0.0044	-0.0085	0.0045	0.0207	0.0102	0.03	0.0159	0.2261	0.1253
Status	3	2	3	1	1	1	1	1	1	1	1	1	1	2	2	1	1	1	1	1	1	1	1	1	1
Value		17.112	10.926	4.1833	1.9748	-5.7426	1.7899	35.0808	11.51	12.0871	3.9388	42.5234	15.8494	0.0431	0.0263	0.0076	0.0044	-0.0085	0.0045	0.0217	0.0106	0.0299	0.0158	0.2257	0.125
Status	4																								
Value																									
Status	5																								
Value																									
Status	6																								
Value																									

Table 31: RRA iterative residual “hand of god” forces and moments on the pelvis for Nominal Tai Chi TFA=177.16. All parameters shown were minimized until they could not be minimized any further. Green= sufficient value, yellow=tolerable value, and red=insufficient value. Threshold values can be found in Table 6.

	Iteration	FX_Max	FX_RMS	FY_Max	FY_RMS	FZ_Max	FZ_RMS	MX_Max	MX_RMS	MY_Max	MY_RMS	MZ_Max	MZ_RMS	tx_Max	tx_RMS	ty_Max	ty_RMS	tz_Max	tz_RMS	rx_Max	rx_RMS	ry_Max	ry_RMS	rz_Max	rz_RMS
Status	1	2	3	3	3	1	1	1	1	1	1	1	1	2	1	2	1	2	1	1	1	1	1	1	1
Value		21.4916	10.8691	-25.9755	13.9038	-8.1481	4.2003	33.8285	17.3398	6.3066	1.9573	23.9139	9.5681	0.0212	0.0104	-0.0325	0.0154	-0.0286	0.0156	-0.1055	0.0619	-0.1021	0.0419	-0.0366	0.016
Status	2	2	3	2	1	1	1	1	1	1	1	1	1	3	3	2	1	3	2	1	1	1	1	1	1
Value		17.3468	11.2378	-16.5689	4.6024	-7.9378	4.2162	33.8927	17.2959	6.2136	1.958	24.7253	9.6904	0.1468	0.1056	0.0334	0.0128	-0.0621	0.0261	0.1076	0.0625	-0.0888	0.0375	-0.0369	0.016
Status	3	2	3	2	1	1	1	1	1	1	1	1	1	3	3	2	1	3	2	1	1	1	1	1	1
Value		17.4456	10.6006	-16.5646	4.6093	-9.4229	4.4792	33.8407	17.3016	6.191	1.95	24.7418	9.6727	0.0886	0.0516	0.0335	0.0129	-0.052	0.0254	-0.1082	0.0628	-0.1052	0.0409	-0.0369	0.0164
Status	4	2	3	2	1	1	1	1	1	1	1	1	1	2	2	2	1	3	2	1	1	1	1	1	1
Value		16.8662	10.3306	-16.5611	4.6291	-9.4222	4.4785	33.8248	17.2995	6.2063	1.9465	24.7422	9.6467	0.0445	0.025	0.0337	0.0129	-0.052	0.0254	-0.1082	0.0628	-0.1018	0.0412	-0.0364	0.0163
Status	5	2	3	2	1	1	1	1	1	1	1	1	1	2	2	2	1	2	2	1	1	1	1	1	1
Value		19.7834	10.6521	-16.5581	4.6522	-9.2689	4.3657	33.8209	17.2906	6.3027	1.9523	24.7428	9.6594	0.0344	0.0171	0.0338	0.0129	-0.0448	0.0226	-0.1084	0.063	-0.1055	0.0426	-0.0359	0.0163
Status	6	2	3	2	1	1	1	1	1	1	1	1	1	2	2	2	1	2	2	1	1	1	1	1	1
Value		15.6948	10.1742	-12.893	4.1127	-9.2443	4.3584	33.8029	17.278	6.2846	1.9523	24.8897	9.6575	0.0458	0.0291	0.0389	0.0148	-0.0448	0.0225	-0.1081	0.063	-0.0997	0.0389	-0.0358	0.0161
Status	7	2	3	2	1	1	1	1	1	1	1	1	1	3	3	2	2	2	2	1	1	1	1	1	1
Value		14.6142	10.5068	10.0578	3.8411	-9.1841	4.3243	33.7853	17.2102	6.3119	1.9427	25.0137	10.2375	0.0932	0.0674	0.0475	0.0201	-0.0443	0.0223	-0.107	0.063	-0.086	0.0341	-0.0354	0.0156
Status	8	2	3	2	1	1	1	1	1	1	1	1	1	2	2	2	1	2	2	1	1	1	1	1	1
Value		19.7835	10.6521	-16.558	4.6523	-9.2689	4.3657	33.8209	17.2906	6.3027	1.9523	24.7428	9.6594	0.0344	0.0171	0.0338	0.0129	-0.0448	0.0226	-0.1084	0.063	-0.1055	0.0426	-0.0359	0.0163
Status	9	2	3	2	1	1	1	1	1	1	1	1	1	2	2	2	1	2	2	1	1	1	1	1	1
Value		19.7823	10.6516	10.6487	3.8815	-9.2592	4.3659	33.8186	17.2955	6.3033	1.9526	24.8934	9.6736	0.0344	0.0171	0.0445	0.0185	-0.0449	0.0226	-0.1082	0.063	-0.1053	0.0426	-0.0361	0.0164
Status	10	2	3	1	1	1	1	1	1	1	1	1	1	2	2	2	2	2	2	1	1	1	1	1	1
Value		17.2614	10.4289	-9.7621	4.9409	-6.4014	2.0974	-36.31	16.2797	6.8515	2.3575	-40.3617	19.3524	0.0366	0.0214	-0.0482	0.0223	-0.0467	0.0211	-0.1136	0.0638	-0.1405	0.0687	-0.0786	0.0377
Status	11	2	3	1	1	1	1	1	1	1	1	1	1	2	2	2	1	2	2	1	1	1	1	1	1
Value		19.6961	10.6603	-8.4876	2.6788	-6.9639	3.3227	18.2997	7.6817	6.7037	2.319	24.4643	9.8322	0.034	0.017	0.0308	0.013	-0.026	0.0128	-0.0505	0.0268	0.0556	0.0255	-0.0347	0.0167

Table 32: RRA iterative residual “hand of god” forces and moments on the pelvis for Varus Tai Chi TFA=177.16. All parameters shown were minimized until they could not be minimized any further. Green= sufficient value, yellow=tolerable value, and red=insufficient value. Threshold values can be found in Table 6.

	Iteration	FX_Max	FX_RMS	FY_Max	FY_RMS	FZ_Max	FZ_RMS	MX_Max	MX_RMS	MY_Max	MY_RMS	MZ_Max	MZ_RMS	tx_Max	tx_RMS	ty_Max	ty_RMS	tz_Max	tz_RMS	rx_Max	rx_RMS	ry_Max	ry_RMS	rz_Max	rz_RMS
Status	1	2	3	3	3	2	1	1	1	1	1	2	1	2	1	3	3	2	1	1	1	1	1	1	1
Value		19.582	10.677	-38.584	14.191	-10.479	3.633	47.39	11.6587	6.7326	2.4828	54.7182	12.2954	0.0327	0.017	-0.0822	0.0555	-0.0272	0.0137	0.2343	0.0443	0.1857	0.0352	0.1259	0.0249
Status	2	2	3	2	1	2	1	1	1	1	1	2	1	2	1	2	1	2	1	1	1	1	1	1	1
Value		19.3	10.63	-20.873	4.9922	-10.823	3.55	46.7731	11.305	6.7853	2.4623	56.6693	12.4431	0.0333	0.0169	0.0452	0.0199	-0.0253	0.0126	0.2356	0.0439	0.1876	0.036	0.1285	0.0253
Status	3																								
Value																									
Status	4																								
Value																									
Status	5																								
Value																									
Status	6																								
Value																									

Table 33: RRA iterative residual “hand of god” forces and moments on the pelvis for Valgus Tai Chi TFA=177.16. All parameters shown were minimized until they could not be minimized any further. Green= sufficient value, yellow=tolerable value, and red=insufficient value. Threshold values can be found in Table 6.

	Iteration	FX_Max	FX_RMS	FY_Max	FY_RMS	FZ_Max	FZ_RMS	MX_Max	MX_RMS	MY_Max	MY_RMS	MZ_Max	MZ_RMS	tx_Max	tx_RMS	ty_Max	ty_RMS	tz_Max	tz_RMS	rx_Max	rx_RMS	ry_Max	ry_RMS	rz_Max	rz_RMS
Status	1	2	3	2	3	1	1	1	1	1	1	1	1	2	1	3	3	2	1	1	1	1	1	1	1
Value	1	19.618	10.77	-21.205	13.346	-6.5443	3.2427	18.1445	7.47	6.4353	2.262	26.4979	10.1518	0.0338	0.0172	-0.0849	0.0566	-0.0275	0.0131	-0.0465	0.0249	0.0613	0.0242	-0.0369	0.0171
Status	2	2	3	2	1	1	1	1	1	1	1	1	1	2	1	2	1	2	1	1	1	1	1	1	1
Value	2	19.832	10.724	-11.005	2.9828	-6.7405	3.2112	17.6783	7.3201	6.4941	2.2584	27.3564	10.252	0.0344	0.0172	0.0296	0.0139	-0.0247	0.0121	-0.0461	0.0253	0.0633	0.0258	-0.0364	0.0175
Status	3	2	3	2	1	1	1	1	1	1	1	1	1	2	1	2	1	2	1	1	1	1	1	1	1
Value	3	19.834	10.732	-11.015	2.9443	-6.7198	3.1931	17.2235	7.2414	6.4949	2.2594	27.3761	10.1961	0.0344	0.0172	0.0289	0.0138	-0.0246	0.0121	-0.0455	0.0251	0.0631	0.0258	-0.0357	0.0174
Status	4																								
Value	4																								
Status	5																								
Value	5																								
Status	6																								
Value	6																								

Appendix C: Left Leg Joint Reaction Plots and Statistics

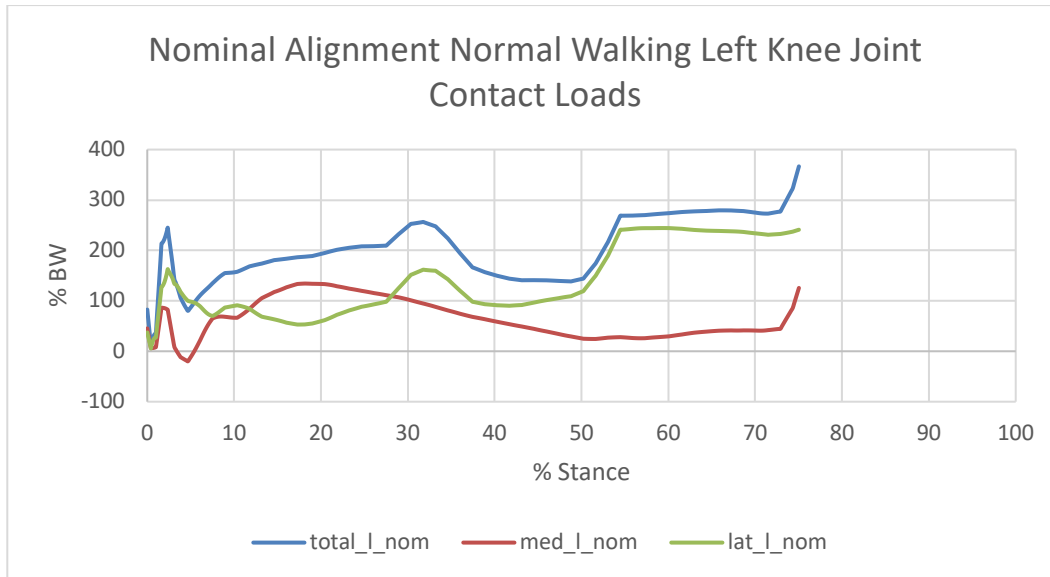


Figure 97: Normalized joint contact loads of the total, medial, and lateral left knee compartments during stance phase of Normal Walking gait with nominal alignment, TFA=177.16 degrees.

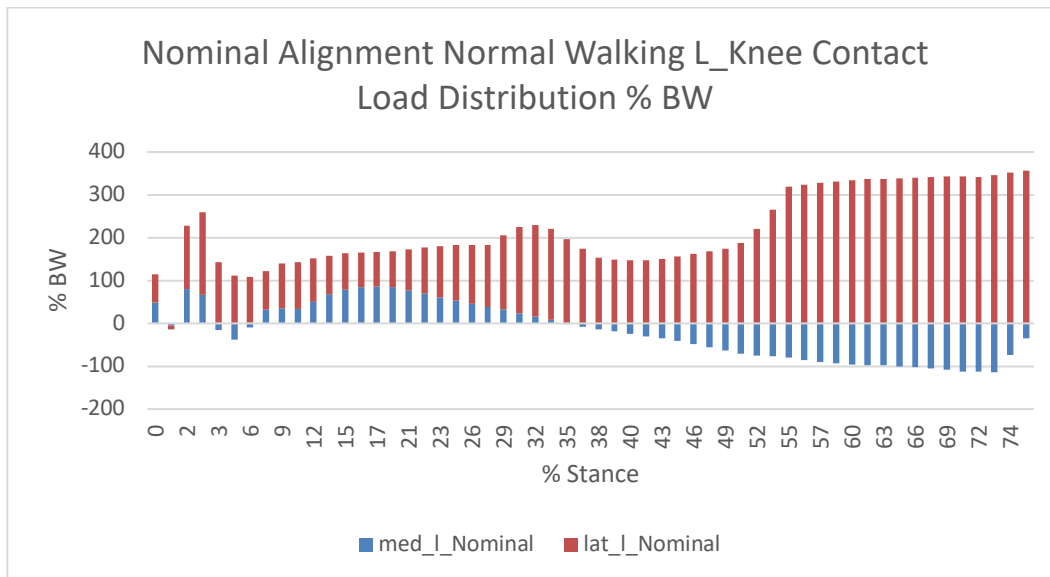


Figure 98: Left medial and lateral normalized joint contact loads summed to show the total contact loads as a percentage of body weight during stance phase of Normal Walking gait with nominal alignment, TFA=177.16 degrees.

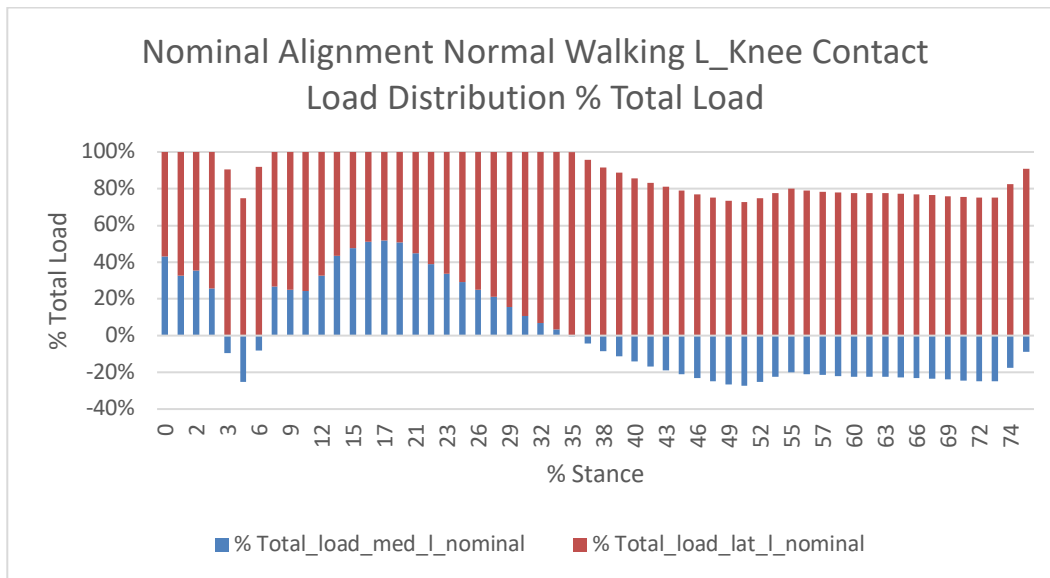


Figure 99: Left medial and lateral normalized joint contact load distribution as a percentage of the total contact load during stance phase of Normal Walking gait with nominal alignment, TFA=177.16 degrees.

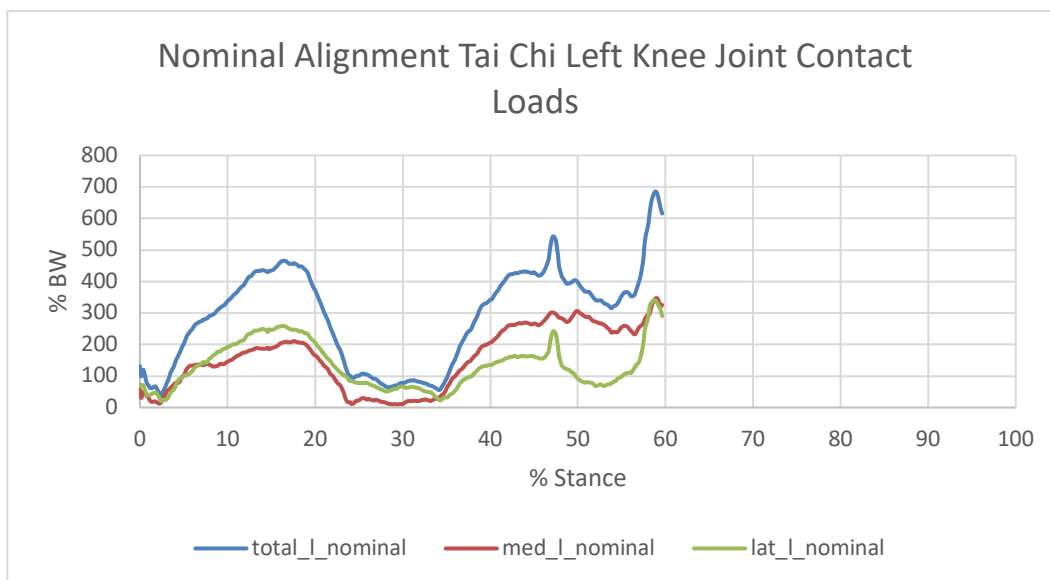


Figure 100: Normalized joint contact loads of the total, medial, and lateral left knee compartments during stance phase of Tai Chi gait with nominal alignment, TFA=177.16 degrees.

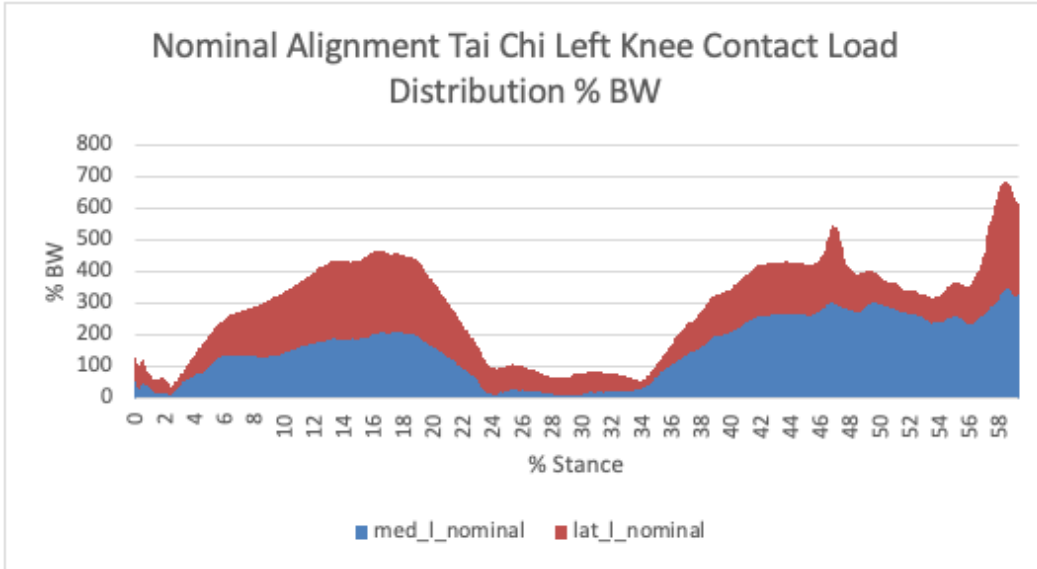


Figure 101: Left medial and lateral normalized joint contact loads summed to show the total contact loads as a percentage of body weight during stance phase of Tai Chi gait with nominal alignment, TFA=177.16 degrees.

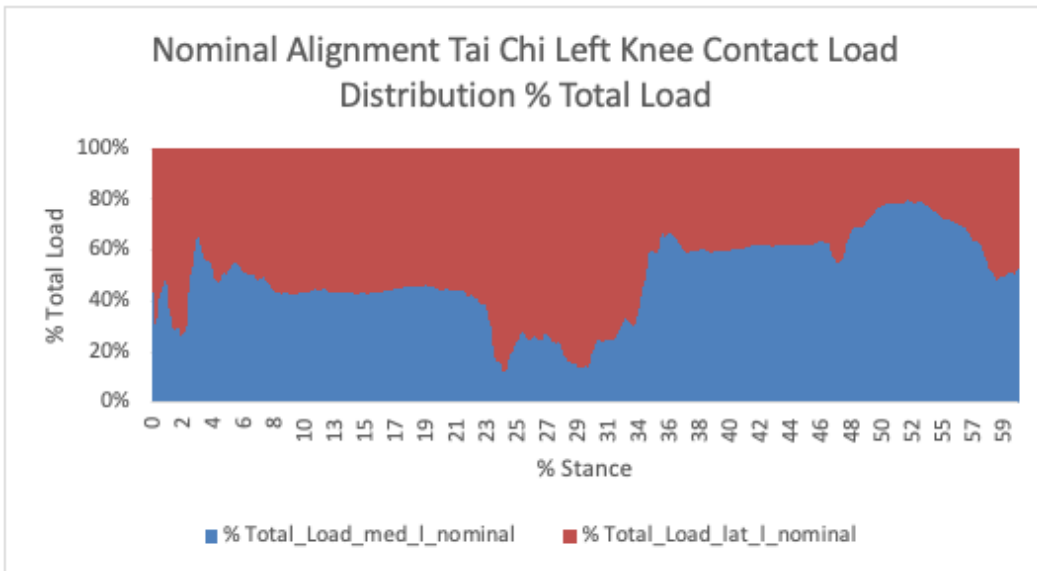


Figure 102: Left medial and lateral normalized joint contact load distribution as a percentage of the total contact load during stance phase of Tai Chi gait with nominal alignment, TFA=177.16 degrees.

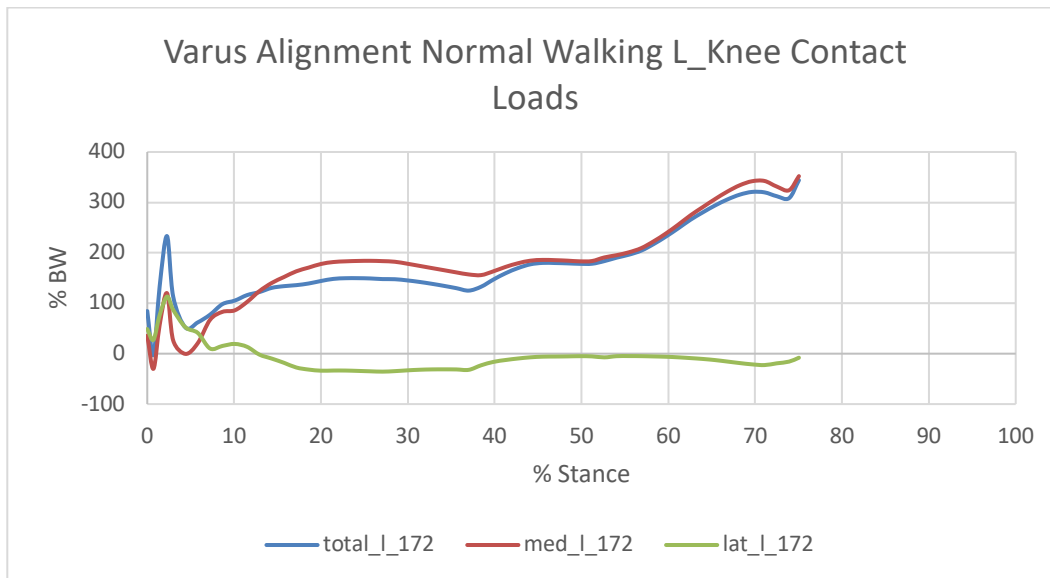


Figure 103: Normalized joint contact loads of the total, medial, and lateral left knee compartments during stance phase of Normal Walking gait with varus alignment, TFA=172 degrees.

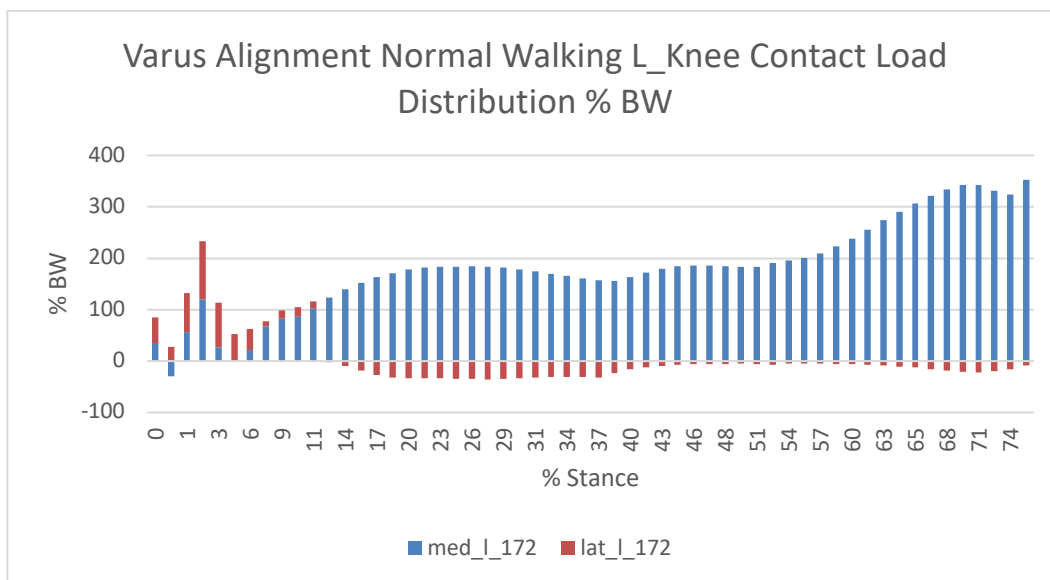


Figure 104: Left medial and lateral normalized joint contact loads summed to show the total contact loads as a percentage of body weight during stance phase of Normal Walking gait with varus alignment, TFA=172 degrees.

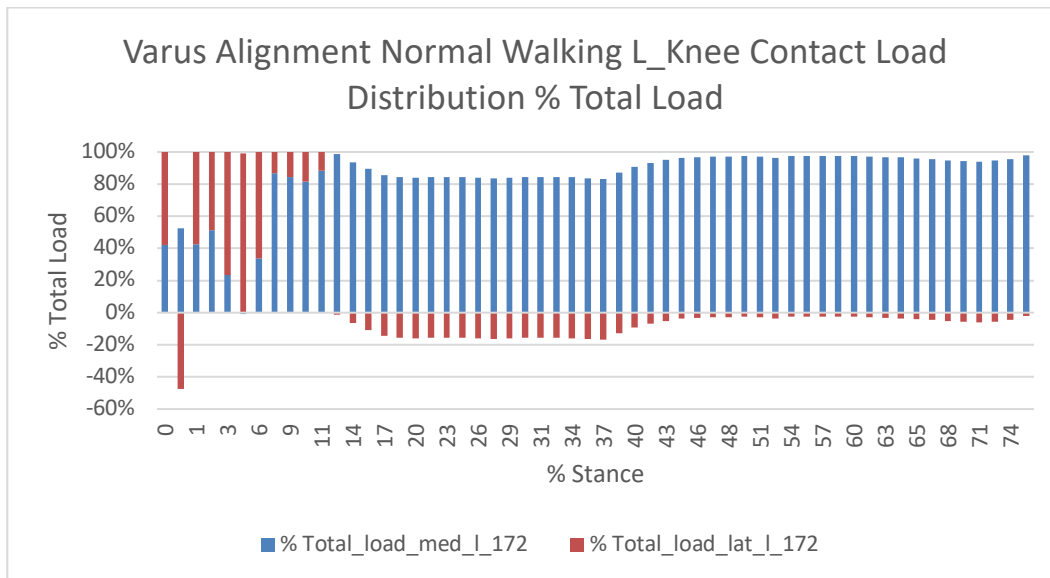


Figure 105: Left medial and lateral normalized joint contact load distribution as a percentage of the total contact load during stance phase of Normal Walking gait with varus alignment, TFA=172 degrees.

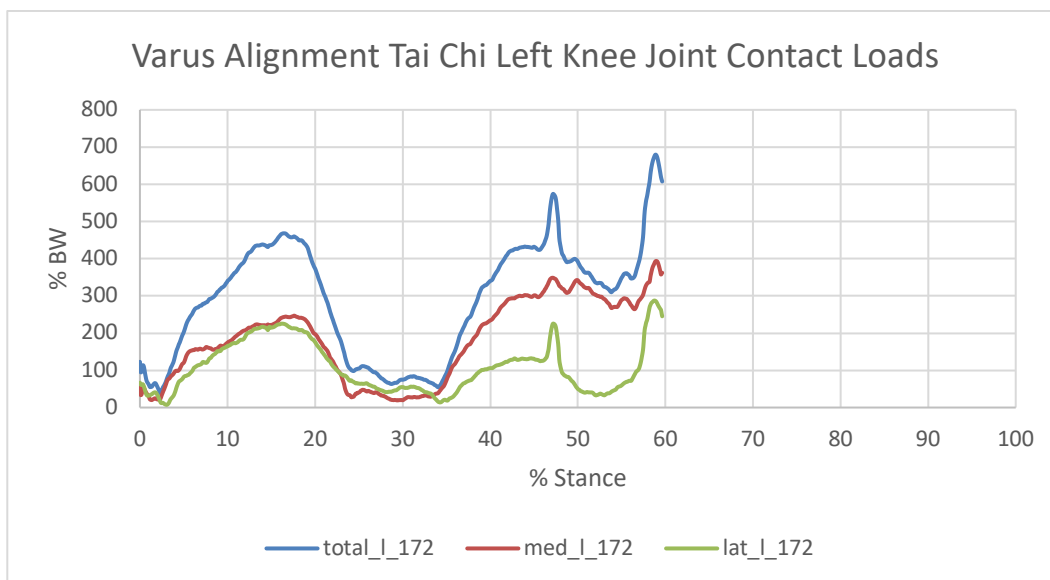


Figure 106: Normalized joint contact loads of the total, medial, and lateral left knee compartments during stance phase of Tai Chi gait with varus alignment, TFA=172 degrees.

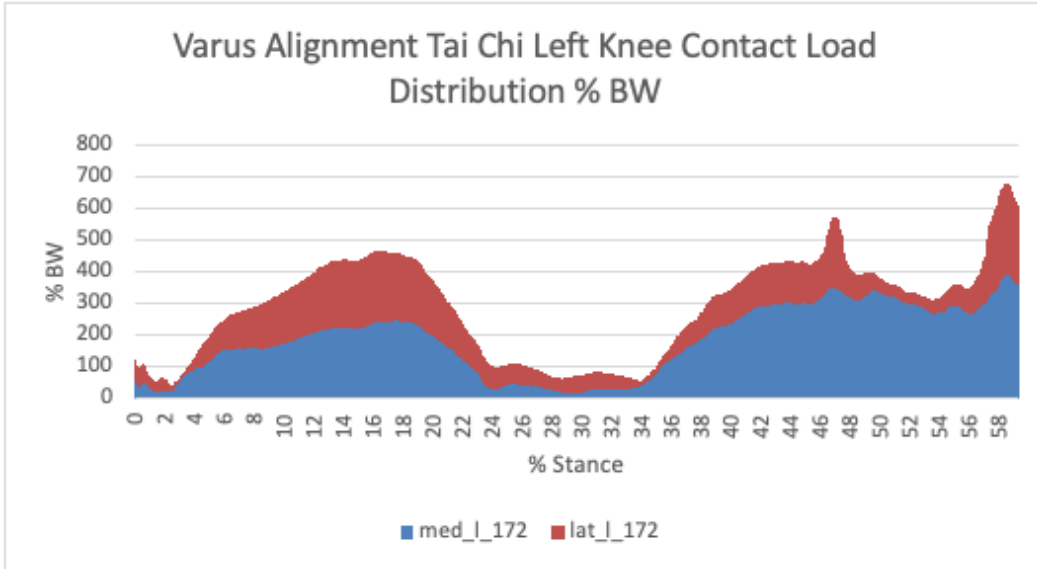


Figure 107: Left medial and lateral normalized joint contact loads summed to show the total contact loads as a percentage of body weight during stance phase of Tai Chi gait with varus alignment, TFA=172 degrees.

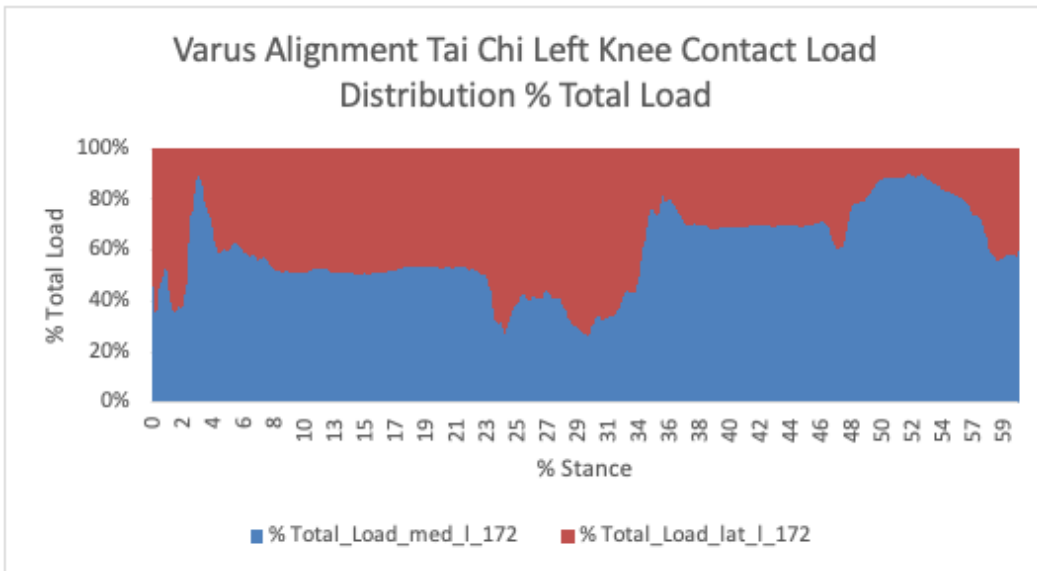


Figure 108: Left medial and lateral normalized joint contact load distribution as a percentage of the total contact load during stance phase of Tai Chi gait with varus alignment, TFA=172 degrees.

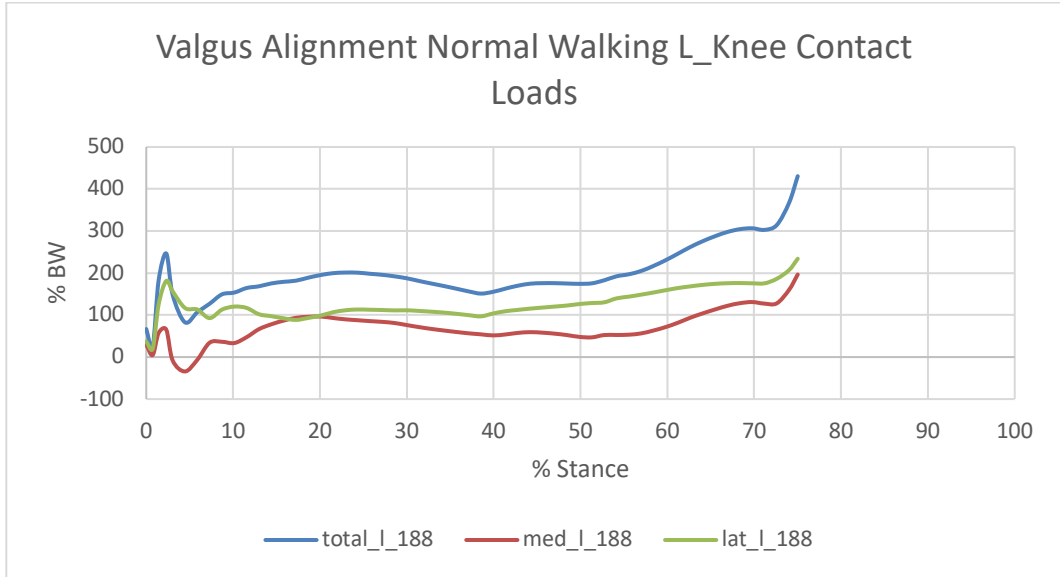


Figure 109: Normalized joint contact loads of the total, medial, and lateral left knee compartments during stance phase of Tai Chi gait with valgus alignment, TFA=188 degrees.

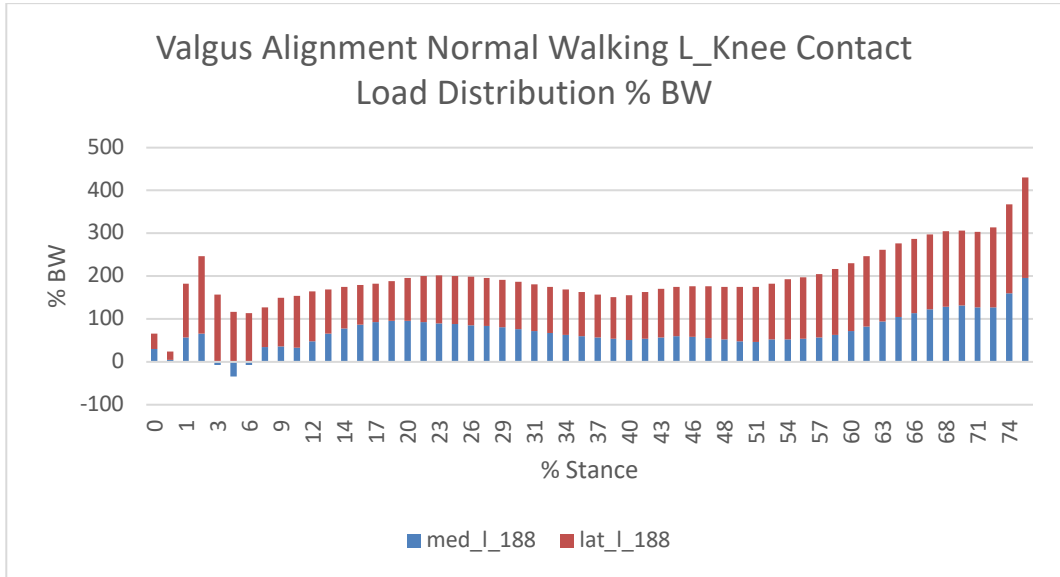


Figure 110: Left medial and lateral normalized joint contact loads summed to show the total contact loads as a percentage of body weight during stance phase of Normal Walking gait with valgus alignment, TFA=188 degrees.

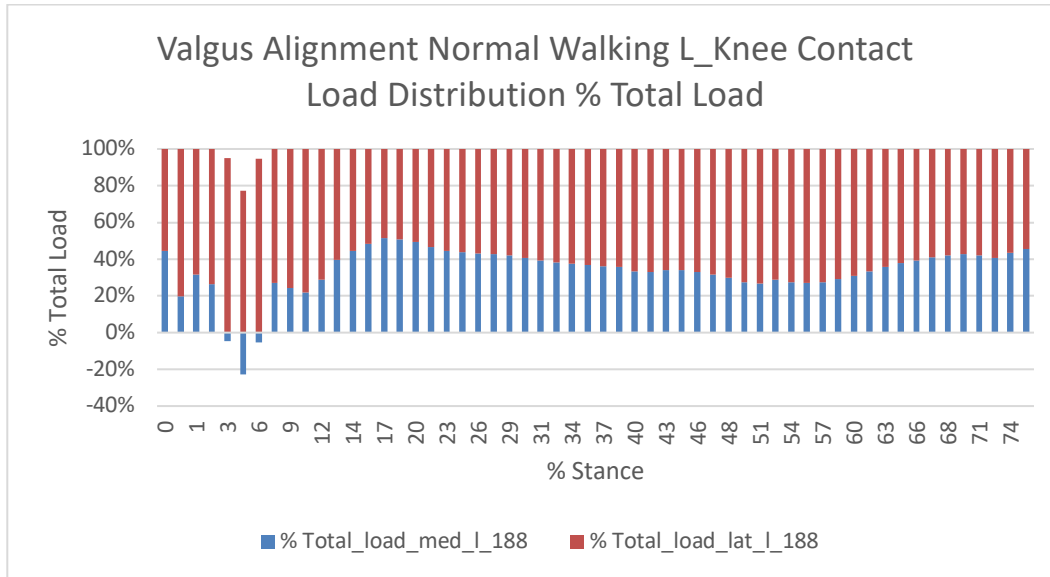


Figure 111: Left medial and lateral normalized joint contact load distribution as a percentage of the total contact load during stance phase of Normal Walking gait with valgus alignment, TFA=188 degrees.

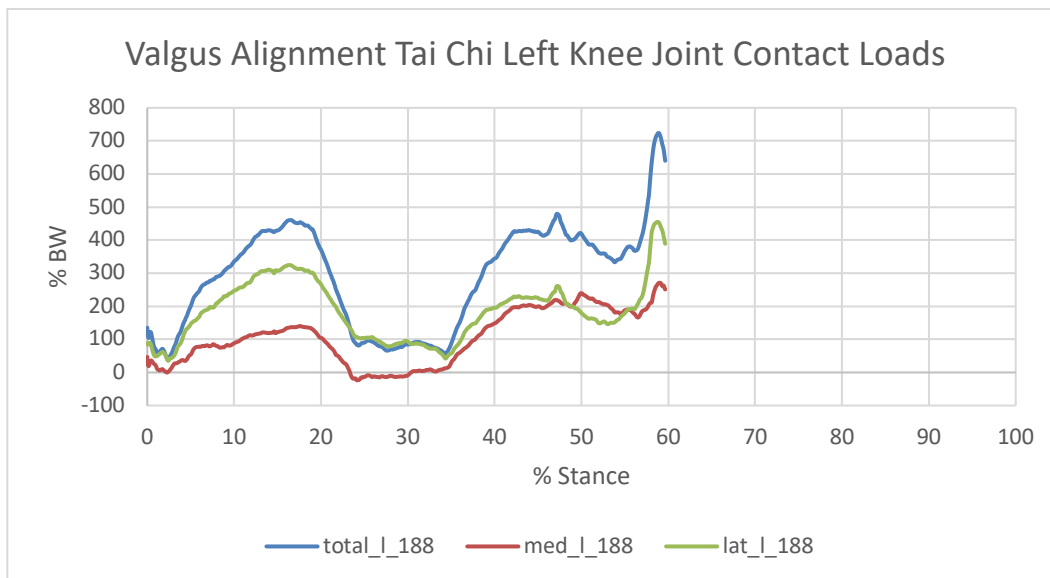


Figure 112: Normalized joint contact loads of the total, medial, and lateral left knee compartments during stance phase of Tai Chi gait with valgus alignment, TFA=188 degrees.

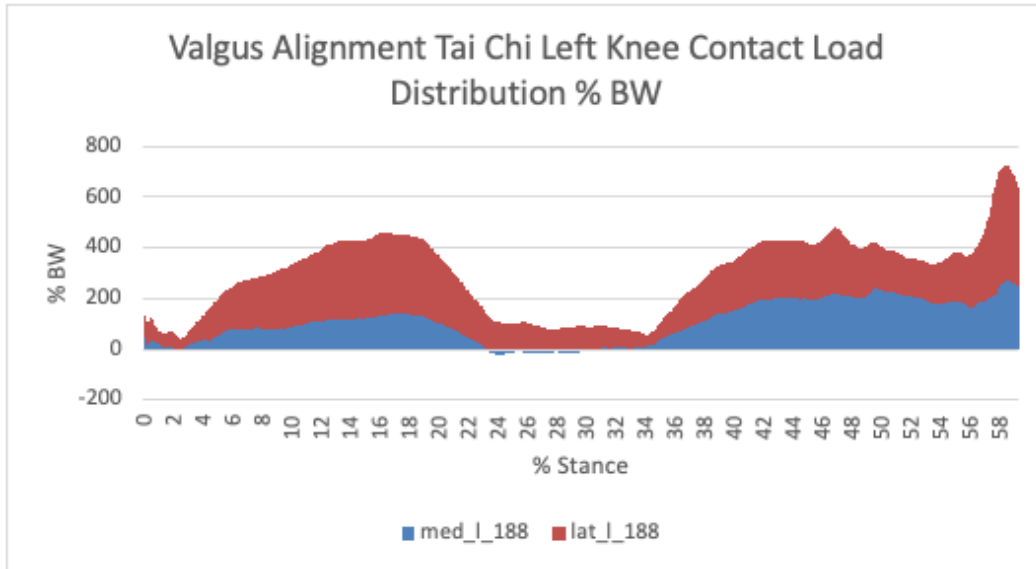


Figure 113: Left medial and lateral normalized joint contact loads summed to show the total contact loads as a percentage of body weight during stance phase of Tai Chi gait with valgus alignment, TFA=188 degrees.

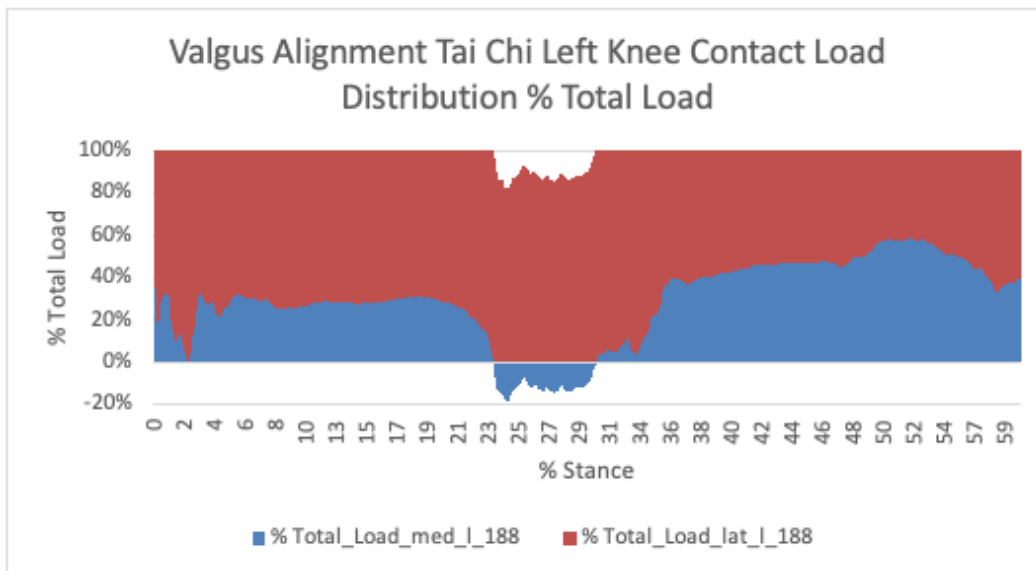


Figure 114: Left medial and lateral normalized joint contact load distribution as a percentage of the total contact load during stance phase of Tai Chi gait with valgus alignment, TFA=188 degrees.

Table 34: Statistical comparisons of normalized joint contact forces for the left knee nominal alignment of Tai Chi and Normal Walking.

Nominal Tai Chi Vs. Normal Walking Left Knee Comparative Statistics					
	NW	TC	Diff (TC-NW)		P-Value
Max_total	321.80	685.66	363.87	%BW	
Max_med	86.48	347.17	260.69	%BW	
Max_lat	357.07	340.36	-16.71	%BW	
Mean_total	179.12	291.72	112.61	%BW	p<0.005
Mean_med	-17.06	158.20	175.26	%BW	p<0.005
Mean_lat	196.18	133.52	-62.66	%BW	p<0.005
Mean_%TotalLoad_med	-7.54	49.74	57.28	%TL	p<0.005
Mean_%TotalLoad_lat	107.54	50.26	-57.28	%TL	p<0.005
Time_MLA_med	5.36	48.58	43.23	%ST	
Time_MLA_lat	94.64	51.42	-43.23	%ST	

Appendix D: Left Leg Altered TFA Plots and Statistics

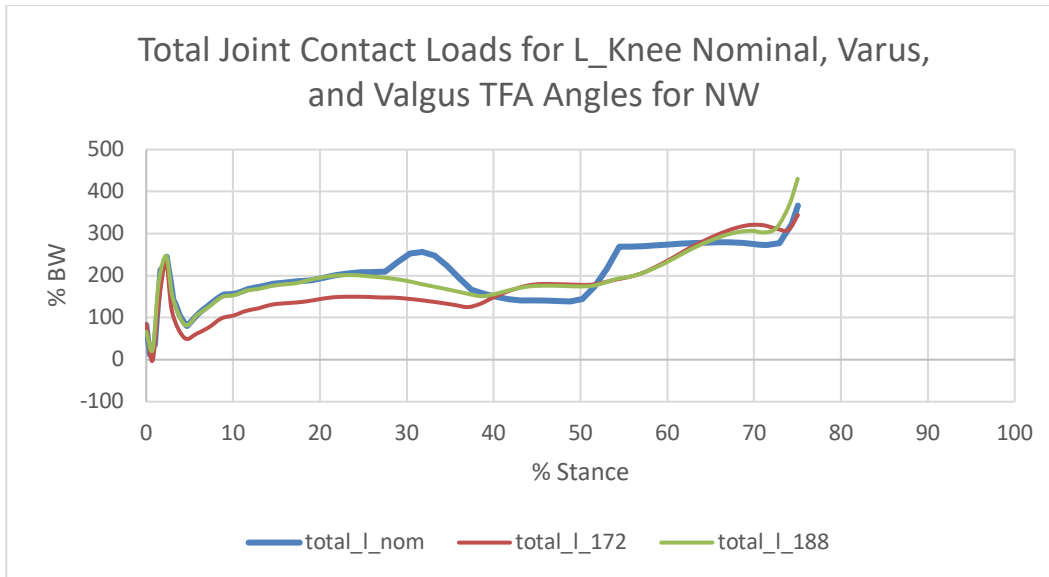


Figure 115: Normalized, left knee, stance phase, total joint contact loads of Normal Walking gait for nominal (TFA=177.16 deg.), varus (TFA=172 deg.), and valgus (TFA=188 deg.) tibiofemoral alignments.

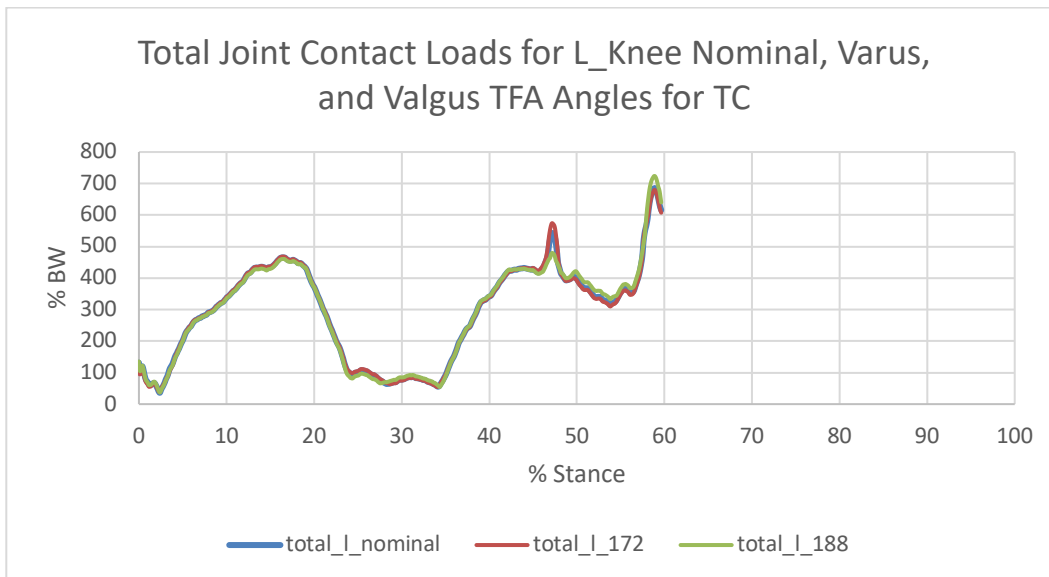


Figure 116: Normalized, left knee, stance phase, total joint contact loads of Tai Chi gait for nominal (TFA=177.16 deg.), varus (TFA=172 deg.), and valgus (TFA=188 deg.) tibiofemoral alignments.

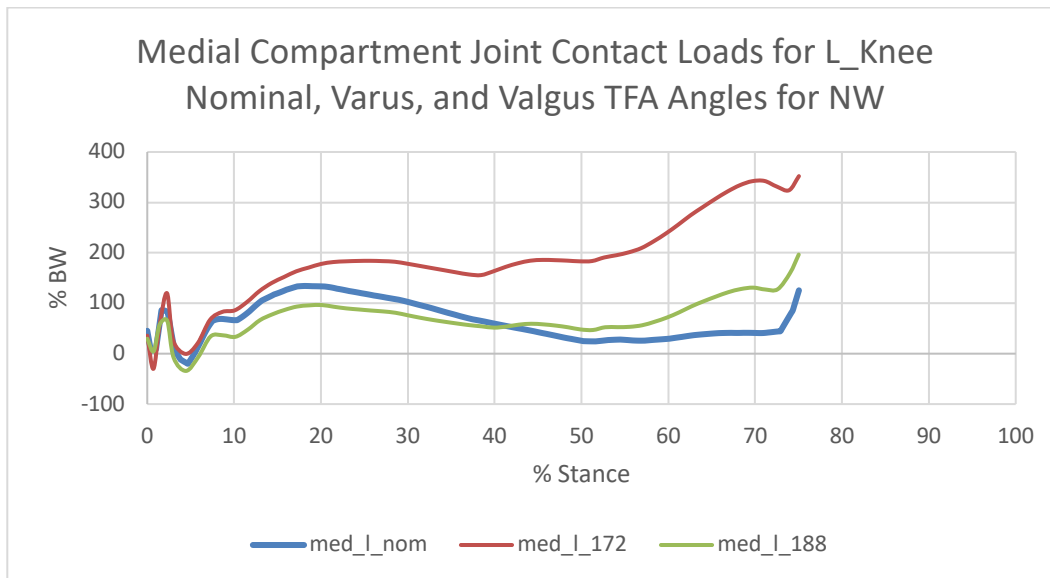


Figure 117: Normalized, left knee, stance phase, medial joint contact loads of Normal Walking gait for nominal (TFA=177.16 deg.), varus (TFA=172 deg.), and valgus (TFA=188 deg.) tibiofemoral alignments.

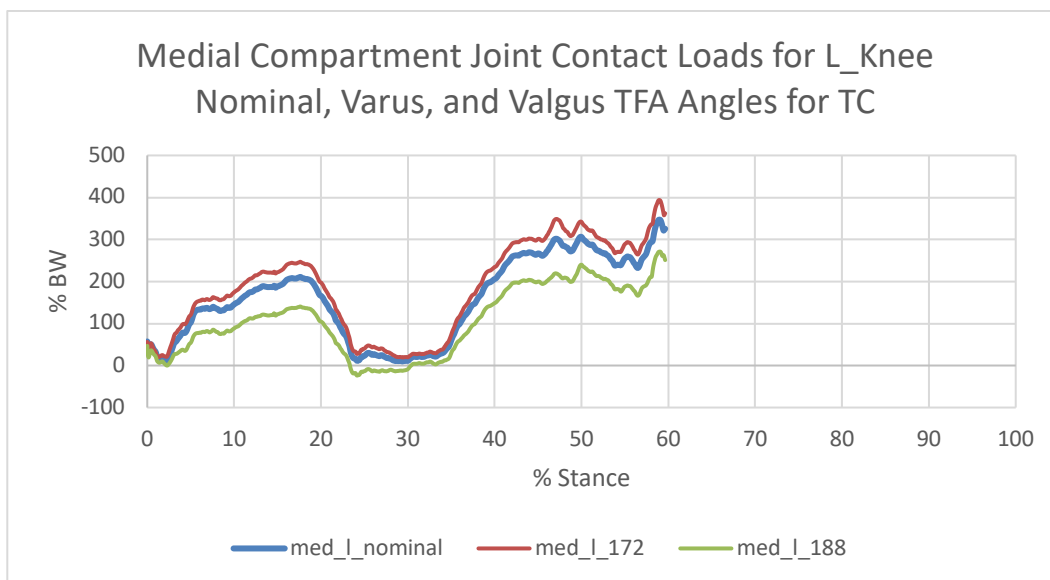


Figure 118: Normalized, left knee, stance phase, medial joint contact loads of Tai Chi gait for nominal (TFA=177.16 deg.), varus (TFA=172 deg.), and valgus (TFA=188 deg.) tibiofemoral alignments.

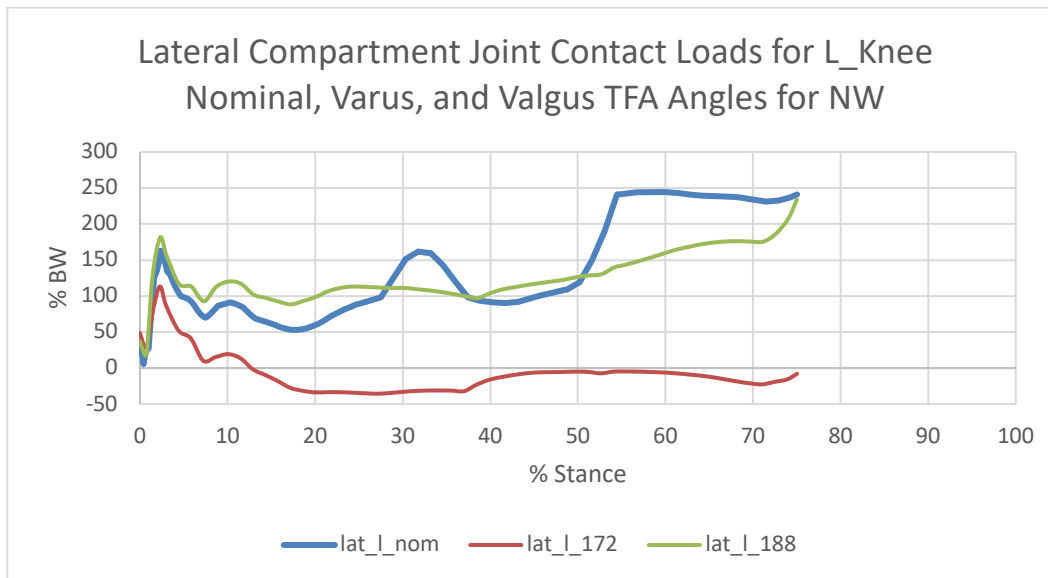


Figure 119: Normalized, left knee, stance phase, lateral joint contact loads of Normal Walking gait for nominal (TFA=177.16 deg.), varus (TFA=172 deg.), and valgus (TFA=188 deg.) tibiofemoral alignments.

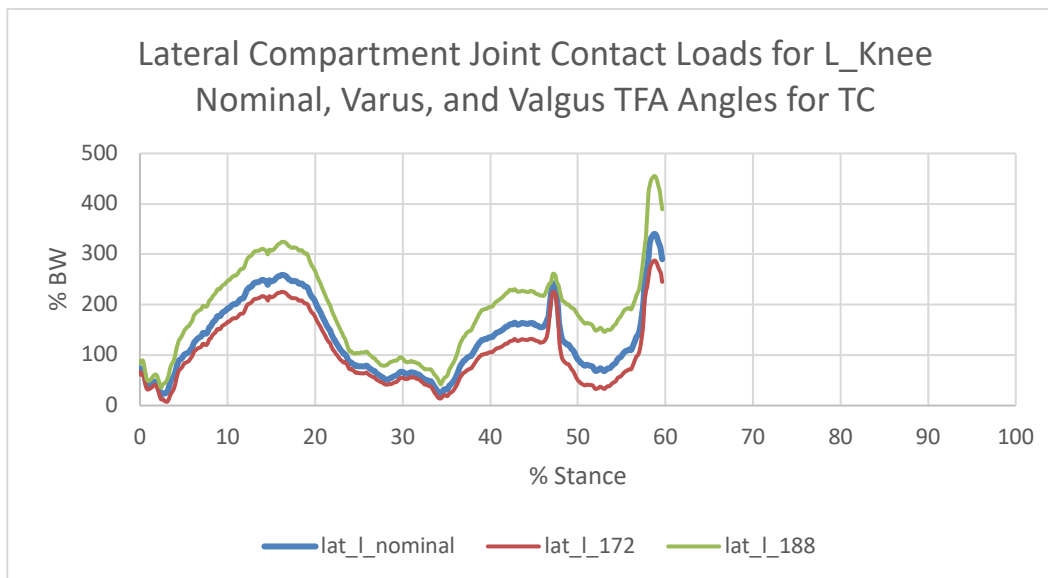


Figure 120: Normalized, left knee, stance phase, lateral joint contact loads of Tai Chi gait for nominal (TFA=177.16 deg.), varus (TFA=172 deg.), and valgus (TFA=188 deg.) tibiofemoral alignments.

Table 35: Statistical comparisons of normalized joint contact forces for the left knee altered tibiofemoral alignment of Normal Walking.

Normal Walking Left Knee Comparative Statistics for Altered TFA									P-Value One-Sided		
	Nominal	Varus	Valgus	Diff (Vr-N)	Diff (Vg-N)	Units	% Diff (Vr-N)	% Diff (Vg-N)	Vr-N	Vg-N	Vr-Vg
Max_total	321.80	344.12	430.56	22.33	108.76	%BW	6.94	33.80			
Max_med	86.48	352.12	196.54	265.63	110.06	%BW	307.15	127.26			
Max_lat	357.07	113.22	234.01	-243.85	-123.06	%BW	-68.29	-34.46			
Mean_total	179.12	175.12	197.69	-4.00	18.57	%BW	-2.23	10.37	0.546	p<0.005	p<0.005
Mean_med	-17.06	180.56	70.80	197.62	87.86	%BW	-1158.38	-515.00	p<0.005	p<0.005	p<0.005
Mean_lat	196.18	-5.44	126.89	-201.62	-69.29	%BW	-102.77	-35.32	p<0.005	p<0.005	p<0.005
Mean_%TotalLoad_med	-7.54	118.44	33.58	125.98	41.12	%TL	-1670.94	-545.34	p<0.005	p<0.005	p<0.005
Mean_%TotalLoad_lat	107.54	-18.44	66.42	-125.98	-41.12	%TL	-117.15	-38.23	p<0.005	p<0.005	p<0.005
Time_MLA_med	5.36	91.07	3.57	85.71	-1.79	%ST	1600.00	-33.33			
Time_MLA_lat	94.64	8.93	96.43	-85.71	1.79	%ST	-90.57	1.89			

Table 36: Statistical comparisons of normalized joint contact forces for the left knee altered tibiofemoral alignment of Tai Chi.

Tai Chi Left Knee Comparative Statistics for Altered TFA									P-Value One-Sided		
	Nominal	Varus	Valgus	Diff (Vr-N)	Diff (Vg-N)	Units	% Diff (Vr-N)	% Diff (Vg-N)	Vr-N	Vg-N	Vr-Vg
Max_total	685.66	679.43	723.84	-6.24	38.18	%BW	-0.91	5.57			
Max_med	347.17	393.78	271.10	46.61	-76.07	%BW	13.43	-21.91			
Max_lat	340.36	287.45	455.09	-52.91	114.74	%BW	-15.54	33.71			
Mean_total	291.72	291.50	292.97	-0.23	1.25	%BW	-0.08	0.43	0.307	0.009	0.026
Mean_med	158.20	183.81	106.29	25.60	-51.92	%BW	16.18	-32.82	p<0.005	p<0.005	p<0.005
Mean_lat	133.52	107.69	186.68	-25.83	53.16	%BW	-19.35	39.82	p<0.005	p<0.005	p<0.005
Mean_%TotalLoad_med	49.74	59.93	28.52	10.19	-21.23	%TL	20.48	-42.67	p<0.005	p<0.005	p<0.005
Mean_%TotalLoad_lat	50.26	40.07	71.48	-10.19	21.23	%TL	-20.27	42.24	p<0.005	p<0.005	p<0.005
Time_MLA_med	48.58	78.95	0	30.36	-48.58	%ST	62.50	-100.00			
Time_MLA_lat	51.42	21.05	100	-30.36	48.58	%ST	-59.06	94.49			

Table 37: Percent difference of normalized joint contact force data comparisons of left knee varus and valgus tibiofemoral alignment for Tai Chi and Normal Walking.

Tai Chi and Normal Walking Comparative Statistics for Left Knee Altered TFA				
	TC % Diff (Vr-N)	NW % Diff (Vr-N)	TC % Diff (Vg-N)	NW % Diff (Vg-N)
Max_total		-0.91	6.94	33.80
Max_med		13.43	307.15	127.26
Max_lat		-15.54	-68.29	-34.46
Mean_total		-0.08	-2.23	10.37
Mean_med		16.18	-1158.38	-515.00
Mean_lat		-19.35	-102.77	-35.32
Mean_%TotalLoad_med		20.48	-1670.94	-545.34
Mean_%TotalLoad_lat		-20.27	-117.15	-38.23
Time_MLA_med		62.50	1600.00	-33.33
Time_MLA_lat		-59.06	-90.57	1.89

Table 38: Normalized percent difference per degree of malalignment of normalized joint contact force data comparisons of left knee varus and valgus tibiofemoral alignment for Tai Chi and Normal Walking.

Tai Chi and Normal Walking Left Knee Comparative Statistics for Altered TFA Normalized Per Degree TFA				
	TC %Diff(Vr-N)/deg.	NW %Diff(Vr-N)/deg.	TC %Diff(Vg-N)/deg.	NW %Diff(Vg-N)/deg.
Max_total	-0.18	1.34	0.51	3.12
Max_med	2.60	59.52	-2.02	11.74
Max_lat	-3.01	-13.23	3.11	-3.18
Mean_total	-0.02	-0.43	0.04	0.96
Mean_med	3.14	-224.49	-3.03	-47.51
Mean_lat	-3.75	-19.92	3.67	-3.26
Mean_%TotalLoad_med	3.97	-323.83	-3.94	-50.31
Mean_%TotalLoad_lat	-3.93	-22.70	3.90	-3.53

Appendix E: Left Leg Muscle Forces and Contact Load Contributions

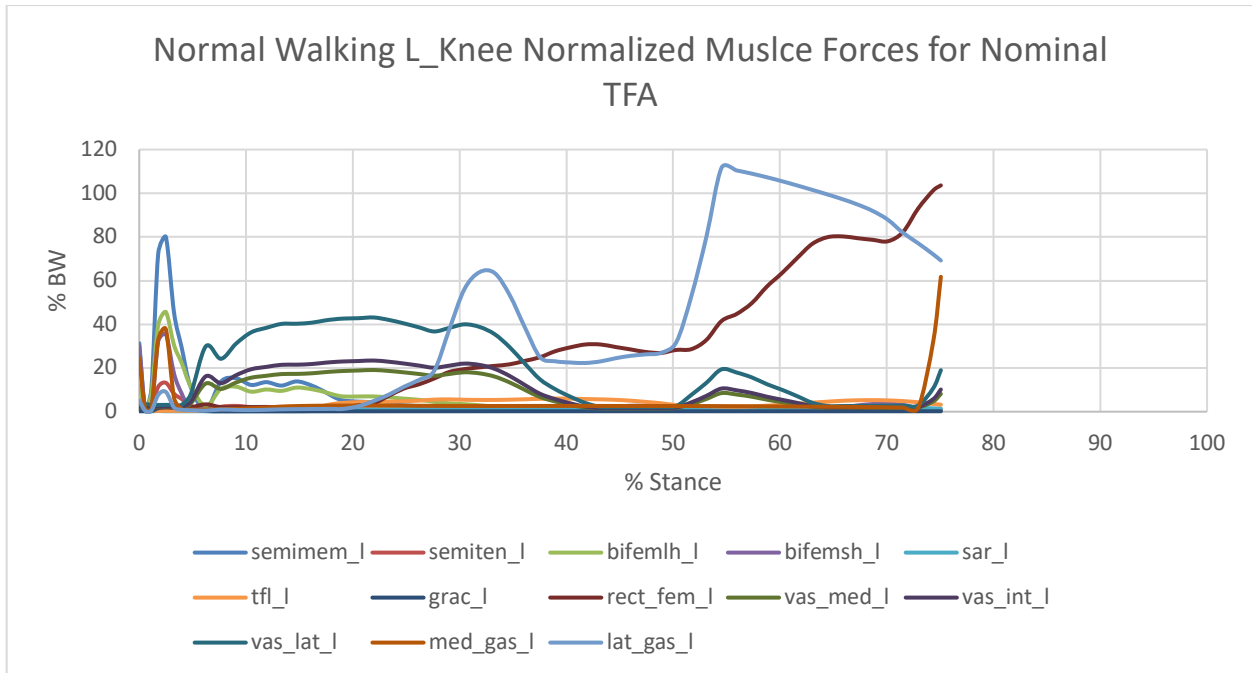


Figure 121: Normalized muscle forces that traverse the left knee during stance phase for Normal Walking, nominal tibiofemoral alignment (TFA=177.16deg.)

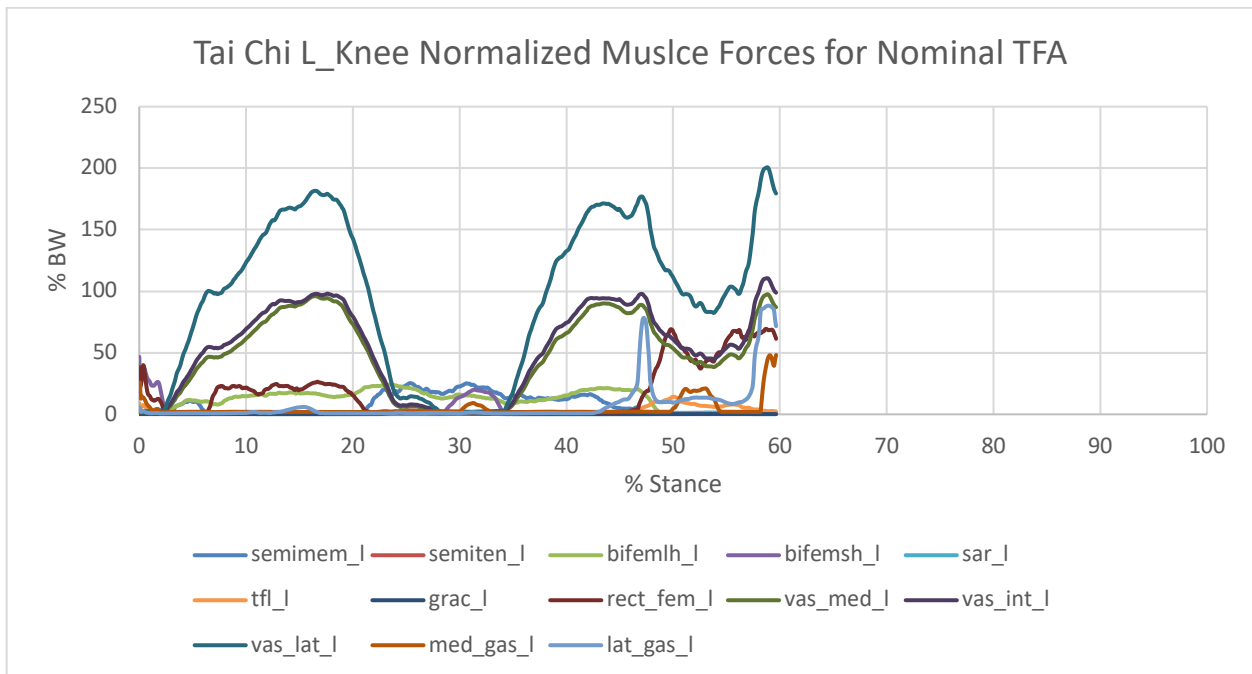


Figure 122; Normalized muscle forces that traverse the left knee during stance phase for Tai Chi, nominal tibiofemoral alignment (TFA=177.16deg.)

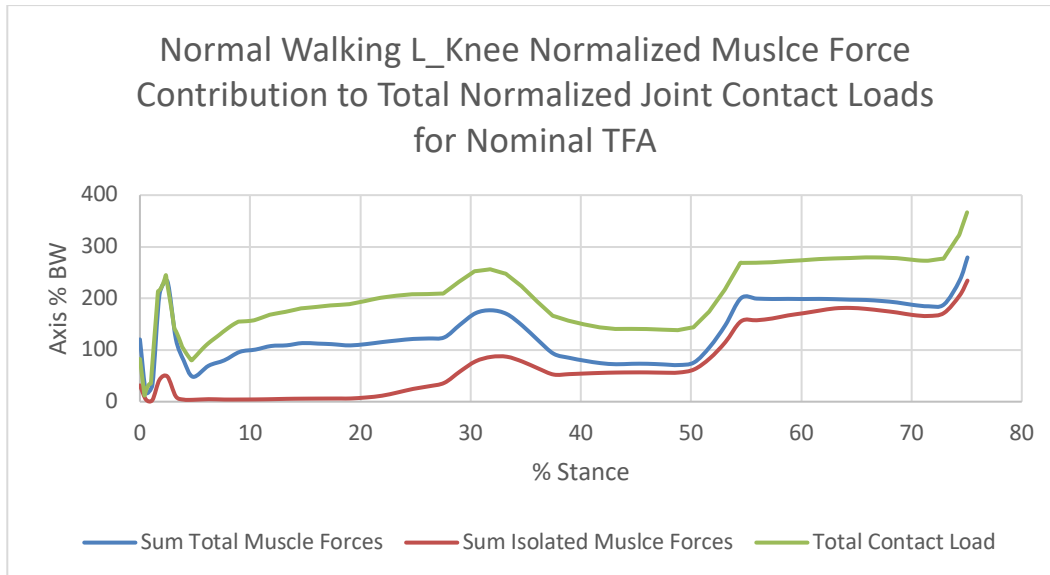


Figure 123: Normalized joint contact forces compared to the sum of the three most influential muscle forces (Sum Isolated Muscle Forces), rectus femoris, lateral gastrocnemius, medial gastrocnemius and the total muscle forces that traverse the left knee, stance phase, Normal Walking, nominal tibiofemoral alignment (TFA=177.16)

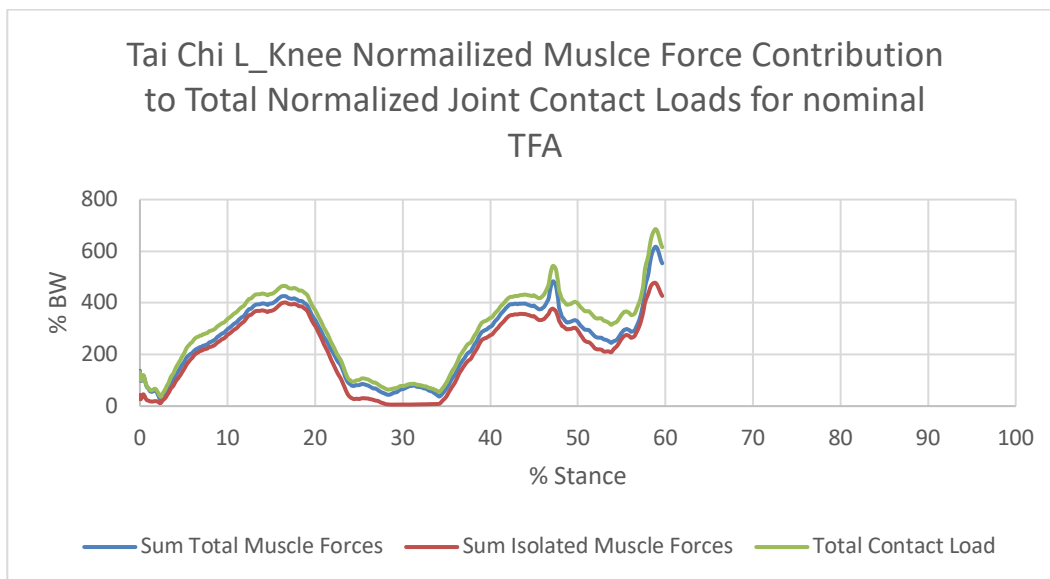


Figure 124: Normalized joint contact forces compared to the sum of the three most influential muscle forces (Sum Isolated Muscle Forces), medial and lateral gastrocnemius, vastus medialis, vastus lateralis, vastus intermedius, rectus femoris, muscle forces that traverse the left knee, stance phase, Tai Chi, nominal tibiofemoral alignment (TFA=177.16)

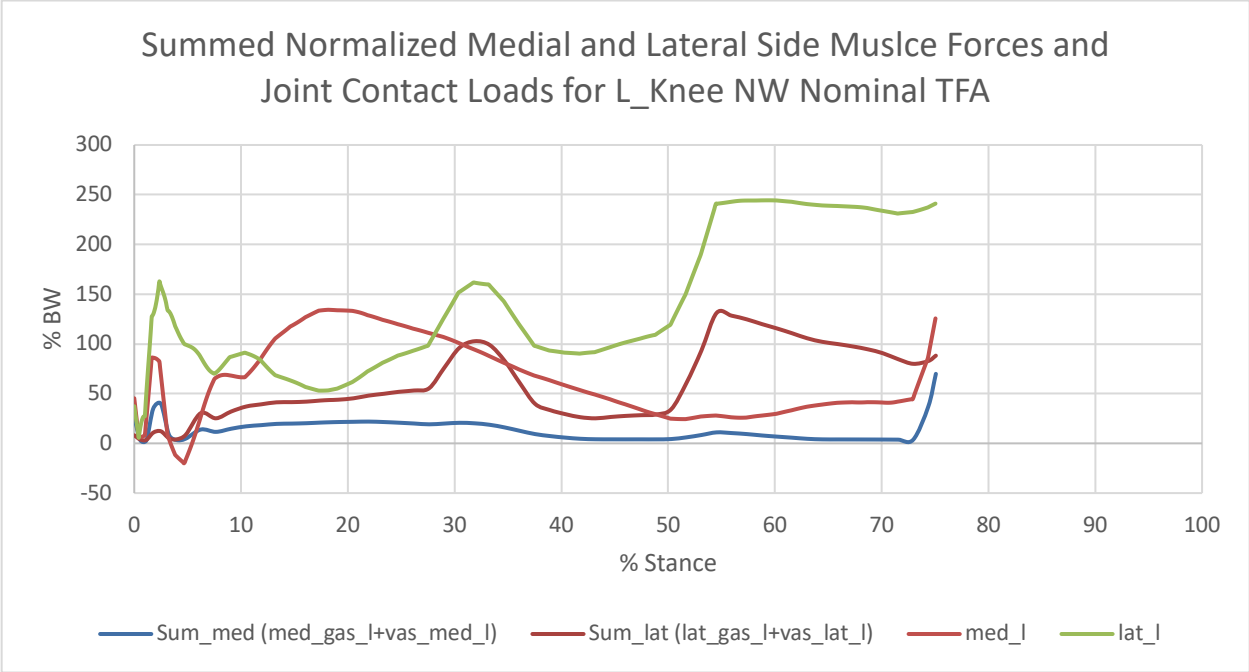


Figure 125: Summed normalized muscle forces for the medial and the lateral sides compared to the medial and lateral joint contact forces of the left knee during stance phase of Tai Chi gait.

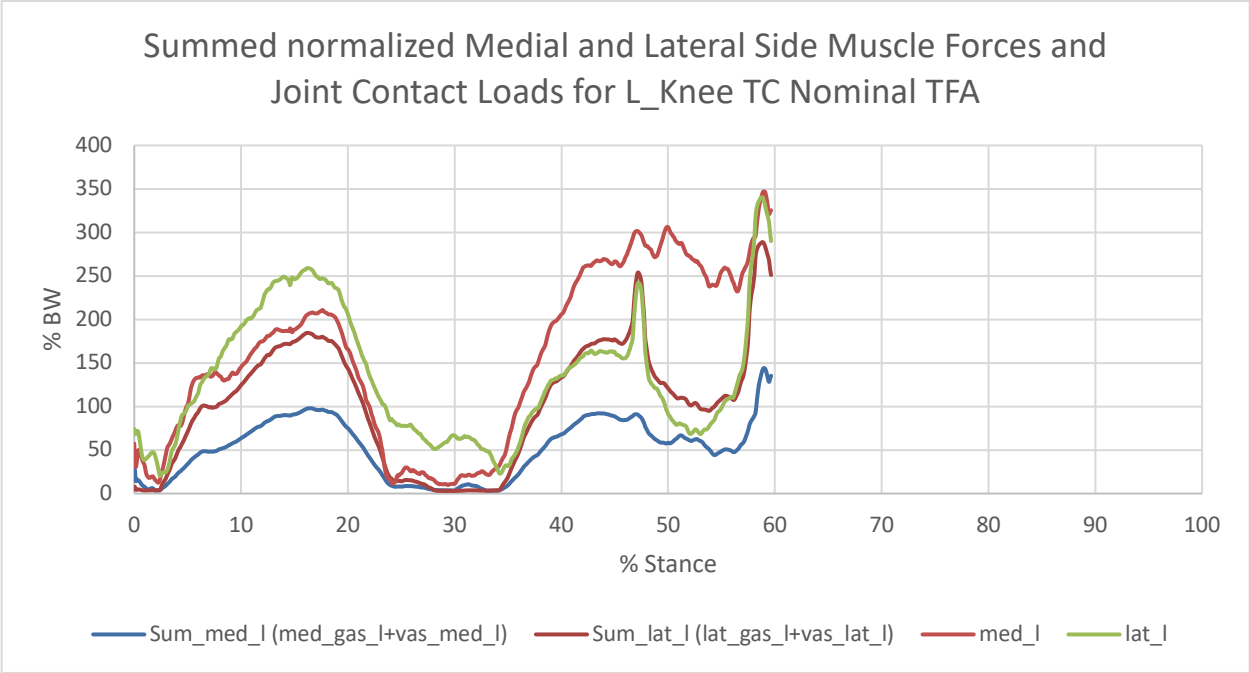


Figure 126: Summed normalized muscle forces for the medial and the lateral sides compared to the medial and lateral joint contact forces of the left knee during stance phase of Tai Chi gait.

Table 39: Mean sum medial side muscle force and lateral side muscle forces that contribute the medio-lateral compartmental joint contact loads in the left knee.

Mean Sum Normalized Influential Left Medial and Lateral Muscle Forces			
	Tai Chi	Normal Walking	
Mean_Sum_Med	52.28	13.75	%BW
Mean_Sum_Lat	103.65	57.72	%BW

Appendix F: Calibration Results

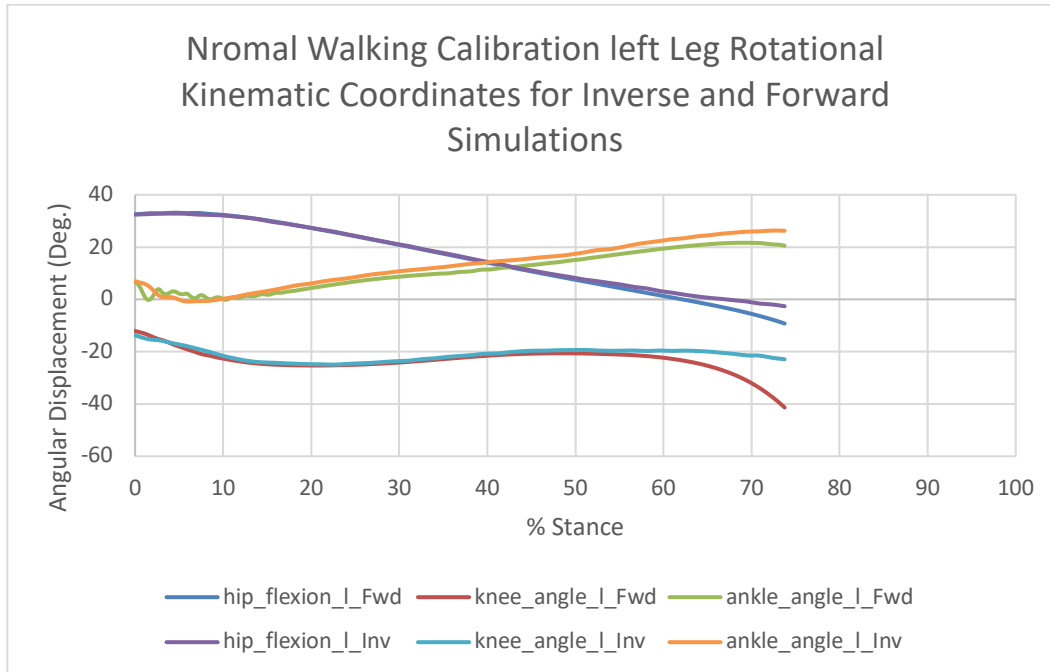


Figure 127: Calibration results for the Normal Walking trial of the nominal model. A comparison of the inverse kinematic and forward dynamic rotations of the hip, knee, and ankle coordinates for left leg, stance phase.

Table 40: Statistical results of paired t-tests for the difference of means for kinematic coordinates calculated by inverse dynamics and forward dynamics. All values are for the left leg stance phase of the Normal Walking trial.

Normal Walking Calibration Statistical Results Left Leg				
Coordinate	Inv_Mean	Fwd_Mean	Diff_Mean	P-Value
Hip_flexion_1	16.42	15.50	-0.92	p<0.005
Knee_angle_1	-21.09	-23.36	-2.28	p<0.005
Ankle_angle_1	13.00	10.88	-2.12	p<0.005

Table 41: The mean the percent differences in kinematic coordinate values at all time steps for inverse kinematics and forward dynamics throughout left leg stance phase of gait for the Normal Walking trial.

Mean % Differences of Normal Walking Kinematic Coordinates Left Leg		
Coordinate	Mean_%Diff	Unit
Hip_flexion_1	-18.17	%
Knee_angle_1	10.60	%
Ankle_angle_1	-0.92	%

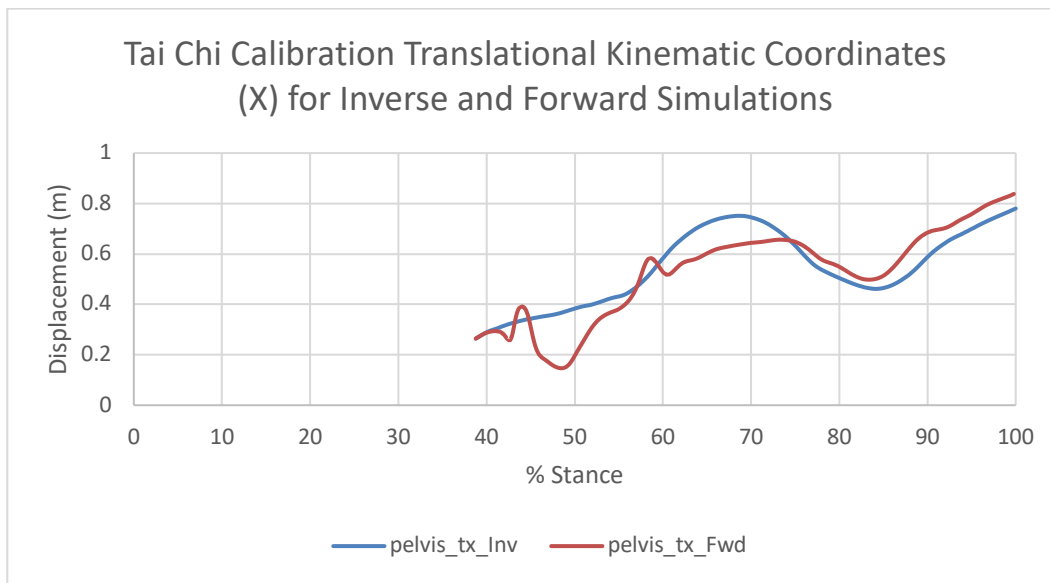


Figure 128: Calibration results for the Tai Chi trial of the nominal model. A comparison of the inverse kinematic and forward dynamic X translational coordinate of the pelvis for right leg, stance phase

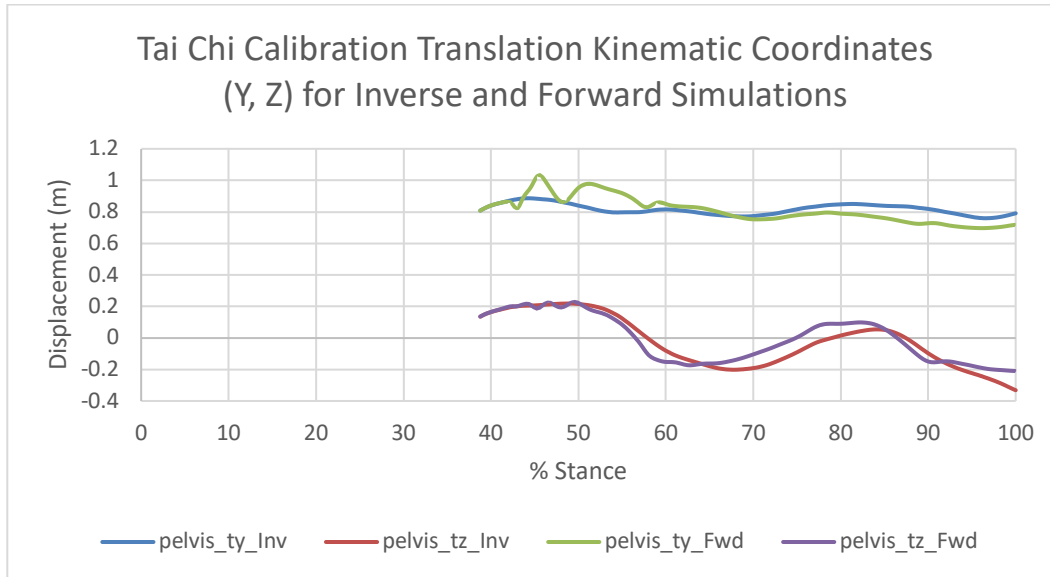


Figure 129: Calibration results for the Tai Chi trial of the nominal model. A comparison of the inverse kinematic and forward dynamic Y & Z translational coordinates of the pelvis for right leg, stance phase

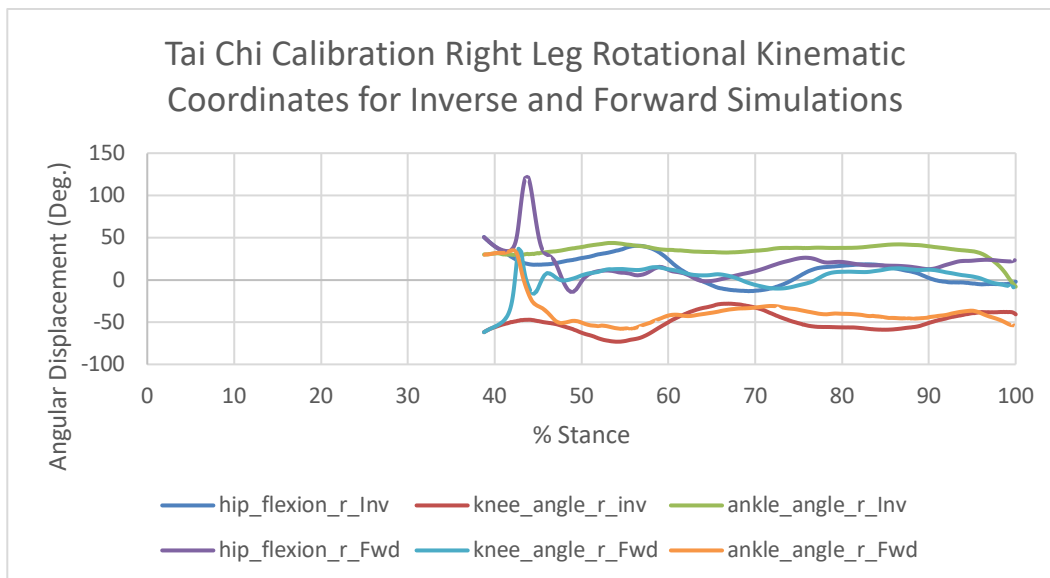


Figure 130: Calibration results for the Tai Chi trial of the nominal model. A comparison of the inverse kinematic and forward dynamic rotations of the hip, knee, and ankle coordinates for right leg, stance phase.

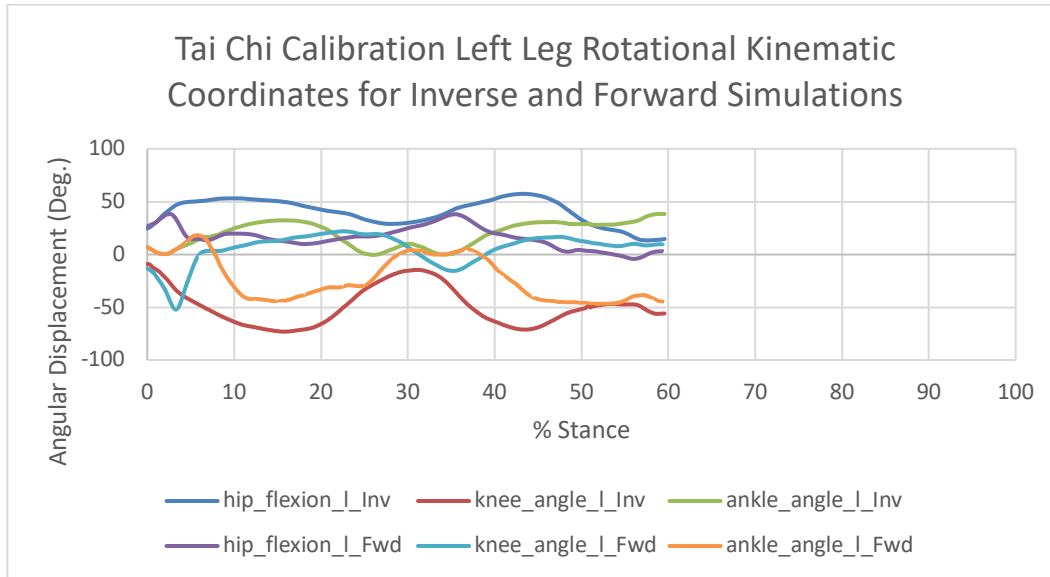


Figure 131: Calibration results for the Tai Chi trial of the nominal model. A comparison of the inverse kinematic and forward dynamic rotations of the hip, knee, and ankle coordinates for left leg, stance phase.

Appendix G: Internal Validation Error Plots

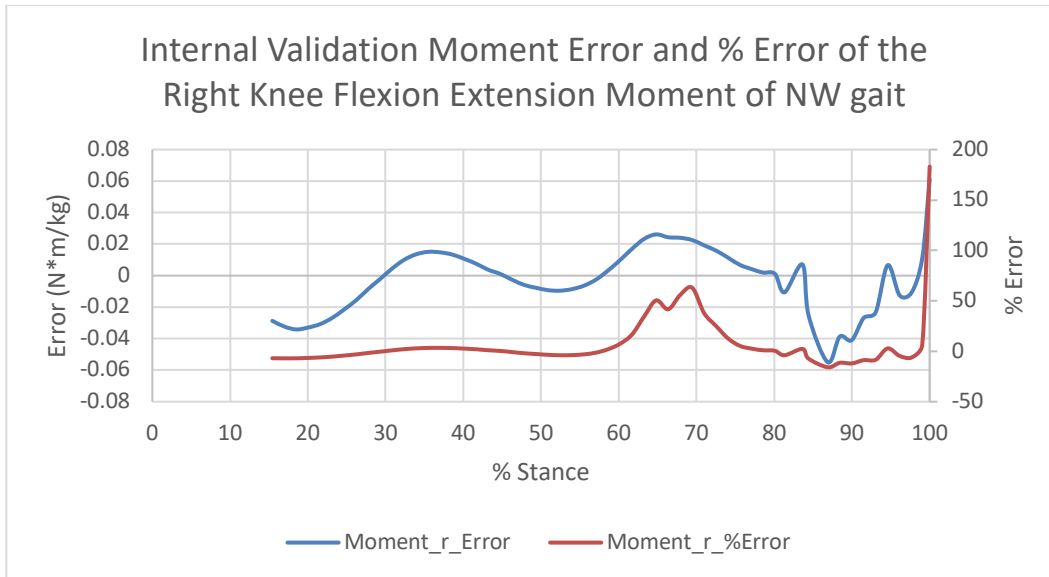


Figure 132: Moment Error, i.e. the error between the moments about the knee generated by the muscle forces and the inverse dynamics moment, calculated by Equation 47 about the right knee joints for stance phase Normal Walking.

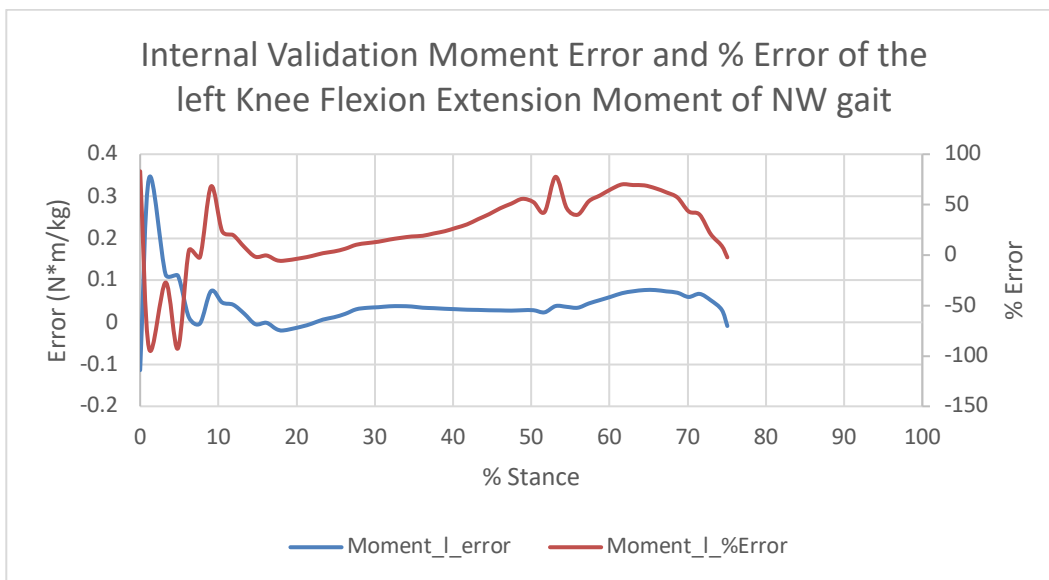


Figure 133: Moment Error, i.e. the error between the moments about the knee generated by the muscle forces and the inverse dynamics moment, calculated by Equation 47 about the left knee joints for stance phase Normal Walking.

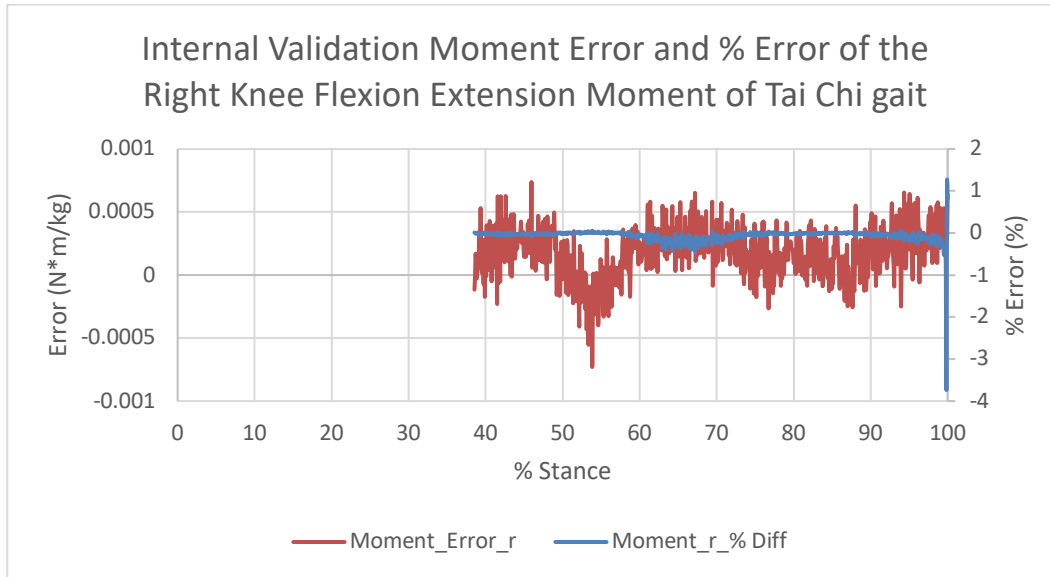


Figure 134: Moment Error, i.e. the error between the moments about the knee generated by the muscle forces and the inverse dynamics moment, calculated by Equation 47 about the right knee joints for stance phase Tai Chi.

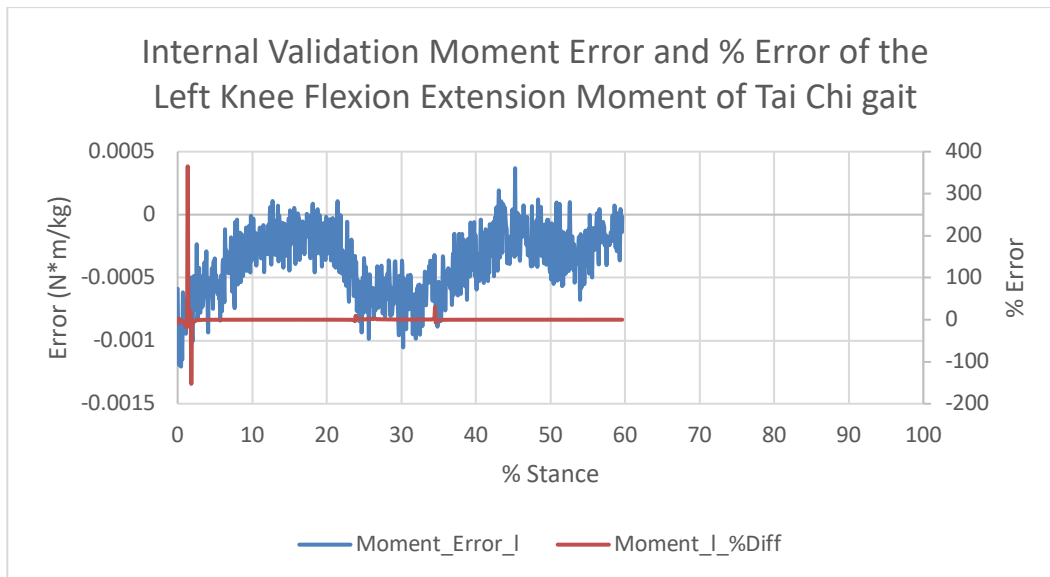


Figure 135: Moment Error, i.e. the error between the moments about the knee generated by the muscle forces and the inverse dynamics moment, calculated by Equation 47 about the left knee joints for stance phase Tai Chi.